

**Synthesis and Characterization of pyridyl/quinolyl imine ruthenium(II) and palladium
(II) complexes in catalysis**



**UNIVERSITY of the
WESTERN CAPE**

By

Leoni Destine Swartz

A dissertation submitted in partial fulfilment of the requirements for the degree



of

**UNIVERSITY of the
WESTERN CAPE**

Magister Scientiae in Chemistry

Faculty of Science

University of the Western Cape
Cape Town, South Africa

Supervisor: Prof Martin Onani

November 2015

University of the Western Cape

KEYWORDS

Diimines

Ruthenium(II)

Palladium(II)

Oxidative cleavage

Styrene

Catalysis

Heck reaction

Methyl acrylate

Iodobenze

TGA



ABSTRACT

Synthesis and characterization of pyridyl/quinolyl imine ruthenium(II) and palladium(II) complexes and their application in catalysis

L.D. Swartz

MSc dissertation, Department of Chemistry, University of the Western Cape

We report the successful syntheses of a family of tetradentate N-donor pyridyl and quinolyl-imine ligands N1,N2-bis((pyridin-2-yl)methylene)ethane-1,2-diamine (L1), N1,N3-bis(pyridin-2-ylmethylene)propane-1,3-diamine (L2), N1,N4-bis(pyridin-2-ylmethylene)butane-1,4-diamine (L3), N1,N2-bis((quinolin-2-yl)methylene)ethane-1,2-diamine (L4), N1,N3-bis(quinolin-2-ylmethylene)propane-1,3-diamine (L5) and N1,N5-bis(pyridin-2-ylmethylene)pentane-1,5-diamine (L6). All the ligands were fully characterized by FT-IR, ¹H and ¹³C NMR, GC-MS, Elemental analysis, UV-Vis and TGA. We report for the first time the thermogravimetric analysis of N1,N2-bis((pyridin-2-yl)methylene)ethane-1,2-diamine (L1) and N1,N2-bis((quinolin-2-yl)methylene)ethane-1,2-diamine (L4). The tetradentate N-donor pyridyl and quinolyl-imine ligands were subsequently utilised to synthesise neutral mononuclear and cationic homobimetallic ruthenium(II) complexes and new bimetallic palladium(II) complexes using the appropriate metal precursors. The ruthenium(II) complexes were evaluated for the oxidative cleavage of styrene using a Sharpless biphasic solvent system (CCl₄:CH₃CN:H₂O) and sodium periodate (NaIO₄) as the cooxidant. The bimetallic palladium(II) complexes were evaluated for their catalytic activity towards the standard Heck coupling reaction. The ruthenium(II) catalysts exhibited efficient catalytic activity, yielding conversions of 69-77%. The palladium(II) catalysts showed an overall low catalytic activity of 41-49 % conversion and analysed by GC.

November 2015

DECLARATION

I declare that *Synthesis and Characterization of pyridyl/quinolyl imine ruthenium(II) and palladium(II) complexes in catalysis* is my own work, that it has not been submitted for any degree or examination in any other university, and that all the sources I have used or quoted have been indicated and acknowledged by complete references.



Leoni Destine Swartz

Year: November 2015

Signature.....

ACKNOWLEDGEMENTS

This dissertation was only possible by the grace of God; with you my Lord everything is possible. To my parents and aunt, I humbly thank you for all the support and sacrifices throughout the years. To my extended family and friends thank you for the encouragement and roles you have played in my life. To the love of my life, thank you for all the motivation; you kept me sane throughout this degree. I love you.

I want to express my gratitude to my supervisor Prof MO Onani for all the knowledge I accumulated while working under his guidance. The road was not always easy, but it was worth the while. I am grateful for your support. Thank you.

To my Organometallic and Nanomaterials research group I am thankful for your support and guidance; you became more than family. Special thanks to Leandre, I am grateful we could experience this journey together. To Asanda, thank you for all the wonderful advice and assistance your input helped in finishing this work; you were the only person who truly understood how tedious the work was. Thank you for being a mentor. Shane, Kip and Mdu thank you for not only your input and motivation but your friendship aswell.

To Mr Lesch, thank you for assisting me with GC-MS analysis and Dr Edith for assisting with NMR analysis. Thanks to the UWC Pharmacy department for assisting with thermogravimetric analyses.

Lastly I would like to thank the National Research Foundation (NRF) for awarding me a Masters Innovation Scholarship and EUROSA your financial support is greatly appreciated.

DEDICATION

This dissertation is dedicated to my siblings Virgil and Nicole. May this work reflect your ability to reach your goals and aim for the stars. Strive to be the best you can be. I Love you.



“Insanity: doing the same thing over and over again and expecting different results.”

Albert Einstein (1879-1955).

CONFERENCE CONTRIBUTIONS

Leoni Swartz, Martin Onani, and Ebbe Nordlander, Some nitrogen based ruthenium complexes for transfer hydrogenation reaction of ketones, CATSA annual conference, Arabella Hotel & Spa, Kleinmond, South Africa, 15-18 November 2015.



ABBREVIATIONS AND SYMBOLS

CCl ₄	Carbon tetrachloride
CDCl ₃ - <i>d</i>	Deuterated chloroform
CH ₃ CN	Acetonitrile
COD	1,5-cyclooctadiene
<i>d</i>	Doublet
DCM	Dichloromethane
DMSO	Dimethylsulfoxide
DMSO- <i>d</i> 6	Deuterated dimethylsulphoxide
EtOAc	Ethyl acetate
FT-IR	Fourier Transform Infra Red
GC-MS	Gas chromatography Mass spectrometry
H ₂ O	Water
H ₂ O ₂	Hydrogen peroxide
hr(s)	Hour(s)
Hz	Hertz
<i>J</i>	Coupling constant
KMnO ₄	Potassium permanganate
<i>m</i>	Multiplet
<i>m/z</i>	Mass to charge ratio
MeOH	Methanol
MHz	Megahertz
min	Minutes
ml	Millilitres
mmol	Millimole
MP	Melting point
NaBH ₄	Sodium borohydrite
NaBrO ₃	Sodium bromate

NaIO ₄	Sodium periodate iii
NMR	Nuclear Magnetic Resonance
O ₃	Ozone
ppm	Parts per million
q	Quintet
RT	Room temperature
s	Singlet
t	Triplet
THF	Tetrahydrofuran
TON	Turn over number
δ	Chemical shift



TABLE OF CONTENTS

Content	Page
Title Page	i
Keywords	ii
Abstract	iii
Declaration	iv
Acknowledgements	v
Dedication	vi
Conferences Contributions	vii
Abbreviations and Symbols	viii
Table of contents	x
List of figures	xvi
List of schemes	xix
List of tables	xxi



CHAPTER 1

Chapter overview	1
1.0 Introduction	1
1.1 Background	1
1.2 Problem Identification, approach, research aims and objectives	2

CHAPTER 2

Chapter overview	7
2.0 Literature review	7
2.1 Schiff base complexes	7

2.1.1	Introduction	6
2.1.2	Pyridyl-imine complexes	9
2.1.3	Quinolyl-imine complexes	12
2.2	Application of ruthenium and palladium complexes in homogenous catalysis	16
2.2.1	Ruthenium complexes in oxidation reactions	16
2.2.1.1	Introduction	16
2.2.1.2	Oxidative cleavage	17
2.2.2	Ruthenium complexes in reduction reactions	24
2.2.2.1	Introduction	24
2.2.2.2	Ruthenium-catalysed transfer hydrogenation	25
2.2.3	Palladium-catalyzed cross coupling reactions	33
2.2.3.1	Introduction	33
2.2.3.2	Heck reaction	33
2.3	Conclusion	36
CHAPTER 3		44
	Chapter overview	44
3.0	Experimental Section	44
3.1	General	44
3.2	Materials and Instrumentation	45
3.2.1	Chemicals	45
3.2.2	Instrumentation	45
3.3	Characterization techniques	46
3.3.1	Fourier transform infrared spectroscopy (FT-IR)	47
3.3.2	Nuclear Magnetic Resonance (^1H and ^{13}C NMR)	48
3.3.3	Ultraviolet-visible spectroscopy (UV-Vis)	49
3.3.4	Thermogravimetric analysis (TGA)	50
3.4	Synthesis of tetradentate pyridyl and quinolyl-imine ligands	51



3.4.1	N1,N2-bis((pyridin-2-yl)methylene)ethane-1,2-diamine, L1	51
3.4.2	N1,N3-bis(pyridin-2-ylmethylene)propane-1,3-diamine, L2	52
3.4.3	N1,N4-bis(pyridin-2-ylmethylene)butane-1,4-diamine, L3	53
3.4.4	N1,N2-bis((quinolin-2-yl)methylene)ethane-1,2-diamine, L4	53
3.4.5	N1,N3-bis(quinolin-2-ylmethylene)propane-1,3-diamine, L5	54
3.4.6	N1,N5-bis(pyridin-2-ylmethylene)pentane-1,5-diamine, L6	55
3.5	Synthesis of ruthenium(II) and palladium(II) precursors	55
3.5.1	Dichlorotetrakis(dimethylsulfoxide)ruthenium(II), RuCl ₂ (dms _o) ₄	55
3.5.2	Dichloro(<i>p</i> -cymene)ruthenium(II) dimer, [RuCl ₂ (<i>p</i> -cymene)] ₂	56
3.5.3	Dichloro(1,5-cyclooctadiene)palladium(II), Pd(COD)Cl ₂	56
3.6	Synthesis of neutral mononuclear and cationic homobimetallic pyridyl/quinolyl-imine ruthenium(II) complexes	56
3.6.1	dichloro-[N1,N2-bis((pyridin-2-yl)methylene)ethane-1,2-diamine]ruthenium (II), C1	56
3.6.2	dichloro-[(N1,N3-bis(pyridin-2-ylmethylene)propane-1,3-diamine]ruthenium (II), C2	57
3.6.3	dichloro-[N1,N4-bis(pyridin-2-ylmethylene)butane-1,4-diamine]ruthenium (II), C3	58
3.6.4	dichloro-[N1,N2-bis((quinolin-2-yl)methylene)ethane-1,2-diamine]ruthenium (II), C4	58
3.6.5	dichloro-[N1,N3-bis(quinolin-2-ylmethylene)propane-1,3- diamine]ruthenium(II), C5	59
3.6.6	Synthesis of cationic homobimetallic ruthenium(II) complex, C6	59
3.7	Synthesis of neutral bimetallic palladium(II) pyridyl-imine complexes	60
3.7.1	dichloro-[N1,N2-bis((pyridin-2-yl)methylene)ethane-1,2- diamine]palladium(II), C7	60
3.7.2	dichloro-[N1,N3-bis(pyridin-2-ylmethylene)propane-1,3- diamine]palladium(II), C8	61

3.7.3	dichloro-[N1,N4-bis(pyridin-2-ylmethylene)butane-1,4-diamine]palladium(II), C9	61
3.7.4	dichloro-[N1,N5-bis(pyridin-2-ylmethylene)pentane-1,5-diamine]palladium(II), C10	62
3.8	Procedure for the oxidative cleavage of styrene by pyridyl and quinolyl-imine ruthenium(II) complexes	62
3.9	Procedure for the Heck coupling reaction of iodobenzene with methylacrylate by bimetallic palladium(II) complexes	63
CHAPTER 4		66
	Chapter overview	66
4.0	Results and Discussion	66
4.1	Pyridyl and Quinolyl-imine ligands	66
4.1.1	Introduction	66
4.1.2	FT-IR spectroscopic analysis of pyridyl and quinolyl-imine ligands	68
4.1.3	¹ H NMR spectroscopic analysis of pyridyl and quinolyl-imine ligands	73
4.1.4	¹³ C NMR spectroscopic analysis of pyridyl and quinolyl-imine ligands	78
4.1.5	Mass spectroscopic analysis of pyridyl and quinolyl-imine ligands	82
4.1.6	Electronic absorption analysis of pyridyl and quinolyl-imine ligands	84
4.1.7	Thermogravimetric analysis of pyridyl and quinolyl-imine ligands	87
4.1.8	Analytical and physical studies of pyridyl and quinolyl-imine ligands	88
4.2	Ruthenium(II) and palladium(II) precursors	90
4.2.1	FT-IR spectroscopic studies of ruthenium(II) and palladium(II) precursors	90
4.2.2	¹ H NMR spectroscopic analysis of ruthenium(II) and palladium(II) precursors	91
4.3	Pyridyl/quinolyl-imine ruthenium(II) and bimetallic pyridyl-imine palladium(II) complexes	92

4.3.1	FT-IR spectroscopic analysis of pyridyl/quinolyl-imine ruthenium(II) complexes and bimetallic pyridyl-imine palladium(II) complexes	92
4.3.2	¹ H NMR and ¹³ C NMR spectroscopy analysis of pyridyl/quinolyl-imine ruthenium(II) complexes and bimetallic pyridyl-imine palladium(II) complexes	97
4.3.3	Electronic absorption analysis of pyridyl/quinolyl-imine ruthenium(II) complexes and bimetallic pyridyl-imine palladium(II) complexes	107
4.3.4	Analytical and physical studies of pyridyl/quinolyl-imine ruthenium(II) and bimetallic pyridyl-imine palladium(II) complexes	112
CHAPTER 5		118
	Chapter overview	118
5.0	Catalytic application of pyridyl and quinolyl-imine palladium and ruthenium(II) complexes	118
5.1	Ruthenium-catalyzed oxidative cleavage reactions	118
5.1.1	Introduction	118
5.1.2	Oxidative cleavage of styrene	119
	5.1.2.1 FT-IR analysis of the oxidative cleavage product	124
	5.1.2.2 ¹ H NMR analysis of the oxidative cleavage product	125
5.2	Palladium-catalyzed Heck coupling reactions	126
5.2.2	Arylation of methyl acrylate with Iodobenzene	126
	5.2.2.1 FT-IR analysis of the Heck coupling products	134
	5.2.2.2 ¹ H NMR analysis of the Heck coupling products	135
5.3	Conclusions	136
CHAPTER 6		139
	Chapter overview	139
6.0	Conclusion and Recommendations	139

6.1	General conclusion	139
6.2	Recommendations and future work	141
6.3	Appendix	142



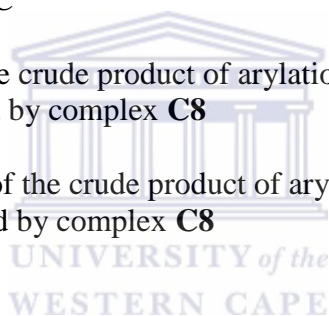
LIST OF FIGURES

Chapter 2	Page
Figure 2.1: (a) General structure of carbon-nitrogen double bond, C=N; (b) Example Of Diimine ligands (I-II)	9
Figure 2.2: Structural variability in manganese(II) complexes of N,N'-bis(2-pyridinylmethylene) ethane (and propane) diamine ligands	11
Figure 2.3: (a) hemi-labile imino-pyridyl Pd(II) complexes; (b) thiophene linked imino-pyridyl Pd(II) complexes	12
Figure 2.4: Examples of some quinoline derivative ligands	13
Figure 2.5: Synthesis of the dinuclear Zn(II) dichloride complexes of symmetric Schiff-base with extended quinoline side arms	15
Figure 2.6: Cabtree and Wilkinsons catalyst	28
Figure 2.7: Examples of transfer hydrogenation polydentate ligands for Ru Catalysts	29
Figure 2.8: (a): BINAP-phosphine based chiral ligands; (b) Ru(CH ₃ COO) ₂ ((R)-binap); (c): RuCl ₂ ((S)-binap)((S)-daipen)	30
Figure 2.9: [RuCl(η ⁶ -Arene)(N-arylsulfonyl-DPEN)]	30
Figure 2.10: Chiral P,N,N,P Ru complexes	31
Figure 2.11: Ru(II) chiral bidentate P, N-containing ligands	31
Figure 2.12: Ruthenium(III) containing (pyridyl)benzazole catalyst	32
Figure 2.13: (η ⁶ -C ₆ H ₆)RuCl ₂ [μ-(PPh ₂ CH ₂ N) ₂ CH ₂ (C ₁₀ H ₆)]RuCl ₂ (η ⁶ -C ₆ H ₆) (1) and RuCl ₂ (PPh ₃)[(PPh ₂ CH ₂ N) ₂ CH ₂ (C ₁₀ H ₆) (2) in the TH of ketones	33
Figure 2.14: Pd(NN') complexes	34
Figure 2.15: Dicarboxamide/dipyridyl palladium complexes	35
Chapter 4	
Figure 4.1: FT-IR of N1,N4-bis(pyridin-2-ylmethylene)butane-1,4-diamine, L3	68
Figure 4.2: FT-IR of N1,N2-bis((quinolin-2-yl)methylene)ethane-1,2-diamine, L4	69

Figure 4.3: ^1H NMR of N1,N4-bis(pyridin-2-ylmethylene)butane-1,4-diamine, L3	73
Figure 4.4: ^1H NMR of N1,N2-bis((quinolin-2-yl)methylene)ethane-1,2-diamine, L4	74
Figure 4.5: ^{13}C NMR of N1,N4-bis(pyridin-2-ylmethylene)butane-1,4-diamine, L3	78
Figure 4.6: ^{13}C NMR of N1,N2-bis((quinolin-2-yl)methylene)ethane-1,2-diamine, L4	79
Figure 4.7: Spectra of N1,N5-bis(pyridin-2-ylmethylene)pentane-1,5-diamine, L6	82
Figure 4.8: UV/Vis of N1,N4-bis(pyridin-2-ylmethylene)butane-1,4-diamine, L3	85
Figure 4.9: UV/Vis of N1,N2-bis((quinolin-2-yl)methylene)ethane-1,2-diamine, L4	85
Figure 4.10: TGA of N1,N2-bis((pyridin-2-yl)methylene)ethane-1,2-diamine, L1	87
Figure 4.11: TGA of (N1,N2-bis((quinolin-2-yl)methylene)ethane-1,2-diamine, L4	87
Figure 4.12: ^1H NMR of Dichloro(<i>p</i> -cymene)ruthenium(II) dimer, $[\text{RuCl}_2(\textit{p}\text{-cymene})]_2$	91
Figure 4.13: FT-IR for dichloro-N1,N2-bis((pyridin-2-yl)methylene)ethane-1,2-diamine-ruthenium(II), C1	93
Figure 4.14: FT-IR for dichloro-N1,N2-bis((quinolin-2-yl)methylene)ethane-1,2-diamine-ruthenium(II), C4	93
Figure 4.15: FT-IR for dichloro-N1,N2-bis((pyridin-2-yl)methylene)ethane-1,2-diamine palladium(II), C7	94
Figure 4.16: ^1H NMR for dichloro-N1,N2-bis((pyridin-2-yl)methylene) ethane-1,2-diamine-ruthenium(II), C1	98
Figure 4.17: ^1H NMR for dichloro-N1,N2-bis((quinolin-2-yl)methylene)ethane-1,2-diamine-ruthenium(II), C4	98
Figure 4.18: ^1H NMR for dichloro-[N1,N5-bis(pyridin-2-ylmethylene)pentane-1,5-diamine]palladium(II), C10	99
Figure 4.19: UV/vis of N1,N3-bis(pyridin-2-ylmethylene)propane-1,3-diamine-RuCl ₂ , C2	108
Figure 4.20: UV/vis of cationic homobimetallic ruthenium(II) complex, C6	108
Figure 4.21: UV/vis of dichloro-[N1,N2-bis((pyridin-2-yl)methylene)ethane-1,2-diamine]palladium(II), C7	109

Chapter 5

- Figure 5.1:** Representation of neutral mononuclear and cationic homobimetallic (N,N) Ru(II) Catalysts 122
- Figure 5.2:** FT-IR spectrum of the crude product of oxidation of styrene, after 2 hrs Catalyzed by complex, **C6** 125
- Figure 5.3:** ^1H NMR spectrum of the crude product of oxidation of styrene, after 2 hrs catalyzed by complex, **C6** 126
- Figure 5.4:** Dendrimeric iminopyridyl-palladium complex, **C3** 129
- Figure 5.5:** Unconjugated di-imine Pd(II) complexes 130
- Figure 5.6:** Thiophene linked iminopyridyl Pd(II) complexes 130
- Figure 5.7:** Bimetallic pyridyl-imine Pd(II) catalysts 131
- Figure 5.8:** Conversion as a function of time for the arylation of methyl acrylate with iodobenzene at 110 °C 132
- Figure 5.9:** FT-IR spectrum of the crude product of arylation of methyl acrylate, after 24 hrs catalyzed by complex **C8** 134
- Figure 5.10:** ^1H NMR spectrum of the crude product of arylation of methyl acrylate, after 8hrs catalyzed by complex **C8** 135



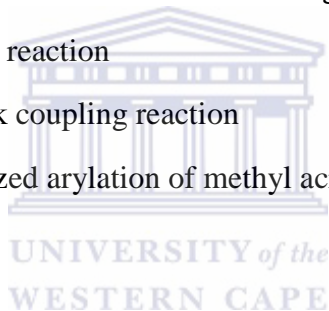
LIST OF SCHEMES

Chapter 2	Page
Scheme 2.1: Synthesis of ruthenium(II) complexes with 2,6-pyridyl-diimine ligands	12
Scheme 2.2: Palladium(II) mononuclear and palladium(II)/ ruthenium(II) heterodinuclear complexes	15
Scheme 2.3: Synthesis of a 2-quinolinecarboxylate-substituted ruthenium(II) complex	16
Scheme 2.4: The first catalytic oxidations by RuO ₄	18
Scheme 2.5: Addition of acetonitrile to the traditional CCl ₄ /H ₂ O solvent system	19
Scheme 2.6: Catalytic cycle for oxidative cleavage of alkenes to acids by <i>cis</i> -[RuCl ₂ (bpy) ₂].2H ₂ O/IO(OH) ₅	21
Scheme 2.7: Transformation of ethynyl alcohol (1a) (100 °C, toluene, 16 h) into alkene In an isolated yield of 33%	22
Scheme 2.8: Ru-catalyzed cleavage of carbon–carbon triple bonds of ethynyl alcohols	23
Scheme 2.9: Reduction of an aldehyde moiety by NaBH ₄	25
Scheme 2.10: Preparation of Wilkinson’s Catalyst	28
Scheme 2.11: Heck cross coupling reaction	34
Chapter 3	
Scheme 3.1: Diagram of FT-IR spectrometer	47
Scheme 3.2: Diagram of the NMR spectrometer	49
Scheme 3.3: Diagram of UV-Visible spectrometer	50
Scheme 3.4: Diagram of a TGA	51
Chapter 4	
Scheme 4.1: A synthetic pathway for pyridyl and quinolyl-imine ligands, L1-L6	67
Scheme 4.2: A schematic representation of synthesised diimine ligands, with numbering	72

Scheme 4.3: Plausible fragmentation pathway for pyridyl-imine ligands	84
Scheme 4.4: A synthetic pathway for precursor, Dichloro(<i>p</i> -cymene)ruthenium(II) dimer	91
Scheme 4.5: Examples of the synthetic pathway of neutral mononuclear pyridyl and quinolyl-imine Ru(II) and bimetallic pyridyl-imine Pd(II) complexes	104
Scheme 4.6: A synthetic pathway for the synthesis of complex, C6	113

Chapter 5

Scheme 5.1: Oxidative cleavage of alkenes using O ₃	119
Scheme 5.2: Catalytic cycle for oxidative cleavage of alkenes to acids by <i>cis</i> -[RuCl ₂ (bpy) ₂].2H ₂ O/IO(OH) ₅	120
Scheme 5.3: Epoxidation of styrene	121
Scheme 5.4: Schematic representation for oxidative cleavage of styrene	123
Scheme 5.5: Heck cross coupling reaction	127
Scheme 5.6: Mechanism for Heck coupling reaction	128
Scheme 5.7: Palladium(II) catalyzed arylation of methyl acrylate with iodobenzene	132



LIST OF TABLES

Chapter 4	Page
Table 4.1: FT-IR data for tetradentate pyridyl and quinolyl-imine ligands, L1-L6	69
Table 4.2: ^1H NMR spectral data of tetradentate pyridyl and quinolyl-imine ligands L1-L6 , recorded in CDCl_3 at 25°C	74
Table 4.3: ^{13}C NMR spectral data of tetradentate pyridyl and quinolyl-imine ligands L1-L6 , recorded in CDCl_3 at 25°C	79
Table 4.4: Summary of mass spectra data for pyridyl and quinolyl-imine ligands L1-L6 , recorded in DCM at room temperature	83
Table 4.5: Electronic absorption data of pyridyl and quinolyl-imine ligands L1-L6 , recorded, in DCM at room temperature	85
Table 4.6: Analytical and Physical Data of the Compounds, L1-L6	89
Table 4.7: FT-IR data of pyridyl/quinolyl-imine ruthenium(II) and bimetallic pyridyl-imine palladium(II) complexes	94
Table 4.8: ^1H NMR spectral data of N-donor ruthenium(II) (C1-C6) ^a and palladium(II) (C7-C10) ^b Schiff base complexes, recorded at 25°C	99
Table 4.9: ^{13}C NMR spectral data of N-donor ruthenium(II) complexes, recorded in CDCl_3 at 25°C	105
Table 4.10: Electronic absorption data of pyridyl and quinolyimine ruthenium(II) complexes	109
Table 4.11: Analytical and Physical Data of pyridyl/quinolyl-imine ruthenium(II) and Pyridyl-imine palladium(II) complexes	113
Chapter 5	
Table 5.1: Oxidative cleavage of styrene by ruthenium catalysts (C2, C4 and C6)	124
Table 5.2: Conversions of iodobenzene during arylation with methyl acrylate	133

CHAPTER 1

1.0 Introduction

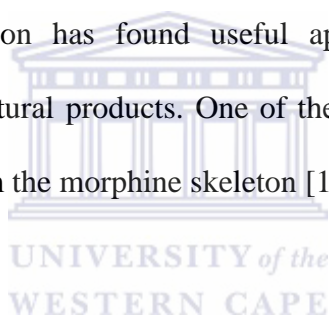
Chapter overview

This chapter gives a brief overview on the background of catalytic reactions, concentrating specifically on the oxidative cleavage and Heck coupling reactions. This chapter also includes the problem identification, research aims, objectives and approach.

1.1 Background

Catalytic reactions are an important topic in the field of organometallic chemistry, one of the many catalytic reactions includes oxidative cleavage and Heck coupling. Some transition metals have been investigated for their activities in olefin oxidation; as part of their participation in catalysis from reported literature, ruthenium holds a prominent position in the oxidation chemistry [1]. Oxidation reactions include the transformation of alcohols or olefins to their corresponding carbonyl compounds and carboxylic acids, transformation of sulfides to sulfoxides and the oxidation of olefins to epoxides. These type of reactions can follow many reaction pathways such as free-radical autoxidation, oxidative cleavage of the double bond, epoxidation, dihydroxylation, and Wacker-type oxidations. The ruthenium-catalyzed oxidative cleavage of olefins can be carried out employing a catalytic amount of RuCl_3 or RuO_2 with a variety of biphasic solvent systems such as $\text{CCl}_4/\text{CH}_3\text{CN}/\text{H}_2\text{O}$ [2], $\text{AcOEt}/\text{water}$ [3] and $\text{AcOEt}/\text{Me}_2\text{CO}/\text{water}$ [4], and co-oxidants; periodate [5], periodic acid [6], or hypochlorite [7]. The oxidation of organic compounds with high selectivity is of extreme importance in synthetic chemistry.

The Palladium-catalyzed cross-coupling is the formation of new carbon-carbon or C-Heteroatom bonds. Some of these reactions includes Negishi, Stille, Kumada, Hiyama, Sonogashira, Suzuki and Heck reactions. The Pd-catalyzed cross-coupling reaction was first discovered and developed by Prof. Richard Heck along with Akira Suzuki, and Ei-ichi Negishi, for which they shared a noble prize in chemistry in 2010 [8]. The Heck cross coupling reaction involves the organic transformation of the aryl halides and various substituted olefins in the presence of a base to form organic olefinic compounds [9]. Throughout the years, efficient catalytically active palladium complexes with a variety of ligands especially anchored to phosphine containing ligands have been developed. Most recently nitrogen containing ligands have become the more preferred ligands in this type of reaction [10]. The Heck reaction has found useful application in the fine chemical, pharmaceutical industries and natural products. One of the natural products transformations involves obtaining morphine from the morphine skeleton [11].



This study focused on the synthesis of N-donor tetradentate neutral mononuclear and cationic homobinuclear ruthenium(II) and bimetallic palladium(II) catalysts for the oxidative cleavage of styrene and the Heck coupling reaction of methyl acrylate.

1.2 Problem Identification, approach, research aims and objectives

Shoair *et al.* reported the unsuccessful oxidative cleavage of olefins to their corresponding carboxylic acids by the catalyst system $\text{cis-}[\text{RuCl}_2(\text{bpy})_2]\cdot 2\text{H}_2\text{O}$ in the presence of $\text{IO}(\text{OH})_5$ [12]. In Heck coupling reactions the ligand choice is one of the most important parameter.

In general, phosphines and its derivatives is the ligand of choice, due to the ligands being good stabilizers of the palladium in its zero oxidation state and accelerating the oxidative addition of the catalyst to the substrate by increasing electron density around the metal centre [13-14]. However, the phosphine ligands were reported to be prone to oxidation and air/moisture sensitive.

Therefore this MSc project aims at preparing N-donor tetradentate neutral mononuclear and cationic homobimetallic ruthenium(II) catalysts which will be subsequently tested for the oxidative cleavage of styrene to its carboxylic acid analogue in a sharpless biphasic solvent system containing the solvent acetonitrile in the presence of a co-oxidant, since it has been reported that CH₃CN aids in the formation of carboxylic acids. We also sought to overcome the drawbacks encountered with previous invented systems which include low overall conversion by employing these bulky catalyst systems. The MSc project also aims at the synthesis of N-donor tetradentate bimetallic palladium (II) catalysts for the Heck coupling reaction, in order to overcome the drawbacks encountered with phosphine ligands. The use of nitrogen containing ligands has proven to be friendlier in terms of cost and stability and can potentially replace phosphine ligands in Heck reactions [15-17].

Therefore, the research aims and objectives include:

- (i) Synthesis of N-donor tetradentate pyridyl and quinolyl-imine ligands.
- (ii) Synthesis of Ru(II) and Pd(II) precursors.
- (iii) Complexation of diimine ligands in (I) towards ruthenium(II) and palladium precursors(II) in (II) to form catalysts.

- (iv) Characterisation of all synthesized ligands and complexes by various spectroscopic techniques such as FT-IR, ^1H NMR, ^{13}C NMR, GC-MS, UV-Vis and elemental analysis.
- (v) Oxidative cleavage of styrene by the synthesized ruthenium(II) complexes
- (vi) Heck coupling reaction of methyl acrylate by bimetallic palladium(II) catalysts.

The summarized outline for the dissertation is depicted below:

Chapter 1 provides a general background on the oxidative cleavage and Heck coupling reactions.

Chapter 2 provides comprehensive literature found with respect to the synthesis, characterisation and application of pyridyl and quinolyl-imine complexes. Furthermore the applications of ruthenium and palladium complexes in homogenous catalysis are highlighted especially in the oxidative cleavage and the Heck coupling reactions.

Chapter 3 outlines the synthesis of tetradentate pyridyl and quinolyl-imine ligands, ruthenium(II) and palladium(II) precursors and their respective neutral mononuclear and cationic homobimetallic ruthenium(II) complexes as well as the neutral bimetallic palladium(II) complexes in preparation for the catalytic studies.

Chapter 4 discusses the results of the prepared tetradentate pyridyl and quinolyl-imine ligands, ruthenium(II) and palladium(II) precursors and their respective neutral mononuclear and cationic homobimetallic ruthenium(II) complexes as well as the neutral bimetallic palladium(II) complexes.

Chapter 5 finally presents the preliminary results obtained for the oxidation of alkenes by the ruthenium(II) complexes, and the Heck coupling reactions of methyl acrylate with iodobenzene catalysed by the palladium (II) complexes.

Chapter 6 lastly summarises the general conclusion and future prospects of the research.

References

1. Chakraborti AK, Ghatak UR, *J. Chem. Soc., Perkin. Trans.*, **1985**, *1*, 2605.
2. Carlsen PH, Katsuki T, Martin VS, Sharpless KB, *J. Org. Chem.*, **1981**, *46*, 3936.
3. Yoshifuji S, Arakawa Y, Nitta Y, *Chem. Pharm. Bull.*, **1985**, *33*, 5042.
4. Albarella L, Musumeci D, Sica D, *Eur. J. Org. Chem.*, **2001**, 99.
5. Mander LN, Williams CM, *Tetra.*, **2003**, *59*, 1105.
6. Nufiez MT, Martin VS, *Y. Org. Chem.*, **1990**, *55*, 1928.
7. Gore S, *Platinum Met. Rev.*, **1983**, *27*, 111.
8. Seechurn CC, Kitching MO, Colacot TJ, Snieckus V, *Angew. Chem. Int. Ed.*, **2012**, *51*, 5062.
9. Heck RF, *Acc. Chem. Res.*, **1979**, *12*, 146.
10. Patra GK, Goldberg I, *New J. Chem.*, **2003**, *27*, 1124.
11. Hong CY, Kado N, Overman LE, *J. Am. Chem. Soc.*, **1993**, *115*, 11028.
12. Shoair AG, Mohamed RH, *Synth. Comm.*, **2006**, *36*, 59.
13. Heck RF, Nolley JP, *J. Org. Chem.*, **1972**, *37*, 2320.
14. Heck RF, *Org. React.*, **1982**, *27*, 345.
15. Grasa GA, Singh R, Stevens ED, Nolan SP, *J. Organomet. Chem.*, **2003**, *687*, 269.
16. Mino T, Shirae Y, Sasai Y, Sakamoto M, Fujita T, *J. Organ. Chem.*, **2006**, *71*, 6834.
17. Buchmeiser MR, Wurst K, *J. Am. Chem. Soc.*, **1999**, *121*, 11101.

CHAPTER 2

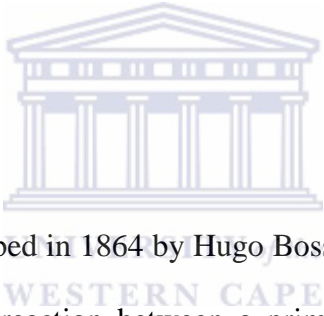
2.0 Literature review

Chapter overview

This chapter first introduces Schiff base ligands, thereafter it shifts the focus to the synthesis of diimine ligands and their transitional metal complexes found in literature. These compounds form a major part of this dissertation. Lastly, we report the catalytic activities of ruthenium(II) and palladium(II) catalysts found in literature. Particular references are made to oxidative cleavage, transfer hydrogenation and Heck coupling reactions since our complexes were applied in this type of reactions.

2.1 Schiff base complexes

2.1.1 Introduction



The Schiff bases were first described in 1864 by Hugo Boss and are a special class of ligands resulting from the condensation reaction between a primary amine and an aldehyde or a ketone in an organic medium [1]. The general formula of the resultant imines are $\text{RHC}=\text{N}-\text{R}'$ (figure 2.1 a), where R and R' are alkyl, aryl, cyclo alkyl or heterocyclic groups which may be variously substituted. These ligands are characterised by the azomethine group observed as a carbon-nitrogen double bond, $\text{C}=\text{N}$, and possess selective and active sites by allowing the fine tuning of the steric and electronic environment at the coordinated metal. Studies have shown that the azomethine group have a lone pair of electrons in either p or sp^2 hybridized orbital on the nitrogen, with considerable biological and catalytic importance and is involved in binding with the metal ions [2]. A lot of researchers have showed great interest in Schiff base complexes due to their ease of synthesis, high reactivity toward transitional metals, possible variation of donor atoms and wide applications [3].

Schiff base metal complexes are generally synthesised by the reaction of a Schiff base ligand and a transitional metal, the reactions are normally carried out in an organic solvent, at room temperature or refluxed under nitrogen conditions, using general schlenk line techniques. There exists numerous types of Schiff base ligands which have been greatly expanded beyond the scope of this study.

The diimine ligands are a family of Schiff bases, consisting of two or more nitrogen donor sites. There exist three well known types of di-imine ligands, which include α di-imine, β di-imines and γ di-imines. Brookhart and co-workers were the first to report on the novel cationic diimine Pd(II) and Ni(II) complexes [4a]. Following this discovery, recently Nyamoto *et al.* reported some imino-pyridine palladium (II) complexes as selective ethylene dimerization catalysts producing mainly butenes [4b]. The diimine complexes have also been used as catalyst precursors for many catalytic processes such as Heck and Suzuki coupling reactions [5a-6a]. Potier *et al.* reported novel Pd(II) complexes containing multifunctional cyclodextrin-based N,N-bidentate ligands for the Heck coupling reaction. These novel Pd(II) water soluble complexes, exhibited efficient catalytic activity for the Heck reaction of aryl iodides in an aqueous medium [5b].

While a series of water-soluble α diimine Pd(II) complexes was reported by Zhou *et al.* for the Suzuki reaction to efficiently catalysed arylbromide and arylboronic acid [6b]. The pyridyl and quinolyl-imine ligands are typical examples of α di-imine ligands. Their complexes are easily synthesized by reacting the imine ligands and a metal ion, thereby forming stable complexes with different metals in various oxidation states [7-8]. A series of stable novel α di-imine palladium (II) complexes was reported by Sunjuk *et al.* [8b].

The palladium (II) complexes were synthesized by reacting the precursor $\text{Pd}(\text{NCPH})_2\text{Cl}_2$ with their corresponding α di-imine ligands in acetone at room temperature. The successful syntheses of the complexes were confirmed by their azomethine fragment using FT-IR and ^1H NMR. The pyridyl and quinolyl-imine complexes are of great interest to us, since it formed a major part of the success of the study. Below are a few examples of diimine ligands (figure 2.1b).

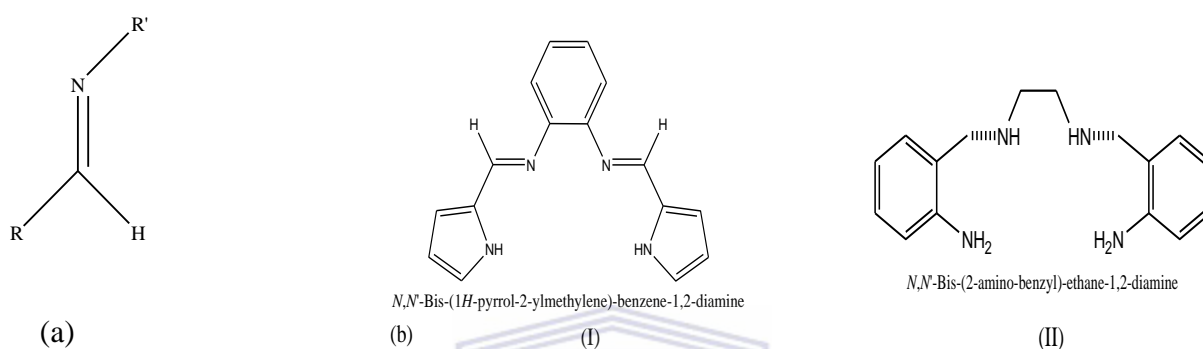
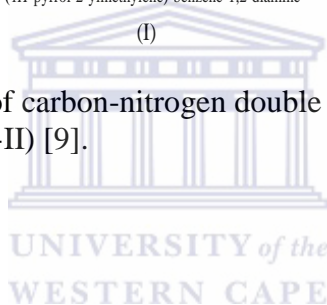


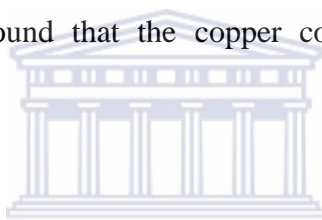
Figure 2.1: (a) General structure of carbon-nitrogen double bond, $\text{C}=\text{N}$; (b) Example of Diimine ligands (I-II) [9].



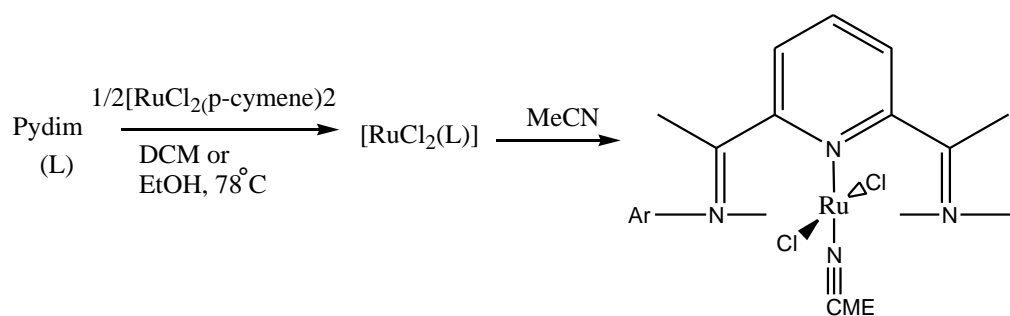
2.1.2 Pyridyl-imine complexes

Pyridyl-imine complexes consist of pyridyl-imine ligands and metal ions. The pyridyl-imine ligands and their corresponding metal complexes are characterized by the $\text{C}=\text{N}$ moiety, upon coordination the $\text{C}=\text{N}$ moiety is reported to shift either upfield or downfield in comparison to the free ligand [10]. Pyridyl-imine ligands can be readily prepared by the Schiff base condensation reaction of pyridinecarboxaldehyde and its derivatives with corresponding amine in an alcoholic medium and using an anhydrous magnesium sulphate to remove the water formed during the reaction. Their complexes can be easily prepared by reflux or at room temperature by reacting pyridyl-imine ligands with most metal ions in a suitable organic solvent.

Ebraldidze *et al.* investigated the structural variability in manganese (II) complexes containing N,N-bis(2-pyridinylmethylene)ethane and propane diamine ligands (figure 2.2a) [11]. The manganese (II) complexes were prepared by reacting the pyridyl-imine ligands with manganese perchlorate hexahydrate in ethanol to yield the novel manganese complexes. Solid-state magnetic susceptibility measurements as well as the DFT calculations confirm that each of the manganese centers is high-spin where $S = 5/2$. The X-ray analysis of the complex $Mn_2L^1_3 (ClO_4)_4$ confirmed the dinuclear nature and the complex has a distorted trigonal-bipyramidal geometry while complex $MnL_2(H_2O)_2(ClO_4)_2$ has an octahedral geometry. Pandiyan *et al.* and co-workers reported a similar procedure for the synthesis of their pyridyl-imine copper (II) complexes, and subsequently a DFT and experimental studies was carried out [12]. It was found that the copper complex of L1 has *cis* and *trans* geometrical isomers.



Simple pyridyl-imine complexes can be tailored, by fine tuning their steric and electronic environment. The diimine ligands bearing 2,2'-bipyridine (bipy) ligands led to the design of numerous active Schiff base ligands. The coordination of bipy ligands is of a bridging type, they form stable complexes due to the $d\pi-p\pi^*$ back bonding of the metal to the pyridine ring and the chelating effect [13]. Choudhury and co-workers studied and reported new tris-chelate ruthenium(II) complexes diimine ligands bearing 2,2'-bipyridine ligands [13]. The complexes with the general formula $[RuLn (bipy)_{3-n}] [ClO_4]_2 \cdot H_2O$ [$L =$ aryl (2-pyridylmethylene) amine, $n = 0-3$] was synthesized by reacting $cis-[RuCl_2L^2_2]$ with $[Ag(bipy)_2][ClO_4]$ in ethanol and refluxed for 2 hours. The FTIR of these complexes displayed a stretch at 1620 cm^{-1} and $1100-1095\text{ cm}^{-1}$ and 620 cm^{-1} which were attributed to the C=N moiety and ClO_4 respectively. The complexes also display a metal-to-ligand charge transfer (MLCT) transitions in the visible range at 475nm.



Scheme 2.1: Synthesis of ruthenium(II) complexes with 2,6-pyridyl-diimine ligands [14].

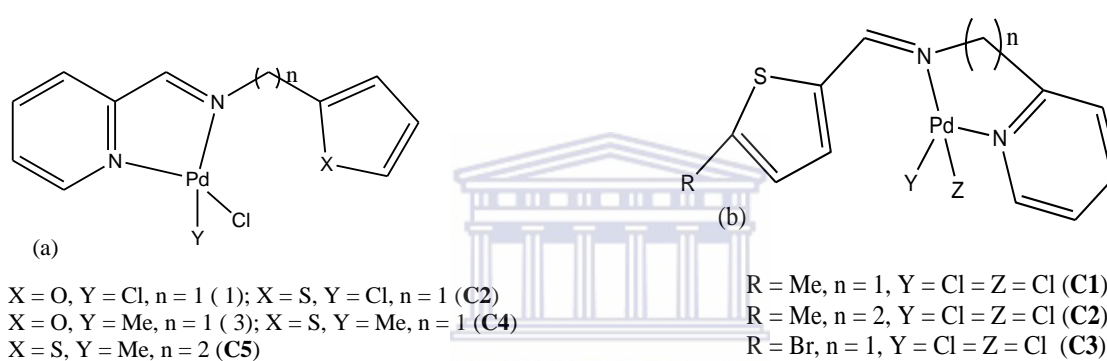


Figure 2.3: (a) hemi-labile imino-pyridyl Pd(II) complexes [16]; (b) thiophene linked iminopyridyl Pd(II) complexes [17].

2.1.3 Quinolyl-imine complexes

Similar to pyridyl-imine ligands above, the quinolyl-imine ligands can be prepared by the Schiff base condensation reaction of a quinolinecarboxaldehyde derivative with amine, in an alcoholic medium and using anhydrous magnesium sulphate to remove the water formed during the reaction. Examples of some quinoline ligands are given below (figure 2.4).

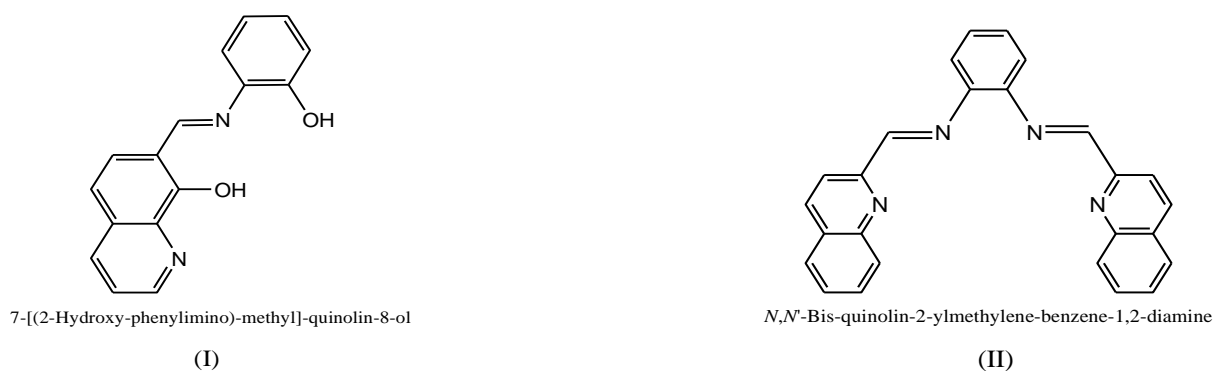


Figure 2.4: Examples of some quinoline derivative ligands.

Patra *et al.* reported the synthesis and characterisation of novel quinolyl-imine Ag (I) complexes; the complexes were synthesized by the reaction of quinolyl-imine ligands and AgClO_4 in acetonitrile while stirring at room temperature for 30 min [18]. The X-ray diffraction and a number of spectroscopic measurements of the Ag (I) complexes revealed that they form a pseudo-tetrahedral geometry around the metal centre. Prema *et al.* reported the synthesis of four enantiomerically-pure bis(imine-quinoline) zinc complexes (figure 2.5). The complexes was synthesized by refluxing or stirring the precursor, anhydrous zinc(II)chloride, at room temperature with their respective bis(imine-quinoline) ligands in a suitable solvent (ethanol, methylene chloride, or toluene). They found that the bimetallic zinc complexes have helical structures in the solid state, and prefer the M helical form [19]. Two types of monodentate Pd(II) complexes and a palladium(II)/ruthenium(II) heterodinuclear complex (3), bearing 2-quinolyl-substituted (pyridine-2-carbonyl)hydrazine ligands was reported by Mori *et al.* (Scheme 2.2) [20]. The first type of monodentate Pd(II) complex was a dichlorido complex (2), in which the zwitterionic HL' is coordinated through the pyridine-N and hydrazonato-N to act as a bidentate ligand. The other monodentate Pd (II) complex is where the anionic hydrazonate (L^-) is ligating through pyridine-N, hydrazonato-N and quinoline-N to act as a tridentate ligand (1) (Scheme 2.2).

Others reported the synthesis and applications of quinoline ligands and their complexes as follows, Shiraishi *et al.* reported a quinoline–polyamine ligand bearing two end quinoline fragments for the quantitative detection of Zn (II) in water at pH 5–12 [21]. The ligand was synthesized by the condensation reaction of diethylenetriamine and 2-quinolinecarboxaldehyde followed by reduction with NaBH₄. The ligands were reported to exhibit both linear and stoichiometrical responses to Zn (II) at pH 5-12. Funaki *et al.* reported a 2-quinolinecarboxylate-substituted ruthenium(II) complex as a new type of sensitizer for dye-sensitized solar cells [22]. The synthesis of the 2-quinolinecarboxylate-substituted ruthenium(II) complex occurred in two steps. First a 2-quinolinecarboxylate-substituted ruthenium(II) precursor (**1**) was synthesized by the reaction of 2-quinolinecarboxylic acid, LiCl, and triethylamine with the precursor Ru(4,4',4''-trimethoxycarbonyl-2,2':6',2''-terpyridine)Cl₃ in EtOH. The desired quinolinecarboxylate-substituted ruthenium(II) complex was then achieved by the hydrolysis of the ester groups of the terpyridine ligand and the coordination of the thiocyanato ligand (NCS) towards the ruthenium atom using the precursor Ru(4,4',4''-trimethoxycarbonyl-2,2':6',2''-terpyridine)(2-quinolinecarboxylato)Cl (scheme 2.3). The UV/Vis spectra of the complex revealed π - π^* transitions and were reported to be due to the coordinated ligands and the MLCT transition was observed at 518 nm. Leung *et al.* reported a synthetic method of several tris(8-quinolinolato)ruthenium(III)/(II) complexes, resulting in yields of up to 75 % [23a]. A series of 8-Quionolinolato ruthenium(III) complexes were synthesized by heating various 8-Quionolinolato derivatives with the starting material Ru(acac)₃ at 180 °C under argon for 24 hours. The syntheses of the various tris(8-quinolinolato)ruthenium(III) complexes, resulted in a higher yield of >75% compared to the previously reported yield which was 40% [23b]. The synthesized tris(8-quinolinolato)ruthenium(III) complexes, served as convenient precursors for the synthesis of a series of tris(8-quinolinolato)ruthenium(II) complexes.

The synthesis of the tris(8-quinolinolato)ruthenium(II) complexes containing π -acceptor ligands such as pyridine, alkene, dimethylsulfoxide and diazadiene was achieved by the reduction of RuQ_3 ($\text{Q} = 8\text{-quinolinolato}$) using Zn/Hg in the presence of the π -acceptor ligands in refluxing EtOH . The geometry of the complexes was cis or trans or trans, cis configurations.

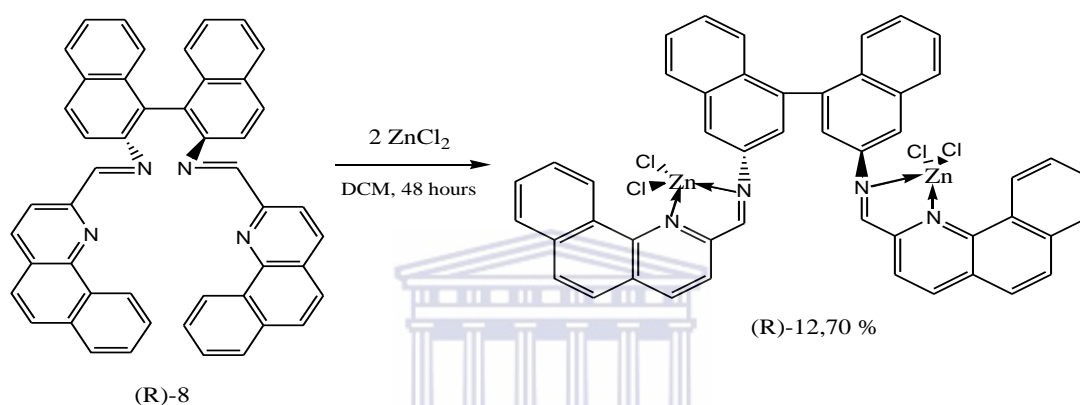
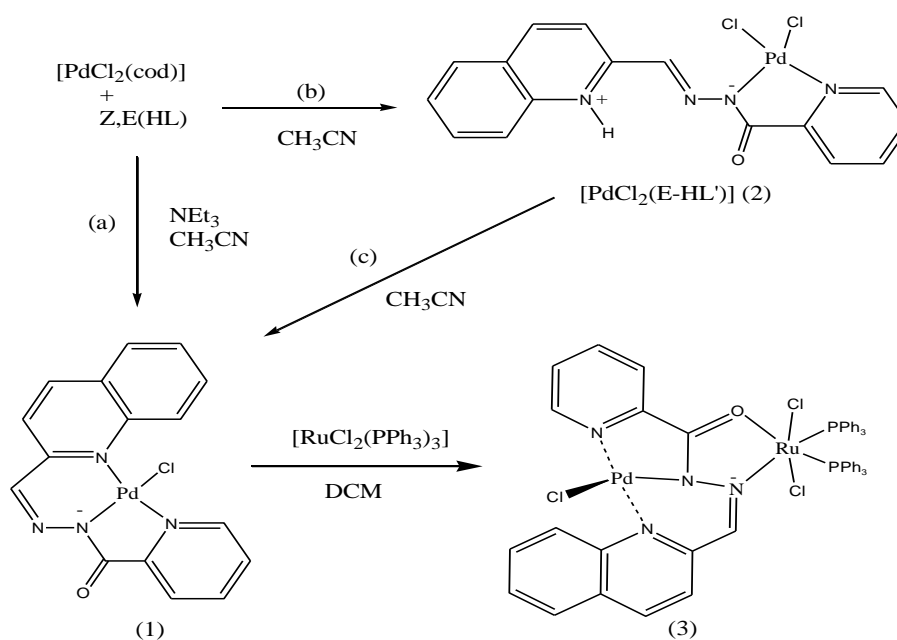
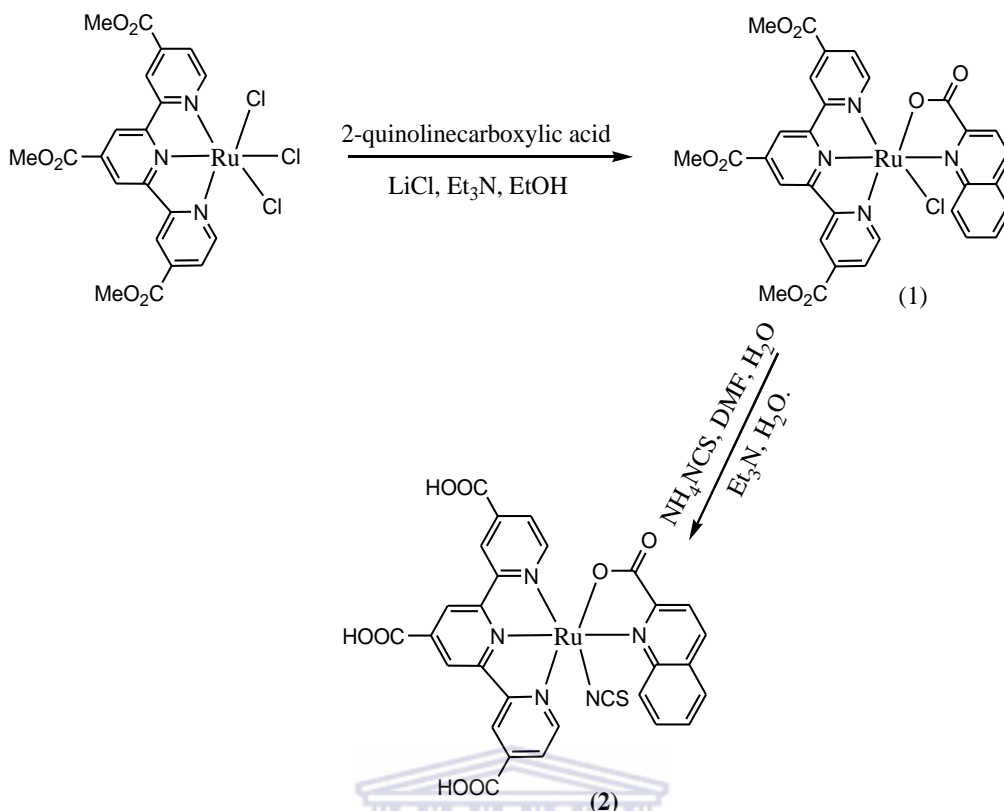


Figure 2.5: Synthesis of the dinuclear Zn(II) dichloride complexes of symmetric Schiff-base with extended quinoline side arms [19].



Scheme 2.2: Palladium(II) mononuclear and palladium (II)/ ruthenium(II) heterodinuclear complexes [20].



Scheme 2.3: Synthesis of a 2-quinolinecarboxylate-substituted ruthenium(II) complex [22].

2.2 Application of ruthenium and palladium complexes in homogenous catalysis

2.2.1 Ruthenium complexes in oxidation reactions

2.2.1.1 Introduction

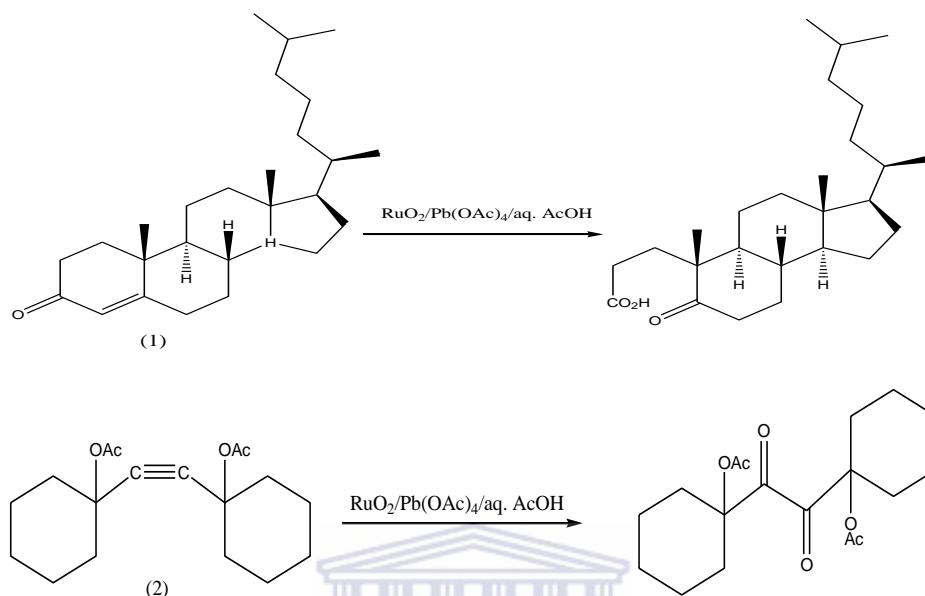
Ruthenium chemistry holds a prominent position in catalysis and is employed in a variety of catalytic reactions. This is due to the attractive properties which the metal possesses. Ruthenium has an electron configuration of $[\text{Kr}] 4d^7 5s^1$, therefore compared to other transitional metals ruthenium holds variable oxidation states from -2 in $\text{Ru}(\text{CO})_4$ to +8 in RuO_4 and each of these oxidation states has a preferred coordination geometry, such as trigonal-bipyramidal and octahedral for $\text{Ru}(0)$, (II) and (III) respectively making it one of the most explored metals [24]. Along with osmium they are the only elements which exhibit octavalency.

The element was first discovered in Kazan (capital of the Tatarstan Republic, Russian federation) by Karl Karlovich Klaus (1796-1864) in 1844 and was the last of the six platinum metals to be isolated [25]. Klaus was first to make RuO_4 , $\text{trans-K}_2[\text{Ru}(\text{OH})_2(\text{O})_3]$ as well as $\text{RuCl}_3/\text{RuCl}_3 \cdot x\text{H}_2\text{O}$. These materials serve as useful precursors for the synthesis of a variety of ruthenium complexes for various catalytic reactions. Some of the catalysis application includes reduction and oxidation reactions [26, 27], transfer hydrogenation [28] and carbon-carbon bond formation [29]. The metal is specially important player in the ruthenium oxidation chemistry. Below a more in depth account of oxidation reactions reported in literature are discussed.

2.2.1.2 Oxidative cleavage

The oxo complex of ruthenium, RuO_4 , was studied as an oxidant in this reaction by Djerassi and Engle in 1953 [30]. Till today it is still the major and most powerful oxidant for oxidative cleavage type reactions compared to its counterpart, OsO_4 . The peruthenate ion, $[\text{RuO}_4]^-$, is also more oxidising than $[\text{OsO}_4]^-$. This is due to the element being in the second row of the periodic table, therefore its outer electrons is more tightly bound than osmium and therefore generally acts as the more stronger oxidant. Since this material is a strong oxidant, but toxic, volatile and not easily handled, it is made *in situ* from standard starting materials such as hydrated ruthenium chloride ($\text{RuCl}_3 \cdot x\text{H}_2\text{O}$) and ruthenium(IV) oxide ($\text{RuO}_2 \cdot x\text{H}_2\text{O}$) with aqueous sodium periodate (NaIO_4) [31], potassium periodate $\text{K}(\text{IO}_4)$ [32] or periodic acid ($\text{IO}(\text{OH})_5$) [33] as co-oxidants. The first use of RuO_4 as a catalyst was by Pappo *et al.* in 1956 [34]. It was used *in situ* for the oxidation of cholest-4-en-3-one using a mixture of the catalyst precursor $\text{RuO}_2/\text{Pb}(\text{OAc})_4/\text{aq.AcOH}$ which was also used for the alkyne oxidation of 1,2-*bis*(1-acetoxycyclohexyl)ethyne which resulted in the formation of a diketone (scheme 2.4).

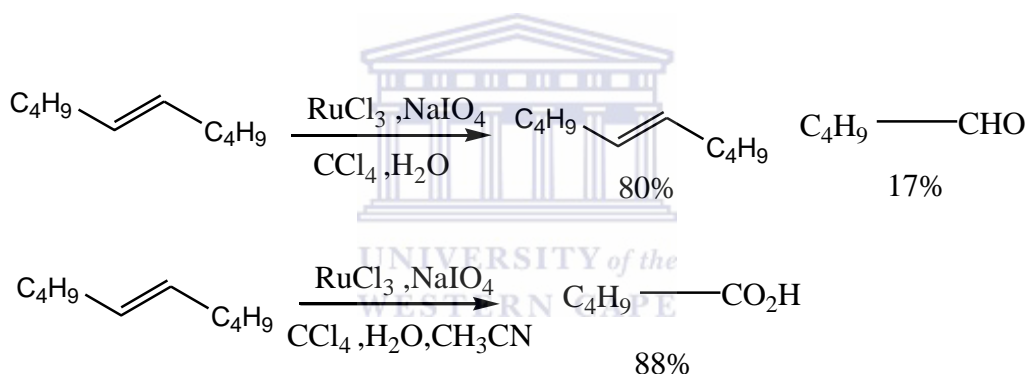
Its utility for a variety of oxidative transformations has been recognized immensely since the discovery of RuO_4 .



Scheme 2.4: The first catalytic oxidations by RuO_4 [34].

Later, Carlsen *et al.* reported an optimized system known as the sharpless system to the traditional $\text{CCl}_4\text{-H}_2\text{O-IO}_4$ system, which resulted in a sluggish and incomplete reaction [35]. The flaw in the system was reported due to the inactivation of ruthenium catalysts by carboxylic acids through the formation of low-valent ruthenium carboxylate complexes. The flawed system was improved by the addition of acetonitrile to disrupt the low-valent ruthenium carboxylate complexes (scheme 2.5). To test their modified system, Carlsen and co-workers synthesized a μ_3 -oxo-triruthenium carboxylate complex, $[(\text{Ru}_3\text{O}(\text{OAc})_6(\text{H}_2\text{O}_3)^+ \text{OAc})]$. The synthesized Ru(III)/Ru(II) mixed valence catalyst exhibited no catalytic activity for the oxidation of 1-octene in the $\text{CCl}_4\text{-H}_2\text{O-IO}_4$ biphasic system, however when CH_3CN was added, the oxidative cleavage of 1-octene resulted in the rapid formation of the pentanoic acid product.

The addition of acetonitrile to the traditional system was reported to disrupt the insoluble low-valent ruthenium-carboxylate complexes causing the reactivation of the catalytic cycle. The Sharpless system, $\text{CCl}_4\text{-CH}_3\text{CN-H}_2\text{O}$ is a biphasic solvent system and is employed in the presence of NaIO_4 as a co-oxidant and ruthenium trichloride (RuCl_3) as the metal for the *in situ* generation of the active RuO_4 species [35]. During their investigation Carlsen and Sharpless reported that the electron-rich olefins such as *cis* 5-decene, 1-decene and *cis*-cyclooctene, citronellyl acetate are converted into carboxylic acids with high yields (75-89%) (scheme 2.5). The oxidative cleavage of olefins results in the production of important intermediates for the pharmaceutical and agrochemical industry and this Sharpless system provides a framework for this type of reaction which has been widely explored.

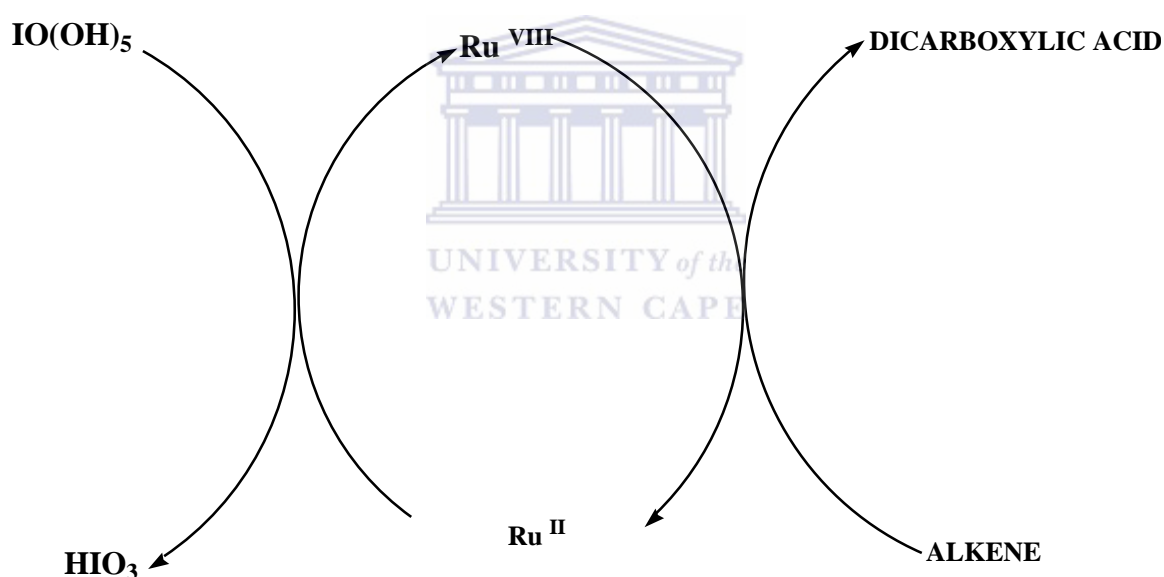


Scheme 2.5: Addition of acetonitrile to the traditional $\text{CCl}_4/\text{H}_2\text{O}$ solvent system

Griffith *et al.* reported an optimised procedure for the catalytic cleavage of alkynes and alkenes to carboxylic acids by ruthenium trichloride in the presence of the co-oxidant periodic acid, $\text{IO}(\text{OH})_5$ using the biphasic H_2O -cyclohexane- CH_3CN system by replacing CCl_4 [36]. The oxidative cleavage of alkyne substrates such as 1-hexyne and 1-heptyne resulted in yields of 60% for products pentanoic acid and hexanoic acid respectively. The substrates 1-decyne and phenylacetylene gave yields of 75% for products 1-nonanoic acid and benzoic acid respectively.

Other reports of oxidative systems are as follows; Giddings *et al.* reported the optimization of the system $\text{CCl}_4/\text{H}_2\text{O}$ for the oxidation of octan-2-ol with sodium bromate as the oxidizing agent in combination with $\text{RuO}_2 \cdot x\text{H}_2\text{O}$ and investigated factors that might influence the rate of the alcohol oxidation [37a]. The factors included choice of ruthenium starting material, pH variation of the aqueous phase, concentration of the oxidizing agent (NaBrO_3) and the degree of dispersion between the organic and aqueous phase. A test system was used to investigate whether the starting materials $\text{RuCl}_3 \cdot x\text{H}_2\text{O}$ or $\text{RuO}_2 \cdot x\text{H}_2\text{O}$ was a good material to use in their biphasic system for the efficient generation of the active species RuO_4 responsible for the initiation of the catalytic cycle. Upon the investigation it was found the starting material $\text{RuCl}_3 \cdot x\text{H}_2\text{O}$ undergoes hydrolysis and air oxidation forming $\text{RuO}_2 \cdot x\text{H}_2\text{O}$. The reaction mixture was also observed as orange instead of the usual yellow color. The NaBrO_3 concentration was investigated and was varied in 2-10 fold excess than the alcohol substrate, the results obtained from the $t_{0.25}$ values revealed only a slight variation over a fivefold increase in bromate concentration. From the results Giddings *et al.* concluded $\text{RuO}_2 \cdot x\text{H}_2\text{O}$ was an efficient ruthenium starting material, since $\text{RuO}_2 \cdot x\text{H}_2\text{O}$ was found to be stable and can be oxidized rapidly to the active RuO_4 species based on previous work [37b]. The optimum pH range for the alcohol oxidation to occur with no formation of Br_2 was reported at pH 5-8. Also when NaBrO_3 is in excess the rate of the alcohol oxidation was reported to be independent on the NaBrO_3 concentration. Daw *et al.* reported the selective oxidative cleavage of olefins to aldehydes using the abnormal-NHC–Ru(II) complex in an $\text{EtOAc}/\text{CH}_3\text{CN}/\text{H}_2\text{O}$ solvent mixture at room temperature. The catalytic oxidation of electron-rich styrene derivatives resulted in the quantitative conversions to their corresponding aldehydes, while electron-deficient styrenes gave lower yields of 92-94%. Daw *et al.* also reported the catalyst displayed superior activity for highly functionalized substrates derived from sugars and amino acids [38].

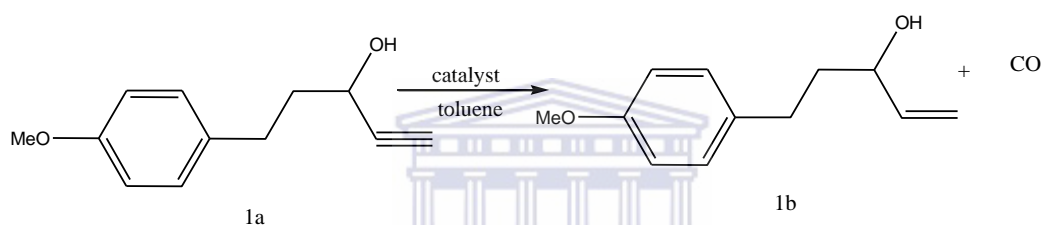
Busa *et al.* investigated the oxidative cleavage of 1-octene with the reaction was carried out in the biphasic solvent system $\text{CCl}_4\text{-CH}_3\text{CN-H}_2\text{O}$ (1:1:2 v/v), and was carried out in our lab. The catalytic systems were found to be active for the oxidative cleavage of 1-octene, resulting in moderate to good yields [15]. A mechanism for the oxidative cleavage of olefins was proposed by Shoair *et al.* using the catalyst system $\text{cis-}[\text{RuCl}_2(\text{bpy})_2]\cdot 2\text{H}_2\text{O}/\text{IO}(\text{OH})_5$ (Scheme 2.6) [39]. The mechanism proceed as follows, the formed RuO_4 cleaves the alkene to acid and subsequently converts into RuO_2 , and further oxidized to RuO_4 by excess $\text{IO}(\text{OH})_5$.



Scheme 2.6: Catalytic cycle for oxidative cleavage of alkenes to acids by *cis-}[\text{RuCl}_2(\text{bpy})_2]\cdot 2\text{H}_2\text{O}/\text{IO}(\text{OH})_5 [39].*

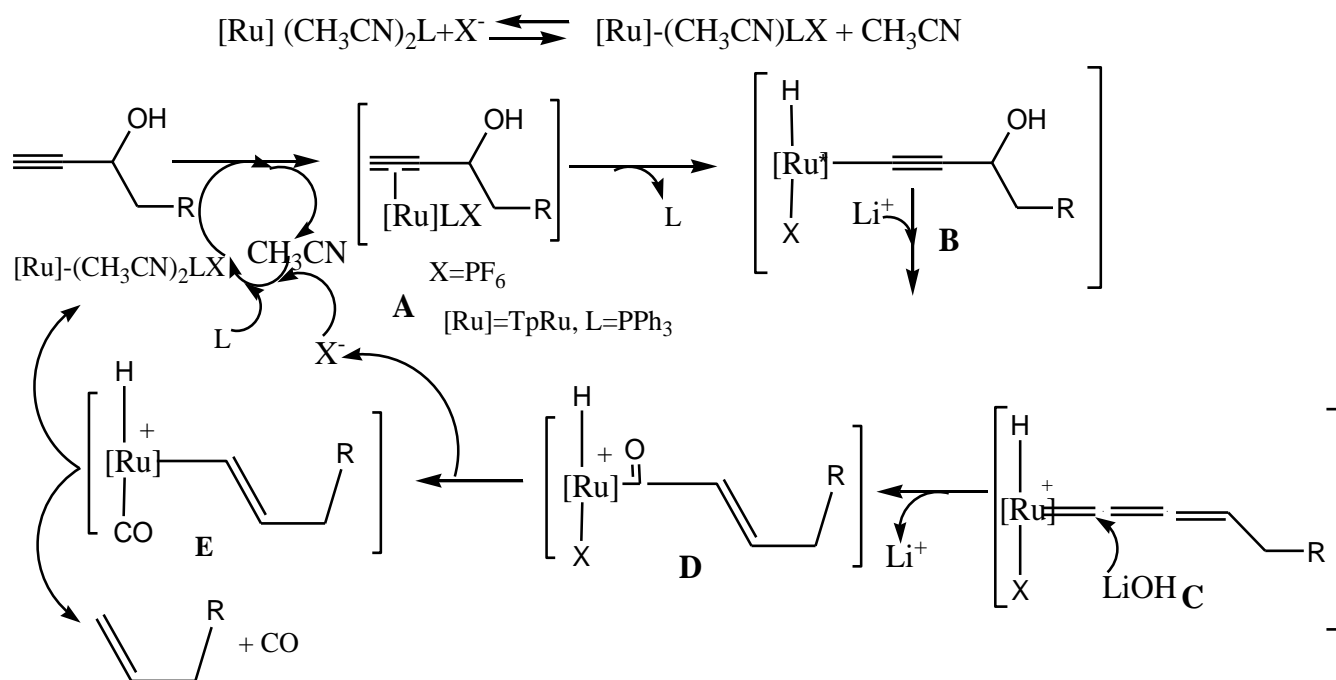
Other oxidative cleavage reactions include C-C triple bond cleavage. The catalytic oxidative cleavage of alkynes can be classified into three categories namely, alkyne metathesis [40], tandem reactions that involve the addition of an external organic compound to the alkyne moiety and the subsequent retro-Mannich and retro-Diels-Alder reactions [41] and reactions that do not require external organic promoters [42].

Only a few successful examples in literature on carbon-carbon triple bond oxidative cleavage via catalytic reactions exist [43a]. Oxidative cleavage of alkynes has been investigated by employing ruthenium, rhodium and palladium catalysts. The metal vinylidene species has been reported as the active species formed during the catalysed alkyne oxidation. Ruthenium readily forms the metal vinylidene species in the presence of alkyne [44]. Datta *et al.* reported the efficient catalytic cleavage of ethynyl alcohol into alkene and carbon monoxide by a ruthenium catalyst coordinated to tris(1-pyrazolyl)borate), triphenylphosphine and acetonitrile, $\text{TpRu}(\text{PPh}_3)(\text{CH}_3\text{CN})_2\text{PF}_6$ (scheme 2.7) [43a].



Scheme 2.7: Transformation of ethynyl alcohol (**1a**) (100 °C, toluene, 16 h) into alkene in an isolated yield of 33% [43a].

Herein Datta *et al.* details the transformation of ethynyl alcohols occurring in the absence of organic promoters via the generation of a metal vinylidene intermediate and the isotope mechanism involved (scheme 2.7). The yield of alkene and CO is further increased by employing the Lewis acid, LiOTf (20 mol %).



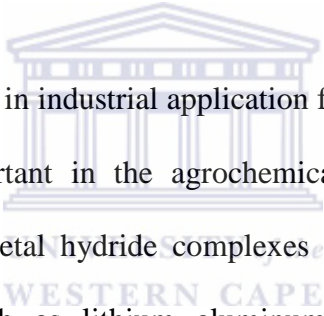
Scheme 2.8: Ru-catalyzed cleavage of carbon-carbon triple bonds of ethynyl alcohols [43a].

An isotope labelling experiment was done to elucidate the reaction mechanism (scheme 2.8). They suggested a mechanism (scheme 2.8) which forms a ruthenium η^1 -alkynyl-hydride species **B** via the proton migration of the initially formed ruthenium λ -alkyne complex **A** [45]. Species **B** undergoes ionisation via the elimination of the OH group in the presence of the Lewis acid co-catalyst, LiOTf, to form the ruthenium-allenylidene intermediate **C** [46]. Furthermore, the counter attack by the hydroxide ion at the electrophilic C_α of species **C** resulted in the formation of the ruthenium-acyl species **D** [47], which underwent de-insertion of carbon monoxide to induce the cleavage of the C-C bond derived from the alkyne moiety forming the vinylruthenium hydride species **E** [47]. As a continuation of this work, but in another study Shen *et al.* [43b] reported the efficient transformation of aryl and alkynyl propargyl ethers into aryl and alkynyl ketones via cleavage of a carbon-carbon triple bond using a ruthenium-catalyzed transformation. The Aryl and alkynyl propargyl ethers was treated with water using the same catalyst, TpRuPPh₃(CH₃CN)₂PF₆ synthesised in the previous study [43a].

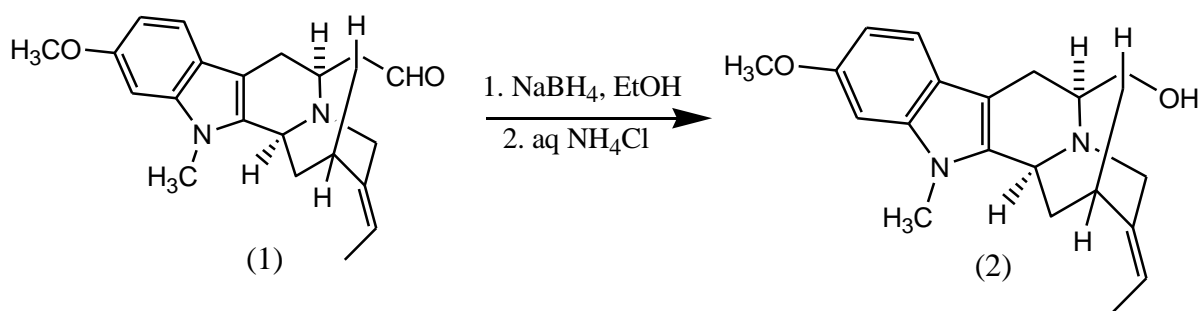
Shen group carried out the reaction in hot dichloroethane leading to the efficient removal of the propargyl ether group, resulting in the production of aryl and alkynyl ketones. In the study, the effect of the solvent and catalysts employed during the catalytic reaction was carried out. The group reported that 1,2-dichloroethane was the most efficient solvent in the introduction of the alkynyl ketone, with a yield of 83% except that the absence of water resulted in only 36% yield. While the use of other solvents which includes CH₃CN, DME, and benzene, EA, DMF and DCE was less effective only producing yields between 0-34% and showed recovery of ether, which was the starting material.

2.2.2 Ruthenium complexes in reduction reactions

2.2.2.1 Introduction



Reduction reactions are important in industrial application for the production of perfumes and fine chemicals which are important in the agrochemical and pharmaceuticals industry. Reduction reactions involving metal hydride complexes are easily achieved by using the common reducing reagents such as lithium aluminum hydride (LiAlH₄) and sodium borohydride (NaBH₄). The LiAlH₄ is a more powerful reducing reagent than NaBH₄ and can be used to reduce ketones, aldehydes, carboxylic acids, esters, amides, acid anhydrides and chlorides; similarly NaBH₄ were often used to reduce ketones, aldehydes, or acid chlorides in the presence of other reducible functional groups making it a selective reagent [48]. Despite LiAlH₄ being a powerful reducing reagent, it has numerous disadvantages such as being explosive when in contact with even the slightest amount of moisture [49]. Sodium borohydride reduces aldehydes and ketones in the presence of other functional groups such as epoxides, esters, lactones, acids, nitriles or nitro groups [50]. Cook and co-workers reported the reduction of the aldehyde moiety (1) using NaBH₄ and achieved an alcohol product (2) in as much as 95% in yield (scheme 2.9).



Scheme 2.9: Reduction of an aldehyde moiety by NaBH_4 [50].

Consequently the past few years has seen the shift from the above mentioned reducing reagents to the ruthenium-catalysed hydrogenation reactions. The ruthenium-catalysed hydrogenation reaction serve as a simpler and easier method for the reduction of saturated compounds compared to the above mentioned, hazardous reducing reagents.

2.2.2.2 Ruthenium-catalysed transfer hydrogenation

There are two types of hydrogenation reactions namely direct hydrogenation and transfer hydrogenation. The reaction involves the organic transformation of carbonyls to saturated compounds. In comparison the former uses molecular hydrogen. The transfer hydrogenation using hydrogen donors are more advantageous, due the addition of hydrogen coming from a source other than gaseous hydrogen and can be considered as a more economical and environmental friendlier reaction. The former method requires the use of expensive gaseous hydrogen, the use of high pressures and hazardous reducing hydrides such as NaBH_4 and LiAlH_4 [51]. The metal-catalyzed transfer hydrogenation reactions can be used to reduce unsaturated compounds (unfunctionalized or functionalized olefins, ketones and aldehydes, other carbonyl compounds, imines, nitriles, and nitro compounds) to their corresponding saturated compounds by employing a hydrogen donor under appropriate conditions [52].

A transfer hydrogenation of commercial Meerwein-Ponndorff-Verley process uses stoichiometric amounts of $\text{Al}(\text{O}i\text{Pr})_3$ to produce acetone and the alkoxides of the alcohols desired from the reduction of ketones [53]. The widely used method for transfer hydrogenation reactions is performed in a round bottom flask/schlenk tube under an argon/nitrogen atmosphere, followed by analysis using GC/NMR [54-55]. Prakash *et al.* reported the transfer hydrogenation reaction of glycerol in a round bottom flask, and the final products were confirmed by ^1H NMR experiments [55].

The first catalytic hydrogenation found in the literature dates back to 1874, when von Wilde *et al.* studied the reduction of acetylene and ethylene in the presence of platinum black [56]. However, only in 1912 did this type of reaction become popular when Sabatier *et al.* developed the reaction between hydrogen and organic compounds to a universal reduction method for which he received a Nobel prize in 1912 [57]. The ruthenium complex $[\text{RuCl}_2(\text{PPh}_3)_3]$ was reported by Sasson and Blum much later in the 1970s to be active in the biphasic TH of acetophenone with isopropanol at high temperature [58-60]. Later, Chowdhury and Backväll reported an optimised procedure by employing a catalytic amount of NaOH, this resulted in the $[\text{RuCl}_2(\text{PPh}_3)_3]$ -promoted reaction being 103–104 times faster [61].

The hydrogen donor, catalyst loading and temperature parameters play an important role in the optimisation of the reaction conditions. Here the hydrogen donor is the source of hydrogen in a reaction which ranges from alcohols, hydrazines, cyclic olefins to formic acids and its salts [62-65]. The donors' "work" is to transfer hydrogen to the surface of the substrate. This function is activated by the metal complex as shown in equation 1 (eq 1).

The hydrogen donor influences the activity and selectivity of the reduction. In principle any compound can serve as a hydrogen donor as long as the oxidation potential is low enough for hydrogen to be transferred under mild reaction conditions [66]. Typically the secondary alcohol, 2-propanol is used for the reduction of ketones to alcohols due to favourable properties; high selectivity, inexpensive, a good solvent for majority substrates and can be easily disposed. Upon dehydrogenation 2-propanol converts to acetone which is environmentally friendly. The uses of hydrogen donors are advantageous due to their ease to handle, easily accessible and eco-friendly.



The appropriate solvents are important media for transfer hydrogenation reactions. They include NaOH and KOH among others. Numerous articles have reported how the type of solvent employed during transfer hydrogenation reactions influences the yield of the product [67]. It has been reported that the presence of the base facilitates the formation of a ruthenium alkoxide by abstracting a proton from the alcohol, followed by a β -elimination to provide a ruthenium hydride which is the active species in the reaction [68].

One of the earlier hydrogenation catalysts where gaseous hydrogen was employed is the Cabtree and Wilkinsons catalysts (figure 2.6); they have long been used to hydrogenate a variety of alkenes. The Rhodium (I) complex also known as Wilkinson's catalyst, $\text{RhCl}(\text{PPh}_3)_3$ (scheme 2.10), discovered by Geoffrey Wilkinson in 1964 was the first highly active homogenous hydrogenation catalyst [69a]. Equally R. Coffey discovered it approximately the same time while working for ICI (Imperial Chemical Industries) [69b].



Scheme 2.10: Preparation of Wilkinson's Catalyst



Figure 2.6: (a) Wilkinson and (b) Cabtree and catalysts.

Wilkinson's catalyst is used in the hydrogenation of olefins; the catalyst is compatible with a range of functional groups, because the reaction mechanism does not involve a hydride ion transfer. A shortfall of the catalyst is that the ethylene hydrogenation is not possible due to the formation of a strongly bonded ethylene complex.

Transfer hydrogenation reactions are a prominent subject and have been well investigated, the uses of Schiff base ligands in this type of reaction are well known. Numerous transfer hydrogenation catalyst has been designed and developed over the past decades which includes tridentate NNN,PNP, P₂N₂,NPN,NNP, PNO and tetradentate, NNNN, ligands [70-76] anchored to transitional metals (figure 2.7).

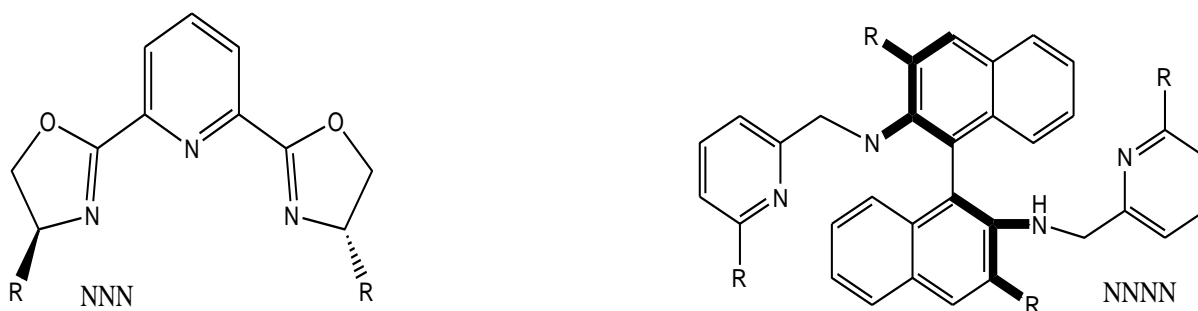


Figure 2.7: Examples of transfer hydrogenation polydentate ligands for Ru Catalysts [72a, 73b].

Great progress has been made on another hydrogenation process known as asymmetric hydrogenations (ATH); this reaction is an important producer of chiral compounds, which are important building blocks in the pharmaceuticals, agrochemicals, and fragrance industries [77]. Literature reports the successful asymmetric transfer hydrogenation of ketones with homogeneous ruthenium complexes especially bearing chiral phosphine ligands. Excellent results were achieved by Noyori *et al.* [78], Bäckvall *et al.* [79] and Xiao *et al.* [80]. Noyori, received a Nobel Prize in 2001 for his outstanding work on asymmetric hydrogenation which he shared with Knowles. Noyori introduced the BINAP-phosphine based chiral ligands in 1987 for which it was used in combination with ruthenium in ATH reactions (figure 2.8a) [78]. The complex $\text{Ru}(\text{CH}_3\text{COO})_2((\text{R})\text{-binap})$ (figure 2.8b) in the presence of HCl is used in the ATH of functionalized or chelatable ketones, the (S) enantiomer $\text{Ru}(\text{CH}_3\text{COO})_2((\text{S})\text{-binap})$ produced the pharmaceutical drug Naproxen(figure 2.8c) [81].

A second generation catalyst $\text{RuCl}_2(\text{binap}/\text{diamine})$ was designed by Noyori in 1995, below the compound $\text{RuCl}_2((\text{S})\text{-binap})((\text{S})\text{-daipen})$ represents the catalyst precursor (figure 2.8c) [82].

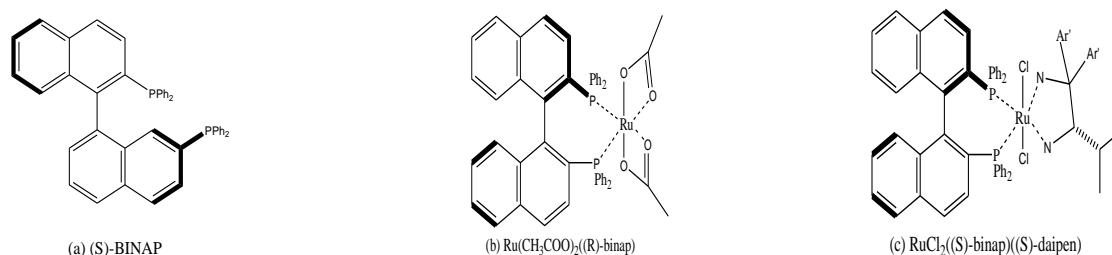


Figure 2.8: (a) BINAP-phosphine based chiral ligands [78]; (b) $\text{Ru}(\text{CH}_3\text{COO})_2((\text{R})\text{-binap})$ [81]; (c) $\text{RuCl}_2((\text{S})\text{-binap})((\text{S})\text{-daipen})$ [81].

The second generation catalyst is employed for the ATH reaction of unfunctionalized or non-chelatable simple ketones. Since its discovery Ru-BINAP catalysts and its derivatives has played a vital role in ATH reactions [83].

In earlier work done by Noyori and co-workers, the asymmetric transfer hydrogenation of aromatic ketones and imines employing a η^6 -arene ruthenium complex bearing a chiral N-arylsulfonyl diphenyl ethylenediamine (DPEN) ligand, and using 2-propanol or $\text{HCOOH-Et}_3\text{N}$ as hydrogen donor was also reported (figure 2.9) [84]. Since then a number of chiral ruthenium, rhodium and iridium systems bearing chiral diamine, amino alcohol, or amino acid derivative has been designed for the asymmetric transfer hydrogenation.

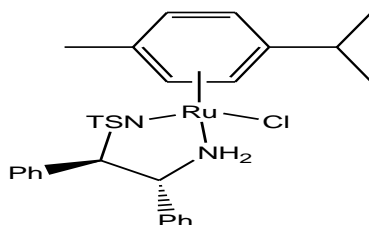


Figure 2.9: $[\text{RuCl}(\eta^6\text{-Arene})(\text{N})\text{-arylsulfonyl-DPEN}]$ [84].

Noyori and co-workers also designed significant ruthenium(II) complexes with chiral diamine/diphosphine ligand containing an o-phenylene linker for the asymmetric transfer hydrogenation of ketones [85 a]. The product was obtained in high yields for the diamine ruthenium complex with 97% ee at 45°C, compared to the diimine/diphosphine ruthenium (figure 2.10). The results indicated that the presence of the NH group on the complex had a superior effect on the reaction. Noyori and group could not account for the results since both complexes have similar geometrical parameters. They concluded the rate and stereoselectivity for the catalytic reaction was affected by the bulkiness and electronic properties of the ring substituent and also the alkyl group [85 a].



Figure 2.10: Chiral P,N,N,P Ru complexes [85].

Other significant transfer hydrogenation catalyst found in recent literature was reported by Li *et al.* which included a successful asymmetric transfer hydrogenation reaction of various ketones to chiral secondary alcohols with up to 99% conversion and up to 60% ee by a novel chiral bidentate P,N-ruthenium(II) complex (figure 2.11) [86].

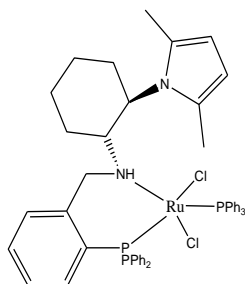


Figure 2.11: Ru(II) chiral bidentate P, N-containing ligands [86].

Ruthenium(III) bearing a (pyridyl)benzoazole ligand for the transfer hydrogenation of ketones was reported by Ogweno group, they found out that during their investigation the oxidation state of the metal centre, the nature of the ligand and the phosphine donor moiety control the activities of the complexes (figure 2.12) [87]. From the study the catalyst bearing ruthenium(II) metal coordinated to PPh₃ ligands showed more activity than the trichloride ruthenium(II) complexes. The mechanism was described as involving ruthenium (II) hydride species from the catalyst precursor.

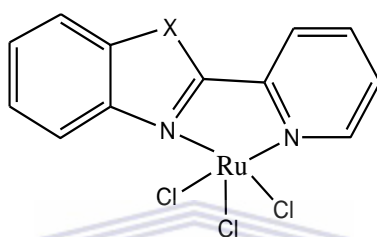


Figure 2.12: Ruthenium(III) containing (pyridyl)benzoazole catalyst [87].

As noted in numerous reported literatures the use of half-sandwich ruthenium complexes containing η^6 -*p*-cymene or η^6 -benzene unit also form superior catalysts for asymmetric transfer hydrogenation reactions. Fu *et al.* reported new ruthenium(II) phosphine complexes containing dihydroperimidine derived phosphine ligands, $(\eta^6\text{-C}_6\text{H}_6)\text{RuCl}_2[\mu\text{-}(\text{PPh}_2\text{CH}_2\text{N})_2\text{CH}_2(\text{C}_{10}\text{H}_6)]\text{RuCl}_2(\eta^6\text{-C}_6\text{H}_6)$ (1) and $\text{RuCl}_2(\text{PPh}_3)[(\text{PPh}_2\text{CH}_2\text{N})_2\text{CH}_2(\text{C}_{10}\text{H}_6)]$ (2) (Figure 2.13) [88]. Complex 1 (figure 2.13) exhibited efficient activity for the transformation of ketones to alcohols in good yields and at mild reaction conditions. Whereas the ruthenium phosphine complex (2) (figure 2.13) showed a lower initial activity however, the final conversions of both complexes were almost the same [88]. It was reported complex 1 had almost no catalytic activity after 2 hours, while complex (2) still showed high catalytic activity. Complex (1) achieved a 98 % conversion for *o*-chloroacetophenone within 0.5 h.



Figure 2.13: $(\eta^6\text{-C}_6\text{H}_6)\text{RuCl}_2[\mu\text{-(PPh}_2\text{CH}_2\text{N)}_2\text{CH}_2(\text{C}_{10}\text{H}_6)]\text{RuCl}_2(\eta^6\text{-C}_6\text{H}_6)$ (1) and $\text{RuCl}_2(\text{PPh}_3)[(\text{PPh}_2\text{CH}_2\text{N)}_2\text{CH}_2(\text{C}_{10}\text{H}_6)]$ (2) in the TH of ketones [88].

2.2.3 Palladium-catalyzed cross coupling reactions

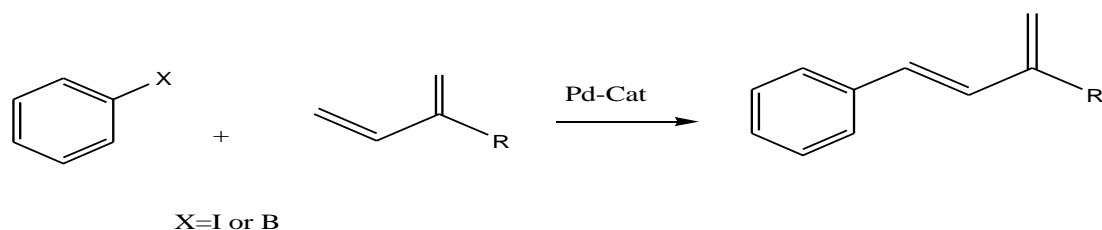
2.2.3.1 Introduction

Another important metal in our study was palladium, which was extracted by William Wollaston in 1802 [89]. The metal was isolated when Wollaston *et al.* dissolved ordinary platinum in aqua regia and a residue was deposited. Palladium is the most common used precious metal for cross coupling reactions such as Heck and Suzuki to mention but a few. These processes are especially dominated by the use of Pd(0) and Pd(II) states. The palladium-catalyzed arylation of unsaturated hydrocarbons for carbon-carbon forming reactions is of interest to us. Below we report on some of the literature found on Heck reactions.

2.2.3.2 Heck reaction

Heck coupling reactions is an important organic transformation involving the arylation of unsaturated hydrocarbons for carbon-carbon forming reactions (scheme 2.11). Palladium complexes have been reported to be good candidates for this type of reactions, especially when anchored to phosphines and nitrogens [90].

Generally the use of nitrogen ligands is preferred over phosphine ligands due to the phosphines being easily decomposed, toxic and expensive [91]. The imino-pyridyl complexes have been successfully applied in Heck reactions [17].



Scheme 2.11: Heck cross coupling reaction.

Pelagatti *et al.* reported the Heck coupling between iodobenzene and methyl acrylate by investigating the catalytic activity of pyridyl-imine palladium(0) and palladium(II) complexes (scheme 2.11) [92]. The reactions were conducted in DMF at 80 °C with a complete conversion of iodobenzene into *trans*-methylcinnamate observed within 2.5 h, with a TOF value of 1253. The palladium (II) complexes were found to be more active than their analogous neutral palladium (0) complexes.

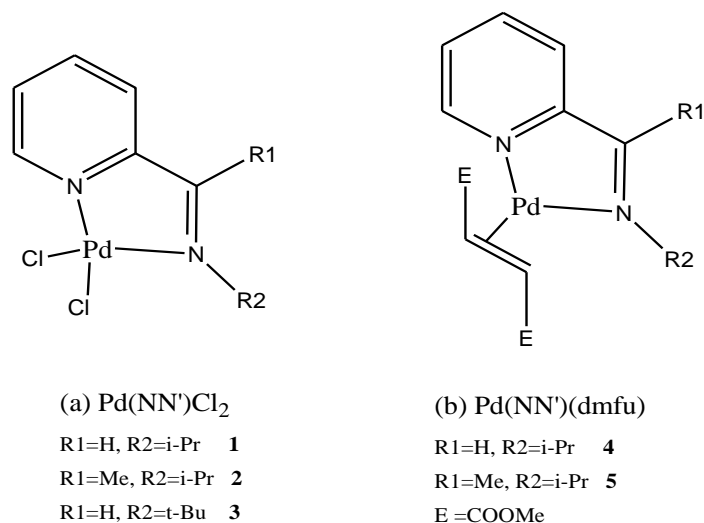
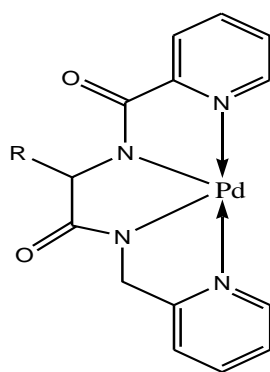


Figure 2.14: Pd(NN') complexes [92].

Motswainyana *et al.* investigated the activity of phenylene bridged binuclear bis(iminoquinolyl) palladium (II) complexes [93]. The complexes showed high activity towards methyl and butyl acrylate with iodobenzene, the reactions were conducted in DMF at 80 °C. The complexes exhibited the efficient arylation of methyl acrylate, resulting in good yields of over 95% in 8 hours; and good selectivity for the formation of trans-methyl cinnamate in the range of 90-94% [93]. Lee *et al.* evaluated amido-functionalized NHC Pd(0) and Pd(II) complexes for the Heck coupling between 4-chloroacetophenone and styrene in N,N-dimethylacetamide (DMA) to yield 4-acetylstilbene [94]. The catalytic activity was reported to be low for both Pd(II) and Pd(0) at low temperature; but by raising temperature from 120 to 140 °C yields of 96% and 99% were achieved. Srinivas *et al.* investigated the activity of dicarboxyamidate/dipyridyl palladium complexes (scheme 2.12) [5]. The thermogravimetric analysis of the complexes revealed they are very stable up to 350 °C. Under harsh reaction conditions of 160 °C for 44 hrs, using the base, LiOH·H₂O the complex 6a successfully catalyzed arylation of 4-chlorotoluene and 4-methylstyrene of turnovers ca. 620 and a yield of 74 %.



6a: R = CH₂C₆H₅
6b: R = CHMe₂

Figure 2.15: Dicarboxyamidate/dipyridyl palladium complexes [5].

2.3 Conclusion

Oxidative cleavage reactions have been studied for decades, and ruthenium complexes have proven to be the superior catalyst precursors. Therefore considering the reported literature our synthesized Ru(II) complex was evaluated for oxidative cleavage of styrene. Following the good results obtained from Busa *et al.* we extend the scope of his investigation by evaluating an aromatic substrate i.e. styrene [15]. The Ru(II) complexes synthesized during this MSc was also intended to be evaluated for the transfer hydrogenation of ketones since it has been reported that these type of complexes are good candidates for this type of reactions; unfortunately due to the unavailability of GC, the reactions could not be carried out. Ruthenium complexes coordinated to “hard” nitrogen and “soft” phosphorous-donor ligands have been reported to form excellent catalysts towards transfer hydrogenation [95], but recently nitrogen donor ligands are preferred over phosphorous-donor ligands due to it being easily decomposed for this reason our synthesized tetradentate N-donor Ru(II) complexes would serve as good candidates to study the reaction conditions since our systems has not yet been tested for these type of transformations to the best our knowledge.

The chapter also highlights on the Pd-catalysed Heck reaction, and the replacement of phosphine ligands with nitrogen based ligands as an alternative are of greater demand and has sparked great interest, since they are easily prepared, and stability in air and/or moisture and lower costs are involved compared to phosphine. Therefore our synthesized tetradentate N-donor Pd(II) complexes would serve as good candidates to study the reaction conditions since our systems has not yet been tested for these type of transformations as far as our knowledge.

References

1. Schiff H, *Ann. Suppl.*, **1864**, 3, 343.
2. Sukanya D, Evans M, Zeller M, Natarajan K, *Polyhedron.*, **2007**, 26, 4314.
3. (a) Cozzi PG, *Chem. Soc. Rev.*, **2004**, 33, 410; (b) Gröger H, *Chem. Rev.*, **2003**, 103, 2795; (c) Sun W, Wang H, Xia C, Li J, Zhao P, *Angew. Chem. Int. Ed.*, **2003**, 42, 1042.
4. (a) Killian CM, Johnson LK, Brookhart M, *J. Am. Chem. Soc.*, **1995**, 117, 6414; (b) Nyamato GS, Ojwach SO, Akerman MP, *Organometallics.*, **2015**, 34, 5647.
5. (a) Srinivas P, Likhari PR, Maheswaran H, Sridhar B, Ravikumar K, Kantam MK, *Chem. Eur. J.*, **2009**, 15, 1578; (b) Potier J, Menuel S, Rousseau J, Tumkevicius S, Hapiot F, Monflier E, *App. Cat. A: General.*, **2014**, 479, 1.
6. (a) Suzuki MN, *Chem. Rev.*, **1995**, 95, 2457; (b) Zhou J, Guo X, Tu C, Li X, Sun H, *J. Organomet. Chem.*, **2009**, 694, 697.
7. Lalrempuia R, Carroll PJ, Kollipara MR, *J. Chem. Sci.*, **2004**, 116, 21.
8. (a) Wu F, Thummel RP, *Inorg. Chim. Acta.*, **2002**, 327, 26; (b) Sunjuk M, Abu-Surrah AS, Abu Safieh KA, Qaroush AK, Al-Qaisi FM, *Arab. J. Chem.*, **2013**, doi:10.1016/j.arabjc.2013.02.019.
9. Vrieze K, van Koten G, *Inorg. Chim. Acta.*, **1995**, 117, 6414.
10. Volpe EC, Wolczanski PT, Lobkovsky EB, *Organometallics.*, **2010**, 29, 364.
11. Ebralidze II, Leitus G, Shimon LJW, Wang Y, Shaik S, Neumann R, *Inorg. Chim. Acta.*, **2009**, 362, 4713.

12. Pandiyan T, Guadalupe HJ, Cruz J, Bernès S, Ugalde-Salvdivar VM, González I, *Eur. J. Inorg. Chem.*, **2008**, 3274.
13. (a) Newkome GR, Patri AK, Holder EU, Schubert S, *Eur. J. Org. Chem.*, **2004**, 2, 235;
(b) Schubert US, Eschbaumer C, *Angew. Chem. Int. Ed.*, **2002**, 41, 2892; (c) Choudhury S, Deb AK, Goswami S, *J. Chem. Soc. Dalt. Trans.*, **1994**, 1305.
14. Cetinkaya B, Cetinkaya E, Brookhart M, White PS, *J. Mol. Cat. A: Chem.*, **1999**, 142, 101.
15. Busa AV, University of the Western Cape (South Africa), MSc dissertation, **2012**.
16. Motswainyana WM, Ojwach SO, Onani MO, Iwuoha EI, Darkwa J, *Polyhedron.*, **2011**, 30, 2574.
17. Radebe M, University of the Western Cape (South Africa), MSc dissertation, **2012**.
18. Patra GK, Goldberg I, *Crystal Growth & Design*, **2003**, 3, 321.
19. Prema D, Wiznycia AV, Scott BMT, Hilborn J, Desper J, Levy CJ, *Dalton. Trans.*, **2007**, 4788.
20. Mori A, Suzuki T, Nakatani Y, Sunatsuki Y, Kojimaa M, Nakajima K, *Dalton. Trans.*, **2015**, 44, 15757.
21. Shiraishi Y, Ichimura C, Hirai T, *Tetra. Lett.*, **2007**, 48, 7769.
22. Funaki T, Yanagida M, Onozawa-Komatsuzaki N, Kasuga N, Kawanishi Y, Sugihara H, *Inorg. Chim. Acta.*, **2009**, 362, 2519.

23. (a) Leung C-F, Wonga C-Y, Ko C-C, Yuen M-C, Wong WT, Wong WW, Lau T-C, *Inorg. Chim. Acta.*, **2009**, *362*, 1149; (b) Lahiri GK, Bhattacharya S, Ghosh BK, Charkravorty A, *Inorg. Chem.*, **1987**, *26*, 4324.
24. Jabłońska-Wawrzycka A, Rogala P, Michałkiewicz S, Hodorowicz M, Barszcz B, *Dalton Trans.*, **2013**, *42*, 6092.
25. Claus C, *Ann Chem Phys (Poggendorff, Leipzig)*, **1845**, *64*, 192.
26. Chen QA, FA Cruz, Dong VM, *J. Am. Chem. Soc.*, **2015**, *137*, 3157.
27. (a) Kuwabara T, Saito T, Kumobayashi H, Akutagawa S, *J. Am. Chem. Soc.*, **1990**, *112*, 7812; (b) Miyata A, Furukawa M, Irie R, Katsuki T, *Tetra. Lett.*, **2002**, *43*, 3481.
28. (a) Himeda Y, Sugihara N, Arakawa H, Kasuga K, *J. Mol. Catal, A: Chem.*, **195**, 95 (2003); (c) Ahlford K, Ekström J, Zaitsev AB, Ryberg P, Eriksson L, Adolfsson H, *Chem.*, **2009**, *15*, 197; (d) González RM, Chávez D, Aguirre G, Hake MP, Somanathan R, *J. Braz. Chem. Soc.*, **2010**, *21*, 431.
29. Lin W, Wilson SR, Girolami GS, *Organometallics.*, **1997**, *16*, 2356.
30. Djerassi C, Engle RR, *J. Am. Chem. Soc.*, **1953**, *75*, 3838.
31. Oberender FG, Dixon JA, *J. Org. Chem.*, **1959**, *24*, 1226.
32. Morris PE, Kiely DE, Vigee GS, *J. Carbohyd. Chem.*, **1990**, *9*, 661.
33. Stock LM, Tse KT, *Fuel.*, **1983**, *62*, 974.
34. Pappo R, Becker A, *Bull. Res. Counc. Israel.*, **1956**, *5A*, 300.

35. Carlsen PHJ, Martin TKVS, Sharpless KB, *J. Org. Chem.*, **1981**, *46*, 3936.
36. Griffith WP, Kwong E, *Synth. Commun.*, **2003**, *33*, 2945.
37. (a) Giddings S, Mills A, *J. Org. Chem.*, **1988**, *53*, 1103; (b) Mills A, Giddings S, Patel I, *J. Chem. Soc., Faraday Trans*, **1987**, *83*, 2317.
38. Daw P, Petakamsetty R, Sarbajna A, Laha S, Ramapanicker S, Bera J, *J. Am. Chem. Soc.*, **2014**, *136*, 13987.
39. Shoair AGF, Mohamed RH, *Synthesis. Commun.*, **2006**, *36*, 59.
40. Fürstner A, Davies PW, *Chem. Commun.*, **2005**, *18*, 2307.
41. Jun C-H, *Chem. Soc. Rev.*, **2004**, *33*, 610.
42. Tobisu M, Chatani N, *Chem. Soc. Rev.*, **2008**, *37*, 300.
43. (a) Datta S, Chang C-L, Yeh K-L, Liu RS, *J. Am. Chem. Soc.*, **2003**, *125*, 9294; (b) Shen H-C, Su H-L, Hsueh Y-C, Liu R-S, *Organometallics.*, **2004**, *23*, 4332; (c) Liu R-S, Shen H-C, Liu Y, Song F, Guo S, *J. Am. Chem. Soc.*, **2006**, *128*, 11332.
44. Sung H-L, Her T-M, Su W-H, Cheng C-P, *Molecules.*, **2012**, *17*, 8533.
45. (a) Bruneau C, Dixneuf P, *Acc. Chem. Res.*, **1999**, *32*, 311; (b) Bustelo E, Carbo J J, Lledos A, Mereiter K, Puerta MC, Valerga P, *J. Am. Chem. Soc.*, **2003**, *125*, 3311.
46. (a) Trost B M, Flygare JA, *J. Am. Chem. Soc.*, **1992**, *114*, 5476; (b) Trost BM, Flygare JA, *Tetra.Lett.*, **1994**, *35*, 4059; (c) Nishibayashi Y, Wakiji I, Hidai M, *J. Am. Chem. Soc.*, **2000**, *122*, 11019; (d) Yeh K-L, Lo C-Y, Huang HL, Liu R-S, *J. Am. Chem. Soc.*,

- 2002**, *124*, 6510; (e) Madhushaw RJ, Li C-L, Shen K-H, Hu C-C, Liu R-S, *J. Am. Chem. Soc.*, **2001**, *123*, 7427.
47. (a) O'Connor JM, Pu L, *J. Am. Chem. Soc.*, **1990**, *112*, 9013; (b) Bianchini C, Casares J A, Peruzzini M, Romerosa A, Zanolini F, *J. Am. Chem. Soc.*, **1996**, *118*, 4585.
48. Chaikin SW, Brown WG, *J. Am. Chem. Soc.*, **1949**, *71*, 122.
49. Gaylord NG, *J. Chem. Educ.*, **1957**, *34*, 367.
50. Liao X, Zhou H, Wearing XZ, Ma J, Cook JM, *Org. Lett.*, **2005**, *7*, 3501.
51. (a) Jiang H, Qiao QD, Gong H, *React. Kinet. Catal. Lett.*, **1998**, *65*, 1193; (b) Fidalgo EG, Plasseraud L, Su'ss-Fink G, *J. Mol. Cat. A: Chem.*, **1998**, *132*, 5.
52. Keleş M, Şahinoğlu C, Emir DM, Mart M, *Appl. Organ. Chem.*, **2014**, *28*, 768.
53. De Grauw CF, Peters JA, van Bekkum H, Huskens J, *Synth.*, **1994**, 1007.
54. Szatmári I, Papp G, Joó F, Kathó A, *Cat. Today*, **2014**, *247*, in press.
55. Prakash O, Sharma KN, Joshi H, Gupta PL, Singh AK, *Organometallics.*, **2014**, *33*, 2535.
56. von Wilde MP, *Deutsch. Chem. Ber.*, **1874**, *7*, 352.
57. Sabatier P, Senderens JB. *C. R. Chim.*, **1897**, *124*, 1358.
58. Sasson Y, Blum J, *Tetra. Lett.*, **1971**, *12*, 2167.
59. Blum J, Sasson Y, Iflah S, *Tetra. Lett.*, **1972**, *13*, 1015.
60. Sasson Y, Blum J, *J. Org. Chem.*, **1975**, *40*, 1887.
61. Chowdhury RL, Bäckvall, J-E, *J. Chem. Soc., Chem. Commun.*, **1991**, 1063.

62. He LP, Chen T, Xue DX, Eddaoudi M, Huang KWJ, *Organomet. Chem.*, **2012**, 700, 202.
63. Ye W, Zhao M, Yu Z, *Chem. Eur. J.*, **2012**, 18, 10843.
64. Mc Skimming A, Bhadbhade MM, Colbran SB, *Angew. Chem., Int. Ed.*, **2013**, 52, 3411.
65. Furst A, Berlo RC, Hooton S, *Chem. Rev.*, **1965**, 65, 51.
66. Brieger G, Nestruck TJ, *Chem. Rev.*, **1974**, 74, 567.
67. Li K, Niu J-L, Yang M-Z, Li Z, Wu L-Y, Hao X-Q, Song M-P, *Organometallics.*, **2015**, 34, 1170.
68. Clapham, SE, Hadzovic A, Morris RH, *Coord. Chem. Rev.*, **2004**, 248, 2201.
69. (a) Jardine FH, Osborn JA, Wilkinson G, Young GF, *Chem. Ind.*, **1965**; (b) Coffey R (ICI), *British Patent 1*, **1965**, 121, 642,
70. (a) Moore CM, Szymczak NK, *Chem. Commun.*, **2013**, 49, 400; (b) Ito J-I, Ujiie S, Nishiyama H, *Organomet.*, **2009**, 28, 630; (c) Beach NJ, Spivak GJ, *Inorg. Chim. Acta.*, **2003**, 343, 244.
71. Gao JX, Yi X-D, Xu P-P, Tang C-L, Wan H-L, Ikariya T, *J. Organomet. Chem.*, **1999**, 592, 290.
72. (a) Cuervo D, Gamasa MP, Gimeno J, *Chem. Eur. J.*, **2004**, 10, 425; (b) Jiang Y, Jiang Q, Zhang X, *J. Am. Chem. Soc.*, **1998**, 120, 3817.
73. Jiang Q, Van Plew D, Murtuza S, Zhang X, *Tetrahed. Lett.*, **1996**, 37, 797; (b) Huang H, Okuno T, Tsuda K, Yoshimura M, Kitamura M, *J. Am. Chem. Soc.*, **2006**, 128, 8716.
74. Braunstein P, Naud F, Pfaltz A, Rettig S J, *Organometallics.*, **2000**, 19, 2676.
75. Clarke ML, Díaz-Valenzuela B, Slawin AMZ, *Organometallics.*, **2007**, 26, 16.
76. Yang H, Alvarez-Gressier M, Lugan N, Mathieu R, *Organometallics.*, **1997**, 16, 1401.
77. Pugin B, Blaser HU, *Top. Catal.*, **2010**, 53, 953.
78. Noyori R, Ohkuma T, Kitamura M, Takaya H, *J. Am. Chem. Soc.*, **1987**, 109, 5856
79. Ell AH, Johnson JB, Bäckvall JE, *Chem. Commun.*, **2003**, 1652.

80. Wu X, Li X, Zanotti-Gerosa A, Pettman A, Liu J, Mills AJ, Xiao J, *Chem. Eur. J.*, **2008**, *14*, 2209.
81. Ohta T, Takaya H, Kitamura M, Nagai K, Noyori R, *J. Organ. Chem.*, **1987**, *52*, 3174.
82. Okhuma T, Ooka H, Hashiguchi T, Noyori R, *J. Am. Chem. Soc.*, **1995**, *117*, 2675.
83. Yoshimiro M, Tanaka S, Masato K, *Tetra. Lett.*, **55**, 3635.
84. Hashiguchi S, Fujii A, Takehara J, Ikariya T, Noyori R, *J. Am. Chem. Soc.*, **1995**, *117*, 7562.
85. (a) Gao JX, Ikariya T, Noyori R, *Organometallics.*, **1996**, *15*, 1087; (b) Zhang H, Yang C-B, Li Y-Y, Donga Z-R, Gao J-X, Nakamura H, Murata K, Ikariya T, *Chem. Commun.*, **2003**, 142.
86. Zeng L, Wu F, Li Y-Y, Dong Z-R, Gao J-X, *J. Organomet. Chem.*, **2014**, *762*, 34.
87. Ogwen A, Ojwach S, Akerman P, *Dalton Trans.*, **2014**, 43, 1228.
88. Fu Q, Zhang L, Yi T, Zou M, Wang X, Fu H, Li R, Chen H, *Inorg. Chem. Comm.*, **2013**, *38*, 28.
89. Wollaston WH, *Philos. Trans. R. Soc.*, **1805**, *95*, 316 .
90. Smith GS, Mapolie SF, *J. Mol. Catal. A: Chem.*, **2004**, *213*, 187.
91. Zhang Z, Chen S, Zhang X, Li H, Ke Y, Lu Y, Hu Y, *J. Mol. Catal. A: Chem.*, **2005**, *230*, 1.
92. Pelagatti P, Carcelli M, Costa M, Ianelli S, Pelizzi C, Rogolino D, *J. Mol. Catal. A: Chem.*, **2005**, *226*, 107.
93. Motswainyana WM, Onani MO, *Inorg. Chem. Comm.*, **2012**, *24*, 221.
94. Lee J-Y, Cheng P-Y, Lin G-R, Liu S-P, Sie M-H, Lee HM, *Organometallics.*, **2010**, *29*, 3901.
95. (a) Wang Y, Guo H, Ding KL, *Tetra. Asymm.*, **2000**, *11*, 4153; (b) Chelucci G, Orru GA, Pinna GA, *Tetra.*, **2003**, *59*, 9471.

CHAPTER 3

3.0 Experimental Section

Chapter overview

The chapter outlines the general conditions at which the synthesis of all the compounds were carried out and the various special chemicals used in the study. This is followed by the principles of the various spectroscopic techniques employed to characterise the tetradentate pyridyl and quinolyl-imine Schiff base ligands and their corresponding metal complexes. A detailed summary of the techniques is described below; the techniques include Fourier transform infrared spectroscopy (FT-IR), Proton and Carbon Nuclear Magnetic Resonance (^1H NMR and ^{13}C NMR), Ultraviolet-visible spectroscopy (UV-Vis) and Thermogravimetric analysis (TGA). The chapter also details the synthesis of tetradentate diimine ligands, synthesis of various ruthenium(II) and palladium(II) precursors and their coordinated neutral monometallic, cationic homobimetallic and bimetallic ruthenium(II) and palladium(II) complexes respectively and the catalytic studies used in the present study. Lastly, the chapter provide full characterisation data for all the compounds which were obtained from various spectroscopic techniques.

3.1 General

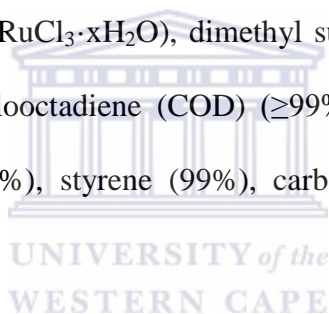
All manipulations were performed under nitrogen conditions, using a dual vacuum/nitrogen line and general schlenk line techniques. Air/moisture-sensitive compounds were performed in a nitrogen-filled glove box. All reagents were used as received, unless otherwise stated. All solvents were distilled prior to use following the literature procedure [1] and stored with activated molecular sieves in tightly sealed solvent bottles.

Reactions progress and product mixture were monitored by thin layer chromatography (TLC) on pre-coated alumina-gel plated in a suitable solvent system using the ascending technique and the plates were viewed under a UV light.

3.2 Materials and Instrumentation

3.2.1 Chemicals

The following specialized chemicals purchased from Sigma Aldrich (South Africa) were used in the study; Ethylenediamine ($\geq 99\%$), 1,3-diaminopropane ($\geq 99\%$), 1,4-diaminobutane ($\geq 99\%$), 1,5-diaminopentane (97%), 2-pyridinecarboxaldehyde (98%), 2-quinolinecarboxaldehyde (97%), anhydrous magnesium sulphate (MgSO_4) ($\geq 99\%$), ruthenium(III) chloride hydrate ($\text{RuCl}_3 \cdot x\text{H}_2\text{O}$), dimethyl sulphoxide (DMSO), palladium(II) chloride (PdCl_2) (99%), 1,5-cyclooctadiene (COD) ($\geq 99\%$), neutral aluminium oxide and sodium periodate (NaIO_4) (99,8%), styrene (99%), carbon tetrachloride, methyl acrylate ($\geq 99\%$) and iodobenzene (98%).



3.2.2 Instrumentation

The ^1H (400 MHz) and ^{13}C (100 MHz) NMR spectra were recorded on a Bruker spectrometer at the University of the Western Cape, South Africa (Chemical science department) and on a Bruker (^1H NMR, 500 MHz; ^{13}C NMR, 200 MHz) spectrometer at Lund University, Sweden (Physical chemistry department). The NMR spectrometers chemical shifts are given in δ values (ppm) using TMS as the internal standard. The deuterated chloroform (CDCl_3-d) and dimethyl sulphoxide ($\text{DMSO}-d_6$) were used as solvents.

The coupling constants are given in hertz (Hz). Elemental analyses for carbon, hydrogen and nitrogen were determined on a Fissons EA 110 CHNS analyzer at the Microanalytic

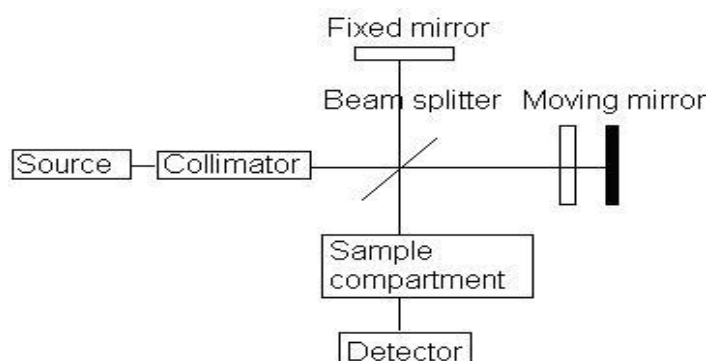
laboratory at the University of Cape Town, South Africa. Fourier transformation infrared spectra (FT-IR) were recorded as Nujol mulls as neat films on NaCl plates or KBr pellets at room temperature using a PerkinElmer Spectrum 100 FT-IR spectrometer in the range 450-4000 cm^{-1} . Gas Chromatograph-Mass spectrometry (GC-MS) was recorded on an Agilent Technologies 7820A GC 5977E MSD COLUMN: DB-5 (30 m). The samples were recorded on a GC-FID with auto injector Agilent Technologies 7890 A on a HP-5, 30 m, 0.32 mm, 2 capillary column. The GC method applied throughout the analysis is as follows: the column temperature was 40 °C at the beginning of the program and it was heated with a rate of 10 °C/min up to 150 °C, then it was kept at this temperature for 3 min. It was then heated with a rate of 20 °C/min up to 200 °C. Throughout the analysis the injector and detector temperatures were kept constant at 200 °C. Ultraviolet-visible spectroscopy was recorded on a Nicolet evolution 100 (Thermo Electron Corporation, UK). Thermogravimetric analyses (TGA) were recorded on a TGA 4000 PerkinElmer at the University of the Western Cape (Pharmacy Department). Melting points were determined in open capillaries using SMP10 melting point apparatus.

3.3 Characterization Techniques

A brief overview of the principles of various spectroscopic techniques employed to confirm the successful syntheses of the tetradentate pyridyl and quinolyl-imine ligands, various ruthenium(II) and palladium(II) precursors and their coordinated monometallic and bimetallic complexes are outlined below.

3.3.1 Fourier transform infrared spectroscopy (FT-IR)

FT-IR is a sensitive, rapid inexpensive analytical vibrational spectroscopy technique; used to determine both qualitative and quantitative features of molecules in organic or inorganic samples. In the FT-IR spectrometer, the IR radiation usually excites molecules into a higher vibrational state. The wavelength of light absorbed by a particular molecule is a function of the energy difference between the at-rest and excited vibrational states. The FT-IR spectrometer uses an interferometer to modulate the wavelength from a broad band infrared source and measures the intensity of transmitted or reflected light as a function of its wavelength [2]. The signal obtained from the detector is an interferogram, which must be analyzed with a computer using Fourier transforms to obtain a single-beam infrared spectrum (scheme 3.1). The spectra are obtained when the IR radiation is passed through the sample and some of the infrared radiation is absorbed by the sample or transmitted [3]. The spectrum contains absorption peaks which correspond to the frequencies of vibrations between the bonds of the atoms making up the material creating a molecular fingerprint of the sample, hence providing information about the functional groups present in compounds. The FT-IR spectra are usually presented as plots of intensity versus wavenumber (cm^{-1}). A correlation chart is available to identify the absorption peaks.



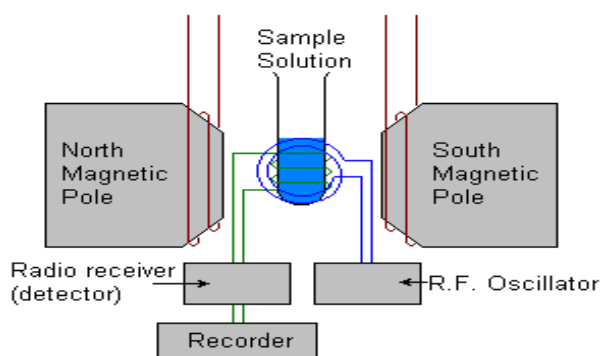
Scheme 3.1: Diagram of FT-IR spectrometer [4].

In this study the technique was used to characterise the diimine ligands to confirm the formation of the imine (C=N) functional group and the disappearance of the carbonyl band (1700 cm^{-1}) of the starting aldehyde. This technique was also used to investigate the complexation of diimine ligands towards their corresponding metal complexes by determining whether coordination occurred via the azomethine nitrogen.

3.3.2 Nuclear Magnetic Resonance (^1H NMR and ^{13}C NMR)

The NMR spectroscopy is a powerful, non-destructive dominant technique used for the determination of organic compounds by identifying its carbon/hydrogen framework [5].

In the NMR spectrometer, the sample is immersed in a magnetic field and irradiated with radio waves (scheme 3.2). The nuclei align with the external applied magnetic field, absorb energy and change their orientation with respect to the field, i.e. to a higher energy state. The absorption or emission of electromagnetic energy by the compound at characteristic frequencies provides analytical information of a compounds unique structure. The ^1H NMR technique provides information about the environment of a proton or group of protons relevant to tetramethylsilane (TMS). The ^{13}C NMR is based on the same fundamentals as ^1H NMR. However the spectrum does not show any splitting patterns it consists only of single peaks, one for each carbon or each set of equivalent carbons in a molecule. Definitions are available for the various spectral regions, identifying the various functional groups present in a molecule.



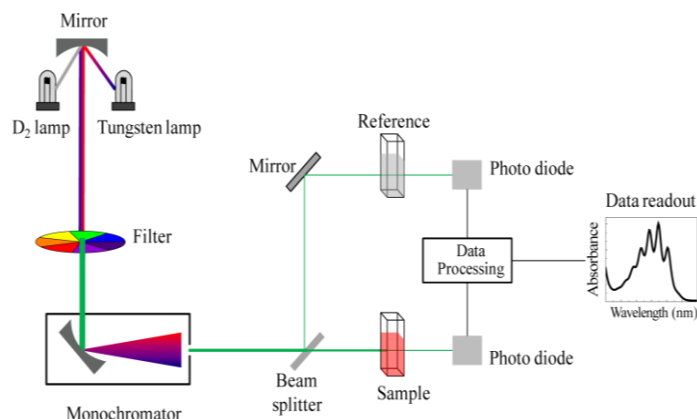
Scheme 3.2: Diagram of the NMR spectrometer [6].

3.3.3 Ultraviolet-visible spectroscopy (UV-Vis)

The UV-Vis spectroscopy is a quick, accurate and inexpensive tool employed for quantitative analysis and provides limited qualitative results [7]. The latter provides information on the identity of certain compounds and the former estimate the amount of compound present in the sample. In UV-Vis the sample (sample cell) and reference cell (scheme 3.3) are exposed to a series of wavelengths of light derive from the spectrometer having an energy that matches a possible electronic transition within the molecule, some of the light energy are absorbed as the electron is promoted to a higher energy orbital in the ultraviolet and visible regions of the electromagnetic spectrum [8]. The instrument generates a spectra based on the absorption of radiation of the sample presented as a graph of absorbance (A) versus wavelength. The bands observed are usually not specific enough to allow a positive identification of an unknown sample, although this data may be used to confirm its nature deduced from its infrared spectrum or by other techniques. A correlation chart has been set by the Joint Committee on Nomenclature in Applied Spectroscopy. The wavelengths of light through the reference cell and sample cell are defined by I_0 and I respectively (I = Intensity) this can expressed as transmittance (T) (Eqn 3.2.1). If I is less than I_0 , then the sample has absorbed some of the light, the computer then converts this into absorbance, A [9]. Lambert-Beer law is then derived as Eqn 3.2.2 which states that there is a linear relationship between absorbance and path length at a fixed concentration [10], where ϵ is the molar extinction coefficient (ϵ , $L \cdot mol^{-1} \cdot cm^{-1}$). However the linearity of the Beer-Lambert law is limited by chemical and instrumental factors.

$$T = I/I_0 \quad (\text{eqn 3.2.1})$$

$$A = -\log T = -\log I/I_0 = \log I_0/I = \epsilon bc \quad (\text{eqn 3.2.2})$$

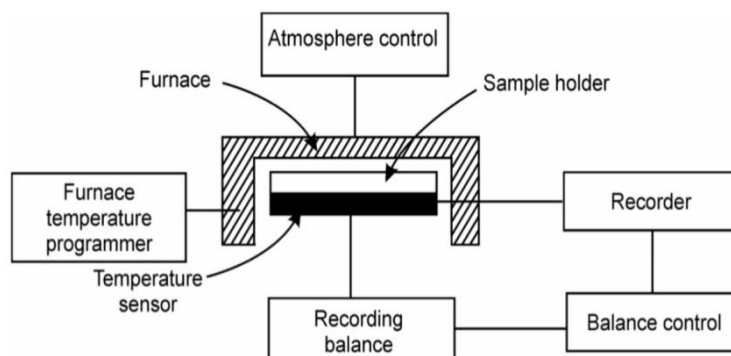


Scheme 3.3: Diagram of UV-Visible spectrometer [9].

UV-Vis studies were performed on all the synthesized ligands and complexes to understand their electronic transitions.

3.3.4 Thermogravimetric analysis (TGA)

The thermogravimetric analysis is a technique in which the mass of a substance is monitored as a function of temperature or time as the sample specimen is subjected to a controlled temperature program in a controlled atmosphere [11]. The technique is carried out by placing the sample in a crucible that is supported by a precision balance (scheme 3.4). The crucible resides in a furnace and is heated or cooled during the experiment. The temperature is between 0.5 and 50 K/min the final temperature is usually very high 600 °C for organic compounds and ≥ 1000 °C for inorganic compounds. The mass of the sample is monitored during the experiment. A sample purge gas controls the sample environment. This gas may be inert or a reactive gas that flows over the sample and exits through an exhaust. The instrument generates a thermal curve, the X-axis can be displayed as time or temperature and the Y-axis can be displayed as weight (mg) or weight percent (%). The graph display information of loss of water, loss of solvent, loss of plasticizer, decarboxylation, pyrolysis, oxidation, reduction and decomposition etc. [12].



Scheme 3.4: Diagram of a TGA [13].

3.4 Synthesis of tetradentate pyridyl and quinolyl-imine ligands

The pyridyl and quinolylimine ligands (L1-L6) were synthesised based on literature work done by Haddleton *et al.* [14], Chen *et al.* [15], and Cloete *et al.* [16]. The tetradentate diimine ligands were synthesized by a Schiff base condensation reaction from the reaction of 2-pyridinecarboxaldehyde or 2-quinolinecarboxaldehyde and appropriate amine (1,2-ethylenediamine, 1,3-diaminopropane, 1,4-diaminobutane and 1,5-diaminopentane) in a 2:1 ratio, using an alcohol medium and general schlenk techniques. The anhydrous sodium sulphate (MgSO_4) was used to remove any water formed during the reaction.

3.4.1 N1,N2-bis((pyridin-2-yl)methylene)ethane-1, 2-diamine, L1

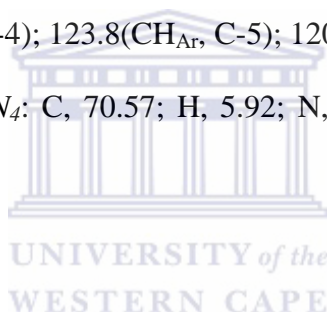
The synthesis of L1 was carried out by reacting 2-pyridinecarboxaldehyde (1.9 ml, 20 mmol) with ethylenediamine (0.67 ml, 10 mmol) in a 2:1 ratio by a condensation reaction using general schlenk techniques. The amine, ethylenediamine was dissolved separately in dry methanol (MeOH) and was added drop wise to the stirred solution of 2-pyridinecarboxaldehyde in dry MeOH, whilst the reaction mixture was cooled in an ice bath. The reaction mixture was then refluxed for 3 hours. After the allotted time the solvent was removed using a rotarvapor, an oily residue was obtained and redissolved in dichloromethane (DCM) (20 ml).

The product was extracted with H₂O (10 x 20 ml portions) and the organic layer was dried over MgSO₄, filtered and the solvent removed under reduced pressure using liquid nitrogen. The ligand was further purified by dissolving in diethylether and cooling overnight at -5°C in order to precipitate out any unreacted aldehyde. The product was filtered off, dried under reduced pressure using liquid nitrogen and obtained as brown solids. Yield (2.30 g, 97%). Molecular formula, C₁₄H₁₄N₄. MP 50-53°C.

FT-IR (KBR), $\tilde{\nu}$ /cm⁻¹: 1647ν(C=N)_{imine}, 1584ν(C=N)_{ring}, 1564ν(C=C).

¹H NMR (500MHz, CDCl₃-d, δppm) δ 8.63(d, H-6, ³J_{H-H} 4.4 Hz); 8.42(s, H-7); 7.98(d, H-3, ³J_{H-H} 7.8 Hz); 7.73(t, H-4, ³J_{H-H} 6.8 Hz); 7.30(t, H-5, ³J_{H-H} 6.3 Hz); 4.07(s, H-8). ¹³C NMR (100MHz, CDCl₃-d), δppm = 61.3(CH₂, C-8); 162.6(CH_{imine}, C-7); 153.3(CH_{Ar}, C-2); 148.4(CH_{Ar}, C-6); 135.4(CH_{Ar}, C-4); 123.8(CH_{Ar}, C-5); 120.4(CH_{Ar}, C-3).

Analytical data *calc. for* C₁₄H₁₄N₄: C, 70.57; H, 5.92; N, 23.51. [M]⁺: m/z = 239. *Found*: 70.20; 5.89; 23.88, [M]⁺ = 237.



3.4.2 N1,N3-bis(pyridin-2-ylmethylene)propane-1,3-diamine, L2

The synthesis of L2 was carried out by reacting 2-pyridinecarboxaldehyde (3.8 ml, 40 mmol) with 1,3-diaminopropane (1.66 ml, 20 mmol) following the same synthetic procedure that was performed for the above ligand. The product was obtained as low viscous brown oil. Yield (4.6 g, 91%). Molecular formula, C₁₅H₁₆N₄.

FT-IR (nujol), $\tilde{\nu}$ /cm⁻¹: 1650ν (C=N)_{imine}, 1580ν(C=N)_{ring}, 1452ν(C=C).

¹H NMR (400 MHz, CDCl₃-d, δppm) δ 8.39(s, H-7); 8.61(d, H-6, ³J_{H-H} 4.7 Hz); 7.97(d, H-3, ³J_{H-H} 7.8 Hz); 7.71(t, H-4, ³J_{H-H} 7.0 Hz); 7.28(t, H-5, ³J_{H-H} 6.1 Hz); 3.77(t, H-8, ³J_{H-H} 6.6 Hz); 2.14(q, H-9, ³J_{H-H} 6.9 Hz). ¹³C NMR (100 MHz, CDCl₃-d), δppm = 31.2(CH₂, C-9); 58.6(CH₂, C-8); 161.9(CH_{imine}, C-7); 154.1(C_{Ar}, C-2); 120.8(CH_{Ar}, C-3); 136.1(CH_{Ar}, C-4); 124.3(CH_{Ar}, C-5); 149.0(CH_{Ar}, C-6).

Analytical data *calc. for* $C_{15}H_{16}N_4$: C, 71.40; H, 6.39; N, 22.21. $[M]^+$: $m/z = 253$. *Found*: C, 71.88; H, 6.04; N, 20.48; $[M]^+ = 252$.

3.4.3 N1,N4-bis(pyridin-2-ylmethylene)butane-1,4-diamine, **L3**

The synthesis of L3 was done by reacting 2-pyridinecarboxaldehyde (1.98 ml, 21 mmol) with 1,4-diaminobutane (1.87 ml, 25 mmol), following the same synthetic procedure as the above ligands. The product was obtained as orange-brown solids. Yield (2.15g, 88%). MP 69°C-72°C. Molecular formula, $C_{16}H_{18}N_4$.

FT-IR (KBR), $\tilde{\nu}/\text{cm}^{-1}$: 1639 $\nu(\text{C}=\text{N})_{\text{imine}}$, 1586 $\nu(\text{C}=\text{N})_{\text{ring}}$, 1566 $\nu(\text{C}=\text{C})$.

^1H NMR (400MHz, CDCl_3 -*d*, δ) δ 8.62(d, H-6, $^3J_{\text{H-H}}$ 4.9 Hz); 8.37(s, H-7); 7.96(d, H-3, $^3J_{\text{H-H}}$ 8.3 Hz); 7.71(t, H-5, $^3J_{\text{H-H}}$ 7.4Hz); 7.28(t, H-4, $^3J_{\text{H-H}}$ 6.3 Hz); 3.72(m, H-8); 1.82(m, H-9).

^{13}C NMR (200 MHz, CDCl_3 -*d*), δppm =28.3(CH_2 , C-9); 61.1(CH_2 , C-8); 160.8(CH_{imine} , C-7); 154.5(C_{Ar} , C-2); 149.3(CH_{Ar} , C-6); 136.4(CH_{Ar} , C-4); 124.5(CH_{Ar} , C-5); 121.1(CH_{Ar} , C-3).

Analytical data *calc. for* $C_{16}H_{18}N_4$: C, 72.15; H, 6.81; N, 21.04. $[M]^+$: $m/z = 267$. *Found*: C, 71.36; H, 6.59; N, 19.88, $[M]^+ = 265$.

3.4.4 N1,N2-bis((quinolin-2-yl)methylene)ethane-1,2-diamine, **L4**

The synthesis of L4 was carried out by reacting 2-quinolinecarboxaldehyde (3.1 g, 20 mmol) with ethylenediamine (0.6g, 10 mmol), following the same synthetic procedure as for the former ligands mentioned above. During the reaction an orange precipitate formed. After the allotted time the solids were filtered off, washed continuously with diethyl ether and dried under reduced pressure using liquid nitrogen. Yield 62%. Molecular formula $C_{22}H_{18}N_4$. MP 113°C-116°C. FT-IR (KBR), $\tilde{\nu}/\text{cm}^{-1}$: 1642 $\nu(\text{C}=\text{N})_{\text{imine}}$, 1593 $\nu(\text{C}=\text{N})_{\text{ring}}$, 1500 $\nu(\text{C}=\text{C})$.

^1H NMR(400MHz, CDCl_3-d , δ) δ 8.61(s, H-11); 8.15(m, 8-H, H-7); 8.10(d, H-3, $^3J_{\text{H-H}}$ 8.3Hz); 7.8(d, H-9, $^3J_{\text{H-H}}$ 7.6 Hz); 7.71(t, H-4, $^3J_{\text{H-H}}$ 7.3 Hz); 7.54(t, H-6, $^3J_{\text{H-H}}$ 7.2Hz); 4.17(s, H-12).

^{13}C NMR (100 MHz, CDCl_3-d), δppm = 163.6(CH_{imine} , C-11); 154.2(CH_{Ar} , C-10); 147.3(CH_{Ar} , C-2); 136.1(CH_{Ar} , C-5); 129.3(CH_{Ar} , C-3); 129.1(CH_{Ar} , C-4); 128.8(CH_{Ar} , C-6); 127.3(CH_{Ar} , C-9); 127.0(CH_{Ar} , C-8); 118.0(CH_{Ar} , C-7); 61.4(CH_2 , C-12).

Analytical data *calc. for* $\text{C}_{22}\text{H}_{18}\text{N}_4$: C, 78.08; H, 5.36; N, 16.56. $[\text{M}]^+$: $m/z = 339$. *Found*: C, 76.88; H, 4.86; N, 15.92.

3.4.5 N1,N3-bis(quinolin-2-ylmethylene)propane-1,3-diamine, **L5**

The synthesis of L5 was done by reacting 2-quinolinecarboxaldehyde with 1,3-diaminopropane and refluxed overnight using the same procedure outlined above. Yield (2.16 g, 85 %). Molecular formula $\text{C}_{23}\text{H}_{20}\text{N}_4$.

FT-IR (Nujol), $\tilde{\nu}/\text{cm}^{-1}$: 1620 $\nu(\text{C}=\text{N})_{\text{imine}}$, 1508 $\nu(\text{C}=\text{N})_{\text{ring}}$, 1452 $\nu(\text{C}=\text{C})$.

^1H NMR (400 MHz, CDCl_3-d) δ 8.62(s, H-11); 8.19(m, H-8, H-7); 8.14(d, H-3 $^3J_{\text{H-H}}$ 8.41 Hz); 7.85(d, H-9, $^3J_{\text{H-H}}$ 7.9 Hz); 7.75(t, H-4, $^3J_{\text{H-H}}$ 7.6 Hz); 7.59(t, H-6, $^3J_{\text{H-H}}$ 7.3 Hz); 3.92(t, H-12, $^3J_{\text{H-H}}$ 6.3 Hz), 2.26(q, H-13, $^3J_{\text{H-H}}$ 6.5 Hz). ^{13}C NMR (100 MHz, CDCl_3-d), δppm = 162.9(CH_{imine} , C-11); 154.8(CH_{Ar} , C-10); 147.8(CH_{Ar} , C-2); 136.6(CH_{Ar} , C-5); 129.3(CH_{Ar} , C-3) 129.1(CH_{Ar} , C-4); 128.8(CH_{Ar} , C-6); 127.3(CH_{Ar} , C-9); 127.1(CH_{Ar} , C-8); 117.8(CH_{Ar} , C-7); 46.0(CH_2 , C-12); 27.6(CH_2 , C-13). Analytical data *calc. for* $\text{C}_{23}\text{H}_{20}\text{N}_4$: C, 78.38; H, 5.72; N, 15.90; $[\text{M}]^+$: $m/z = 353$. *Found*: C, 77.23; H, 4.14; N, 14.33.

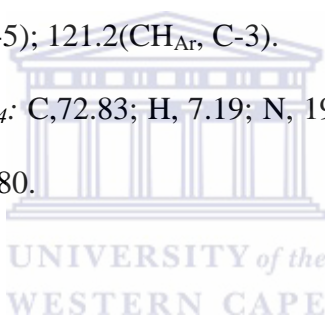
3.4.6 N1,N5-bis(pyridin-2-ylmethylene)pentane-1,5-diamine, L6

The synthesis of L6 was done by reacting 2-pyridinecarboxaldehyde (3.7 ml, 39.0 mmol) with 1,5-diaminopentane (2.26 ml, 19.50 mmol), the same synthetic procedure was performed as the above ligands. The product was obtained as brown oil. Yield (4.02 g, 74%). Molecular formula $C_{17}H_{20}N_4$.

FT-IR (KBR), $\tilde{\nu}/\text{cm}^{-1}$: 1648 $\nu(\text{C}=\text{N})_{\text{imine}}$, 1563 $\nu(\text{C}=\text{N})_{\text{ring}}$, 1479 $\nu(\text{C}=\text{C})$.

^1H NMR (400MHz, CDCl_3-d , δ) δ 8.63 (d, H-6, $^3J_{\text{H-H}}$ 3.7 Hz); 8.35(s, H-7); 7.95(d, H-3, $^3J_{\text{H-H}}$ 7.9Hz); 7.28(t, H-5, $^3J_{\text{H-H}}$ 5.5Hz); 7.71(t, H-4, $^3J_{\text{H-H}}$ 7.0Hz); 3.67(t, H-8, $^3J_{\text{H-H}}$ 6.4 Hz); 1.78 (m, H-9); 1.47(m, H-10). ^{13}C NMR (200 MHz, CDCl_3-d), δppm = 25.0(CH_2 , C-10); 30.5(CH_2 , C-9); 61.4(CH_2 , C-8); 161.8(CH_{imine} , C-7); 154.6(CH_{Ar} , C-2); 149.4(CH_{Ar} , C-6); 136.5(CH_{Ar} , C-4); 124.6(CH_{Ar} , C-5); 121.2(CH_{Ar} , C-3).

Analytical data *calc.* for $C_{17}H_{20}N_4$: C, 72.83; H, 7.19; N, 19.98. $[\text{M}]^+$: $m/z = 281$; *Found*: C, 71.13; H, 6.34; N, 18.78, $[\text{M}]^+ = 280$.



3.5 Synthesis of ruthenium(II) and palladium(II) precursors

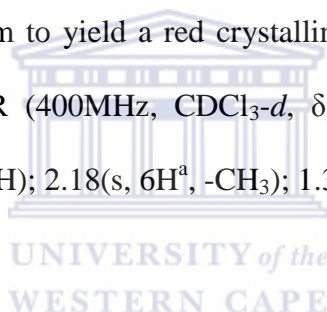
3.5.1 Dichlorotetrakis(dimethylsulfoxide)ruthenium(II), $\text{RuCl}_2(\text{dmsO})_4$

The ruthenium(II) precursor $\text{RuCl}_2(\text{dmsO})_4$, was synthesized by dissolving 2g of $\text{RuCl}_3 \cdot x\text{H}_2\text{O}$ in 50 ml of ethanol according to literature procedure [17]. The reaction was refluxed for 3 hours under nitrogen, using general schlenk techniques. During the reaction a colour change is observed from black to dark green. After the allotted time any unreactive materials is filtered off. The solvent is removed on a rotary evaporator, and thick green oil is observed. 9ml DMSO is added to the reaction mixture and refluxed for another 2hours or more until yellow solids is observed. This is followed by the addition of 60 ml acetone and stored in the fridge overnight. The solvent was removed under reduced pressure using liquid nitrogen and a yellow crystalline powder was collected.

Yield 1.7245g. FT-IR (KBR), ν/cm^{-1} : 1102 (S=O for S bonded DMSO), 921 (S=O for O bonded DMSO), 3014, 2931, (C-H methyl) 655 and 418 (Ru-O and Ru-S).

3.5.2 Dichloro(*p*-cymene)ruthenium(II)dimer, $[\text{RuCl}_2(\textit{p}\text{-cymene})]_2$

The ruthenium(II) dimer was synthesised by dissolving 2g of $\text{RuCl}_3 \cdot x\text{H}_2\text{O}$ in 100 ml of anhydrous ethanol, followed by the addition of α -phellandrene (10 ml) (scheme 4.5) following literature procedure [18]. The reaction was refluxed overnight under nitrogen, using general schlenk techniques. A colour change is observed from black to dark green. The solution is dried in vacuum to a volume of approximately 20ml and stored in the freezer (-4°C) overnight. After the allotted time a red precipitate is filtered off, washed with cold diethyl ether and dried in vacuum to yield a red crystalline powder. Yield 92%, Molecular formula $\text{C}_{20}\text{H}_{28}\text{Cl}_4\text{Ru}_2$, ^1H NMR (400MHz, $\text{CDCl}_3\text{-}d$, δ); 5.48(d, $4\text{H}^{\text{c,c'}}$, $\text{Ar}_{\text{C}_{\text{YE}}}$); 5.35(d, $4\text{H}^{\text{b,b'}}$, $\text{Ar}_{\text{C}_{\text{YE}}}$); 2.94 (sept, 2H^{d} , $-\text{CH}$); 2.18(s, 6H^{a} , $-\text{CH}_3$); 1.3 (d, $12\text{H}^{\text{e,e'}}$, $-(\text{CH}_3)_2$).



3.5.3 Dichloro(1,5-cyclooctadiene)palladium (II), $\text{Pd}(\text{COD})\text{Cl}_2$

A suspension of PdCl_2 (5.00 g, 28.2 mmol) in dry methanol (150 ml) was treated with 1,5-cyclooctadiene (COD) (10.4 ml, 84.6 mmol) and stirred for 48 h at room temperature [19]. During the allotted time a color changed was observed of the suspension from red to yellow. The yellow air stable solid was filtered and collected, continually washed with methanol, and dried under vacuum. Yield: 7.29 g (91%).

3.6 Synthesis of neutral mononuclear and cationic homobimetallic pyridyl/quinolylimine ruthenium(II) complexes

3.6.1 dichloro-[N1,N2-bis((pyridin-2-yl)methylene)ethane-1,2-diamine]ruthenium(II), **C1**

The synthesis of the ruthenium(II) complexes followed reported procedures by Busa *et al.* [21].

To a stirring solution of ligand, L1 (0.41 mmol, 98.0 mg) in dry DCM, the precursor, dichlorotetrakis(dimethylsulfoxide)ruthenium(II) (0.41 mmol, 198.5 mg) which was dissolved separately in dry DCM was added dropwise. The reaction mixture was allowed to stir overnight at room temperature under nitrogen. After the allotted time the volume of the reaction mixture was reduced to 1/5th and neutral aluminium oxide was added, followed by drying under vacuum. A dry neutral aluminium oxide column was packed with DCM. The mobile phase used to elute the first moving blue band were a mixture of DCM and acetone (10:1). The blue solution was collected and dried under vacuum for several hours. Yield: 70 %.

Molecular Formula $C_{14}H_{14}Cl_2N_4Ru$. Solid, Purple-blue. FT-IR (KBR), $\tilde{\nu}/cm^{-1}$: 1590 $\nu(C=N)_{imine}$, 1454 $\nu(C=C)_{ring}$. 1H NMR (500MHz, $CDCl_3-d$) δ 9.26(s, H-7); 9.20(d, H-6, $^3J_{H-H}$ 6.30 Hz); 7.89(t, H-4, $^3J_{H-H}$ 7.48 Hz); 7.80(d, H-3, $^3J_{H-H}$ 7.60 Hz); 4.82(s, H-8). ^{13}C NMR (100MHz, $CDCl_3-d$), δ ppm = 63.1(CH_2 , C-8); 163.9(CH_{imine} , C-7); 153.9(CH_{Ar} , C-2); 150.1(CH_{Ar} , C-6); 137.6(CH_{Ar} , C-4); 125.9(CH_{Ar} , C-5); 121.6(CH_{Ar} , C-3).

Analytical data *calc. for* $C_{14}H_{14}Cl_2N_4Ru$: C, 40.99; H, 3.44; N, 13.66; $[M]^+$: $m/z = 411$; Found: C, 41.23; H, 3.52; N, 14.19.

3.6.2 dichloro-[(N1,N3-bis(pyridin-2-ylmethylene)propane-1,3 diamine]ruthenium(II), C2

The synthesis of complex, C2 follows the same experimental procedure as outlined above. The ligand, L2 was reacted with the precursor dichlorotetrakis(dimethylsulfoxide) ruthenium(II) at room temperature. Yield 64 %. Molecular formula $C_{15}H_{16}Cl_2N_4Ru$. Solid, Purple-blue. FT-IR (KBR), $\tilde{\nu}/cm^{-1}$: 1538 $\nu(C=N)_{imine}$, 1454 $\nu(C=C)_{ring}$. 1H NMR($CDCl_3-d$, δ ppm) δ 9.45(d, H-6, $^3J_{H-H}$ 5.24 Hz); 9.17(s, 7-H); 7.88 (m, H-3 and H-4); 7.64(m, H-5); 4.57(t, H-4, $^3J_{H-H}$ 7.1 Hz); 3.77(m, H-2).

^{13}C NMR (200 MHz, CDCl_3 -*d*), δ ppm= 33.2(CH_2 , C-9); 59.6(CH_2 , C-8); 162.3(CH_{imine} , C-7); 154.5(C_{Ar} , C-2); 121.1(CH_{Ar} , C-3); 136.9 (CH_{Ar} , C-4); 124.6(CH_{Ar} , C-5); 149.9(CH_{Ar} , C-6). Analytical data calc. for $\text{C}_{15}\text{H}_{16}\text{Cl}_2\text{N}_4\text{Ru}$: C, 42.46; H, 3.80; N, 13.20; $[\text{M}]^+$: $m/z = 425$; Found: C, 43.91; H, 4.10; N, 13.86.

3.6.3 dichloro-[N1,N4-bis(pyridin-2-ylmethylene)butane-1,4-diamine]ruthenium(II), C3

The synthesis of complex C3 follows the same experimental procedure as outlined above. The ligand, L3 was reacted with the precursor dichlorotetrakis(dimethylsulfoxide) ruthenium(II) at room temperature. Yield: 73%. Molecular formula $\text{C}_{16}\text{H}_{18}\text{Cl}_2\text{N}_4\text{Ru}$. Solid, Purple-blue. FT-IR (KBR), $\tilde{\nu}/\text{cm}^{-1}$: 1597 $\nu(\text{C}=\text{N})_{\text{imine}}$, 1454 $\nu(\text{C}=\text{C})_{\text{ring}}$. ^1H NMR (500MHz, CDCl_3 -*d*, δ) δ 9.43(d, H-6, $^3J_{\text{H-H}}$ 5.2Hz); 8.96(s, H-7); 7.85(m, H-3 and H-4); 7.57(m, H-5); 4.73(m, H-8); 2.47(m, H-9). ^{13}C NMR (200 MHz, CDCl_3 -*d*), δ ppm= 29.0(CH_2 , C-9); 61.9(CH_2 , C-8); 162.1(CH_{imine} , C-7); 154.7 (C_{Ar} , C-2); 150.5(CH_{Ar} , C-6); 137.1(CH_{Ar} , C-4); 124.7(CH_{Ar} , C-5); 121.5(CH_{Ar} , C-3). Analytical data calc. for $\text{C}_{16}\text{H}_{18}\text{Cl}_2\text{N}_4\text{Ru}$: C, 43.84; H, 4.14; N, 12.78; $[\text{M}]^+$: $m/z = 439$; Found: C, 43.31; H, 4.83; N, 12.65.

3.6.4 dichloro-[N1,N2-bis((quinolin-2-yl)methylene)ethane-1,2-diamine]ruthenium(II), C4

The synthesis of complex C4 follows the same experimental procedure as outlined above. The ligand, L4 was reacted with the precursor dichlorotetrakis(dimethylsulfoxide) ruthenium(II) at room temperature. After the allotted time a dark green precipitate formed. The precipitate was collected, continuously washed with dry DCM and dried under vacuum. Yield: 80 %. Molecular formula $\text{C}_{22}\text{H}_{18}\text{Cl}_2\text{N}_4\text{Ru}$. Solid, Green. FT-IR (KBR), $\tilde{\nu}/\text{cm}^{-1}$: 1520 $\nu(\text{C}=\text{N})_{\text{imine}}$, 1443 $\nu(\text{C}=\text{C})_{\text{ring}}$. ^1H NMR (500MHz, CDCl_3 -*d*) δ 9.52(s, H-11); 8.91(d, H-3, $^3J_{\text{H-H}}$ 8.0 Hz); 8.37(d, H-9, $^3J_{\text{H-H}}$ 7.7 Hz); 7.90(m, H-8, H-9); 7.88(t, H-4, $^3J_{\text{H-H}}$ 7.5 Hz); 7.39(t, H-6, $^3J_{\text{H-H}}$ 7.4 Hz); 4.90(s, H-12).

^{13}C NMR (100 MHz, CDCl_3-d), δppm = 164.6(CH_{imine} , C-11); 154.9(CH_{Ar} , C-10); 148.1 (CH_{Ar} , C-2); 136.9(CH_{Ar} , C-5); 129.6(CH_{Ar} , C-3); 129.3(CH_{Ar} , C-4); 128.9(CH_{Ar} , C-6); 127.5(CH_{Ar} , C-9); 127.3(CH_{Ar} , C-8); 118.5(CH_{Ar} , C-7); 62.1(CH_2 , C-12). Analytical data *calc. for* $\text{C}_{22}\text{H}_{18}\text{Cl}_2\text{N}_4\text{Ru}$: C, 51.77; H, 3.55; N, 10.98; $[\text{M}]^+$: $m/z = 511$. *Found*: C, 51.98; H, 3.67; N, 11.03.

3.6.5 dichloro-[N1,N3-bis(quinolin-2-ylmethylene)propane-1,3-diamine]ruthenium(II), C5

The synthesis of complex C5 follows the same experimental procedure as outlined above. The ligand (L5) was reacted with the precursor dichlorotetrakis(dimethylsulfoxide) ruthenium(II) at room temperature. Yield: 64%. Molecular Formula $\text{C}_{23}\text{H}_{20}\text{Cl}_2\text{N}_4\text{Ru}$. Solid, Green. FT-IR (KBR), $\tilde{\nu}/\text{cm}^{-1}$: 1520 $\nu(\text{C}=\text{N})_{\text{imine}}$, 1442 $\nu(\text{C}=\text{C})$.

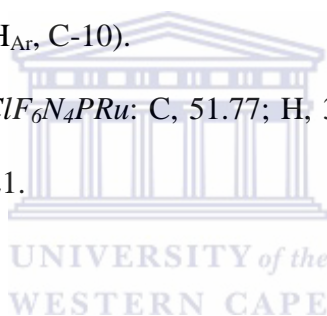
^1H NMR (400 MHz, CDCl_3-d) δ 9.50(s, H-11); 8.91(d, H-3, $^3J_{\text{H-H}}$ 8.4 Hz); 8.45(d, 9H, $^3J_{\text{H-H}}$ 7.9 Hz); 7.90(m, 8-H, 9-H); 7.85(t, H-4, $^3J_{\text{H-H}}$ 7.6 Hz); 7.34 (t, H-6, $^3J_{\text{H-H}}$ 7.3 Hz) 3.97(t, H-12, $^3J_{\text{H-H}}$ 6.4 Hz), 2.31(q, H-13, $^3J_{\text{H-H}}$ 6.0 Hz). ^{13}C NMR (100 MHz, CDCl_3-d), δppm = 163.5(CH_{imine} , C-11); 159.2(CH_{Ar} , C-10); 148.1(CH_{Ar} , C-2); 136.8(CH_{Ar} , C-5); 130.4 (CH_{Ar} , C-3) 129.8(CH_{Ar} , C-4); 129.2(CH_{Ar} , C-6); 127.9(CH_{Ar} , C-9); 127.6(CH_{Ar} , C-8); 118.4 (CH_{Ar} , C-7); 46.6(CH_2 , C-12) 27.8(CH_2 , C-13). Analytical data *calc. for* $\text{C}_{23}\text{H}_{20}\text{Cl}_2\text{N}_4\text{Ru}$: C, 52.68; H, 3.84; N, 10.68; $[\text{M}]^+$: $m/z = 525$; *Found*: C, 53.9; H, 3.72; N, 10.52.

3.6.6 Synthesis of cationic homobimetallic ruthenium(II) complex, C6

The precursor $[\text{Ru}(\eta^6\text{-p-Pr}^i\text{C}_6\text{H}_4\text{Me})\text{Cl}_2]_2$ (0.191 g, 0.312 mmol) was stirred at room temperature for 3 hours in ethanol, followed by filtering of any unreactive material. The ligand (L3) (0.0830 g 0.312 mmol) in (5 ml) ethanol was added dropwise to the stirring solution and allowed to stir overnight. After the allotted time the solution was filtered and the filtrate was concentrated to approximately 10 ml.

TIPF₆ was added to the reaction mixture and allowed to stir at room temperature for 3 hours, a precipitate was observed to form almost immediately. The reaction mixture was stored in the fridge (-4°C) overnight to completely precipitate out the product. The product was filtered off, washed with diethyl ether and dried under reduced pressure. Yield 85 %. Molecular Formula C₂₂H₁₈ClF₆N₄PRu. Solid, Brown, MP 182-184°C. FT-IR (KBR), $\tilde{\nu}/\text{cm}^{-1}$: 1590 ν (C=N)_{imine}, 1460 ν (C=C)_{ring}. ¹H NMR (400 MHz, CDCl₃-d, δ ppm) δ 5.83(t, ³J_{H-H} 6.3 Hz, Ar_{CYE}); 6.10(dd, 4H, ³J_{H-H} 6.3 Hz, Ar_{CYE}); 8.10(m, ³J_{H-H} 5.7 Hz, Pyr); 8.19(m, 4H, 5H ³J_{H-H} 7.7 Hz); 8.66(d, ³J_{H-H} 7.6 Hz); 9.46 (t, H-7, ³J_{H-H} 5.8 Hz). ¹³C NMR (100 MHz, CDCl₃-d) δ ppm = 23.5, 22.6, 24.5 (CH₃, C_{CYE}); 166.23(CH_{imine}, C-7); 156.1(C_{Ar}, C-2); 123.1(CH_{Ar}, C-3); 135.2(CH_{Ar}, C-4); 132.3(CH_{Ar}, C-5); 154.3(CH_{Ar}, C-6); 128.6(CH_{Ar}, C-7); 127.3(CH_{Ar}, C-8); 131.0(CH_{Ar}, C-9); 131.2(CH_{Ar}, C-10).

Analytical data *calc. for C₂₂H₁₈ClF₆N₄PRu*: C, 51.77; H, 3.55; N, 10.98; [M]⁺: m/z = 838; *Found*: C, 52.03; H, 4.02; N, 11.21.



3.7 Synthesis of neutral bimetallic Palladium (II) pyridyl-imine complexes

3.7.1 dichloro-[N1,N2-bis((pyridin-2-yl)methylene)ethane-1,2-diamine]palladium(II), C7

The synthesis of the bimetallic palladium (II) complexes followed reported procedures by Sibanyoni *et al.* with some modification [22]. To a stirring solution of ligand, L1 (0.34 mmol, 80 mg) in dry DCM at room temperature the precursor, Dichloro(1,5-cyclooctadiene)palladium(II) (0.67 mmol, 191 mg) was added dropwise, upon addition the solution changed from colourless to yellow. A precipitate was observed to form after 10 minutes of stirring. The reaction mixture was allowed to stir further for 4 hours, to ensure the completion of the reaction. After the allotted time the reaction mixture was reduced to 1/5 th followed by the addition of diethyl ether or hexane to further precipitate out the yellow solids and dried under vacuum for several hours. Yield 70 %. Molecular Formula C₁₄H₁₄C₁₄N₄Pd₂.

Solid, yellow. FT-IR (KBR), $\tilde{\nu}/\text{cm}^{-1}$; 1588 ν (C=N)_{imine}, ν (C=N)_{ring}, 1442 ν (C=C). ¹H NMR (400 MHz, DMSO-*d*₆) δ 8.93(d, H-6, ³*J*_{H-H} 7.2Hz); 8.76(s, H-7); 8.33(d, H-3, ³*J*_{H-H} 6.1Hz); 8.54(t, H-4, ³*J*_{H-H} 6.4Hz); 7.28(t, H-5, ³*J*_{H-H} 5.4Hz), 4.21(s, H-8). Analytical data *calc. for* C₁₄H₁₄Cl₂N₄Pd₂: C, 28.36; H, 2.38; N, 9.45 [M]⁺: m/z = 593; *Found*: C, 26.55; H, 2.64; N, 8.72.

3.7.2 dichloro-[N1,N3-bis(pyridin-2-ylmethylene)propane-1,3-diamine]palladium(II), C8

The synthesis of complex C8 follows the same experimental procedure as outlined above. The ligand L2 was reacted with the precursor dichloro(1,5-cyclooctadiene)palladium(II) at room temperature. Yield 68%. Molecular Formula C₁₅H₁₆Cl₂N₄Pd₂. Solid, yellow, FT-IR (KBR), $\tilde{\nu}/\text{cm}^{-1}$; 1576 ν (C=N)_{imine}, 1438 ν (C=C).

¹H NMR (400 MHz DMSO-*d*₆) δ 8.94(d, H-6, ³*J*_{H-H} 7.3Hz); 8.62(s, H-7); 8.41(d, H-3, ³*J*_{H-H} 6.3Hz); 8.22(t, H-4, ³*J*_{H-H} 6.2Hz); 7.62(t, H-5, ³*J*_{H-H} 5.2Hz); 3.82 (t, H-8, ³*J*_{H-H} 7.3Hz); 2.16 (m, H-9). Analytical data *calc. for* C₁₅H₁₆Cl₂N₄Pd₂: C, 29.68; H, 2.66; N, 9.23; [M]⁺: m/z = 607. *Found*: C, 30.69; H, 2.49; N, 7.46.

3.7.3 dichloro-[N1,N4-bis(pyridin-2-ylmethylene)butane-1,4-diamine]palladium(II), C9

The synthesis of complex C9 follows the same experimental procedure as outlined above. The ligand, L3 was reacted with the precursor dichloro(1,5-cyclooctadiene)palladium(II) at room temperature. Yield: 76 %. Molecular Formula C₁₆H₁₈Cl₂N₄Pd₂. Solid, yellow. FT-IR (KBR), $\tilde{\nu}/\text{cm}^{-1}$; 1661 ν (C=N)_{imine}, 1480 ν (C=C). ¹H NMR (400 MHz, DMSO-*d*₆) δ 8.93(d, H-6, ³*J*_{H-H} 5.6Hz); 8.63(s, H-7); 8.07(d, H-3 ³*J*_{H-H} 6.5Hz); 8.33(t, H-4, ³*J*_{H-H} 7.4Hz); 7.85(t, H-5, ³*J*_{H-H} 6.5Hz); 3.71(m, H-8); 1.79(m, H-9).

Analytical data *calc. for* C₁₆H₁₈Cl₂N₄Pd₂: C, 30.95; H, 2.92; N, 9.02; [M]⁺: m/z = 624; *Found*: C, 30.12; H, 3.34; N, 8.99.

3.7.4 dichloro-[N1,N5-bis(pyridin-2-ylmethylene)pentane-1,5-diamine]palladium(II),C10

The synthesis of complex C11 follows the same experimental procedure as outlined above. The ligand, L6 was reacted with the precursor dichloro(1,5-cyclooctadiene)palladium(II) at room temperature. Yield:72%. Molecular Formula $C_{17}H_{20}N_4Cl_2Pd_2$. Solid, yellow. FT-IR (KBR), $\tilde{\nu}/\text{cm}^{-1}$:1592 ν (C=N)_{imine}, 1452 ν (C=C). ^1H NMR (400 MHz, DMSO- d_6) δ 8.79(s, H-7); 9.13(d, $^3J_{\text{H-H}}$ 8.1Hz); 8.26(d, $^3J_{\text{H-H}}$ 7.4Hz); 8.51(t, H-4, $^3J_{\text{H-H}}$ 7.6Hz); 8.03(t, H-5, $^3J_{\text{H-H}}$ 7.6Hz); 3.90(t, H-8, $^3J_{\text{H-H}}$ 5.2Hz); 1.98(m, H-9); 1.51(m, H-10). Analytical data *calc. for* $C_{17}H_{20}N_4Cl_2Pd_2$: C, 32.15; H, 3.17; N, 8.82. $[\text{M}]^+$: $m/z = 636$; *Found*: C,32.75; H, 3.02; N,7.25.

3.8 Procedure for the oxidative cleavage of styrene by pyridyl and quinolyl-imine ruthenium(II) complexes

The neutral and cationic mono- and homobimetallic ruthenium(II) catalysts were evaluated for the oxidative cleavage of styrene. The reaction was carried in a biphasic CCl_4 - CH_3CN - H_2O (1:1:2 v/v) solvent system, using NaIO_4 as a co-oxidant. The oxidative cleavage of styrene was carried out by the addition of styrene (0.556 mmol), catalyst (0.002782 mmol), and NaIO_4 (2.782 mmol) to the biphasic solvent system [CH_3CN (5 cm^3), CCl_4 (5 cm^3), and H_2O (10 cm^3)]. The reaction mixture was stirred at room temperature for 2 hours. After the allotted time the reaction mixture was extracted with diethyl ether (3x10 ml), the organic layer was evaporated under reduced pressure and analyse with FT-IR and ^1H NMR.

3.9 Procedure for the Heck coupling reaction of iodobenzene with methylacrylate by bimetallic Palladium (II) complexes

The Heck reaction was carried out with iodobenzene, methylacrylate and triethylamine as a base in a 1:1:1 ratio and added to a solution of the bimetallic palladium (II) catalysts (1 mol %) in anhydrous DMF (10 ml) at 110 °C (scheme 2.1). Mesitylene was used as an internal standard and the reaction was heated for 24 hrs in a 50 ml flask equipped with a reflux condenser and a magnetic stirring bar. The activity of the catalyst was confirmed by GC analysis.



References

1. Perrin DD, Armarego WL, *Purification of Laboratory Chemicals*, Third Ed., New York, Pergamon, **1998**.
2. Colthup NB, Daly LH, Wiberley SE, *Introduction to Infrared and Raman Spectroscopy*, Third Ed., Elsevier, **1990**.
3. Kutz M, *Handbook of Materials Selection*, John Wiley & Sons, Technology & Engineering, **2002**, 607.
4. http://chemwiki.ucdavis.edu/Physical_Chemistry/Spectroscopy/Vibrational_Spectroscopy/Infrared_Spectroscopy/How_an_FTIR_Spectrometer_Operates, accessed on 26/08/15
5. Atta-ur-Rahman, Choudhary MI, *Applications of NMR Spectroscopy*, Elsevier, Science **2015**, *1*, 58.
6. http://sustainability.sellafieldsites.com/resources/labmouse/chemistry_a2/2908.php, accessed on 26 August 2015.
7. Clark BJ, Frost T, Russell MA, *UV Spectroscopy: Techniques, instrumentation and data handling*, Springer Science & Business Media, Science, *4*, **1993**.
8. Morrell DG, *Catalysis of Organic Reactions*, CRC. Press., Science, **2002**, 593.
9. Tabaza W, PhD dissertation, University of the Free State, **2014**.
10. Muda R, Lewis E, O’Keeffe S, Dooly G, Clifford J, *Procedia. Chem.*, **2009**, *1*, 593.
11. (a) Kar A, *Pharmaceutical Drug Analysis*, New Age International, Drugs, **2007**, 194; (b) Gabbott P, *Principles and Applications of Thermal Analysis*, John Wiley & Sons, Science, **2008**.
12. Broido A, *J. Poly. Sci.,: Part A-2*, **1969**, *7*, 1761.
13. <http://www.slideshare.net/KalsoomMohammed/thermogravimetry-analysis-tga>, accessed on 26 August 2015.

14. Haddleton DM, Duncalf DJ, *Eur. J. Inorg. Chem.*, **1998**, 1799.
15. Chen R, Bacsa J, Mapolie SF, *Polyhedron.*, **2003**, 22, 2855.
16. Cloete J, Mapolie SF, *J. Mol. Catal. A:*, **2006**, 243, 221.
17. Bratsos I, Alessio E, *Inorg. Synth.*, **2010**, 35, 148.
18. Fonseca J, p-Cymene, University of Lisboa (Portugal), PhD dissertation, **2011**.
19. Wiedermann J, Mereiter K, Kirchner K, *J. Mol. Catal. A: Chem.*, **2006**, 257, 67.
20. Pal S, Pal S, *Polyhedron.*, **2003**, 22, 867.
21. Busa AV, University of the Western Cape (South Africa), MSc dissertation, **2012**.
22. Sibanyoni JM, University of the Western Cape (South Africa), MSc dissertation, **2007**.

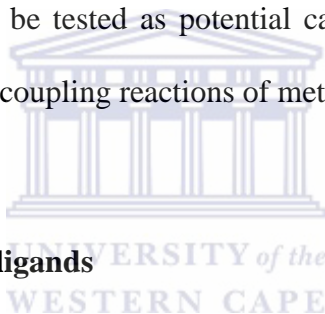


CHAPTER 4

4.0 Results and Discussion

Chapter overview

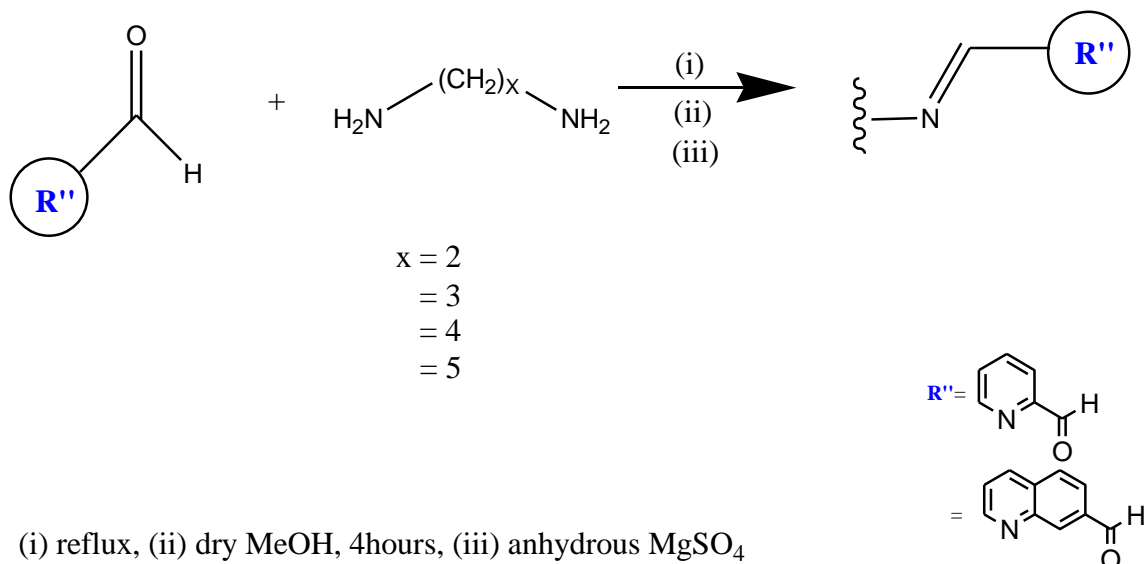
This chapter gives a brief introduction to pyridyl and quinolyl-imine ligands as viable Schiff bases as well as their ruthenium and palladium complexes. Thereafter we report and discuss the results obtained for the characterization of pyridyl and quinolyl-imine ligands, ruthenium (II) and palladium (II) metal precursors and neutral mononuclear and cationic homobimetallic ruthenium(II) and bimetallic palladium(II) complexes by techniques like FT-IR, ^1H and ^{13}C NMR, Elemental analysis, GC-MS and UV/Vis. The prepared ruthenium(II) and palladium (II) complexes will subsequently be tested as potential catalyst precursor for the oxidative cleavage of alkenes and the Heck coupling reactions of methyl acrylate with iodobenzene.



4.1 Pyridyl and Quinolyl-imine ligands

4.1.1 Introduction

The targeted pyridyl and quinolyl ligands belong to a family of diimines [1]. The synthesis of the N-donor pyridyl and quinolyl-imine ligands were carried out by the reaction of 2-pyridinecarboxaldehyde/2-quinolinecarboxaldehyde with *n*-propylamine in a 2:1 ratio, followed by the addition of MgSO_4 to quench any water formed during the reaction (scheme 4.1). The corresponding ruthenium(II) and palladium(II) complexes were synthesized by the reaction of the ligands with their respective metal precursors $\text{RuCl}_2(\text{dmsO})_4$, $\text{Pd}(\text{cod})\text{Cl}_2$ or $[\text{RuCl}_2(p\text{-cymene})]_2$.



Scheme 4.1: A synthetic pathway for pyridyl and quinolyl-imine ligands, L1-L6

The diimine ligands coordinate to the metals readily forming stable and active complexes. The pyridyl and quinolyl-imine complexes were characterised by the functional group carbon-nitrogen double bond, C=N.

Literature reports on the synthesis of pyridyl and quinolyl-imine ruthenium(II) complexes are rare as well as their catalytic activity towards the oxidative cleavage of olefins. Nonetheless a number of literature reports on nickel and copper complexes are available [2, 3]. The pyridyl-imine palladium (II) complexes have been previously reported as active catalyst towards Heck coupling reactions. Chen *et al.*, reported the synthesis and characterization of 2-iminopyridyl palladium dichloride complexes [4]. The complexes was synthesized by the reaction of pyridyl-imine ligand and PdCl₂(CH₃CN)₂ in dry DCM at room temperature. The characterization of the complexes was confirmed by the presence of the C=N moiety in both the ¹H NMR and FT-IR spectra. The Heck reaction of arylbromides and olefins was successfully achieved with the formation of two isomers when electron-rich substrates are employed.

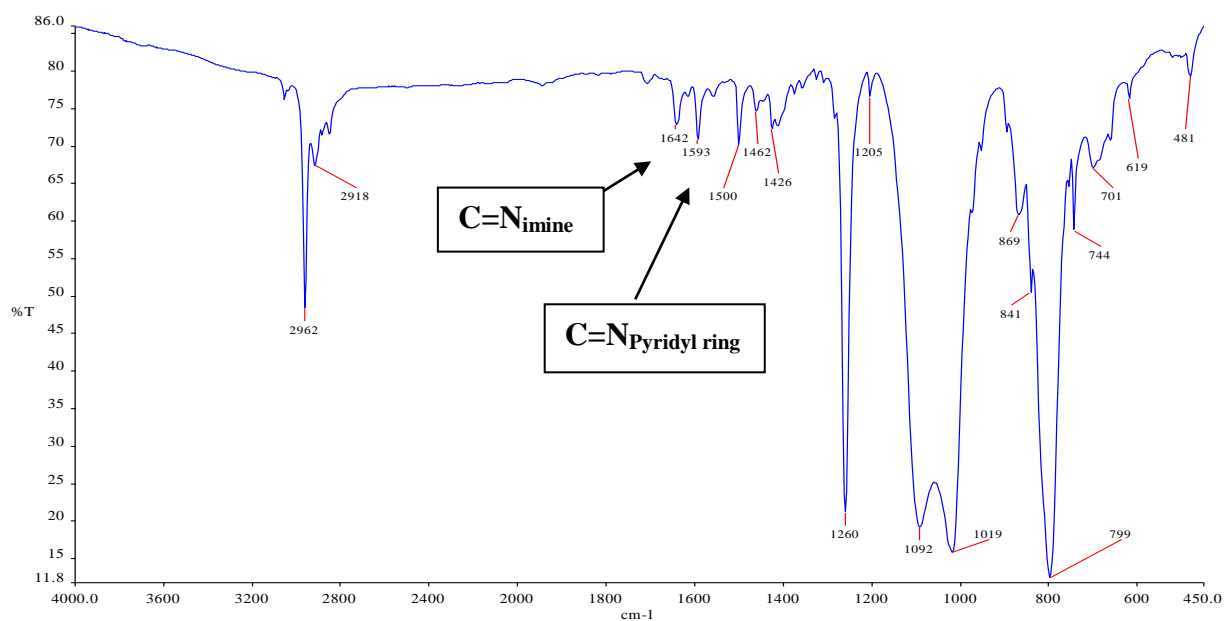


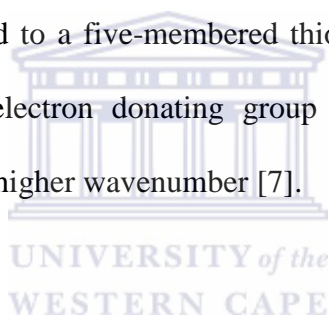
Figure 4.2: FT-IR of N1,N2-bis((quinolin-2-yl)methylene)ethane-1,2-diamine, L4

Table 4.1: FT-IR data for tetradentate pyridyl and quinolyl-imine ligands, L1-L6

Ligand	$\nu(\text{C}=\text{N})_{\text{imine}}$ cm^{-1}	$\nu(\text{C}=\text{N})_{\text{ring}}$ cm^{-1}	$\nu(\text{C}=\text{C})_{\text{ring}}$ cm^{-1}
L1 ^a	1647	1584	1564
L2 ^b	1650	1580	1452
L3 ^a	1639	1586	1566
L4 ^a	1642	1593	1500
L5 ^b	1620	1508	1452
L6 ^b	1648	1563	1479

^aSolids were recorded using KBR pellets, ^bOils were recorded using nujol mulls on NaCl plates.

Fourier transform infrared spectroscopy was used to confirm the formation of the imine functional group and the disappearance of the carbonyl band (1700 cm^{-1}) of the starting aldehyde. The solids, ligands L1, L3 and L4 were recorded using KBr pellets and the oils ligands L2, L5 and L6 were recorded using nujol mulls on NaCl plates. The IR spectra of the pyridyl-imine ligands gave three strong stretching frequencies in the range $1639\text{-}1650\text{ cm}^{-1}$, $1563\text{-}1586\text{ cm}^{-1}$ and $1452\text{-}1566\text{ cm}^{-1}$, which were assigned to the azomethine fragment, $\nu(\text{C}=\text{N})$ vibration, the pyridine-ring $\nu(\text{C}=\text{N})$ and $\nu(\text{C}=\text{C})$ vibrations respectively. Ebralidze *et al.* observed the azomethine C=N moiety in the range $1647\text{-}1649\text{ cm}^{-1}$ for the free pyridyl-imine ligands, which were reported to be in the range of previously reported values [6]. Radebe *et al.* reported similar values for the C=N functional group in the range of $1635\text{-}1650\text{ cm}^{-1}$ for their pyridyl-imine ligands linked to a five-membered thiophene ring, the presence of both the electron withdrawing and electron donating group in the thiophene ring gave the stretching frequency at a slightly higher wavenumber [7].

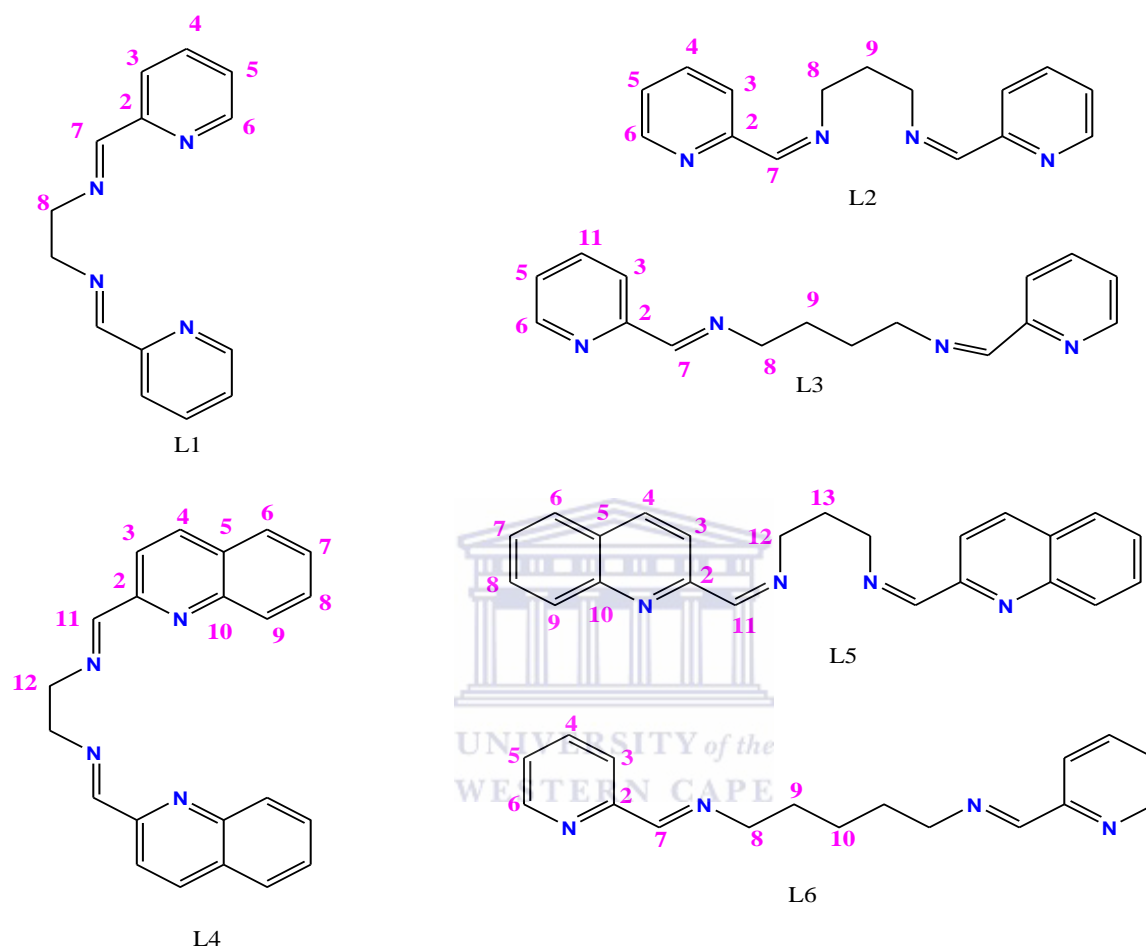


The quinolyl-imine ligands showed three stretching frequencies in the range $1620\text{-}1642\text{ cm}^{-1}$, $1508\text{-}1593\text{ cm}^{-1}$, $1452\text{-}1500\text{ cm}^{-1}$ which were attributed to the azomethine fragment, $\nu(\text{C}=\text{N})$ vibration, the pyridine-ring $\nu(\text{C}=\text{N})$ and $\nu(\text{C}=\text{C})$ vibrations respectively. The azomethine fragment stretching frequencies of the quinolyl-imine ligands appeared at a lower frequency compared to their analogues pyridyl-imines, due to the extra conjugation and an increase in the electron delocalization (resonance) around the quinoline ring. Patra *et al.* observed a strong frequency at 1643 cm^{-1} for quinolyl-imine which were assigned to the C=N moiety, the ligands was synthesised by using the aldehyde 4-quinoline-carboxaldehyde as the starting material [8]. Busa *et al.* also reported a strong frequency at 1646 cm^{-1} for quinolyl-imine ligands which are in strong agreement with our reported values and in the range of previously reported values [9].

The absence of the C=O band in the 1700 cm^{-1} region, and the presence of the imine functional group in the spectra of both pyridyl and quinolyl-imine ligands is a strong indication of the successful condensation reaction between the starting aldehydes and primary amines to yield the corresponding imines (scheme 4.1) [10]. The FT-IR spectra also show bands in the 2845-2856 cm^{-1} and 3042-3038 cm^{-1} region which is attributed to the saturated C-H of the aliphatic and the unsaturated -CH of the pyridine and quinoline ring respectively. The FT-IR data of all the ligands appear within the range of reported literature [8, 9].

From table 4.1 a significant difference in the azomethine stretching vibration of the C=N moiety for the pyridyl ligand L1 compared to the quinolyl ligand L4 was observed at 1647 cm^{-1} and 1642 cm^{-1} respectively. The two compounds differ in the starting aldehyde employed during the synthesis of the ligands; for ligand L1 the aldehyde 2-pyridinecarboxaldehyde was used whereas in L4 the aldehyde 2-quinolinecarboxaldehyde was used. The differences in the C=N stretching frequency thus arise from an increase in the conjugation of the quinoline ring in ligand L4 resulting in the lowering of the stretching frequency. The spectra of pyridyl ligand L2 and quinolyl ligand L5 also gave a difference in the stretching vibration of the C=N moiety at 1650 cm^{-1} and 1620 cm^{-1} respectively. Similar to previously mentioned ligands the differences in the C=N stretching frequency arises from the extra conjugation in the starting quinoline ring for ligand L5 compared to ligand L2, resulting in the lowering of the stretching frequency. The spectra of pyridyl ligands L3 and L6 gave a strong stretching frequency at 1639 cm^{-1} and 1648 cm^{-1} respectively. The above mentioned ligands are structurally similar with the only difference is in the alkyl chain linker; for ligand L3 four carbons separates the pyridyl ring, whereas in ligand L6 five carbon atoms separates the pyridyl ring.

The differences in the C=N stretching frequency is due to an increase in the alkyl chain for ligand L6 compared to ligand L3, since stronger bonds exist in L6 more energy is required to cause a vibration, hence arising in a shift to a higher wavenumber compared to L3.



Scheme 4.2: A schematic representation of synthesised diimine ligands (L1-L6), with numbering for NMR analysis

4.1.3 ^1H NMR spectroscopic analysis of pyridyl and quinolyl-imine ligands

The following ^1H NMR spectra (figure 4.3 and 4.4) were obtained for pyridyl and quinolyl-imine ligands. The ^1H NMR of the remaining ligands follows a similar spectral pattern and are provided in Appendix 5-7. The ^1H NMR spectra of pyridyl/quinolyl-imine ligands were recorded in CDCl_3 solutions at 25°C to probe the solution chemical environment. The chemical shift values of the protons are summarized in table 4.2 and the proton numbering is shown above in scheme 4.2.

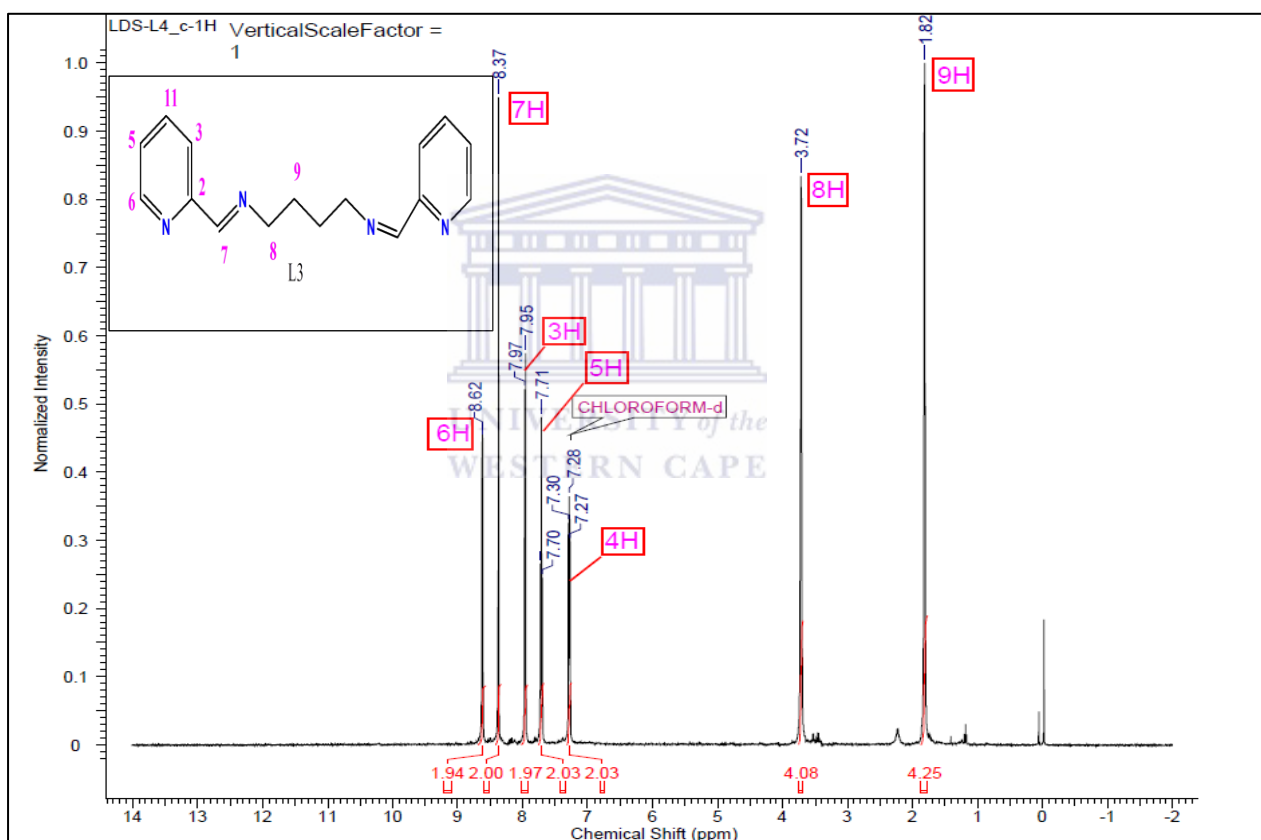


Figure 4.3: ^1H NMR of N1,N4-bis(pyridin-2-ylmethylene)butane-1,4-diamine, L3

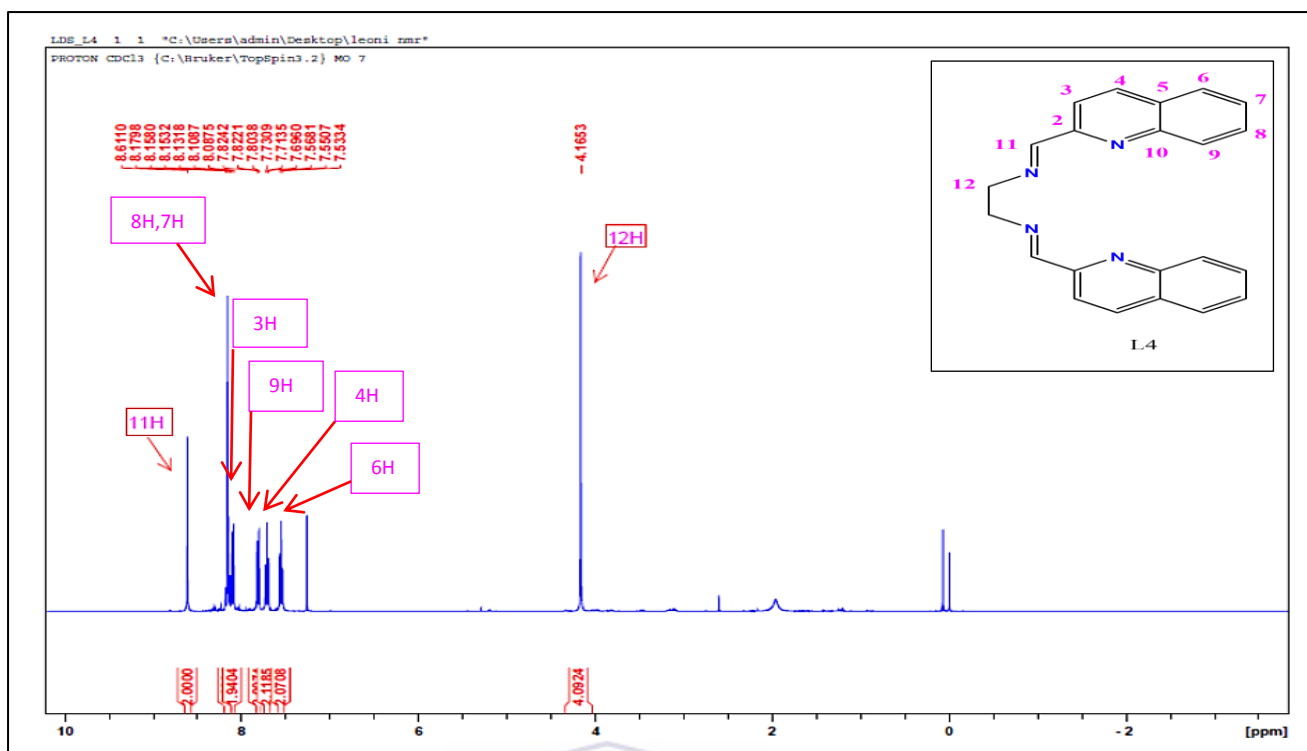


Figure 4.4: ¹H NMR of N1,N2-bis((quinolin-2-yl)methylene)ethane-1,2-diamine, L4.

Table 4.2: ¹H NMR spectral data of tetradentate pyridyl and quinolyl-imine ligands **L1-L6**, recorded in CDCl₃ at 25°C

Ligand	HC=N(δ ppm)	Aromatic protons(δppm)	Methylene protons(δppm)
L1	8.42	7.30-8.63 (m,8H,Ar-H)	4.07 (s,4H)
L2	8.43	7.31-8.66 (m,8H,Ar-H)	3.83 (t,4H); 2.22 (q,2H)
L3	8.37	7.29-8.64 (m,8H,Ar-H)	3.72 (m,4H); 1.82 (m,4H)
L4	8.61	7.55-8.17 (m,12H,Ar-H)	4.17 (s,4H)
L5	8.62	7.59-8.19 (m,12H,Ar-H)	3.94 (t,4H); 2.29 (q,2H)
L6	8.35	8.63-7.28 (m,8H,Ar-H)	3.67 (t,4H); 1.78 (m,4H); 1.47 (m,2H)

The ligands were characterised with ^1H NMR spectroscopy to obtain detailed information of the ligands functional group and their chemical environment. The ^1H NMR spectra revealed the azomethine proton (H-7) for pyridyl-imine ligands L1, L2, L3 and L6 as a singlet in the range, 8.35-8.43 ppm. The azomethine proton appears more upfield (diamagnetic shift) compared to their respective starting aldehyde, because there is an increase in the electron density of the imine moiety, which shields the protons. The proton (H-6) is observed as a doublet within the range 8.61-8.63 ppm and appears downfield (paramagnetic shift) due to the electron withdrawing effect of the nitrogen of the pyridine ring H-6 experiences, compared to the other protons. Proton (H-3) gave rise to a doublet and appears within the range 7.96-7.98 ppm, the proton is shielded (diamagnetic shift) compared to (H-6), therefore appear upfield [11]. Protons (H-4) and (H-5) appears in the range 7.28-7.73 ppm and gave rise to triplets in the ^1H NMR spectra. Ebralidze *et al.* reported the presence of the azomethine proton for pyridyl-imine ligands in the 8.23-8.43 ppm region which was reported to agree with previously reported values [6]. The azomethine proton (H-11) for the quinolyl-imine ligands L4 and L5 is observed as a singlet at 8.35-8.62 ppm. Similar to the pyridyl-imine ligands the quinolyl-imine ligands experiences an upfield shift compared to their starting aldehyde, because there is an increase in the electron density in the imine moiety which shields the protons. Munro *et al.*, reported the azomethine peak as a singlet at 8.92 for their quinolyl-imine ligand, the ligand was synthesized by using the starting aldehyde isoquinoline-1-carbaldehyde giving rise to a different geometry compared to our synthesized ligands [12]. A trend is observed in the ^1H NMR spectra of ligands L1 and L4, the methylene protons appear as singlets at 4.07 ppm (H-8) and 4.17 ppm (H-12) respectively.

The methylene protons of both ligands L1 and L4 were observed at a lower field and are now deshielded compared to their starting primary amine; due to it now being adjacent to the azomethine fragment the ligands experiences the strong electron withdrawing effect of the azomethine nitrogen resulting in a decrease in the electron density around the methylene group protons. Methylene group protons for ligands L2 appear as a triplet and quintet at 3.83 ppm (H-8) and 2.22 ppm (H-9) respectively, the former is assigned to the protons of the terminal methylene group protons and the latter is assigned to the middle methylene group protons of the trimethylene fragment. The terminal methylene group protons (H-8) is more deshielded compared to the middle methylene group protons (H-9) due to the electron withdrawing effect of nitrogen which decreases the electron density around the protons. The observations made are similar to those reported elsewhere [6, 9]. The intensity of the triplet was observed as twice of that of the quintet indicating that the two halves are magnetically equivalent. The alkyl linker for ligand L3 appeared at 3.72 ppm (H-8) and 1.82 ppm (H-9) respectively and was observed as multiplets. The peak at the lower field is assigned to the methylene group protons (H-8) which is attached to the azomethine nitrogen resulting in (H-8) being deshielded, the peak at a higher field is assigned to the terminal (H-9) methylene group protons and is more shielded compared to (H-8). The peak intensity of (H-8) is slightly higher than (H-9). Similar trends were observed by Busa *et al.* [9] and Pal *et al.* [13] for the pyridyl and quinolyl-imines. The presence of the azomethine protons confirms the successful synthesis of the diimines as well as the absence of the CHO peak at 10 ppm in the ¹H NMR spectra of all the ligands. The absence of the CHO peak also confirms the purity of the ligands. From table 4.2 a significant difference in the azomethine proton for the pyridyl ligand L1 compared to the quinolyl ligand L4 was observed at 8.42 ppm and 8.61 ppm respectively.

The two compounds differ in the starting aldehyde used in the synthesis; for ligand L1 the aldehyde 2-pyridinecarboxaldehyde was used whereas in L4 the aldehyde 2-quinolinecarboxaldehyde was used. The differences in the azomethine proton is attributed to the extra conjugation of the quinoline ring in ligand L4 resulting in the shift to a lower field and is deshielded. The spectra of pyridyl ligand L2 and quinolyl ligand L5 also gave a difference in the chemical shifts of the C=N moiety at 8.43 ppm and 8.62 ppm respectively. Similarly the differences in the C=N chemical shifts arises from the extra conjugation and delocalised p electrons in the starting quinoline ring for ligand L5 compared to ligand L2, causing the protons to absorb at a lower magnetic field resulting in the azomethine proton appearing at a lower field and deshielded compared to L2. The azomethine proton for quinolyl-imine ligands L4 and L5 appear at a similar chemical shifts, since these ligands are structurally similar and experiences the same magnetic field. The pyridyl-imine ligands L1 and L2 also appear at a similar chemical shift; again these ligands are structurally similar and will therefore experience more or less the same magnetic field. The pyridyl-imine ligands L3 and L6 also appear at a similar chemical shift; again these ligands are structurally similar with only a difference of one carbon atom in the alkyl chain and will therefore experience more or less the same magnetic field. However the HC=N of the pyridyl-imine ligands L3 and L6 appear upfield compared to the previously mentioned pyridyl-imine ligands (L1, L2), this could be due to the significant increase of the alkyl chain linker resulting in the ligands being shielded. Also the conformational feature of L3 and L6 slightly differ from L1 and L2.

4.1.4 ^{13}C NMR spectroscopic analysis of pyridyl and quinolyl-imine ligands

The ligands were further characterised with the ^{13}C NMR spectroscopy. The following ^{13}C NMR spectra (figure 4.5 and 4.6) are a typical example of the spectra obtained for pyridyl and quinolyl-imine ligands. The other ^{13}C NMR spectra for the ligands are given in Appendix 8-10. The chemical shift values of the carbons are summarized in table 4.3. The ^{13}C NMR spectroscopy assignment for ligands L1-L6 was carried out by means of chemical shift of the relevant protons. The ^{13}C NMR spectra of pyridyl and quinolyl-imine ligands were recorded in CDCl_3 at 25°C solutions to probe the solution structures. The carbon numbering is shown above in scheme 4.2.

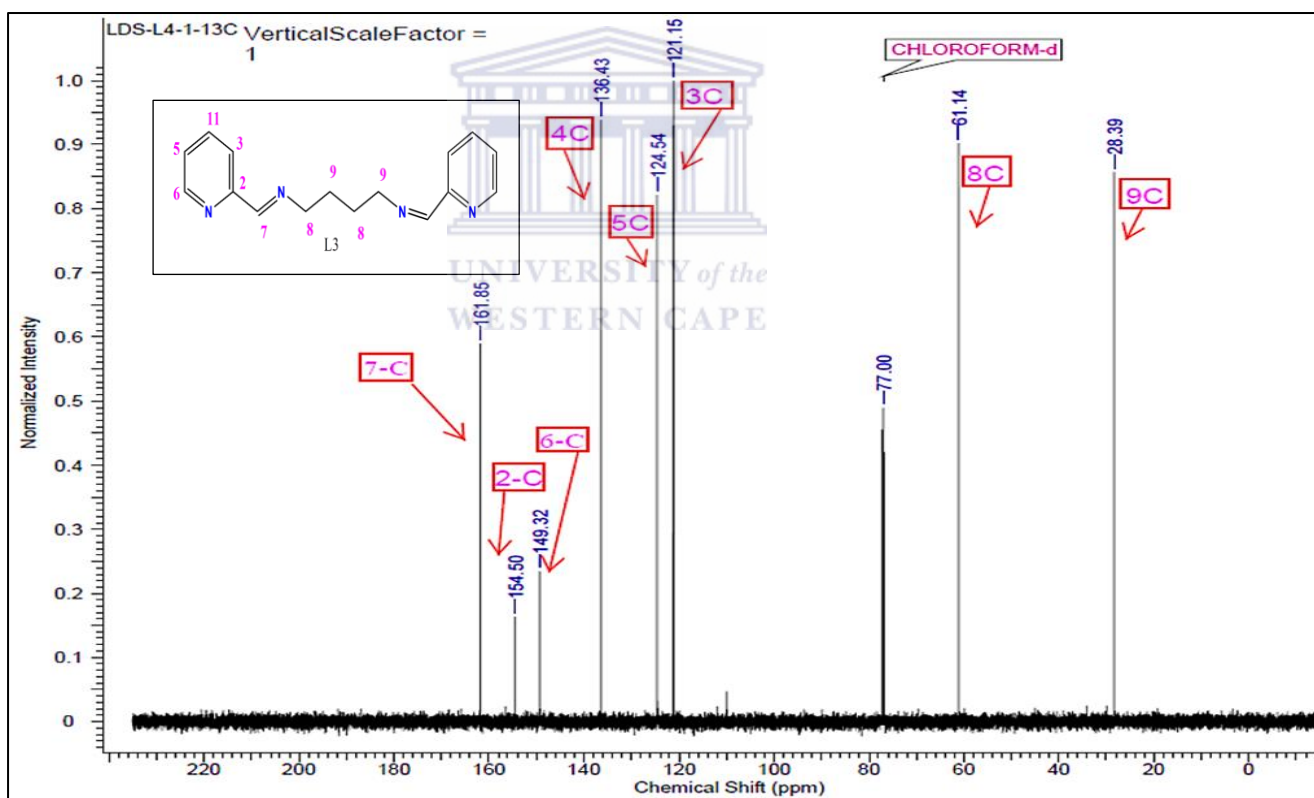


Figure 4.5: ^{13}C NMR of N1,N4-bis(pyridin-2-ylmethylene)butane-1,4-diamine, L3

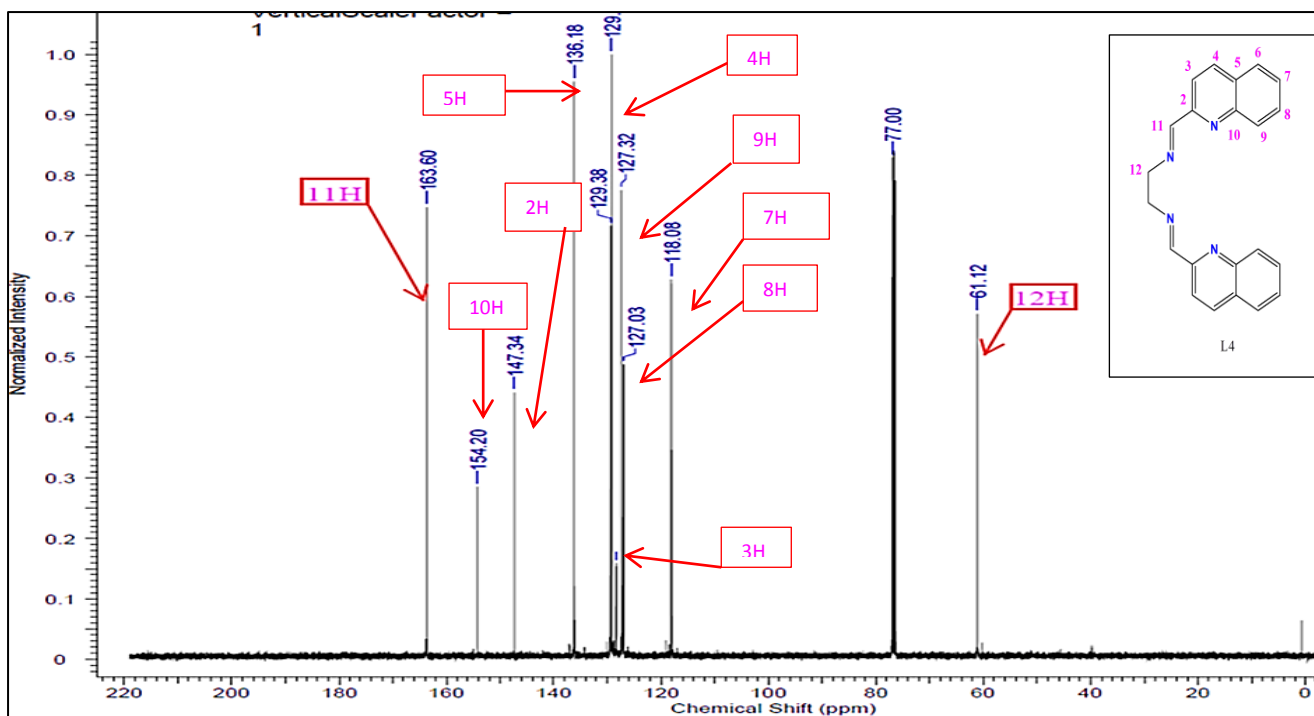
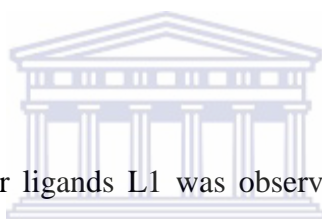


Figure 4.6: ^{13}C NMR of N1,N2-bis((quinolin-2-yl)methylene)ethane-1,2-diamine, L4

Table 4.3: ^{13}C NMR spectral data of tetradentate pyridyl and quinolyl-imine ligands **L1-L6**, recorded in CDCl_3 at 25°C

Ligand	$\text{CH}_{\text{imine}}(\delta \text{ ppm})$	Methylene carbons($\delta \text{ ppm}$)
L1	162.6 (CH_{imine} , C-7)	61.3 (CH_2 , C-8)
L2	161.9 (CH_{imine} , C-7)	31.2 (CH_2 , C-9) 58.6 (CH_2 , C-8)
L3	160.8 (CH_{imine} , C-7)	28.3 (CH_2 , C-9) 61.1 (CH_2 , C-8)
L4	163.9 (CH_{imine} , C-11)	61.4 (CH_2 , C-12)
L5	162.9 (CH_{imine} , C-11)	46.0 (CH_2 , C-12) 27.6 (CH_2 , C-13)
L6	161.8 (CH_{imine} , C-7)	25.0 (CH_2 , C-10) 30.5 (CH_2 , C-9) 61.4 (CH_2 , C-8)

Further characterization of the synthesized pyridyl and quinolyl-imine ligands were carried out using the ^{13}C NMR spectroscopy, the technique provided information about the environment of the carbons in the compounds. The azomethine and methylene carbon signals were observed in the range 161.8-162.6 ppm and 31.2-61.4 ppm respectively for pyridyl-imine ligands. The azomethine and methylene carbons were observed in the range 162.9-163.9 ppm and 27.6-61.4 ppm for quinolyl-imine ligands. The values are consistent with those reported in literature [14]. Sibanyoni *et al.*, reported the observation of the methylene carbons in the range 25.02-61.54 ppm, while the azomethine carbons appeared downfield in the range 161.14-161.77 ppm for their pyridyl-imine ligands [14]. The aromatic carbons of the pyridine and quinolyl ring were observed in the 154.6-118.4 ppm region of the ^{13}C NMR spectra.



The methylene group carbons for ligands L1 was observed at 61.3 ppm (C-8). Methylene carbons for ligands L2 appeared at 58.6 and 31.2 ppm the former is assigned to the terminal methylene carbons (C-8) due to a decrease in the electron density the carbons experience and the latter is assigned to the middle methylene group carbons (C-9) of the trimethylene fragment, the carbons are more shielded from the electron withdrawing effect of the azomethine nitrogen. The tetramethylene fragment for ligand L3 appeared at 61.1 and 28.3 ppm respectively, the former signal at the lower field is assigned to the methylene group carbons (C-8) attached to the azomethine nitrogen and the latter at a higher field is assigned to the terminal (C-9) methylene group carbons. Methylene carbons for ligands L6 appeared at 61.4 ppm (C-8), 30.5 ppm (C-9) and 25.0 ppm (C-10) respectively; the carbon atoms (C-8) attached to the azomethine nitrogen appeared more downfield compared to the terminal methylene group (C-10) which is observed more upfield in the ^{13}C NMR spectra this is due to a decrease in electron density C-10 experience.

The methylene carbons (C-9) are observed at a lower chemical shift, since they are further away from the azomethine nitrogen compared to C-10. Methylene carbons for quinolyl-imine ligands appeared at 61.1 ppm (C-8) for L4, similar peaks appeared at 46.0 ppm (C-8) and 27.6 ppm (C-9) for L5. Similar observations were made by Sibanyoni *et al.* and Busa *et al.*, the methylene group carbons were observed in the 25.02-61.54 ppm and 68.88 ppm for their pyridyl-imine and quinolyl-imine ligands respectively [9,14]. The observation of the azomethine carbon confirms the successful synthesis of the diimine ligands as well as the absence of the starting aldehyde, CHO, peak in the range 190-200 ppm in all the ^{13}C NMR spectra.

From table 4.3, again the chemical shift of the azomethine carbon for the pyridyl ligand L1 compared to the quinolyl ligand L4 was observed at 162.2 ppm and 163.9 ppm respectively. The two compounds differ in the starting aldehyde employed during synthesis; for ligand L1 the aldehyde 2-pyridinecarboxaldehyde was used, whereas in L4 the aldehyde 2-quinolinecarboxaldehyde was used. The differences in the azomethine carbon thus arise from an increase of the conjugation in ligand L4 resulting in the shift to the low field. The ^{13}C NMR spectra of pyridyl ligand L2 and quinolyl ligand L5 gave a chemical shift at 161.9 ppm and 162.9 ppm respectively. The differences in the HC=N chemical shift also arise from an increase of the extra conjugation in the starting quinoline ring for ligand L5 compared to ligand L2, resulting in the lowering of the chemical shift. Although, in general an increase in conjugation has a very small effect on the chemical shift, a trend could still be observed in the ^{13}C NMR spectra of the synthesized pyridyl/quinolyl-imine ligands. The spectra of pyridyl ligands L3 and L6 gave a strong chemical shifts at 160.8 ppm and 161.8 ppm respectively.

The above mentioned ligands are structurally similar with the only difference is in the alkyl chain linker; for ligand L3 four carbons separates the pyridyl ring, whereas in ligand L6 five carbon atoms separates the two pyridyl rings. The differences in the C=N chemical shift is due to an increase in the alkyl chain for ligand L6 compared to ligand L3, similar to ^1H NMR spectroscopy, an increase in carbon substituents results in an increase of the chemical shift and shift to low field.

4.1.5 Mass spectroscopic analysis of pyridyl and quinolyl-imine ligands

Mass spectroscopy was used to determine the molecular weight of the non-metallic based compounds. The following mass spectrum (figure 4.7) is a typical example of the spectra obtained for pyridyl-imine ligands. A summary of the calculated and found m/z values are provided in table 4.4 below. The other mass spectra for the ligands are given in Appendix 11-13. The mass spectra of the ligands were recorded in dichloromethane at room temperature. The general fragmentation patterns are shown in scheme 4.3.

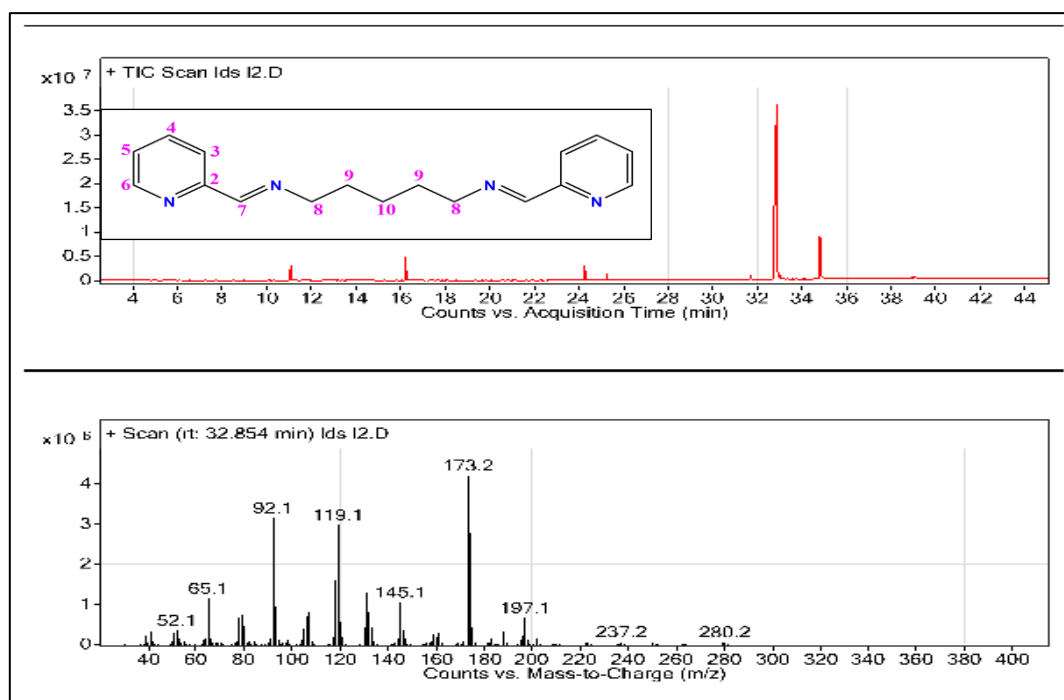
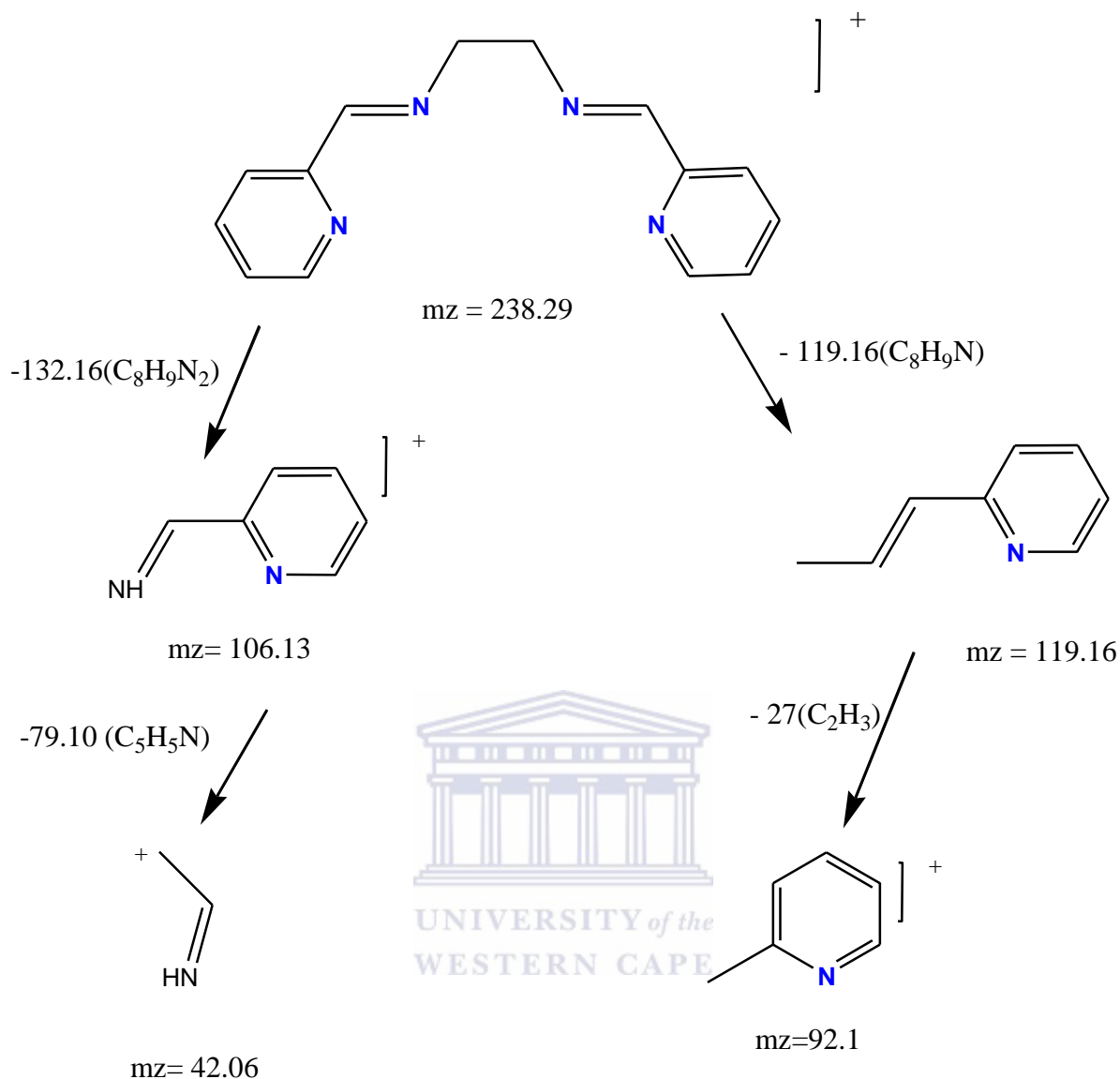


Figure 4.7: Spectra of N1,N5-bis(pyridin-2-ylmethylene)pentane-1,5-diamine,L6

Table 4.4: Summary of mass spectra data for pyridyl and quinolyl-imine ligands **L1–L6**, recorded in DCM at room temperature.

Ligand	ESI-MS [M+H] ⁺ (m/z) Calculated (found)
L1	239 (237)
L2	253 (251)
L3	267 (265)
L4	-
L5	-
L6	281 (280)

Mass spectroscopy was used as a tool to determine the molecular weight of the compounds. The molecular ion (M^+) fragments for the compounds L1, L2, L3 and L6 was calculated at 239, 253, 267 and 281, while the found M^+ values was observed at 237, 252, 265 and 281 respectively. The found M^+ values correlate well with the calculated molecular ion fragments of the compounds. In the mass spectra of the compounds L1, L2, L3 and L6, a typical intense signal at 92.1 m/z and 119.1 m/z were observed. The intense signal observed at 119.1 m/z and 92.1 m/z reveals the loss of C_8H_9N and $C_6H_6N^+$ respectively. Unfortunately attempts to determine the mass spectrometry of L4 and L5 failed due their boiling points being too high; the GC-MS machine used was only capable of operating up to a temperature of 300 °C. The presence of the molecular peak ions were observed in the mass spectra for all the synthesized ligands. A plausible fragmentation pattern of **L1** is showed below (scheme 4.3).



Scheme 4.3: Plausible fragmentation pathway for pyridyl-imine ligands.

4.1.6 Electronic absorption analysis of pyridyl and quinolyl-imine ligands

Ultraviolet-visible spectroscopy was used to identify the electronic transitions within the compounds. The following UV/Vis spectra (figure 4.8 and 4.9) are typical examples of the spectra obtained for pyridyl and quinolyl-imine ligands respectively. The summary of the spectra obtained for pyridyl and quinolyl-imine ligands respectively. The summary of the electronic transitions are provided in table 4.5 below. The other UV/Vis spectra for the ligands are given in Appendix 14-17. The spectra of the ligands were obtained as DCM solutions at room temperature, by using a spectrophotometer and were scan from 200-600 nm.

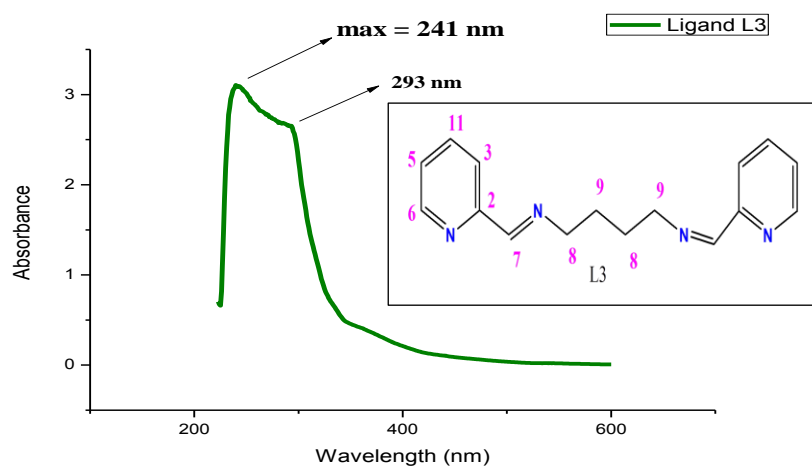


Figure 4.8: UV/Vis of N1, N4-bis(pyridin-2-ylmethylene)butane-1,4-diamine, L3

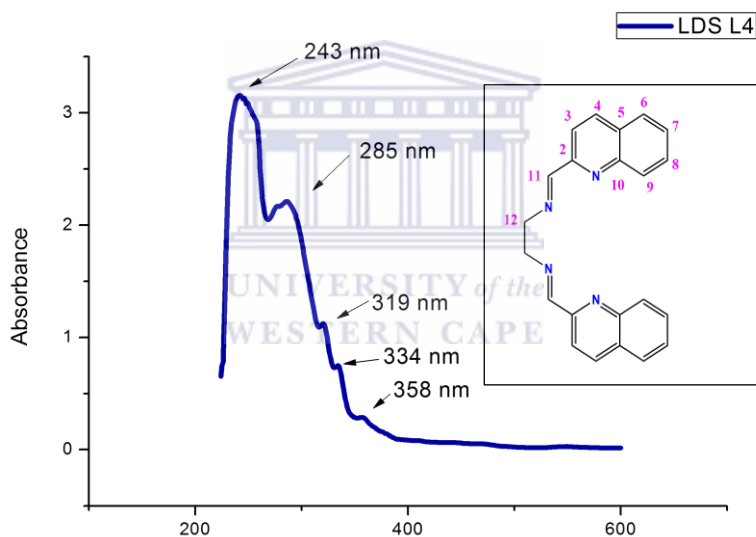


Figure 4.9: UV/Vis of N1,N2-bis((quinolin-2-yl)methylene)ethane-1,2-diamine, L4

Table 4.5: Electronic absorption data of pyridyl and quinolyl-imine ligands L1-L6, recorded in DCM at room temperature.

Ligand	λ_{max} (nm)
L1	241, 327
L2	241, 268
L3	241, 268
L4	243, 285, 319, 334, 358
L5	234, 318
L6	242, 270

For all the pyridyl-imine ligands only two absorption bands were observed. The first band observed as the maximum peak was in the region 241-242 nm and ascribed to the $\pi \rightarrow \pi^*$ charge transfer transition due to the intramolecular ligand transitions of the aromatic pyridine rings [15]. A second peak was observed in the region 268-327 nm, which were assigned to the $n \rightarrow \pi^*$ transition of non bonding electrons present on the nitrogen of the C=N moiety [16]. Similar transitions for the pyridyl-imine ligands were observed by Ebraliidze *et al.* in the range 235-236 nm and 271 nm and was assigned to the $\pi \rightarrow \pi^*$ and $n \rightarrow \pi^*$ transitions respectively, the analysis of the ligands was conducted in EtOH and CH₃CN [6]. In the spectra of the quinolyl-imine ligands L4 and L5, the first band observed as the maximum peak was in the region 234-241 nm and were attributed to the intramolecular ligand ($\pi \rightarrow \pi^*$) transitions of the aromatic quinoline ring. A second peak was observed in the region 285 nm and 318 nm for ligands L4 and L5, which were assigned to the $n \rightarrow \pi^*$ transition of non bonding electrons present on the nitrogen of azomethine. In the spectra of Ligand L4 numerous “shoulders” was observed at 319, 334, 358 nm and was assigned to intra-ligand charge transfer bands. Asadi *et al.* and co-workers reported similar absorption bands for quinolyl-imine ligands, the electronic transitions were observed in the 283-332 nm region and were attributed to intra-ligand charge transfer bands [17].

From table 4.5 the quinolyl-imine ligands was observed to absorb at a longer wavelength in the 243 nm region of the UV/Vis spectra compared to the pyridyl-imine ligands which was observed in the 241 nm region, due to an increase in the delocalisation of the π -electrons and extra conjugation of the quinoline ring.

4.1.7 Thermogravimetric analysis of pyridyl and quinolyl-imine ligands

We report for the first time thermogravimetric studies for the ligands N1,N2-bis((pyridin-2-yl)methylene)ethane-1,2-diamine and (N1,N2-bis((quinolin-2-yl)methylene)ethane-1,2-diamine to the best of our knowledge. The following TGA spectra (figure 4.10 and 4.11) were obtained for pyridyl and quinolyl-imine ligands L1 and L4.

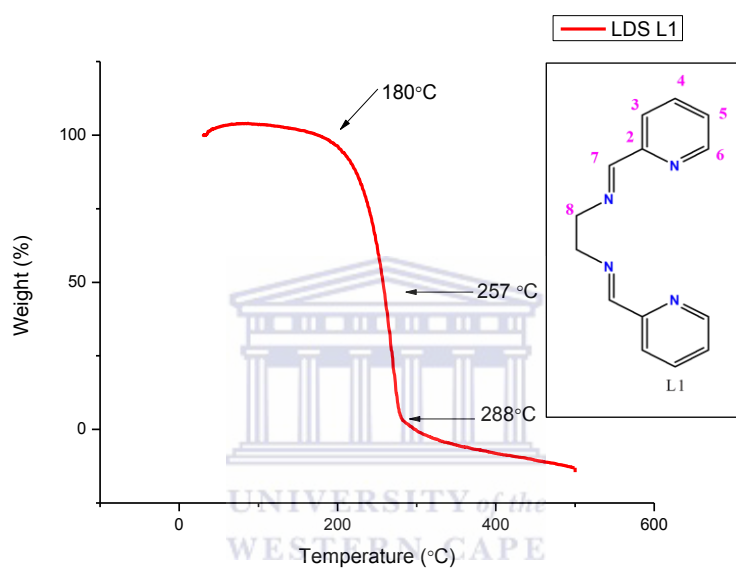


Figure 4.10: TGA of N1,N2-bis((pyridin-2-yl)methylene)ethane-1,2-diamine, L1

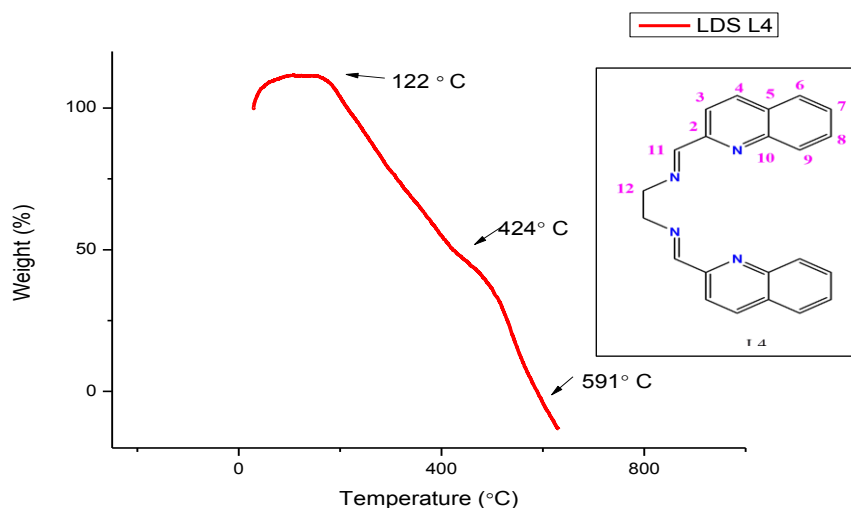


Figure 4.11: TGA of (N1,N2-bis((quinolin-2-yl)methylene)ethane-1,2-diamine, L4

Thermogravimetric analysis was used to investigate the thermal stability of the ligands with variable temperatures. The TGA of the ligands was recorded using a small amount of sample (± 0.4 mg) in a controlled atmosphere, under nitrogen, and at a programmed heating linear rate of $10\text{ }^{\circ}\text{C}/\text{min}$. The thermogram of the pyridyl-imine ligand, L1 illustrates the weight loss of the sample as the temperature is increased. The ligand appeared thermally stable until the initial decomposition occurred at a temperature of 180°C , followed by a continuous weight loss. The d half occurred at 232°C , when 50 wt % of the compound decomposed, which corresponds to the loss of $\text{C}_8\text{H}_9\text{N}$ with a molecular weight = 119.6 g/mol . The molecular fragment was also observed in the mass spectra of L1 ($m/z=119.6$) (scheme 4.3). The whole ligand becomes decomposed in a single step [18] and the final decomposition temperature was observed at 288°C . The shape of the thermogram (figure 4.10) suggests that moisture escapes when the compound melts [19]. The ligand, L4 experienced an increase in weight of approximately 10% until the temperature reached 122°C (figure 4.11). Literature reports that an increase of weight might occur due to a chemical reaction between the compound and the purged gas accompanied by the formation of volatile or non-volatile compounds [19]. The initial decomposition occurred at approximately $122\text{ }^{\circ}\text{C}$ with continuous weight loss. At approximately $424\text{ }^{\circ}\text{C}$ the d half occurred when 50 wt % of the compound decomposed, which corresponds to the loss of $\text{C}_{11}\text{H}_{10}\text{N}_2$ molecular weight = 170.21 g/mol . The final decomposition of the L4 occurred at a temperature of $591\text{ }^{\circ}\text{C}$ [19a].

4.1.8 Analytical and physical studies of pyridyl and quinolyl-imine ligands

The tetradentate pyridyl and quinolyl-imine ligands were prepared only differing in the aldehyde and the backbone (number of CH_2 groups), which separates the imine. The ligands were purified by the addition of diethyl ether and left overnight at -5°C to precipitate out any unreacted aldehyde.

All the synthesized ligands are soluble in common organic solvents such as DCM, CHCl₃, DMSO, toluene, hexane, pentane, CH₃CN and THF. The analytical data and physical data are given in Table 4.6.

Table 4.6: Analytical and physical data of the compounds, **L1-L6**

Compounds	Molecular formula	Molecular weight	Yield%	MP(°C)	Colour	Physical Appearance
L1	C ₁₄ H ₁₄ N ₄	238.29	97	50-53	Brown	Solid
L2	C ₁₅ H ₁₆ N ₄	252.31	90	-	Brown	Oil
L3	C ₁₆ H ₁₈ N ₄	266.34	88	69-72	Brown	Solid
L4	C ₂₂ H ₁₈ N ₄	338.41	62	113-116	Orange	Solid
L5	C ₂₃ H ₂₀ N ₄	352.17	80	-	Orange	Oil
L6	C ₁₇ H ₂₀ N ₄	280.37	74	-	Brown	Oil

From table 4.6 the melting point increased from L1 to L3 for L1 the melting point was recorded in the range 50-53°C, while for L3 the melting point was recorded in the range 69-72°C. For the quinolyl-imine ligands a higher melting point was observed in the range 113-116°C. The melting point of compounds is generally affected by factors such as intermolecular forces, degree of symmetry and geometry of the compounds. Compounds with weak intermolecular forces will have a lower melting point as less energy is needed to overcome these forces. While compounds with stronger intermolecular forces (bulkier structures) will have a higher melting point as more energy is needed to overcome these forces. The melting point of the compounds were observed to increase from L1<L3<L4. This may be due to the increase in the molecular weight of the compounds from L1<L3<L4.

The melting point tests for all the prepared ligands were sharp, indicating a high purity. The ligands were also observed to change from the solid to a crystalline form followed by melting.

The above results also indicated that different colors and physical appearances were observed with different reactions. The tetradentate diimine ligands (**L1, L3 and L4**) were obtained as brown and orange solids in good to moderate yields 97%, 88 % and 62% respectively. Ligands **L2, L5** and **L6** were obtained as low viscosity brown and orange oils respectively in good yields 90%, 80% and 74%. The quinolyl-imine ligands was observed at a longer wavelength in UV/Vis spectra compared to the pyridyl-imine ligands, due to the effect of an increase in the delocalisation and extra conjugation of the quinoline ring, thus also arising in the observation of different colored ligands. The ligands were quite stable and only showed signs of decomposition when stored at room temperature for prolonged periods (2 weeks). Hence ligands were stored at -4°C. Furthermore the elemental analysis results are in close agreement with the calculated values.

4.2 Ruthenium(II) and palladium(II) precursors

4.2.1 FT-IR spectroscopic studies of ruthenium(II) and palladium(II) precursors

FT-IR was used to confirm the successful syntheses of the transitional metal precursors. The FT-IR spectra of precursors $\text{RuCl}_2(\text{dmsO}_4)$ and $\text{Pd}(\text{COD})\text{Cl}_2$ are provided in appendix 18-19, both precursors were recorded in KBR. The FT-IR spectra obtained for $\text{Pd}(\text{COD})\text{Cl}_2$ showed multiple strong absorption similar to the spectral data reported elsewhere [20].

In the spectra of the precursor dichloro(*p*-cymene)ruthenium(II) dimer, the aromatic protons c,c' appears downfield at 5.48 ppm compared to the protons b,b' and is observed as a doublet and split by the neighbouring protons b. The protons b,b' appear at 5.35 ppm and is observed as a doublet, split by neighbours protons c. The septet observed at 2.94 ppm were assigned to protons d, the protons are split by their neighbours e,e'. The chemical shifts observed as a singlet and doublet at 2.18 ppm and 1.3 ppm were assigned to a and e and are split by protons b and d respectively. The ¹H NMR spectra of RuCl₂(dmsO)₄ was recorded in D₂O. The signal observed at 3.5 ppm was assigned to H (CH₃) protons and the signal observed at 2.60 ppm, which was assigned to S-bonded and O-bonded DMSO. The results obtain from the ¹H NMR spectra confirms the successfully syntheses of the precursors.

4.3 Pyridyl/quinolyl-imine ruthenium(II) and bimetallic pyridyl-imine palladium (II) complexes

The synthesis of the neutral mononuclear pyridyl/quinolyl-imine ruthenium(II) complexes (C1-C5) (scheme 4.5) followed the literature procedures [9]. The cationic homobimetallic ruthenium(II) complex, C6 (scheme 4.6) followed a similar synthetic procedure done by Govender *et al.* [22]. The synthetic procedure for bimetallic pyridyl-imine palladium(II) complexes (C7-C10) (scheme 4.5) is similar to that reported by Sibanyoni *et al.* [14], with some modification as described in chapter 3.

4.3.1 FT-IR spectroscopic analysis of pyridyl/quinolyl-imine ruthenium(II) complexes and bimetallic pyridyl-imine palladium(II) complexes

The following FT-IR spectra (figure 4.13, 4.14 and 4.15) are typical examples of spectra obtained for mononuclear pyridyl/quinolyl-imine ruthenium(II) and bimetallic pyridyl-imine palladium(II) complexes respectively.

The FT-IR spectra of the complexes were recorded using KBR pellets. The other FT-IR spectra for the complexes are given in Appendix 20-24. A summary of the stretching frequencies of the main functional groups is given in table 4.7.

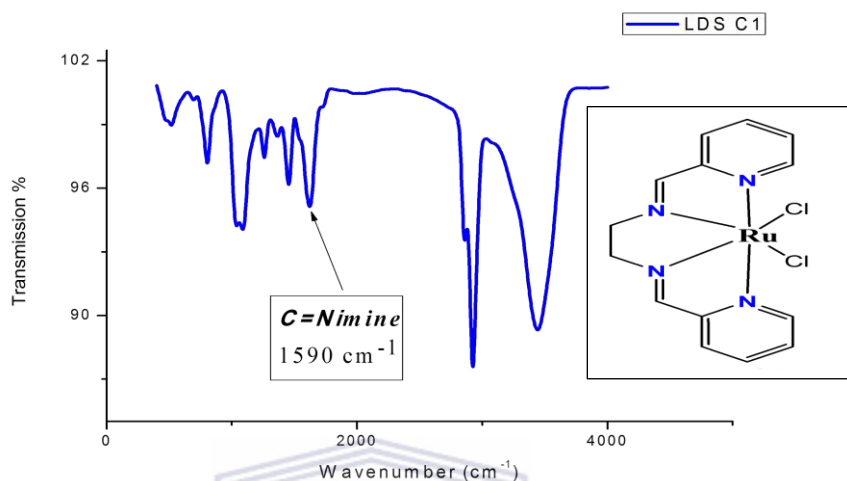


Figure 4.13: FT-IR for dichloro-N1,N2-bis((quinolin-2-yl)methylene)ethane-1,2-diamine-ruthenium(II), C4

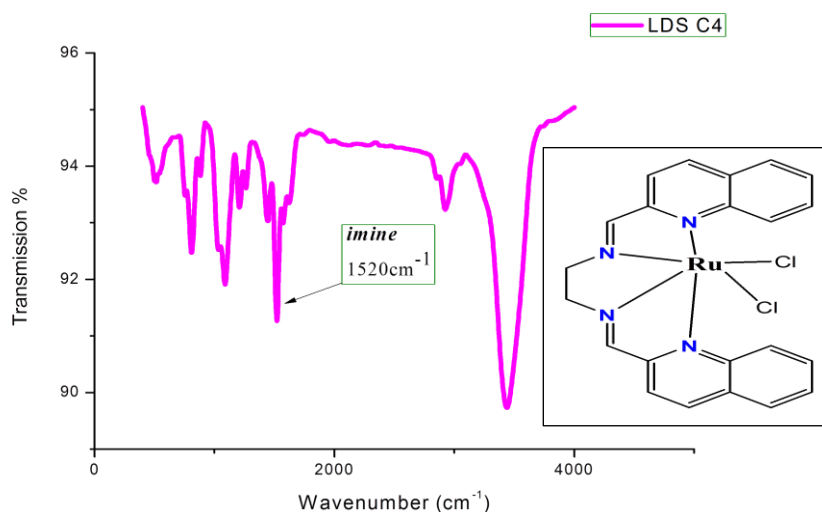


Figure 4.14: FT-IR for dichloro-N1,N2-bis((pyridin-2-yl)methylene)ethane-1,2-diamine-ruthenium(II), C1

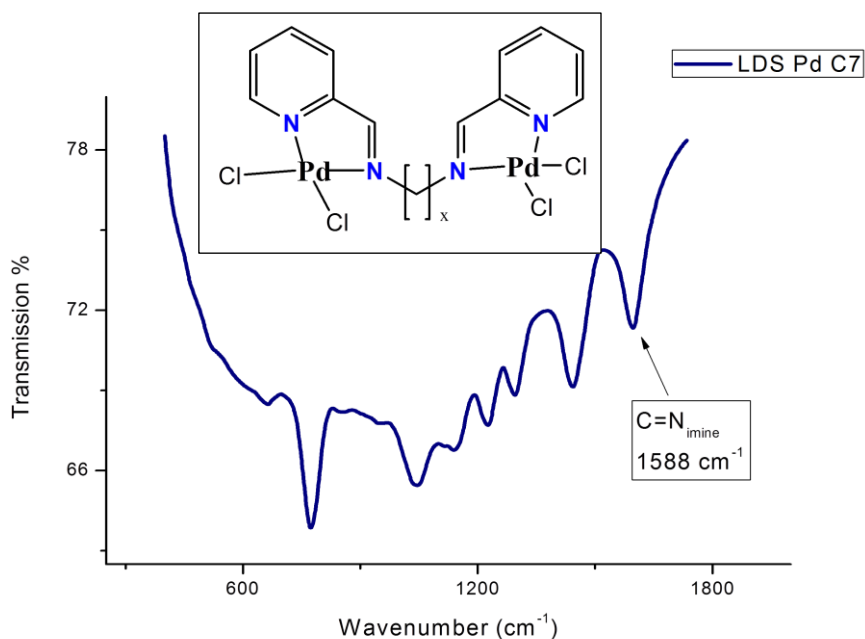
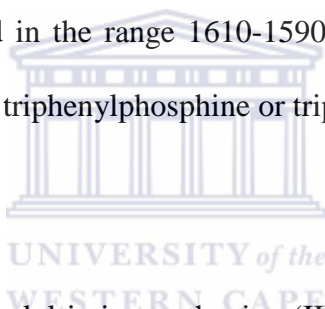


Figure 4.15: FT-IR for dichloro-N1,N2-bis((pyridin-2-yl)methylene) ethane-1,2-diamine-palladium(II), **C7**

Table 4.7: FT-IR data of pyridyl/quinolyl-imine ruthenium(II) and bimetallic pyridyl-imine palladium(II) complexes.

Complexes	Metal complex $\nu_{(C=N)}$ cm^{-1}
C1	1590
C2	1538
C3	1597
C4	1520
C5	1520
C6	1590
C7	1588
C8	1576
C9	1598
C10	1592

Infrared spectroscopy was used as a technique to determine whether the coordination of the imine ligands towards the ruthenium(II) and palladium(II) precursors occurred to form the desired complexes by observing the presence of the azomethine, $\nu(\text{C}=\text{N})$, functional group. The FT-IR spectra of the neutral mononuclear pyridyl-imine ruthenium(II) complexes C1, C2 and C3 displayed a strong stretching frequency in the range 1538-1597 cm^{-1} which were assigned to the azomethine fragment, $\nu(\text{C}=\text{N})$. The C=N vibration appears at a significant lower frequency and underwent a red shift compared to the free ligands previously observed in the range 1639-1650 cm^{-1} . Literature reports indicated this red shift is due to the reduction of the electron density in the C=N bond arising from the electron flow from the ligand to the metal centre [23]. Viswanathamurthi *et al.* reported similar values for the free imine ligands in the range 1610-1630 cm^{-1} and in the range 1610-1590 cm^{-1} for their Ru(II) tetradentate Schiff base complexes containing triphenylphosphine or triphenylarsine ligands [24].

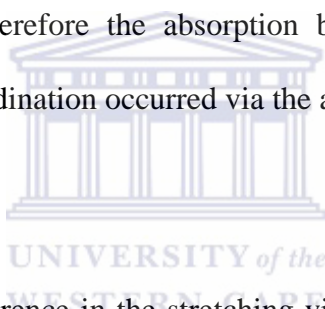


The FT-IR spectra of the quinolyl-imine ruthenium(II) complexes displayed a strong stretching frequency at 1520 cm^{-1} attributed to the C=N moiety, a red shift was also observed for these compounds arising from the electron flow from the ligand to the ruthenium metal. The C=N moiety of the cationic homobimetallic ruthenium(II) complex, C6 appeared at a lower vibration of 1590 cm^{-1} compared to the free ligand observed at 1639 cm^{-1} .

The bimetallic pyridyl-imine palladium(II) complexes showed similar results, the azomethine stretching frequency previously observed at 1639-1650 cm^{-1} for the free ligands shifted to a lower wavenumber in the range 1576-1598 cm^{-1} indicative of a red shift, due to the electron flow between the ligand and metal centre [25].

Similar results were obtained by Moletsane *et al.* for the pyridyl and quinolyl-imine palladium(II) dendrimers, a red shift was observed from 1648 cm^{-1} to 1612 cm^{-1} and 1640 cm^{-1} to 1596 cm^{-1} for the pyridyl- and quinolyl-imine respectively [25]. Furthermore no absorption bands were observed above 1620 cm^{-1} ; which is the characteristic stretching frequency for the uncoordinated imine ligand system.

In the FT-IR spectra of all the synthesized complexes, the red shift observed is due to a decrease in the electron density around the C=N moiety arising from the electron flow from the nitrogen to the d-orbitals of the metal centre resulting in the energy of vibration of the functional group to decrease therefore the absorption bands were observed at a lower frequency. Hence signifying coordination occurred via the azomethine nitrogen [26].



From table 4.7 a significant difference in the stretching vibration of the $\nu(\text{C}=\text{N})$ moiety for the pyridyl-imine ruthenium(II) complex C1 compared to the quinolyl-imine ruthenium(II) complex C4 was observed at 1590 cm^{-1} and 1520 cm^{-1} respectively. The two compounds differ in the starting diimine ligand employed during the synthesis; for complex C1 the pyridyl-imine ligand L1 was used whereas in complex C4 the quinoline-imine ligand was employed. The differences in the C=N stretching frequency thus arise from an increase in the conjugation of the quinoline ring in ligand L4 resulting in the lowering of the stretching frequency. Again the spectra of the pyridyl-imine ruthenium(II) complex C2 and quinolyl-imine ruthenium(II) complex C5 also gave a difference in the stretching vibration of the C=N moiety at 1538 cm^{-1} and 1520 cm^{-1} respectively.

Similar to the previously mentioned complexes the differences in the C=N stretching frequency arises from an increase of the extra conjugation and delocalisation of the electrons in the starting quinoline-imine ligand (L5) compared to ligand L2, resulting in the lowering of the stretching frequency. The spectra of the mononuclear pyridyl-imine ruthenium(II) complex, C3 gave a strong stretching frequency at 1597 cm^{-1} while the cationic homobimetallic ruthenium(II) complex, C6 gave a stretching frequency at a lower wavenumber of 1590 cm^{-1} . Since complex C6 has two metal centres and the presence of the p-cymene rings, the reduction of the electron density around the C=N bond will be more pronounced resulting in a lower wavenumber compared to its analogue compound C3.

4.3.2 ^1H NMR and ^{13}C NMR spectroscopy analysis of pyridyl/quinolyl-imine ruthenium (II) complexes and bimetallic pyridyl-imine palladium(II) complexes

The following ^1H NMR spectra (figure 4.16, 4.17 and 4.18) are typical examples of the spectra obtained for pyridyl/quinolyl-imine ruthenium(II) complexes and bimetallic pyridyl-imine palladium(II) complexes. The other ^1H NMR spectra for the complexes are given in Appendix 25-27. The chemical shift values of the protons are summarized in table 4.8. The ^1H NMR spectroscopy assignment for ligands (C1-C10) was carried out by means of chemical shift of the relevant protons, and was assisted by comparison with the ^1H NMR spectra obtained for the free pyridyl/quinolyl-imine ligands. The ^1H NMR spectra of neutral mononuclear pyridyl/quinolyl-imine ruthenium(II) complexes (C1-C5), cationic homobimetallic ruthenium(II) complexes (C6) and bimetallic palladium(II) complexes (C7-C10) were recorded at 25°C in CDCl_3 -*d*, CD_3OD and $\text{DMSO-}d_6$ solutions respectively. The proton numbering is shown scheme 4.3.

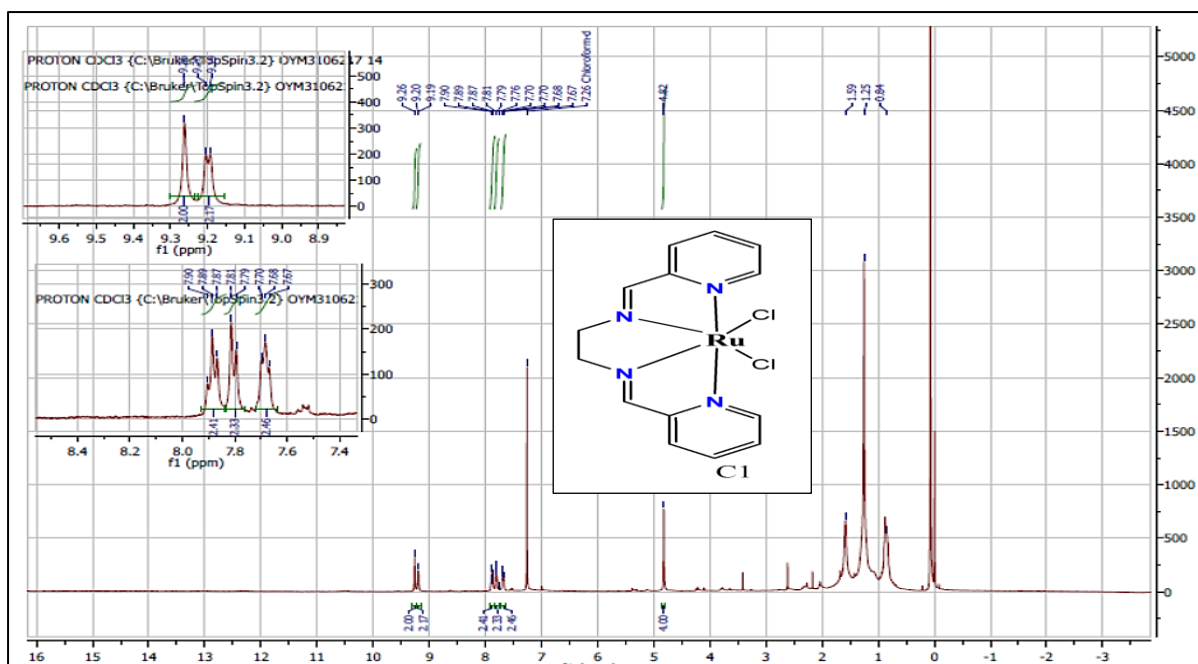


Figure 4.16: ^1H NMR for dichloro-N1,N2-bis((pyridin-2-yl)methylene) ethane-1,2-diamine-ruthenium(II), C1

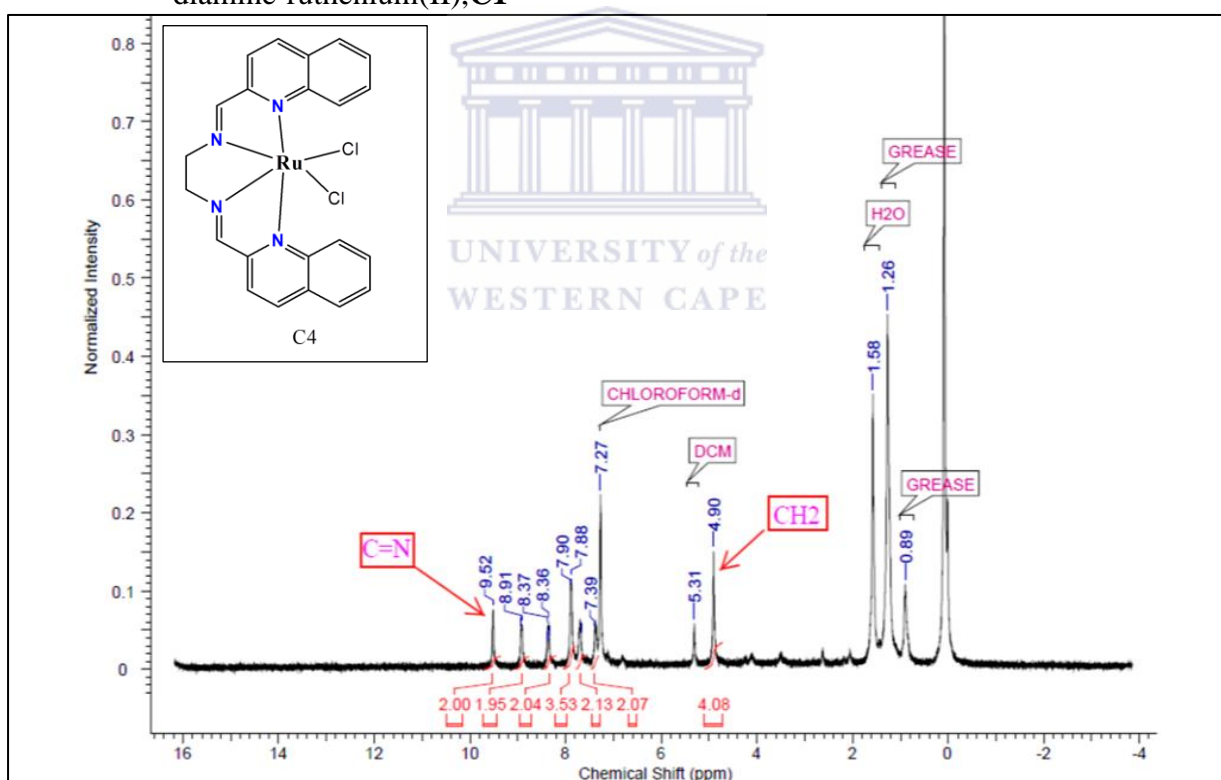


Figure 4.17: ^1H NMR for Dichloro-N1,N2-bis((quinolin-2-yl)methylene)ethane-1,2-diamine-ruthenium(II), C4

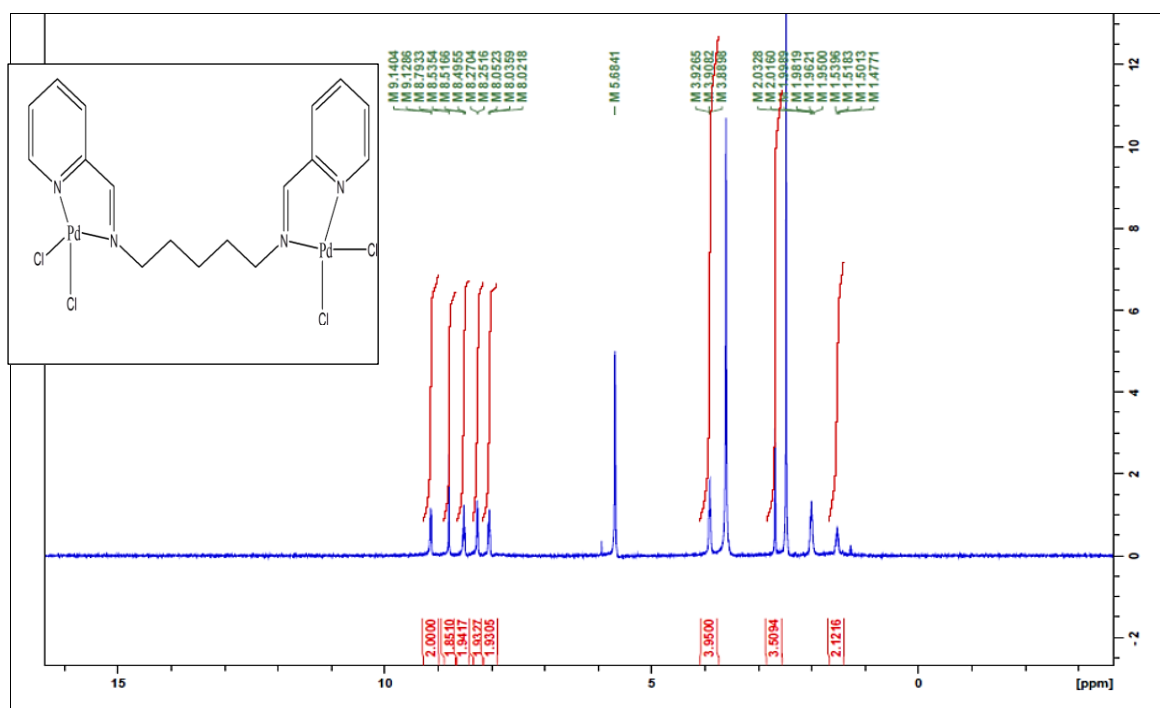


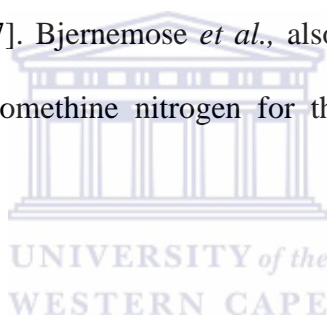
Figure 4.18: ^1H NMR for dichloro-[N1,N5-bis(pyridin-2-ylmethylene)pentane-1,5-diamine]palladium(II), **C11**.

Table 4.8: ^1H NMR spectral data of N-donor ruthenium(II) (C1-C6)^a and palladium(II) (C7-C10)^b Schiff base complexes, recorded at 25°C

Compounds	HC=N (δ ppm)	Methylene protons (δ ppm)
C1	9.26	4.82 (s, 4H)
C2	9.16	4.57 (t, 4H); 3.77 (m, 2H)
C3	8.96	4.73 (m, 4H); 2.47 (m, 4H)
C4	9.51	4.90 (s, 4H)
C5	9.50	3.97 (t, 12-H); 2.31 (q, 13-H)
C6	8.94	2.29 (m, 4H); 2.13 (m, 4H)
C7	8.76	4.21 (s, 4H)
C8	8.62	3.82 (t, 4H); 2.16 (m, 2H)
C9	8.63	3.71 (m, 4H); 1.79 (m, 4H)
C10	8.79	3.90 (t, 4H); 1.98 (m, 4H); 1.51 (m, 2H)

a: Complexes (C1-C6) recorded in CDCl_3 -*d*; b: Complexes (C7-C10) recorded in $\text{DMSO-}d_6$.

Further characterisation by ^1H NMR was done to investigate whether the coordination occurred and the successful synthesis of the proposed complexes. The ^1H NMR spectra of the pyridyl-imine ruthenium(II) complexes displayed the azomethine proton at a lower field in the range 8.96-9.26 ppm compared to the free ligand which was previously observed in the range 8.39-8.43 ppm. The results suggest the deshielding (paramagnetic shift) of the azomethine proton due to the coordination of ruthenium towards the azomethine nitrogen. Busa *et al.* and Pal *et al.* reported similar downfield shifts of the azomethine proton for the pyridyl/quinolyl-imine ruthenium(II) complexes in the range 8.4 ppm to 8.9-9.2 ppm upon coordination with the ruthenium metal [9, 13]. The downfield shift observed in the ^1H NMR spectra therefore confirms the coordination of the ruthenium metal via the azomethine nitrogen of the imine ligands [27]. Bjernemose *et al.*, also reported the coordination of the ruthenium metal through the azomethine nitrogen for their Ru(II) complexes containing polypicolylamine ligands [27].



The $\text{HC}=\text{N}$ moiety for quinolyl-imine Ru(II) complexes underwent a very big shift downfield in the range 9.50-9.51 ppm compared to their free ligand which was previously observed in the range 8.61-8.62 ppm. El-Sonbati *et al.* prepared several new Schiff base complexes based on the quinoline starting material, 7-formyl-8-hydroxyquinoline (oxine) with 2-aminophenol or 2-aminopyridine [28]. El-Sonbati and group also reported a downfield shift from 8.9 ppm to 9.4 ppm in their quinoline Schiff base complexes and the coordination of the metal through both the oxygen atom of the deprotonated phenolic group and the azomethine nitrogen resulting in the azomethine proton being deshielded [28]. In the ^1H NMR spectra of all the synthesized complexes, a decrease in the peak intensity of the azomethine protons was also observed; this effect is attributed to the coordination of the metal center.

The methylene group protons and aromatic protons for the pyridyl and quinolyl-imine ruthenium(II) complexes also experiences a downfield shift compared to the free ligands, due to the deshielding effect of the ruthenium metal coordinated to the ligand. The CH₂ group protons for complexes C1 and C4 experienced a downfield shift to 4.82 ppm and 4.90 ppm respectively and appear as singlets. A similar observation was made by Pal *et al.*, and suggests the two methylene groups of C1 and C4 are magnetically equivalent on an NMR time-scale [9, 13]. The methylene group protons for complexes C2, C3, C4 and C5 experienced a downfield in the range 3.77-4.90 ppm.

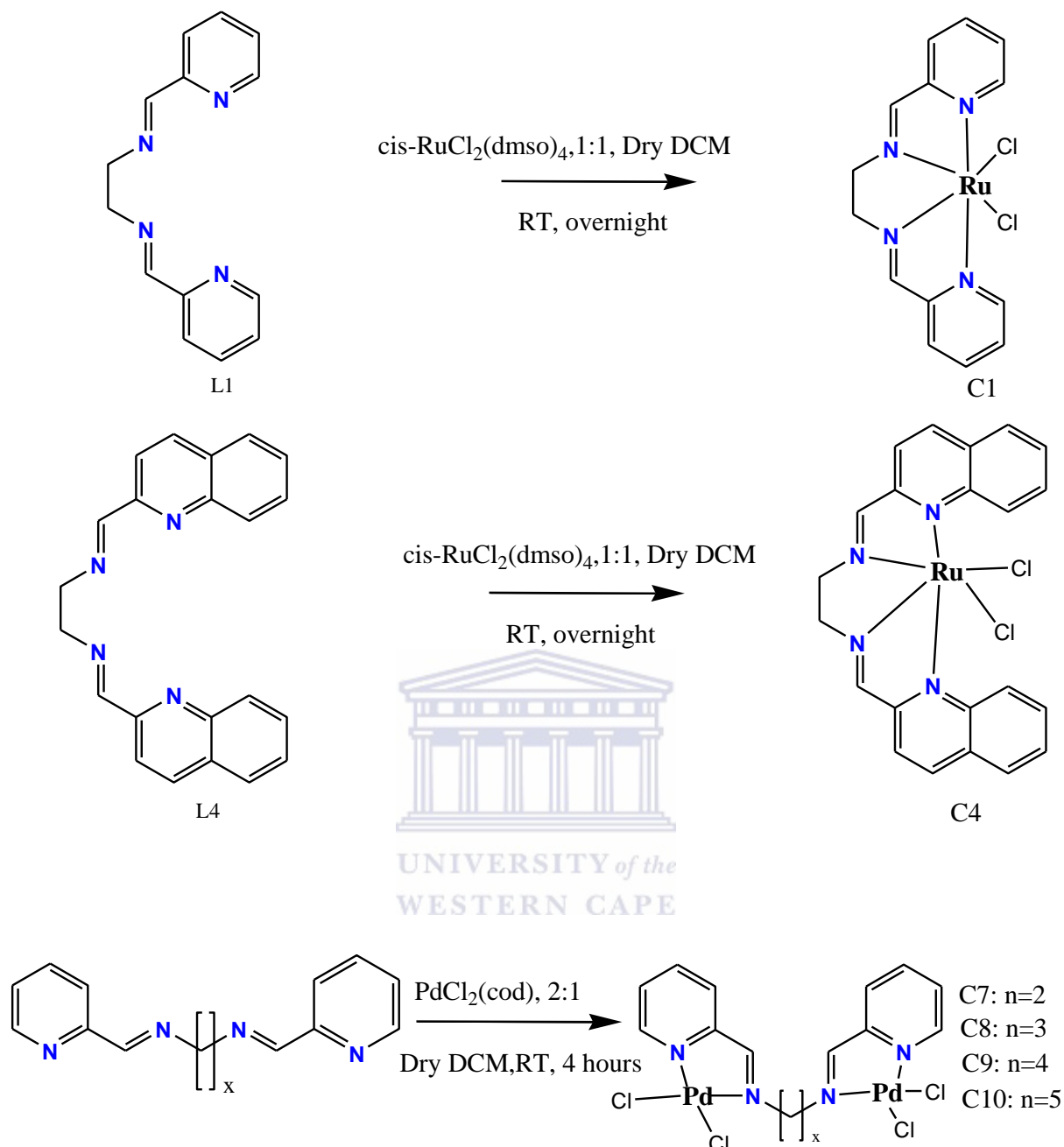
The cationic ruthenium(II) homobimetallic complex, C6 was only partially soluble in CDCl₃-*d* and CD₃OD was used to further dissolve the sample hence two solvent peaks are seen in the ¹H NMR spectrum. The azomethine proton (H-7) peak for the cationic homobimetallic ruthenium(II) complex was seen more downfield at 8.64 ppm compared to the free ligand previously observed at 8.39 ppm. Govender *et al.* also reported a downfield shift of their N,N-ruthenium(II) arene functionalised poly(propylene-imine) dendrimer scaffolds in the range 8-9 ppm [29]. The aromatic protons for the pyridyl-imine complex were also observed downfield in the region 7.75-9.47 ppm (Appendix 1) while the aromatic protons for *p*-cymene (CYE) were observed in the range 5.79-6.17 ppm. The presence of both the CH(CH₃)₂CYE group and the CH(CH₃)₂CYE group appear at 1.06 ppm and 2.63 ppm respectively, these functional groups were earlier noted in the ¹H NMR spectra of the precursor [RuCl₂(*p*-cymene)]₂ (figure 4.12) at 1.3 ppm and 2.18 ppm respectively. Hence it is evident from this results no loss of the *p*-cymene moiety occurred. Rath *et al.* and Lalrempuia *et al.* reported similar values for their *p*-cymene ruthenium(II) Schiff base complexes [30, 31]. Therefore we can conclude the successful synthesis of the cationic homobimetallic ruthenium(II) complex, C6.

The solubility of some palladium(II) complexes was weak and only partially soluble in DMSO. The azomethine proton for pyridyl-imine bimetallic palladium(II) complexes appeared more downfield in the range 8.62-8.79 ppm compared to the free ligands, observed in the range 8.35-8.43 ppm. This is due to the coordination of the palladium to the azomethine nitrogen, resulting in the deshielding of the azomethine proton [32]. However the ^1H NMR spectra of the palladium(II) complexes only showed a slight downfield shift, indicating that the palladium centre is weakly coordinated to the ligands. Similar results were obtained by Ojwach *et al.* and Cloete *et al.* [33, 34]. Cloete *et al.* reported the synthesis of mononuclear pyridyl-imine palladium(II) complexes, the ^1H NMR spectra of the palladium (II) complexes revealed a downfield shift from 8.25 ppm in the free ligand to 8.62 ppm for the coordinated compounds. Cloete and group reported the downfield shift was due to the coordination of the azomethine nitrogen through the metal atom. Ojwach *et al.* reported the synthesis and characterization of substituted (pyridinyl)benzoazole palladium(II) complexes, the ^1H NMR spectra of the complexes revealed a significant downfield shifts of the aromatic and pyridyl protons suggesting the coordination of the palladium atom through the nitrogen of the pyridine and benzoazole rings [34].

From table 4.8 a significant difference in the azomethine proton for the pyridyl-imine complex C1 compared to the quinolyl-imine complex C4 was observed at 8.26 ppm and 8.51 ppm respectively. The two compounds differ in the starting ligand employed; for complex C1 the pyridyl-imine ligand was used whereas for complex C4 the quinoline-imine ligand L4 was used. The differences in the azomethine proton thus arise from an increase in the conjugation of the quinoline ring in ligand L4 resulting in the shift to a lower field and resulting in the azomethine proton for complex C4 being deshielded.

The ^1H NMR spectra of pyridyl-imine complex C2 and quinolyl-imine complex C5 also gave a difference in the chemical shift of the C=N moiety at 9.16 ppm and 9.50 ppm respectively. Again, the differences in the chemical shift arises from the extra conjugation and delocalised p electrons in the starting quinoline-imine ligand L5 compared to ligand L2, causing the protons to absorb at a lower field and being deshielded compared to L2. The azomethine protons for the complexes C3 and C6 appeared at similar chemical shifts of 8.96 ppm and 8.94 ppm respectively, this could be due to the starting ligands being the same. The slight differences in the chemical shift could be representative of the different geometries the two complexes possess; C3 is a mononuclear ruthenium complex and C6 is a bimetallic complex.

From the table the chemical shifts of the pyridyl-imine bimetallic palladium(II) complexes appeared at a high field compared to the pyridyl-imine ruthenium(II) complexes. The azomethine proton for complexes C7 and C10 appear at 8.76 and 8.79 ppm respectively, whereas the ^1H NMR spectra of complexes C8 and C9 reveal the azomethine protons at 8.62 and 8.63 ppm respectively. The different chemical shifts obtained suggest that complexes C7 and C10 could have a similar conformation and complexes C8 and C9 have a similar conformation.



Scheme 4.5: Examples of the synthetic pathway of neutral mononuclear pyridyl and quinolyl-imine Ru(II) and bimetallic pyridyl-imine Pd(II) complexes

The relevant carbon assignments for the pyridyl and quinolyl-imine ruthenium(II) complexes are tabulated below (table 4.9).

Table 4.9: ^{13}C NMR spectral data of pyridyl and quinolyl-imine ruthenium(II), recorded in CDCl_3 at 25°C

Complexes	CH_{imine} (δ ppm)	Methylene carbons (δ ppm)
C1	163.5 (CH_{imine} , C-7)	63.3 (CH_2 , C-8)
C2	162.4 (CH_{imine} , C-7)	31.9 (CH_2 , C-9) 59.0 (CH_2 , C-8)
C3	163.9 (CH_{imine} , C-7)	30.0 (CH_2 , C-9) 68.5 (CH_2 , C-8)
C4	165.2 (CH_{imine} , C-11)	62.5 (CH_2)
C5	164.6 (CH_{imine} , C-11)	47.2 (CH_2 , C-12) 28.0 (CH_2 , C-13)
C6	166.5 (CH_{imine} , C-7)	23.2, 23.6, 25.9 (CH_3 , C_{CYE})

Further characterization of the synthesized pyridyl/quinolyl-imine ruthenium(II) complexes was carried out using the ^{13}C NMR spectroscopy. The azomethine carbon and methylene carbons signals were observed in the range 162.4-163.9 ppm and 30.0-63.3 ppm respectively for mononuclear pyridyl-imine Ru(II) complexes (C1-C3). The azomethine and methylene carbons were observed in the range 164.6-165.2 ppm and 28.0-62.5 ppm for quinolyl-imine complexes (C4-C5). The values are consistent with those reported in literature for the pyridyl and quinolyl-imine complexes. Moletsana *et al.* reported a downfield shift in the azomethine carbon for their pyridine/quinoline-imine palladium(II) dendrimers from 154.1 ppm and 162.5 ppm for the free ligands to 155.0 ppm and 169.3 ppm for the dendrimers.

In the case of our pyridine/quinoline-imine ruthenium(II) complexes a downfield shift was observed in the HC=N peak from 161.8-163.9 ppm for the free ligands to 162.4-165.2 ppm for the complexes. The methylene group protons for ligands C1 was observed at 63.3 ppm (C-8). Methylene carbons for ligands C2 appeared at 59.0 ppm and 31.9 ppm the former is assigned to the carbon of the terminal methylene groups (C-8) and the latter is assigned to the middle methylene group carbons (C-9) of the trimethylene fragment. The tetramethylene fragment for ligand C3 appeared at 68.5 ppm and 30.0 ppm respectively, the former signal at the lower field is assigned to the methylene group carbons (C-8) attached to the azomethine nitrogen and the latter at a higher field is assigned to the terminal (C-9) methylene group carbons. The methylene carbons for the quinolyl-imine complex C4 appeared at 62.5 ppm (C-8), similar peaks appeared at 47.2 ppm (C-12) and 28.0 ppm (C-13) for C5. Similar observations were made by Busa *et al.*, their methylene group protons were observed in the 68.88 ppm region for their pyridyl/quinolyl-imine complexes [9]. The observation of the azomethine carbon confirms the successful synthesis of the pyridyl/quinolyl-imine complexes. The ^{13}C NMR spectra of all the binuclear palladium(II) complexes gave relatively poor quality spectra because of the poor solubility of the compounds.

From table 4.9, the chemical shift of the azomethine carbon for the ruthenium(II) pyridyl/quinolyl-imine complexes C1 and C4 was observed at 163.5 ppm and 165.2 ppm respectively. The two compounds differ in the starting diimine ligand; for C1 the ligand L1 was used whereas in C4 the ligand L4 was used. The differences in the azomethine carbon thus arise from an increase of the conjugation from the quinoline ring in ligand L4 resulting in the shift to the low field. The ^{13}C NMR spectra of complexes C2 and C5 gave a chemical shift at 162.4 ppm and 164.6 ppm respectively.

The differences in the HC=N chemical shift also arise from an increase of the extra conjugation in the starting quinoline ring for ligand C5 compared to ligand C2, resulting in the observation of the chemical shift at a higher ppm. Although in general an increase in the conjugation of the aromatic group has a very small effect on the chemical shift, a trend was observed in the ^{13}C NMR spectra of the synthesized ruthenium(II) pyridyl/quinolyl-imine complexes. The spectra of the neutral mononuclear pyridyl-imine Ru(II) complexes C3 and cationic homobimetallic ruthenium(II) complex C6 gave a strong chemical shifts at 163.9 ppm and 166.5 ppm respectively. The differences in the azomethine carbons chemical shift, could be due to the azomethine carbon of complex C6 experiencing the electron withdrawing effect of the substituent p-cymene ring on the ruthenium atom; resulting in a increase in the paramagnetic deshielding effect and hence a larger chemical shift is observed in the spectra of C6 compared to C3.

4.3.3 Electronic absorption analysis of pyridyl/quinolyl-imine ruthenium(II) complexes and bimetallic pyridyl-imine palladium(II) complexes

The following UV/Vis spectra (figure 4.19, 4.20, 4.21) are a typical example of the spectra obtained for mono- and cationic homobimetallic pyridyl/quinolyl-imine ruthenium(II) complexes and bimetallic pyridyl-imine palladium(II) complexes respectively. The other UV/Vis spectra for the complexes are given in Appendix 28-32. The UV-Visible spectra of the mono- and cationic homobimetallic ruthenium(II) complexes were recorded in dichloromethane at room temperature and the bimetallic palladium(II) complexes were recorded in DMSO, by using a Spectrophotometer and were scanned from 200-1200 nm. The DCM solutions for the pyridyl-imine ruthenium(II) complexes appeared purplish/blue in color while the quinolyl-imine ruthenium(II) complexes were observed as green solutions. The cationic homobimetallic ruthenium(II) complex, C6 appeared as a yellow solution.

The DMSO solutions were orange/yellowish for the bimetallic pyridyl-imine palladium(II) complexes. The electronic absorption spectral data collected using these solutions are reported in Table 4.10.

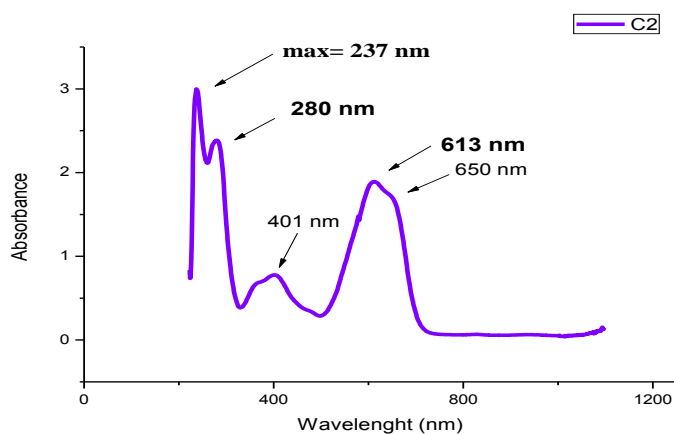


Figure 4.19: UV/vis of N1,N3-bis(pyridin-2-ylmethylene)propane-1,3-diamine-RuCl₂, **C2**

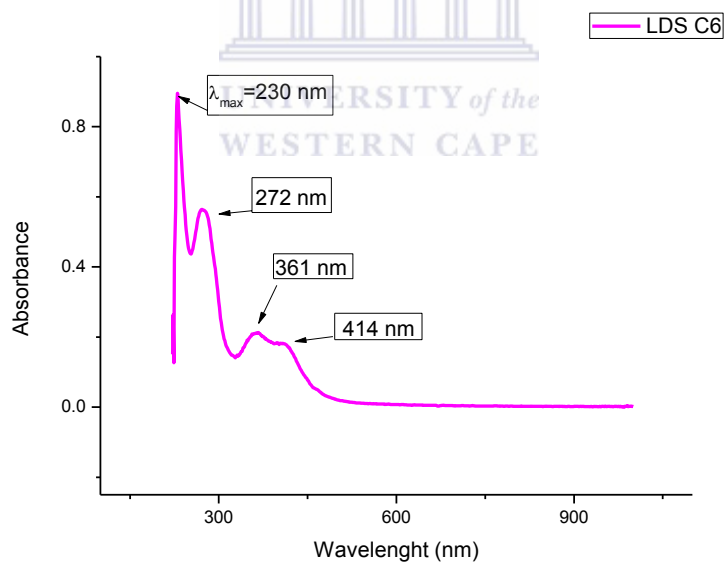


Figure 4.20: UV/vis of cationic homobimetallic ruthenium(II) complex, **C6**

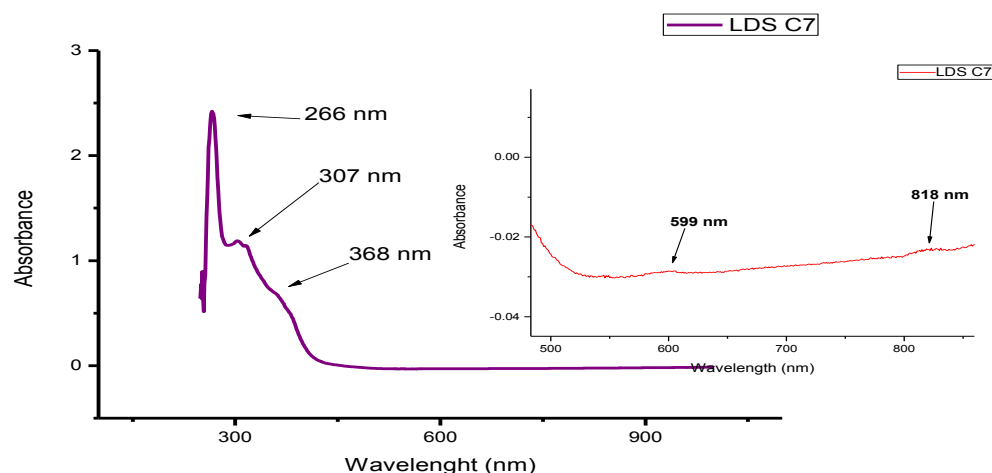


Figure 4.21: UV/vis of dichloro-[N1,N2-bis((pyridin-2-yl)methylene)ethane-1,2-diamine]palladium(II), **C7**

Table 4.10: Electronic absorption data of pyridyl/quinolyl-imine ruthenium(II) complexes(C1-C6)^a and bimetallic palladium(II) complexes (C7-C10)^b

Complex	λ_{\max} (nm)
C1	233, 267, 351, 592
C2	237, 280, 401, 613, 650
C3	230, 274, 364, 561, 602, 656
C4	249, 330, 651
C5	245, 325, 645
C6	230, 272, 361, 414
C7	266, 307, 368, 699, 818
C8	283, 317
C9	283, 317
C10	283, 320

a:Complexes (C1-C6) recorded in DCM; b: Complexes (C7-C10) recorded in DMSO.

The ultraviolet-visible spectroscopy was used to investigate the electronic transitions for the neutral mononuclear/cationic homobimetallic ruthenium(II) complexes and bimetallic palladium(II) complexes. The electronic spectrum of the neutral mononuclear pyridyl-imine ruthenium(II) complexes (C1-C3) displays several bands in the range 230-656 nm. The UV/Vis spectra are similar to those reported by Pal *et al.* who observed several bands in the range 274-656 nm for their ruthenium(II) pyridyl-imine complexes [9].

The first strong peak observed in the range 230-237 nm were assigned to the $\pi \rightarrow \pi^*$ charge transitions of the pyridine ring. Similar peaks were reported to appear at $\lambda_{\text{max}} < 340$ nm and attributed to the $\pi \rightarrow \pi^*$ charge transitions [35-36]. Chen *et al.* reported the presence of the the $\pi \rightarrow \pi^*$ charge transitions at 330 nm for their free bipyridine and phosphine ligands present in the dinuclear copper (I) complexes [35]. The band in the range 267-280 nm were assigned to the $n \rightarrow \pi^*$ transition of the non bonding electrons present on the nitrogen of the C=N moiety, this band was also observed in the UV/Vis of the free ligands. Similar observations were made by Mketto *et al.* which observed this band in the 278-311 nm region for their mononuclear pyridyl -imine copper (I) dendrimers [16]. The third new and weak bands in the range 351-401 nm reflected a report by Pal *et al.* and were possibly due to intra-ligand transitions [9]. The same observations were made by Choudry *et al.* for their diimine bipyridine ruthenium(II) complexes observed at 470 nm [37]. Several strong new bands were also observed in the region above 500 nm due to the metal-ligand ($\text{Ru}(d\pi) \rightarrow \text{L}(\pi^*)$) charge transfer transitions (MLCT). Complex 1 exhibits a high intense absorption peak at 592 nm. Complex 2 exhibits a peak at 613 nm followed by a shoulder at 650 nm, whereas for complex 3 three peaks were observed at 561, 605 and 656 nm respectively. The multiple MLCT bands observed are not uncommon for these types of compounds [37, 38]. Similar bands for the neutral quinolyl-imine ruthenium(II) have been reported. In the spectra of the quinolyl-imine ruthenium(II) complexes (C4-C5) a strong peak was observed in the range 245-249 nm attributed to the $\pi \rightarrow \pi^*$ charge transition of the quinoline ring. Similar transitions were reported by Mketto *et al.* for their mononuclear quinolyl-imine copper (I) dendrimers [16]. The two peaks in the region 325-330 nm and 645-651 nm respectively were assigned to the $n \rightarrow \pi^*$ transition of the non bonding electrons present on the nitrogen of the C=N moiety and the metal-to-ligand charge transfer (MLCT) transitions respectively.

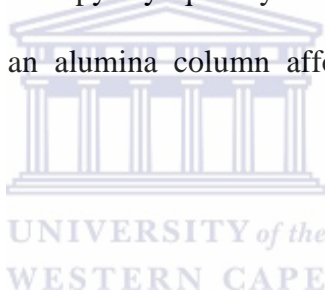
Again similar trends were observed for the cationic homobimetallic ruthenium(II) complex, C6. The UV/Vis displays a λ_{max} peak at 230 nm which is attributed to the $\pi \rightarrow \pi^*$ charge transitions of the aromatic rings. A second peak was observed at 272 nm, which was assigned to the $n \rightarrow \pi^*$ transition of non bonding electrons present on the nitrogen of the C=N moiety. The peak seen at 316 nm is due to intraligand transitions. The absorption band observed at a lower energy of 414 nm is attributed to the metal-to-ligand charge transfer (MLCT) transition.

The UV/Vis of the bimetallic palladium(II) complexes was conducted in DMSO and was only partially soluble. The bimetallic palladium(II) complexes showed several absorption bands in the range 266-818 nm. The first maximum band for the free ligands initially observed in the range 241-243 nm, underwent a shift to a longer wavelength that was observed in the 266-283 nm range. This band was seen at 266 nm for complex C7 and attributed to the $\pi \rightarrow \pi^*$ charge transitions of the pyridine. The $\pi \rightarrow \pi^*$ charge transition appeared at 283 nm for complexes C8, C9 and C10. Again the second band found in the range 307-320 nm were assigned to the $n \rightarrow \pi^*$ transition of the non bonding electrons present on the nitrogen of the C=N moiety, this band was also observed in the UV/Vis of the free ligands. Several other bands were only observed for complex 7 at 368, 699 and 818 nm. The band at 368 nm was attributed to the intraligand transitions. The expanded version of the spectra for complex 7 showed two more bands at longer wavelengths at 699 nm and 818 nm respectively and was attributed to the MLCT transitions [9]. The UV/Vis spectra of all the synthesized compounds revealed a red shift.

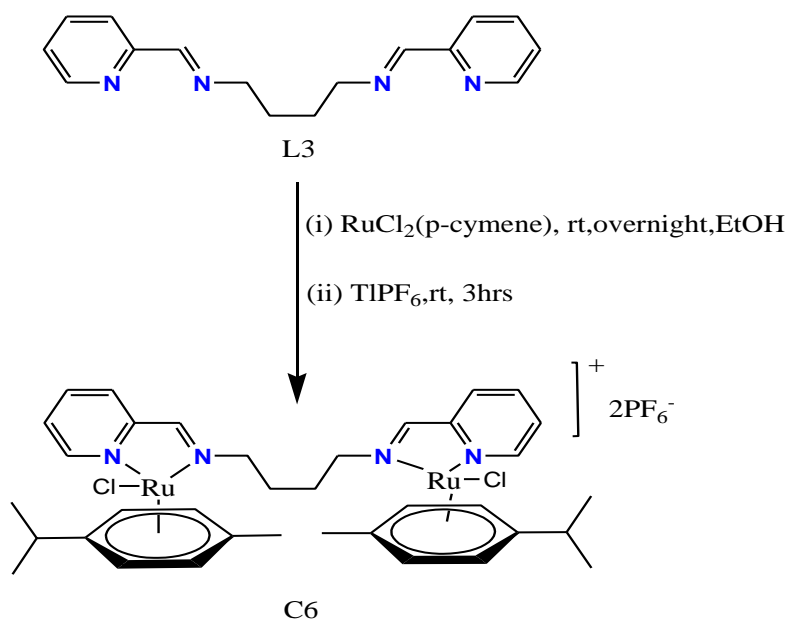
From table 4.10 the ruthenium(II) quinolyl-imine complexes (C4-C5) was observed to absorb at a longer wavelength in the UV/Vis spectra compared to the ruthenium(II) pyridyl-imine complexes (C1-C3), due to an increase in the delocalisation and extra conjugation of the quinoline ring. Similar observations were made for the free pyridyl/quinolyl-imine ligands (table 4.5). All the bimetallic pyridyl-imine palladium(II) complexes (C7-C10) absorbed at a longer wavelength compared to their respective free ligands.

4.3.4 Analytical and physical studies of pyridyl/quinolyl-imine ruthenium(II) and bimetallic pyridyl-imine palladium(II) complexes

Neutral mononuclear dichlororuthenium(II) complexes (C1-C5) was synthesized by reacting the precursor, $[\text{RuCl}_2(\text{dmsO})_4]$ and pyridyl/quinolyl-imine ligands in dry DCM. The compounds were isolated using an alumina column affording the complexes of general formula $[\text{RuLCl}_2]$.



The cationic homobimetallic ruthenium(II) complex, C6 was synthesized by reacting the ligand L3 with the dimer dichloro(*p*-cymene)ruthenium(II) and TIPF_6 and left in the freezer for 12 hrs to precipitate the product which was filtered and washed with ethanol (scheme 4.6). The bimetallic pyridyl-imine palladium(II) complexes (C7-C10) were synthesized by reacting the precursor $\text{Pd}(\text{cod})\text{Cl}_2$ with pyridyl-imine ligands in a 2:1 ratio in dry DCM, affording the complexes of general formula $[\text{Pd}_2\text{LCl}_2]$. The isolation of these compounds generally depended on the choice of the transition metal employed.



Scheme 4.6: A synthetic pathway for the synthesis of complex, C6.

Table 4.11: Analytical and Physical Data of pyridyl/quinolyl-imine ruthenium(II) and Pyridyl-imine palladium(II) complexes

Compounds	Molecular formula	Molecular weight	Yield%	Colour	Physical Appearance
C1	C ₁₄ H ₁₄ Cl ₂ N ₄ Ru	410.26	70	Purple-blue	Solid
C2	C ₁₅ H ₁₆ Cl ₂ N ₄ Ru	424.29	64	Purple-blue	Solid
C3	C ₁₆ H ₁₈ Cl ₂ N ₄ Ru	438.32	73	Purple-blue	Solid
C4	C ₂₂ H ₁₈ Cl ₂ N ₄ Ru	510.38	64	Green	Solid
C5	C ₂₃ H ₂₀ Cl ₂ N ₄ Ru	524.41	69	Green	Solid
C6	C ₂₂ H ₁₈ ClF ₆ N ₄ PRu	837	85	Brown	Solid
C7	C ₁₄ H ₁₄ Cl ₂ N ₄ Pd ₂	592.94	70	Yellow	Solid
C8	C ₁₅ H ₁₆ Cl ₂ N ₄ Pd ₂	606.97	68	Yellow	Solid
C9	C ₁₆ H ₁₈ Cl ₂ N ₄ Pd ₂	620.99	76	Yellow	Solid
C10	C ₁₇ H ₂₀ N ₄ Cl ₂ Pd ₂	635.02	72	Yellow	Solid

The colours of the complexes varied with the nature of the transitional metal and ligand used. During the electronic charge transfer from the the metals d-orbitals to the ligands molecular orbitals to form the coordination bond, the metals degenerate d-orbitals (same energy level) becomes non-degenerate and have different energy levels which can be explained by the crystal field theory based on the d-electron configuration of the complexes. The excited electronic state of this transition occurs in the visible region of the electromagnetic spectrum, which produces the characteristic color of the complexes. The neutral mononuclear pyridyl-imine ruthenium(II) complexes (C1-C3) were isolated and obtained as purplish-blue solids in moderately high yields.

The neutral mononuclear quinolyl-imine ruthenium(II) complexes (C4-C5) were isolated and obtained as green solids in moderately high yields. The compounds appeared to be air sensitive and are soluble in less polar solvents such as CHCl_3 and CH_2Cl_2 and the CH_2Cl_2 solution is blue. The cationic homobimetallic complex C6 was isolated as a brown solid with a melting point in the range 182-184 °C, appeared air stable and is soluble in polar organic solvents.

The bimetallic pyridyl-imine palladium(II) complexes (C7-C10) were isolated as yellow solids and continuously washed with DCM. The palladium(II) complexes showed was only partially soluble in DMSO and not in common organic solvents. All complexes were stored under an inert atmosphere. The above results (table 4.11) also indicated that different colors and physical appearances were observed with different reactions. The elemental analysis results are in close agreement with the expected results.

References

1. Killian CM, Johnson LK, Brookhart M, *J. Am. Chem. Soc.*, **1995**, *117*, 6414.
2. Banerjee S, Gangopadhyay J, Lu C-Z, Chen J-T, Ghosh A, *Eur. J. Inorg. Chem.*, **2004**, 2533.
3. Pandiyan T, Guadalupe HJ, Cruz J, Bernès S, Ugalde-Salvdivar VM, González I, *Eur. J. Inorg. Chem.*, **2008**, 3274.
4. Chen W, Xi C, Yang K, *Appl. Organomet. Chem.*, **2007**, *21*, 641.
5. <http://chemwiki.ucdavis.edu>, accessed on 26 September 2015.
6. Ebralidze I, Leitus G, Shimon LJW, Wangc Y, Shaik S, Neumann R, *Inorg. Chim. Acta.*, **2009**, *362*, 4713.
7. Radebe M, University of the Western Cape, (South Africa), MSc Dissertation, **2012**.
8. Patra GK, Goldberg I, *Crys. Growth & Des.*, **2003**, *3*, 321.
9. Busa AV, University of the Western Cape (South Africa), MSc Dissertation, **2012**.
10. Katwal R, Kaur H, Kapur BK, *Sci. Revs. Chem. Commun.*, **2013**, *3*, 1.
11. Golcu A, Tumer M, Demirelli H, Wheatley RA, *Inorg. Chim. Acta.*, **2005**, *358*, 1785.
12. Munro LB, Catalano VJ, *Eur. J. Inorg. Chem.*, **2014**, 4994.
13. Pal S, Pal S, *Polyhedron.*, **2003**, *22*, 867.
14. Sibanyoni JM, University of the Western Cape (South Africa), MSc Dissertation, **2007**.
15. www.thermoscientific.com, accessed 26 September 2015.
16. (a) Mketi N, Stellenbosch University (South Africa), MSc Dissertation, **2010**; (b) Rahaman SH, Ghosh R, Fun H-K, Ghosh BK, *Struct Chem.*, **2006**, *17*, 553.

17. Asadi M, Absalan G, Zamanpour A, *J. Iran. Chem. Soc.*, **2011**, 8, 1073.
18. Sheikh RA, Wani MY, Shreaz S, Hashm AA, *Arabian. J. Chem.*, 2012, doi:10.1016/j.arabjc.2011.08.003.
19. (a) us.mt.com, accessed 26 September 2015; (b) Oshima S, Hirayama N, Kubono K, Kokusen H, Honjo T, *Anal. Sci.*, **2002**, 18, 1351; (c) Oshima S, Hirayama N, Kubono K, Kokusen H, Honjo T, *Anal. Chim. Acta.*, **2001**, 441, 155.
20. Drew D, Doyle JR, *Inorg. Synth.*, **1990**, 28, 346.
21. Fonseca J, University of Lisboa (Portugal), PhD Dissertation, **2011**.
22. Govender P, Renfrew AK, Clavel CM, Dyson PJ, Therrien B, Smith GS, *Dalton. Trans.*, **2011**, 40, 1158.
23. Yorke J, Dent C, Decken A, Xia A, *Inorg. Chem. Comm.*, **2010**, 13, 54.
24. Viswanathamurthi P, Dharmaraj N, Anuradha S, Natarajan K, *Trans. Met. Chem.*, **1998**, 23, 337.
25. Moletsane AM, University of the Western Cape (South Africa), MSc Dissertation, **2011**.
26. Gupta G, Sharon R, Kapoor RN, *Transition Met. Chem.*, **1978**, 3, 282.
27. Bjernemose J, Hazell A, McKenzie CJ, Mahon MF, Nielsen LP, Raithby PR, Simonsen O, Toftlund H, Wolny JA, *Polyhedr.*, **2003**, 22, 875.
28. El-Sonbati AZ, El-Bindary AA, *Polish J. Chem.*, **2000**, 74, 621.
29. Govender P, Renfrew AK, Clavel CM, Dyson PJ, Therrien B, Smith GS, *Dalton Trans.*, **2011**, 40, 1158.
30. Rath RK, Nethaji M, Chakravarty AR, *Polyhedron.*, **2001**, 20, 2735.
31. Lalrempuia R, Carroll PJ, Kollipara MR, *J. Chem. Sci.*, **2004**, 116, 21.
32. Motswainyana WM, MSc Dissertation, University of the Western Cape, **2010**.
33. Cloete J, Mapolie SF, *J. Mol. Cat. A: Chem.*, **2006**, 243, 221.

34. Ojwach SO, Westman G, Darkwa J, *Polyhedron.*, **2007**, 26, 5544.
35. Chen Y, Chen J-S, Gan X, Fu WF, *Inorg. Chim. Acta.*, **2009**, 362, 2492.
36. Yang P, Yang X-J, Wu B, *Eur. J. Inorg. Chem.*, **2009**, 2951.
37. Choudhury S, Deb AK, Goswami S, *J. Chem. Soc. Dalton. Trans.*, **1994**, 1305.
38. Sullivan BP, Salmon DJ, Meyer TJ, *Inorg. Chem.*, **1978**, 17, 3334.



CHAPTER 5

5.0 Catalytic application of pyridyl and quinolyl-imine palladium and ruthenium (II) complexes

Chapter overview

In this chapter the background on the oxidative cleavage reaction and the Heck coupling reaction are outlined. Thereafter, the catalytic activity of the neutral mono- and cationic homobimetallic ruthenium(II) catalysts towards the oxidative cleavage of styrene is discussed. The catalytic activity of the neutral bimetallic palladium(II) catalysts towards the arylation of methyl acrylate and iodobenzene is also discussed.



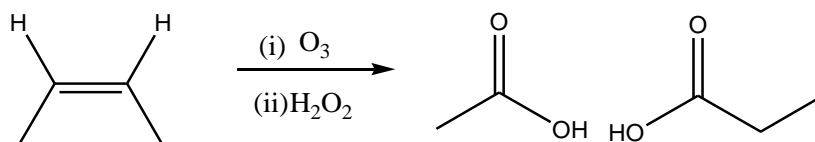
5.1 Ruthenium-catalyzed oxidative cleavage reactions

5.1.1 Introduction

Catalysis continues to be of great interest and has expanded tremendously since its discovery; organometallic chemistry has specifically made a tremendous impact in the field, and has prompted researchers to develop catalytic metal-based systems by moving away from stoichiometric systems for various organic transformations. Ruthenium and palladium organometallic compounds hold a prominent position in catalysis and are employed in a variety of catalytic reactions. Some of these transformations include the oxidative cleavage and the arylation of olefins known as the Heck cross coupling reaction. These types of reactions are beneficial for the production of fine chemicals.

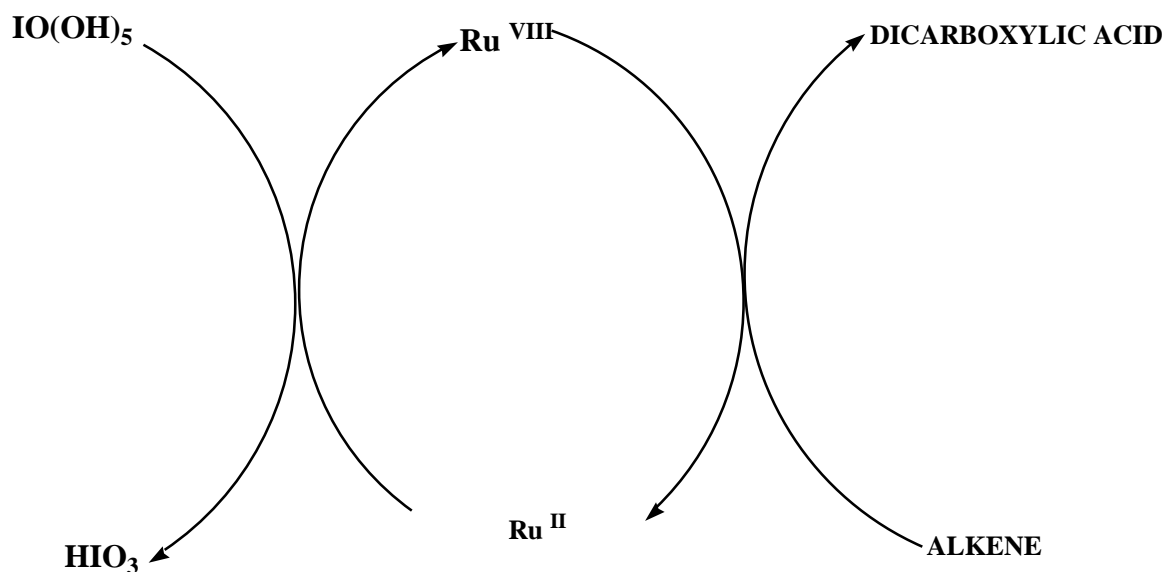
The oxidative cleavage reaction can simply be described as the ‘breaking’ of carbon-carbon or carbon-hydrogen bonds, and the formation of new carbon-oxygen bonds [1].

Previously the reaction was done by ozonolysis using O_3 as the oxidising agent (scheme 5.1) or with $KMnO_4$, but due to safety concerns and the high cost involved the reaction can also now be performed catalytically; in the presence of the oxidants IO_4^- or H_2O_2 and ruthenium complexes which form superior oxidation catalysts.



Scheme 5.1: Oxidative cleavage of alkenes using O_3 .

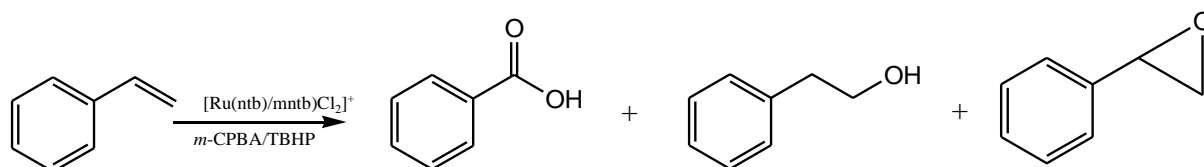
The oxidative cleavage can occur in two main ways, which is the transformation of alkenes into 1,2-diols followed by oxidative cleavage [2] and the direct cleavage of alkenes into a variety of functionalized products [3a]. The direct cleavage of alkenes can be carried out with catalytic amounts of transition metals such as ruthenium in the presence of a co-oxidant [3b, 3c]. Depending on the reaction conditions the oxidative cleavage of alkenes can either lead to the formation of ketones, aldehydes or carboxylic acids. The oxo ruthenium complex, RuO_4 , is the most powerful oxidant documented in literature [4]. Due to the toxicity of RuO_4 the ruthenium-catalysed cleavage of alkenes are mostly done using the Sharpless procedure [5], during which $RuCl_3 \cdot xH_2O$ is used in a biphasic CCl_4 - CH_3CN - H_2O solution in the presence of $NaIO_4$ as a co-oxidant. The reaction mechanism is described to occur via the formation of the ruthenate (VI) ester intermediate (scheme 5.3) [6].



Scheme 5.2: Catalytic cycle for oxidative cleavage of alkenes to acids by *cis*- $[\text{RuCl}_2(\text{bpy})_2] \cdot 2\text{H}_2\text{O}/\text{IO(OH)}_5$ [6].

Kanmani *et al.* reported the oxidative cleavage of styrene by a variety of ruthenium(II) perchlorate complexes using TBHP or H_2O_2 as the oxidizing agents [7]. The oxidation of styrene with TBHP resulted in the formation of both benzaldehyde and styrene oxide as the major and minor product respectively, in the presence of oxygen the yield of benzaldehyde was found to increase. While the use of H_2O_2 as the oxidizing agent, resulted in the formation of benzaldehyde selectively as the product though it was less than 10% in yield.

Several ruthenium complexes of nitrogen-containing ligands have drawn much attention as oxidation catalysts and has been reported as follows; Murali *et al.* investigated the catalytic oxidation activity of Tris[(benzimidazol-2-yl)-methyl]amine ruthenium(III) complexes; it was reported that allylic oxidation of cyclohexene was a more favourable reaction, while the ruthenium catalyst effected the epoxidation reaction for the substrates cyclooctene and styrene [8]. The epoxidation of styrene resulted in a higher TON in the presence of the oxidising agent TBHP than m-CPBA.



Scheme 5.3: Epoxidation of styrene [8].

Liu *et al.* reported the efficient oxidative cleavage of various alkenes to their respective α -diketone counterparts using pyridazine-based N-Heterocyclic carbene dinuclear ruthenium catalysts [9]. The oxidative cleavage of the alkene, (E)-1,2-diphenylethene, was carried out using TBHP as the oxidising agent and CH_3CN as the solvent at room temperature. This resulted in formation of benzil with a 92% yield. Daw *et al.* reported the selective oxidative cleavage of olefins to aldehydes by employing a catalytically active abnormal-NHC–Ru(II) complex, $[Ru(COD)(L1)Br_2]$ [10]. The reaction was carried out in a biphasic solvent mixture, $EtOAc/CH_3CN/H_2O$, using $NaIO_4$ as the co-oxidant at room temperature for 30 min. The oxidative cleavage of styrene and electron-rich substituted styrene led to the quantitative formation of benzaldehyde, while electron-deficient substituted styrene resulted in lower yields of 92-94%. The mechanism was reported to occur via the formation of the high valent Ru–oxo specie [10].

The following section discusses the results obtained for the selective oxidative cleavage of styrene, using our nitrogen-based Ru (II) complexes.

5.1.2 Oxidative cleavage of styrene

Based on previous work done by Busa *et al.* on the oxidative cleavage of straight alkenes, particularly 1-octene we extend the scope of the study to the aromatic compound styrene.

The reaction was carried out in a biphasic sharpless system in the presence of the tetradentate N-donor ruthenium(II) catalysts and the co-oxidant $NaIO_4$ (figure 5.1).

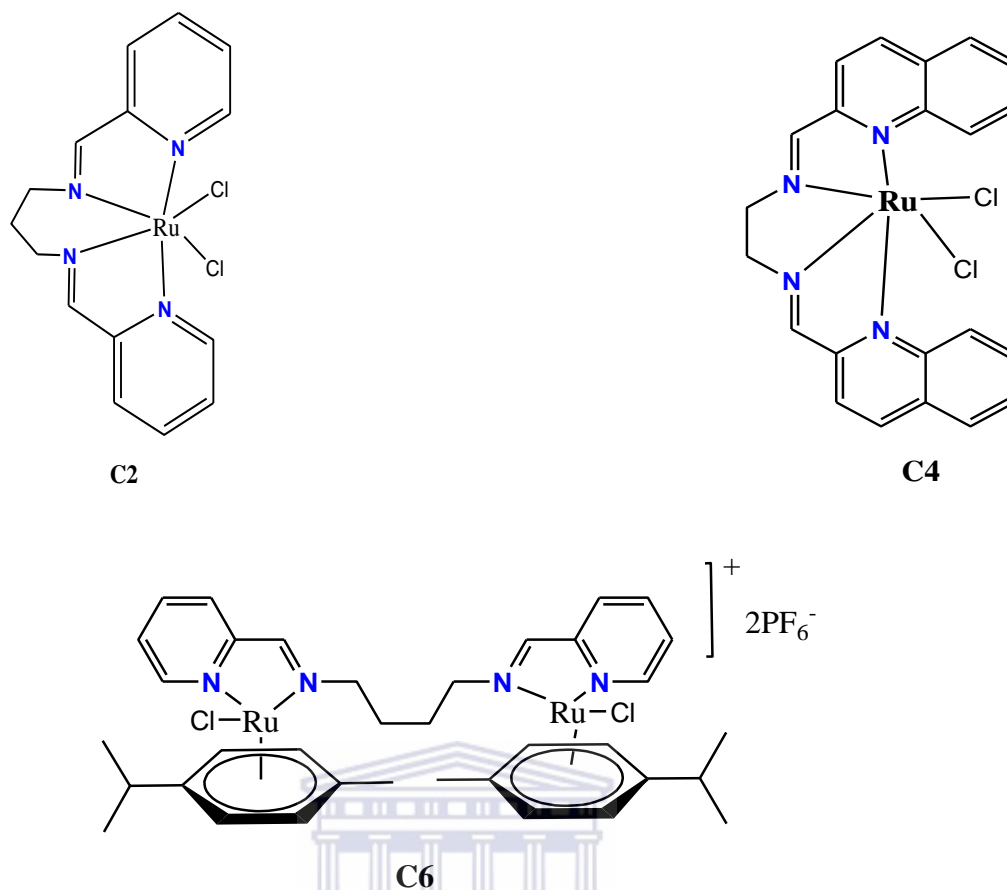
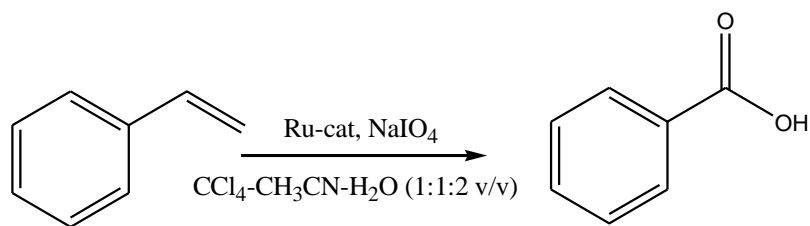


Figure 5.1: Representation of neutral mononuclear and cationic homobimetallic (N,N) Ru(II) catalysts.

The neutral mononuclear ruthenium(II) catalysts C2 and C4, and cationic homobimetallic ruthenium(II) catalyst, C6 was evaluated for the oxidative cleavage of styrene and was carried out in a sharpless biphasic solvent system involving tetrachloromethane, acetonitrile and water (1:1:2 v/v) at room temperature for 2 hours and NaIO_4 as a co-oxidant (scheme 5.6). The reaction progress and product formation were monitored by thin layer chromatography (TLC). The product was identified using analytical techniques such as FT-IR and ^1H NMR.



Ru= **C2, C4, C6**

Scheme 5.4: Schematic representation for oxidative cleavage of styrene

Under the reaction conditions and using the ruthenium(II) mononuclear complexes C2 and C4, a colour change from purple to yellow was observed after an induction period of 10 min. While employing the homobimetallic complex C6, the reaction mixture resulted in a colour change from colourless to pale yellow also after an induction period of 10 min. The colour change observed was also reported by Busa *et al.* and is due to the formation of the active ruthenium species, RuO_4 , involved in the reaction [11]. The oxidative product yields from moderate to good with the major products being benzoic acid for all the catalysts evaluated. The solvent, CH_3CN , in the sharpless system facilitates in the selective formation of carboxylic acids being favoured. All oxidation crude products were extracted with diethyl ether (3x10 ml) and the organic layer was evaporated. The ^1H NMR and FT-IR spectroscopy of the crude product confirmed the cleavage of styrene to benzoic acid. The final product was obtained as white needle-like crystals. A summary of the results is given below in table 5.1.

Table 5.1: Oxidative cleavage of styrene by ruthenium catalysts (C2, C4, and C6)

Entry	Catalyst	Temp (° C)	Time (h)	Yield % [TO]
1	C2	RT	2	69 [139]
2	C4	RT	2	73 [146]
3	C6	RT	2	77 [155]

Reaction conditions: Reaction conditions: alkene (0.556 mmol), catalyst (0.00278 mmol, C-6), and periodic acid (2.78 mmol) were added to a mixture of CCl₄-CH₃CN-H₂O (1:1:2 v/v), stirring at room temperature for 2 h. TO = turnover = moles of the product/moles of the catalyst.

The overall catalytic activity of the catalyst was moderate to good with the major product being benzoic acid, for all the catalysts evaluated. After 2 hours the catalysts C2 and C4 gave conversions of 69 % and 73% respectively. Under identical reaction conditions as the previously mentioned catalysts, C6 gave the highest conversion of 77 % (entry 3). However catalyst C2, exhibited the lowest overall catalytic activity (entry 1). The higher conversions of catalysts C4 and C6 were attributed to the bulkiness of the structures in comparison to catalyst C2.

5.1.2.1 FT-IR analysis of the oxidative cleavage product

The following FT-IR spectra (figure 5.1) is a typical example obtained for the oxidative products and was recorded using KBR.

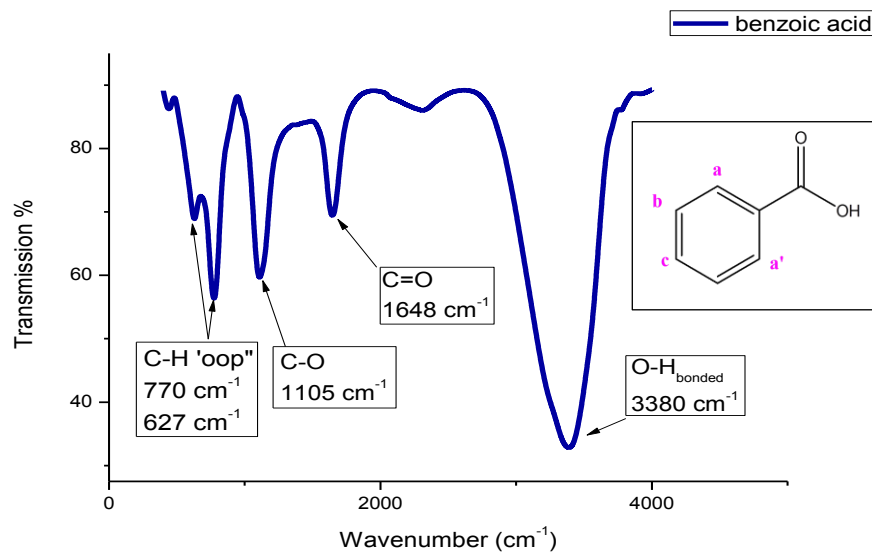


Figure 5.2: FT-IR spectrum of the crude product of oxidation of styrene, after 2 hrs catalyzed by complex, C6

The products formed by the oxidative cleavage of styrene were characterised with the Fourier transform infrared spectroscopy to obtain detailed information of the functional groups and their chemical environment. The FT-IR spectra of benzoic acid displays a band at 1648 cm^{-1} which is attributed to the C=O functional group, the C=O frequency is observed to appear at a lower frequency due to resonance with the phenyl ring. The C-O band at 1105 cm^{-1} confirms the presence of the carboxylic group. The OH (H-bonded) functional group is observed at 3380 cm^{-1} . Characteristic C-Hoop patterns were observed at 770 cm^{-1} and 627 cm^{-1} respectively. The absence of the shoulder bands in the region $2830\text{--}2695\text{ cm}^{-1}$ supports that the final product is a carboxylic acid rather than an aldehyde.

5.1.2.2 ^1H NMR analysis of the oxidative cleavage product

The crude products were further characterized by ^1H NMR and were recorded in $\text{CDCl}_3\text{-}d$ solutions at 25°C . The ^1H NMR spectra showed the formation of the carboxylic acid.

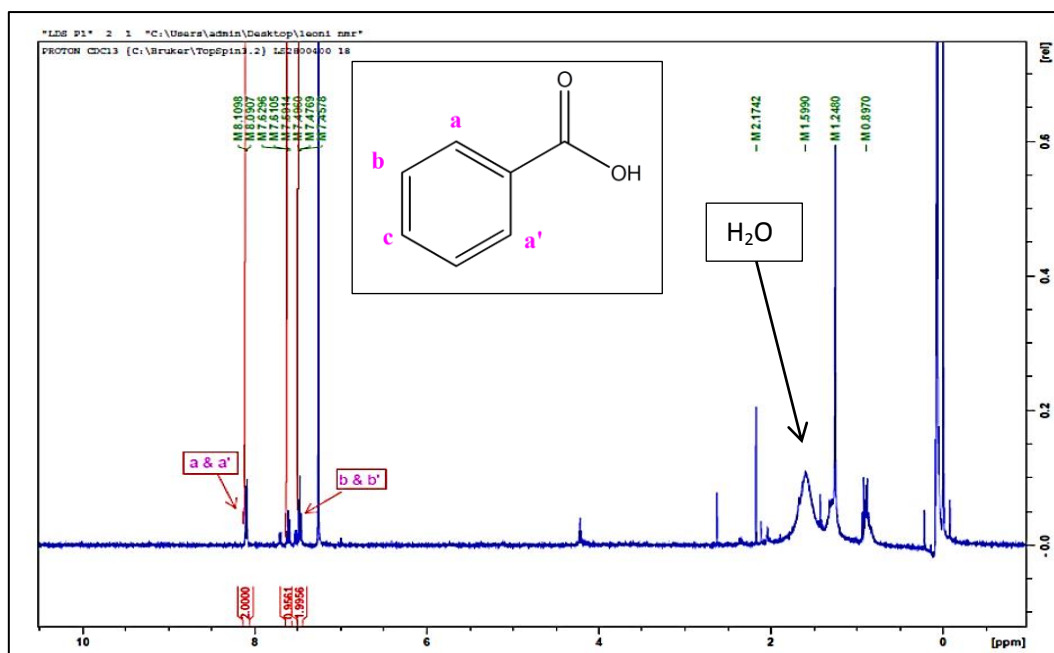


Figure 5.3: ¹H NMR spectrum of the crude product of oxidation of styrene, after 2 hrs catalyzed by complex, C6

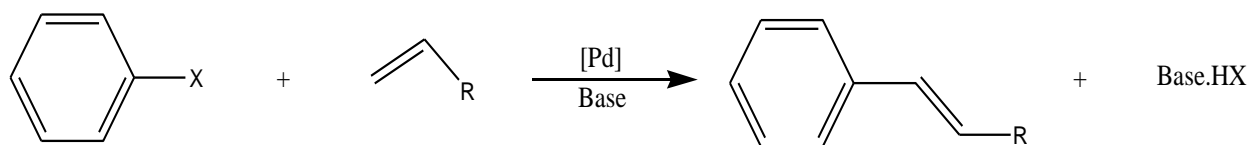
The products formed by the oxidative cleavage of styrene were characterised with the ¹H NMR spectroscopy to obtain detailed information of the functional groups and their chemical environment. The protons a and a' experiences the biggest shift at 8.09 ppm, since they are more deshielded by the carboxylic group compared to protons b and b'. The presence of the hydroxyl hydrogen could not be observed in the spectra which usually appears in the range 10-13 ppm, this could be due to the exchange of the proton with water since traces of water was found in the ¹H NMR spectra.

5.2 Palladium-catalyzed Heck coupling reactions

5.2.1 Introduction

Heck coupling reactions is in contrast to oxidative cleavage. Whereas the latter destroys C-C bonds, the former makes C-C bonds.

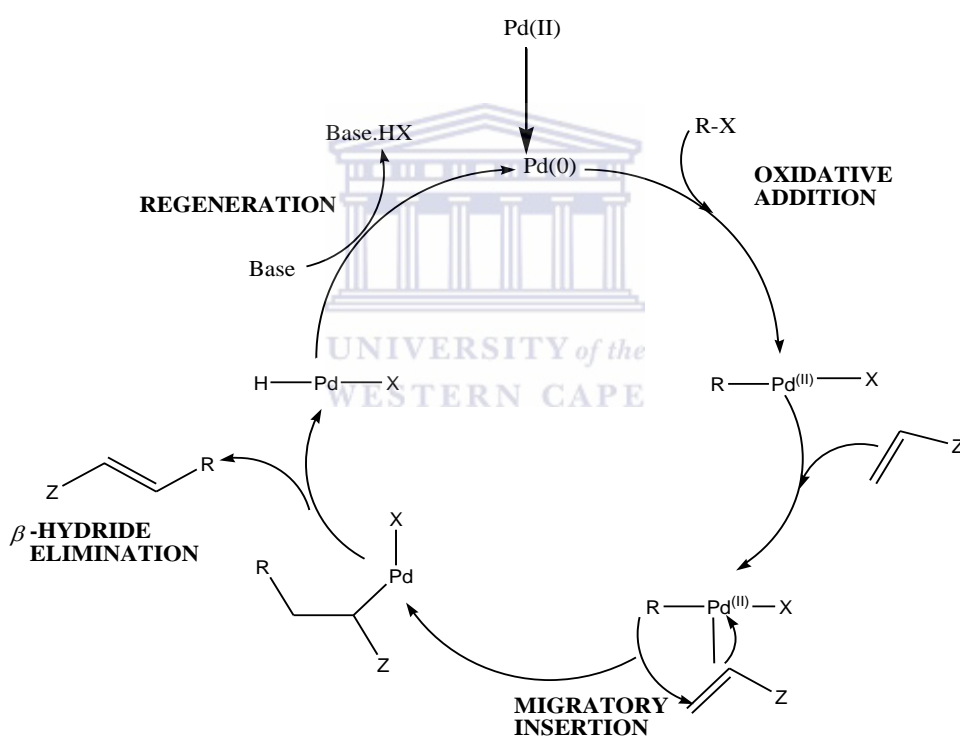
The Heck coupling reactions involves the reaction of aryl halides and various substituted olefins in the presence of a base to form organic olefinic compounds and was first reported by Heck and Mizoroki in the early 1970's independently [12,13]. The reaction is typically carried out in the presence of palladium precursors such as Pd(OAc)₂, Pd₂(dba)₃, Pd(PPh₃)₄ or PdCl₂, a phosphine ligand such as PPh₃ or PR₃ and the base Et₃N as a reducing agent. During the reaction mechanism the catalytically active species Pd(0) is formed in-situ from the pre-catalysts [12]. The choice of ligand plays a pivotal role in the synthesis of an efficient catalytic active catalyst for palladium-catalyzed cross coupling reactions and effects the oxidative addition and the elimination step of the catalytic cycle [14]. During the early years the readily available PPh₃ was considered the ligand of choice, later Heck found that the tri-*o*-tolylphosphine ligand had a better activity compared to [Pd(PPh₃)₄] [15]. The use of the bidentate ligands is also documented in literature to accelerate the reductive-elimination step in the catalytic cycle, resulting in an increase in the overall rate of the reaction and less competition from the β-hydride-elimination side-product formation [16]. The rate of the reaction is also effected by the aryl halide, in the order of I > Br ~ OTf >> C from fastest to slowest rate; the degree of substitution of the olefinic compound. The Heck coupling reaction has found useful application in the pharmaceutical industry and the synthesis of natural products [17].



Scheme 5.5: Heck cross coupling reaction.

The mechanism of the Pd-catalyzed C-C coupling reaction proceeds as follows; the oxidative addition of an organohalide (R-X) to the catalytically active Pd(0) complex occurs, forming a *trans* palladium complex.

The next step follows the insertion of an olefin, into the newly formed palladium(II) carbon bond. This is followed by β -hydride elimination, resulting in the formation of the alkene product and a palladium hydrido halide [18a]. The base then facilitates in the regeneration of the active Pd(0) complex [18b, 18c]. Majority of palladium-catalysed Heck reactions are reported to follow a similar catalytic cycle.



Scheme 5.6: Mechanism for Heck coupling reaction.

Metallodendrimers have also been tested as catalysts for Heck coupling reactions. Krishna *et al.* reported the catalytic activity of poly(ether-imine) Pd(II) phosphine dendrimers [19]. The complexes were air sensitive in the solution phase over an extended period.

The catalytic activities of the catalysts were also reported to increase with an increase in the generation number [19]. Smith *et al.* reported the efficient catalytic activity of the (propylene imine)-iminopyridyl-palladium dendrimers used for the coupling reaction of iodobenzene with methyl acrylate [20]. Moletsane *et al.* reported the arylation of styrene with iodobenzene using iminopyridyl-palladium dendrimer (figure 5.4), which resulted in the arylation of styrene with a 75% yield in only 7 hours [21].

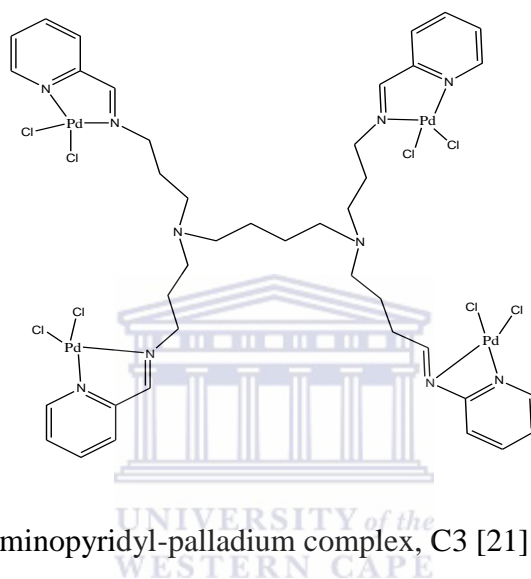
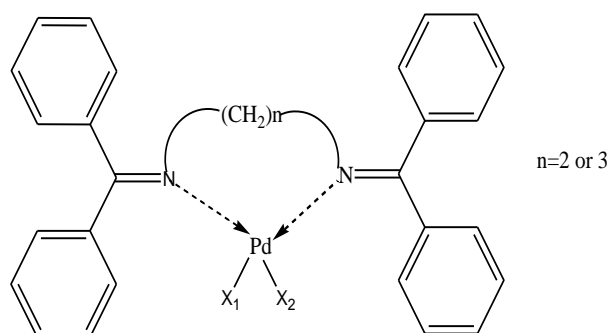


Figure 5.4: Dendrimeric iminopyridyl-palladium complex, C3 [21].

The N-donor palladium complexes have also been tested as catalysts for Heck coupling reactions. Nelana *et al.* reported the catalytic activity of some unconjugated di-imine palladium catalysts for the arylation of methyl acrylate or butyl acrylate with iodobenzene [22]. The palladium(II) complexes were reported to exhibit a higher catalytic activity than their analogous palladium(II) dichloride salt. Radebe *et al.*, reported the catalytic activity of some novel thiophene linked imino-pyridyl Pd (II) catalysts for the arylation of methyl acrylate, in the coupling of iodobenzene, 4-iodotoluene, and 1-iodo-4-nitrobenzene [23]. The major Heck coupling products were reported as α -aryl products, *trans*-methyl cinnamate, at 50-60 yields in 2 hours.



Complex 1: $n = 2$ or 3 ; $X_1 = \text{Cl}$

Complex 2: $n = 2$ or 3 ; $X_1 = \text{Cl}$, $X_2 = \text{CH}_3$

Figure 5.5: Unconjugated di-imine Pd(II) complexes [22].

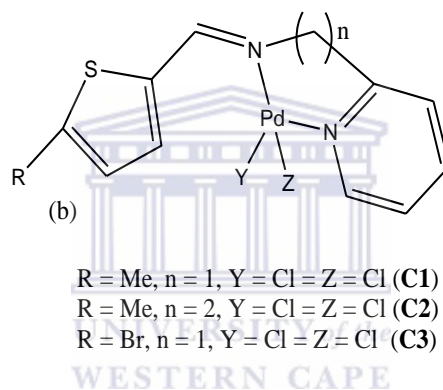


Figure 5.6: Thiophene linked iminopyridyl Pd(II) complexes [23].

Over the past decades a lot of progress has been made, although there are still a few drawbacks encountered with the previously mentioned system one of which includes selectivity and yield issues.

Following literature reports on the successful application and active palladium complexes similar to the palladium N,N catalyst systems prepared during this research, we evaluated the activity and scope of some of the prepared bimetallic palladium(II) complexes. The following section discusses the results of the palladium catalyst which is based on N-donor pyridyl-imine ligands that has not yet been tested for these type of transformations as far as our knowledge. These N-donor ligands are air/moisture stable and inexpensive.

5.2.2 Arylation of methyl acrylate with Iodobenzene

The bimetallic pyridyl-imine palladium(II) catalysts, C9, C10 (figure 5.7) were evaluated for the arylation of methyl acrylate with iodobenzene. The reaction was carried out using iodobenzene with methyl acrylate in dry DMF at 110°C under reflux conditions for 24 hours (scheme 5.7). Small amount of the sample was withdrawn at regular intervals during the reaction time and diluted in DMF for GC analysis. A GC-chromatogram of the arylation of iodobenzene, catalysed by complex **C10** is given in Appendix 1. The Heck coupling product yield was obtained based on the amount of the internal standard, mesitylene. The converted substrate was calculated as a percentage of the initial substrate used and plotted against time (figure 5.8). After the reaction time all the Heck coupling crude products were dissolved in DCM and washed with water and dried over anhydrous magnesium sulphate. The reaction was monitored by TLC and the coupling product was also characterized using the analytical techniques ^1H NMR and FT-IR.

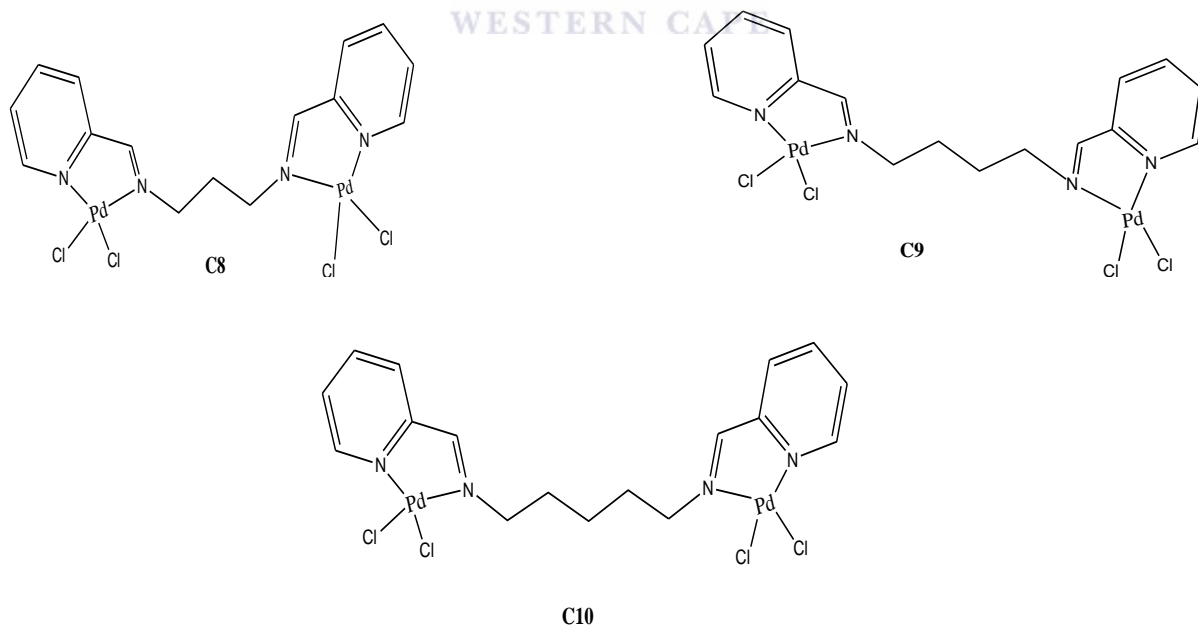
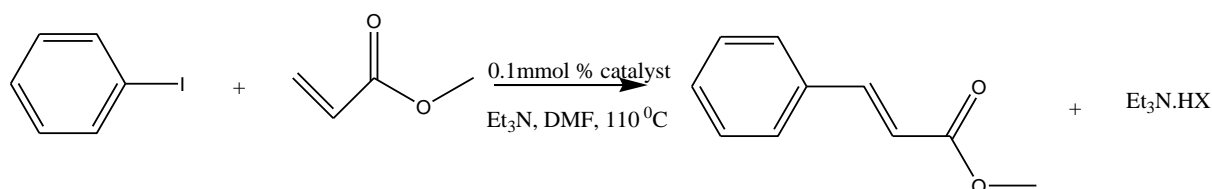


Figure 5.7: Bimetallic pyridyl-imine Pd(II) catalysts



Scheme 5.7: Palladium(II) catalyzed arylation of methyl acrylate with iodobenzene

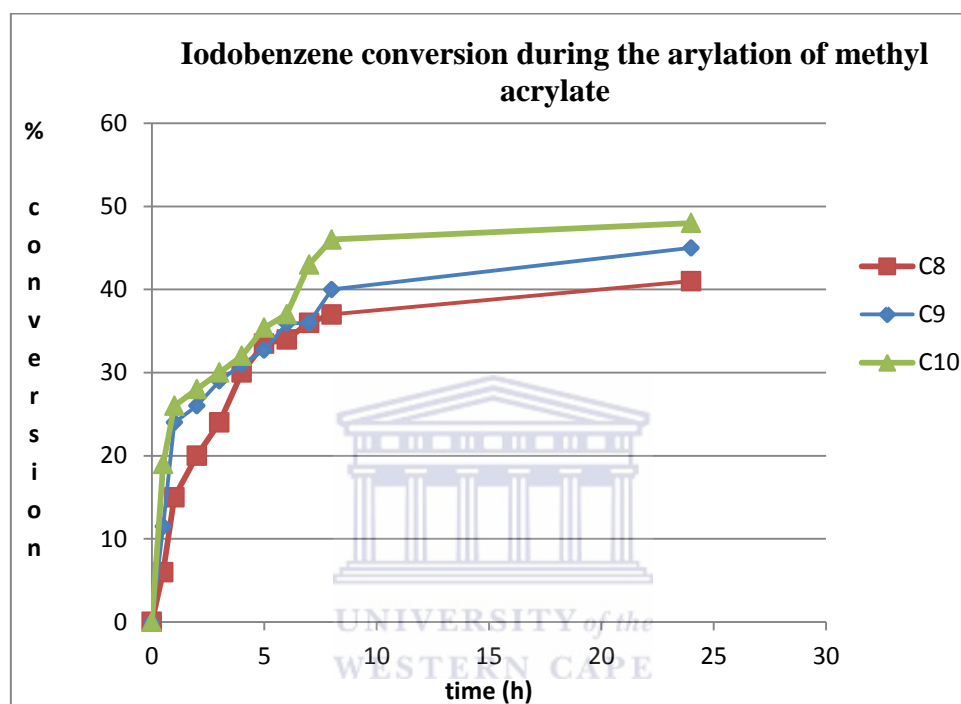


Figure 5.8: Conversion as a function of time for the arylation of methyl acrylate with iodobenzene at 110 °C.

Under the reaction conditions using the bimetallic pyridyl-imine palladium(II) catalysts C9 and C10 a colour change from orange to red was observed after an induction period of 5-10 min. While an induction period of 15 min was observed for catalyst C8. The colour change observed was also reported by Radebe *et al.*, and is due to the formation of the active Pd (0) species when the catalysts are reduced from Pd (II) by triethylamine [23]. The Heck coupling product was obtained as moderate to good yields with the major products *trans*-methyl cinnamate, for all the catalysts evaluated.

The products were evaluated by GC and the ¹H NMR and FT-IR analyses of the crude product also aided in the confirmation of the arylation of methylacrylate to trans-methylcinnamate. The final crude product was obtained as deep maroon oil. A summary of the results is given below in table 5.2.

Table 5.2: Conversions of iodobenzene during arylation with methyl acrylate

Entry	Catalyst	Temp (° C)	Time (h)	Conversion %
1	C8	110	24	41
2	C9	110	24	45
3	C10	110	24	48

Reaction conditions: iodobenzene (10 mmol); Methyl acrylate (10 mmol); Et₃N (10 mmol); Catalyst (0.1mmol); Solvent: DMF (10 ml); Determined by GC with mesitylene as internal standard.

The catalysts were found to have moderate catalytic activity of 45 % in average. All the bimetallic pyridyl-imine palladium(II) complexes successfully catalyzed the coupling of iodobenzene with methyl acrylate. From the graph the catalytic activity of the catalysts followed a similar trend. The catalysts exhibited very low conversion during the initial stages of the reaction, with 15 %, 24 % and 26 % conversions in an hour for catalyst C8, C9 and C10 respectively (table 5.2). After 24 hours the catalysts yield a conversion of almost 50%. From the table catalyst C10 was found to be most active exhibiting the highest conversion of 48 % compared to C8 and C9 which resulted in 41 % and 45 % conversions respectively. A trend was observed with the catalytic activity increasing from C8<C9<C10 this could be due to an increase in the length of the alkyl chain linker from C8<C9<C10. Motswainyana *et al.* reported imino-pyridyl nickel (II) catalysts only differing in their alkyl chain (methyl and ethyl). The catalyst with ethyl linker resulted in an 85 % conversion compared to the analogue catalyst with a methyl linker yielding an 80 % conversion [24].

The longer the alkyl chain the more labile the catalyst precursors. However, there was little cooperative effect observed from the homometals suggesting that the metals need to be different.

5.2.2.1 FT-IR analysis of the Heck coupling products

The following FT-IR spectrum (figure 5.9) is a typical spectrum obtained of the crude product for the arylation of methyl acrylate and was recorded using nujol mulls on NaCl plates.

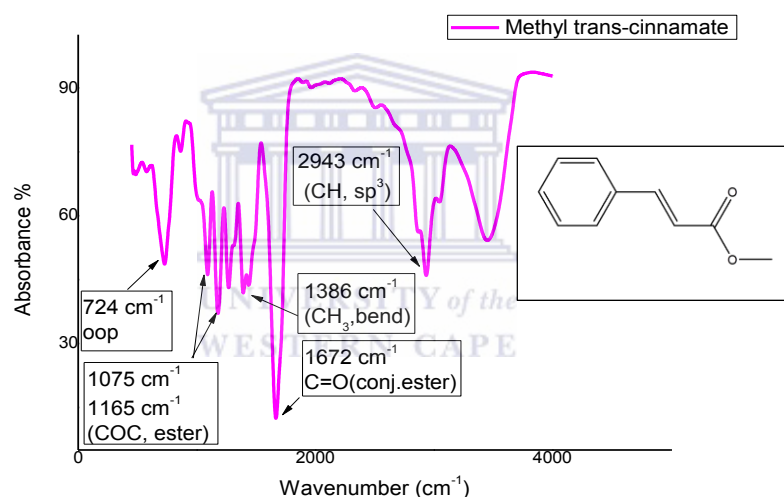


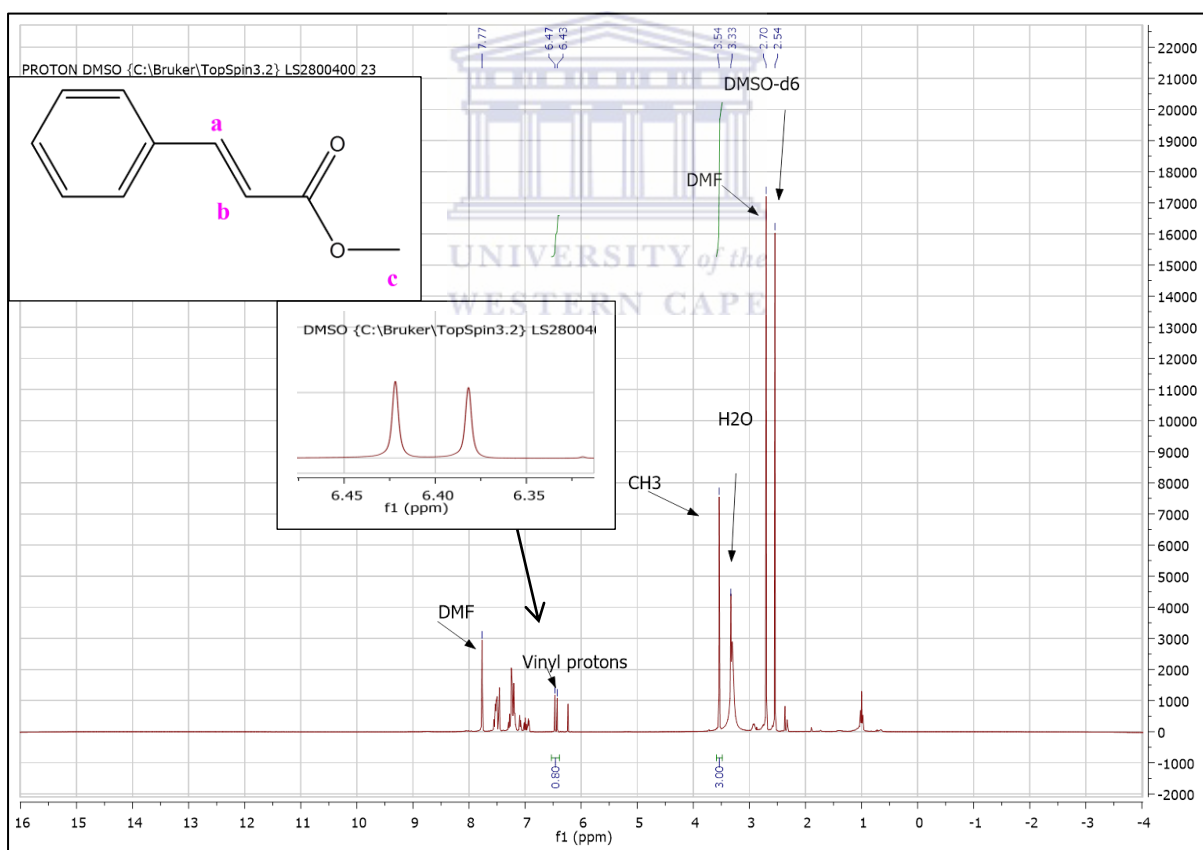
Figure 5.9: FT-IR spectrum of the crude product of arylation of methyl acrylate, after 24 hrs catalyzed by complex C8

The Heck coupling products were characterised with the Fourier transform infrared spectroscopy to obtain detailed information of the arylation products functional group and their chemical environment.

The carbonyl stretch C=O of α , β -unsaturated esters normally appears from 1730-1715 cm^{-1} , but due to the conjugation the ester functional group is observed at a lower frequency of 1672 cm^{-1} . The presence of the C-O-C functional group is observed at 1075 cm^{-1} and 1165 cm^{-1} .

5.2.2.2 ^1H NMR analysis of the Heck coupling products

The crude products were further characterized by ^1H NMR and were recorded in DMSO- d_6 solutions at 25°C. The ^1H NMR spectra showed the formation of *trans* methyl cinnamate as the regioselective major product.



Reaction conditions: iodobenzene (10 mmol); Methyl acrylate (10 mmol); Et₃N (10 mmol); Catalyst (0.1mmol); Solvent: DMF (10 ml); Determined by GC with mesitylene as internal standard.

Figure 5.10: ^1H NMR spectrum of the crude product of arylation of methyl acrylate, after 24 hrs catalyzed by complex C8.

The arylation products were characterised with the ^1H NMR spectroscopy to obtain detailed information of the functional group and their chemical environment. The ^1H NMR spectra revealed the presence of the vinylic protons, α , around 6.47 ppm with typical singlet chemical shifts. The presence of the vinyl protons strongly indicated the formation of the α -aryl product. The CH_3 protons were seen at 3.54 ppm and observed as an intense singlet peak. The aromatic proton was also observed in 7-7.5 ppm.

5.3 Conclusion

In conclusion we have successfully synthesized three mononuclear/bimetallic pyridyl/quinolyl-imine ruthenium(II) complexes and used them as catalyst precursors for the oxidative cleavage of styrene. Three new bimetallic pyridyl-imine complexes were also used as catalyst precursors for the Heck coupling reaction of iodobenzene with methyl acrylate. The preliminary tests of the catalyst precursors for both oxidative cleavage and Heck coupling reactions proved the catalyst can be employed for the above mentioned catalytic reactions. In the oxidative cleavage, benzoic acid was formed from styrene and was confirmed analytically. The catalytic activity of the pyridyl/quinolyl-imine catalysts during the oxidative cleavage showed moderate to good overall activity. On the other hand, the Heck coupling product *trans*-methyl cinnamate was formed from the coupling reaction of methylacrylate with iodobenzene. The bimetallic pyridyl-imine catalysts showed low overall activity during the Heck coupling reaction of iodobenzene, however the catalysts represent some of the few palladium non-phosphine based catalysts.

References

1. Beller M, Bolm C, *Transition Metals for Organic Synthesis: Building Blocks and Fine Chemicals*, Wiley-VCH, Germany, Second ed., **2004**, 1, 201.
2. Shing KT, *Comprehensive Organic Synthesis*, (Ed.: Trost BM, Fleming I), Pergamon Press, Oxford, **1991**, 7, 703.
3. (a) Larock CR, *Comprehensive Organic Transformations*, Wiley-VCH, New York Second ed., **1999**, 1213; (b) Neumann R, Kogan V, Quintal MM, *Org. Lett.*, **2005**, 7, 5039; (c) Jin ZD, Yu WS, Mei Y, Kang Y, Hua ZM, *Org. Lett.*, **2004**, 6, 3217.
4. Griffith WP, *Ruthenium Oxidation Complexes: Their Uses as Homogenous Organic Catalysts*, (Ed.: Bianchini C, Cole-Hamilton DJ, van Leeuwen P, Springer, New York, **2011**, 34, 7.
5. Carlsen PHJ, Martin TKVS, Sharpless KB, *J. Org. Chem.*, **1981**, 46, 3936.
6. Shoair AGF, Mohamed RH, *Synth. Commun.*, **2006**, 36, 59.
7. Kanmani S, Vancheesan S, *J. Mol. Cat. A: Chem.*, **1999**, 150, 95.
8. Murali M, Mayilmurugan R, Palaniandavar M, *Eur. J. Inorg. Chem.*, **2009**, 3238.
9. Liu X, Chen W, *Organometallics.*, **2012**, 31, 6614.
10. Daw P, Petakamsetty R, Sarbajna A, Laha S, Ramapanicker R, Bera JK, *J. Am. Chem. Soc.*, **2014**, 136, 13987.
11. Busa AV, University of the Western Cape (South Africa), MSc Dissertation, **2012**.
12. Heck RF, Nolley JP, *J. Organic Chem.*, **1972**, 37, 2320.
13. a) Mizoroki T, Mori K, Ozaki A, *Bull. Chem. Soc. Jpn.*, **1973**, 46, 1505; b) Mizoroki T, Mori K, Ozaki A, *Bull. Chem. Soc. Jpn.*, **1971**, 44, 581.
14. Galardon E, Ramdeehul S, Brown JM, Cowley A, Hii KK, Jutand A, *Angew. Chem, Int. Ed.*, **2002**, 41, 1760.
15. Heck RF, *Org. React.*, **1982**, 27, 345.

16. (a) Kondolff I, Doucet H, Santelli M, *Organometallics.*, **2006**, 25, 5219; (b) Luo X, Zhang H, Duan H, Liu Q, Zhu L, Zhang T, Lei A, *Org. Lett.*, **2007**, 9, 4571; (c) Melzig L, Gavryushin A, Knochel P, *Org. Lett.*, **2007**, 9, 5529.
17. Hong CY, Kado N, Overman LE, *J. Am. Chem. Soc.*, **1993**, 115, 11028.
18. (b) Hills ID, Fu GC, *J. Am. Chem. Soc.*, **2004**, 126, 13178; c) Barrios-Landeros F, Carrow BP, Hartwig JF, *J. Am. Chem. Soc.*, **2008**, 130, 5842.
19. Krishna TR, Jayaraman N, *Tetrahedron.*, **2004**, 60, 10325.
20. Smith GS, Mapolie SF, *J. Mol.Cat. A: Chem.*, **2004**, 213, 187.
21. Moletsane A, University of the Western Cape (South Africa), MSc Dissertation, **2011**.
22. Nelana S, Cloete J, Lisenskey G, Nordlander E, Guzei I, Mapolie S, Darkwa J, *J. Mol. Catal. A: 2008*, 285,72.
23. Radebe M, University of the Western Cape (South Africa), MSc Dissertation, **2012**.
24. Motswainyana WM, University of the Western Cape (South Africa), MSc Dissertation, 2012.



CHAPTER 6

6.0 Conclusion and Recommendations

Chapter Overview

This chapter outlines the main objectives achieved and discusses the catalytic activity of the pyridyl and quinolyl-imine neutral mononuclear and cationic homobimetallic Ru(II) and bimetallic Pd(II) complexes towards oxidative cleavage of styrene and the Heck coupling reactions of methyl acrylate with iodobenzene respectively. Lastly recommendations are given to improve the catalytic activity of these complexes for future work.

6.1 General conclusion

In conclusion, a family of pyridyl and quinolyl-imine tetradentate Schiff base ligands (**L1-L6**) were successfully synthesized by a Schiff base condensation reaction and fully characterized by various spectroscopic techniques such as FT-IR, ^1H NMR spectroscopy, ^{13}C NMR spectroscopy, mass spectroscopy, ultraviolet-visible spectroscopy, TGA and elemental analysis. The ligands (**L1, L3 and L4**) were obtained as brown and orange solids in good to moderate yields 97%, 88 % and 62% respectively. Ligands **L2, L5 and L6** were obtained as low viscosity brown and orange oils respectively as good yields 90%, 80% and 74%. The successful synthesis of the ligands were confirm by the presence of the C=N moiety around 1620 cm^{-1} in the FT-IR spectra. The successful imine formation was further confirmed by the presence of the azomethine proton observed at around 8.35 ppm in the ^1H NMR spectra of the ligands. The ^{13}C NMR spectra showed the presence of the imine carbons around 160.0 ppm. Analysis of the ligands by UV/Vis showed the presence of both the intramolecular ligand transitions of the respective aromatic rings ($\pi\rightarrow\pi^*$) and non-bonding ($n\rightarrow\pi^*$) charge transitions around 234 nm and 268 nm respectively.

The elemental analyses and mass spectra of the synthesized compounds were in good agreement with the calculated C,H,N values and molecular weight m/z values respectively. The structures of the prepared imines were also confirmed using GC/MS analysis. The TGA thermograms illustrated the initial decomposition of **L1** at a temperature of 180°C and **L4** at 122 °C.

The corresponding neutral mononuclear and cationic homobimetallic ruthenium(II) (**C1-C6**) and bimetallic palladium(II) complexes (**C7-C10**) were successfully synthesized, by reacting the pyridyl/quinolyl-imine ligands and the respective $\text{RuCl}_2(\text{dmsO})_4$, $\text{RuCl}_2(\text{p-cymene})_2$ or $\text{PdCl}_2(\text{cod})$ precursors respectively. The coordination of the ligands towards the metal precursors occurred via the azomethine nitrogen of the lone pair electrons present and the coordination behavior was determined using analytical techniques. The successful coordination of the neutral mononuclear pyridyl/quinolyl-imine ruthenium(II) complexes (**C1-C6**) were confirm by a red shift of the C=N moiety absorption band to around 1520 cm^{-1} in the FT-IR spectra. The successful coordination was further confirmed by the downfield shift of the azomethine proton signal to around 8.94 ppm in the ^1H NMR spectra compared to the free ligands. Analysis of the complexes by UV/Vis showed the presence of both $\pi \rightarrow \pi^*$, $n \rightarrow \pi^*$ and MLCT charge transitions around 230 nm, 267 nm and at 414 nm and above 500 nm respectively. The MLCT bands observed in the UV/Vis spectra of the compounds is attributed to the electron distribution from the metals $d\pi$ -orbitals to the ligands π^* orbitals forming the coordination complexes. The successful coordination of the bimetallic pyridyl-imine palladium(II) complexes (**C7-C10**) was also observed to undergo a red shift to 1515 cm^{-1} . The successful coordination was further confirmed by the downfield shift of the azomethine proton signal to around 8.79 ppm in the ^1H NMR spectra compared to their corresponding free ligands. The elemental analysis of all the synthesized compounds were in good agreement with the calculated C,H,N values.

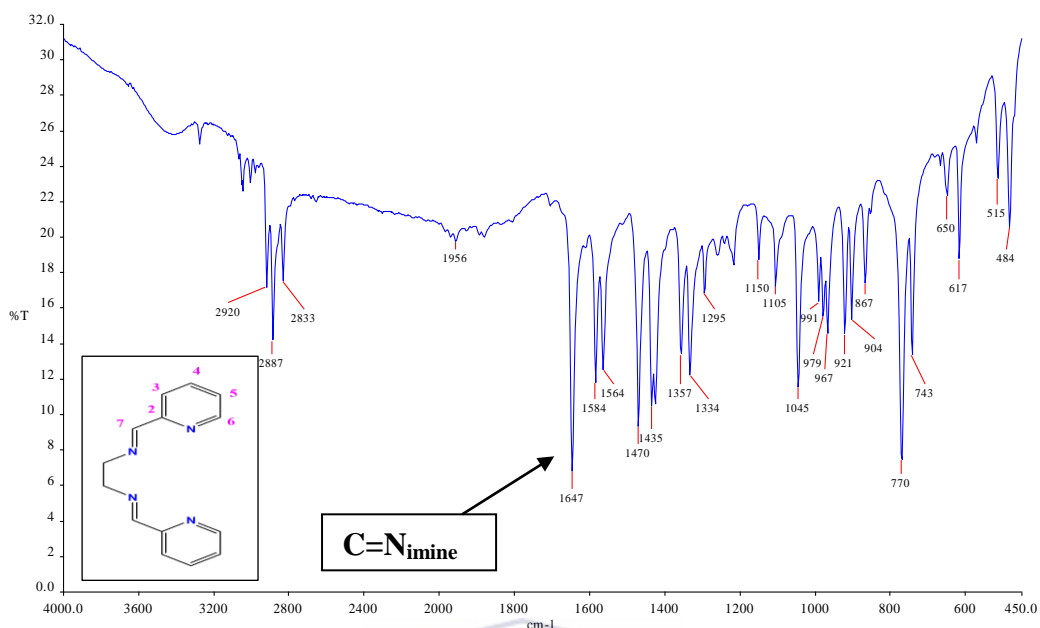
The differences in the chemistry of the pyridyl-imine and quinolyl-imine and their transition metal complexes are of steric effects since there is little difference in basicities of the pyridine and quinoline aromatic rings.

The pyridyl and quinolyl-imine palladium and ruthenium complexes were subsequently tested as catalyst precursors towards the catalytic activity of Heck coupling reactions of methyl acrylate with iodobenzene and the oxidative cleavage of styrene respectively. The ruthenium(II) catalysts exhibited efficient catalytic activity, yielding conversions of 69-77%. The palladium(II) catalysts showed an overall low catalytic activity of 41-49 % conversion and analysed by GC. All the crude products were analysed by the analytical techniques ^1H NMR and FT-IR.

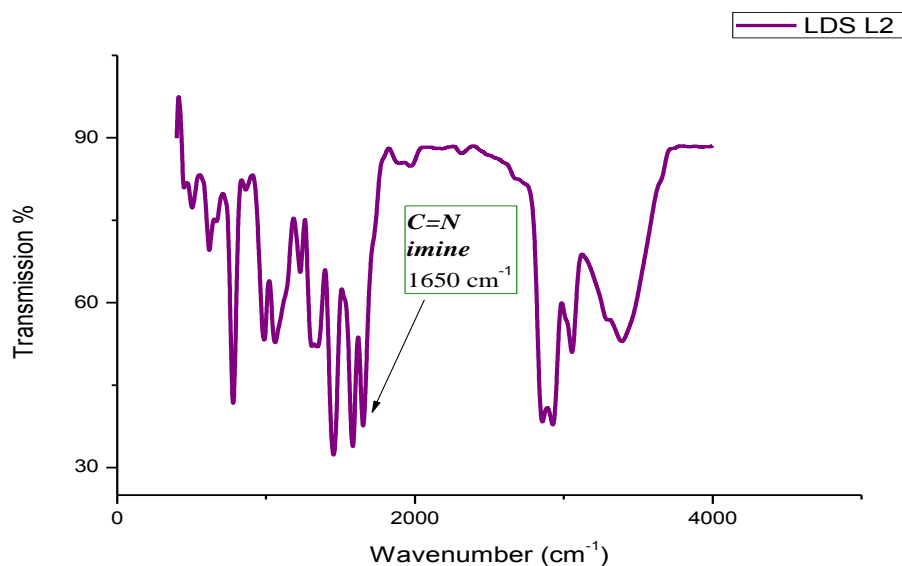
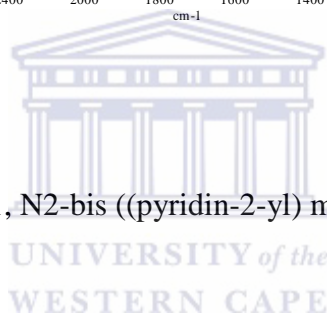
6.2 Recommendations and future work

It is recommended that both functionalized cyclic and aliphatic alkenes also be evaluated for the selective oxidative cleavage of C=C by the prepared pyridyl and quinolyl-imine ruthenium(II) complexes. The variation of the biphasic system, by especially replacing CCl_4 with a more economic friendlier solvent. Crystal structures should be obtained for all the synthesized compounds to better understand their chemical structures. The study of the Heck coupling reaction can be expanded by investigating the scope of the substrate, such as the effect of electron withdrawing/donating substrates on the catalytic activity of the catalyst and optimization of the reaction time. In future pyridyl-imine ligands containing heterodonor atoms (hemi-labile ligands) should be investigated as a means of improving the catalytic activity of the catalysts. Other parameters to be investigated and/or varied include the catalyst loading, various bases and reaction temperature. The characterization of the transitional metal complexes and catalytic products should also be carried out by ESI-Mass spectrometry.

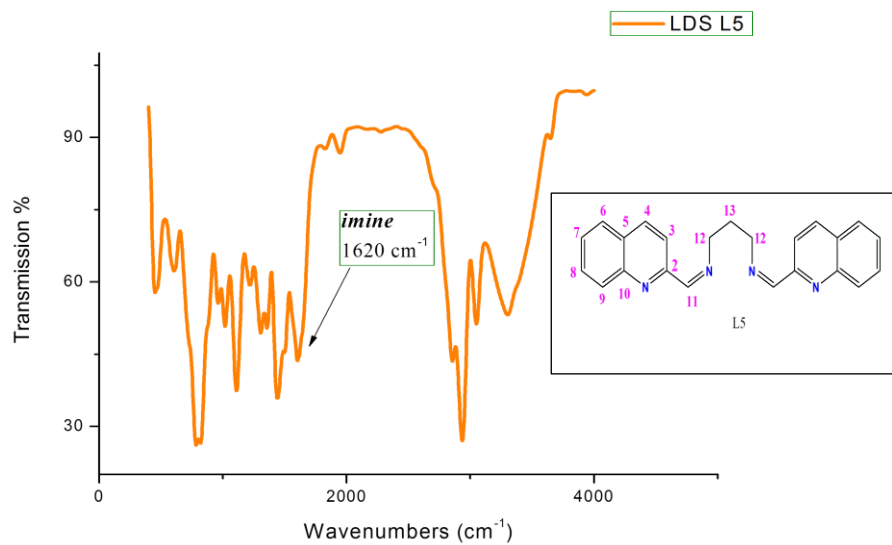
Appendix



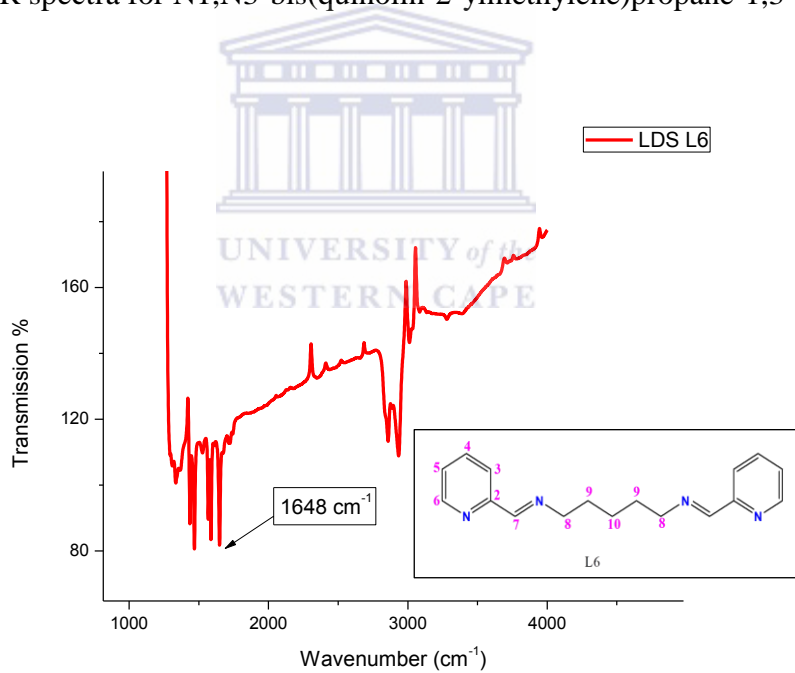
Appendix 1: FT-IR spectra for N1, N2-bis ((pyridin-2-yl) methylene) ethane-1, 2-diamine, L1



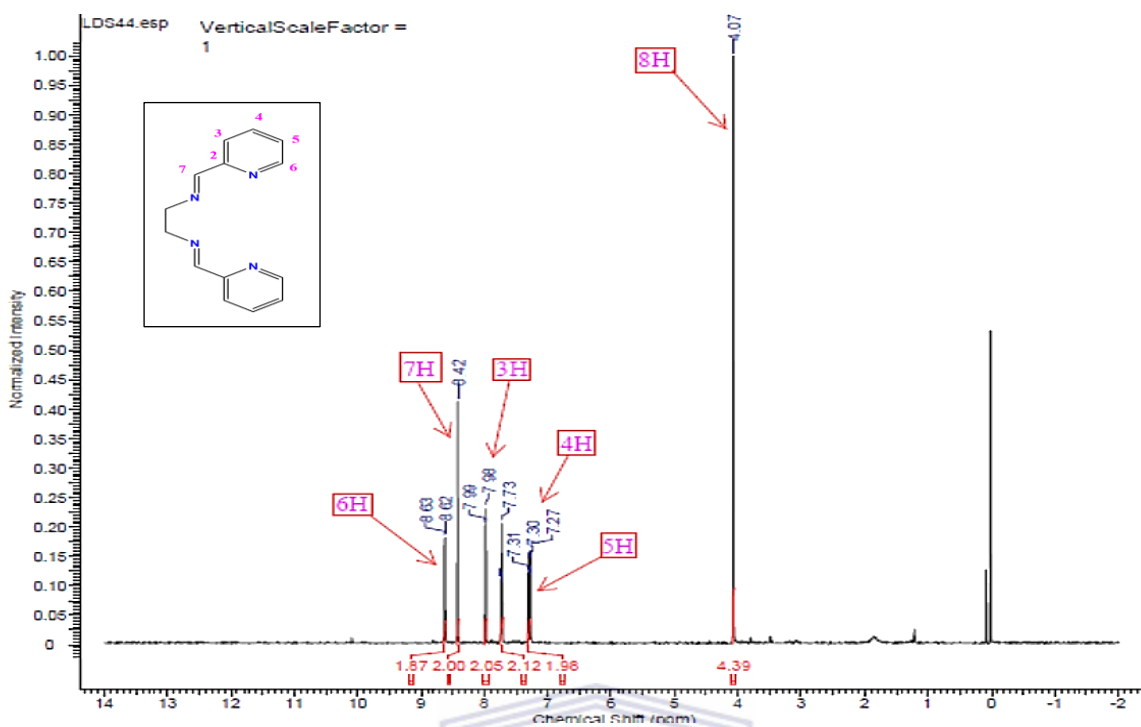
Appendix 2: FT-IR spectra for N1,N3-bis(pyridin-2-ylmethylene)propane-1,3-diamine, L2



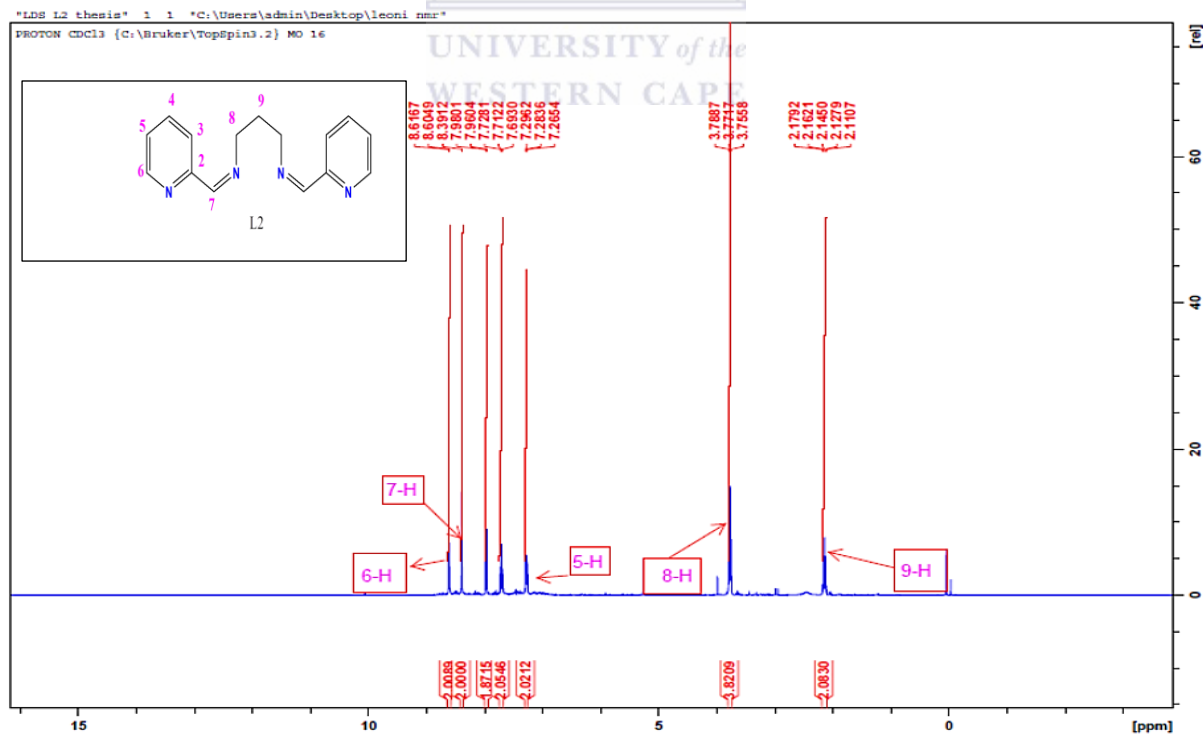
Appendix 3: FT-IR spectra for N1,N3-bis(quinolin-2-ylmethylene)propane-1,3-diamine, L5



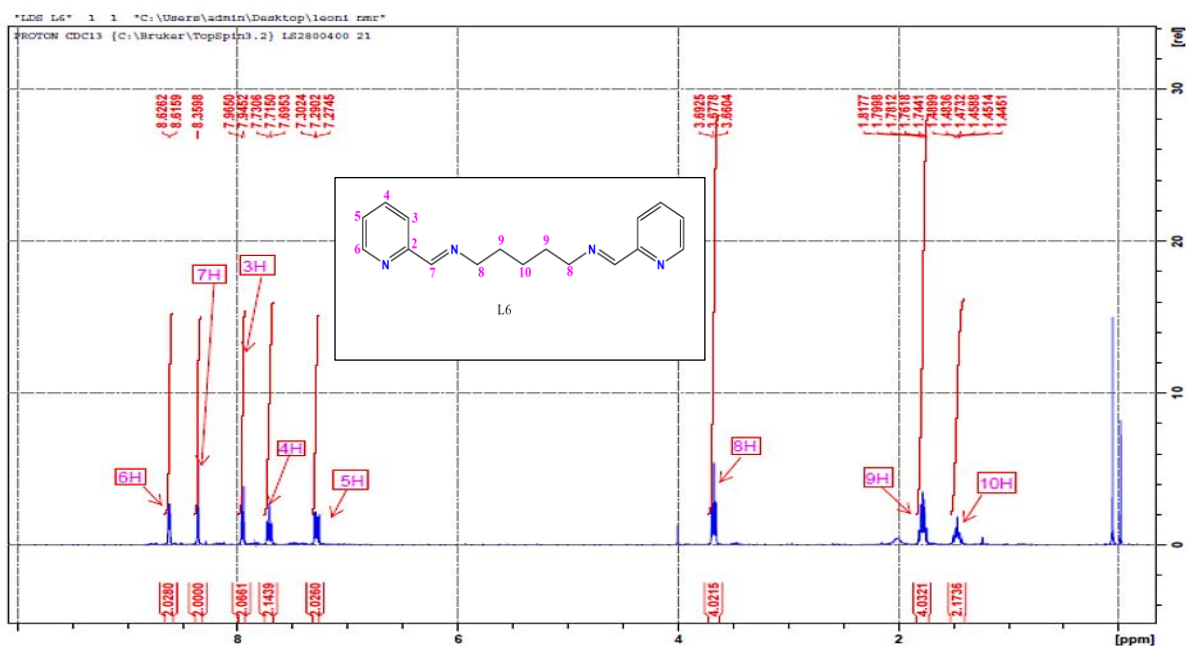
Appendix 4: FT-IR for N1,N5-bis(pyridin-2-ylmethylene)pentane-1,5-diamine, L6



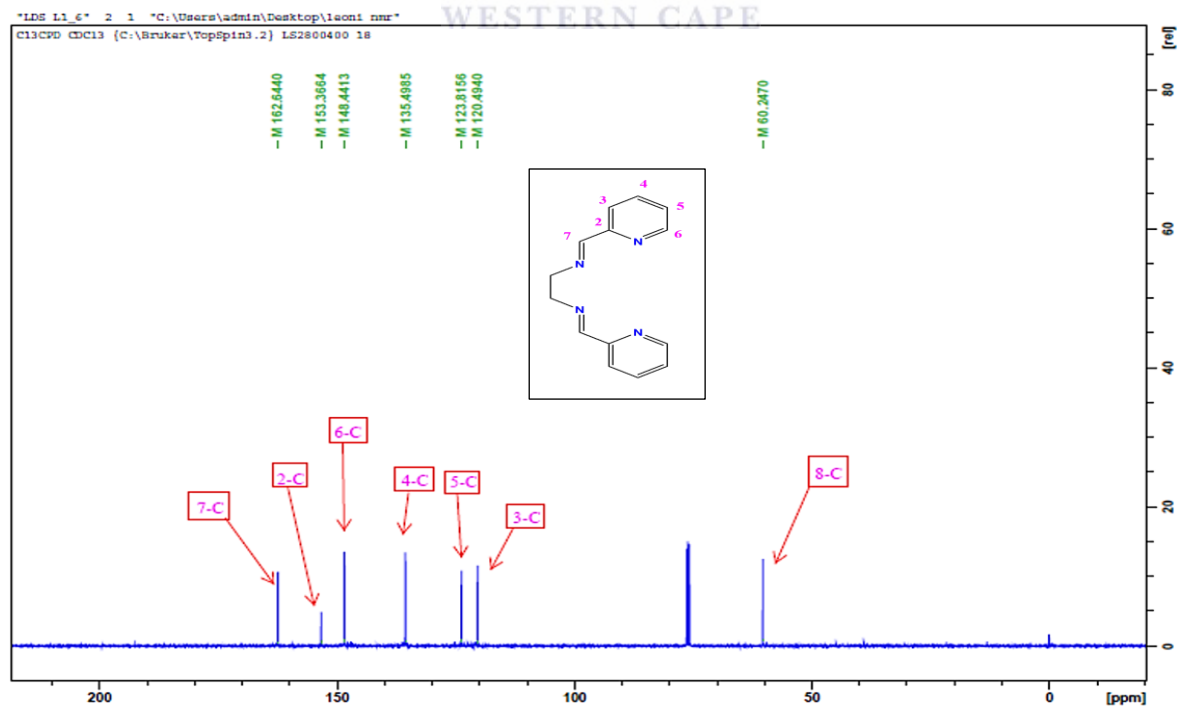
Appendix 5: ^1H NMR for N1, N2-bis((pyridin-2-yl) methylene) ethane-1, 2-diamine, L1



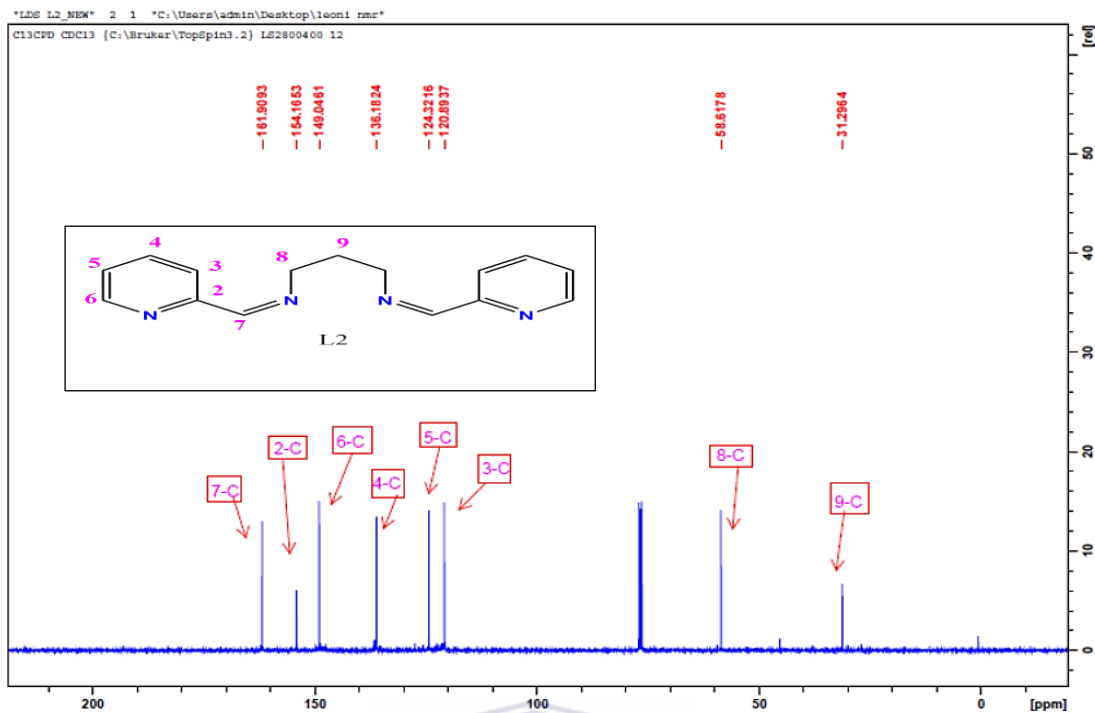
Appendix 6: ^1H NMR for N1, N3-bis((pyridin-2-yl) methylene) propane-1, 3-diamine, L2



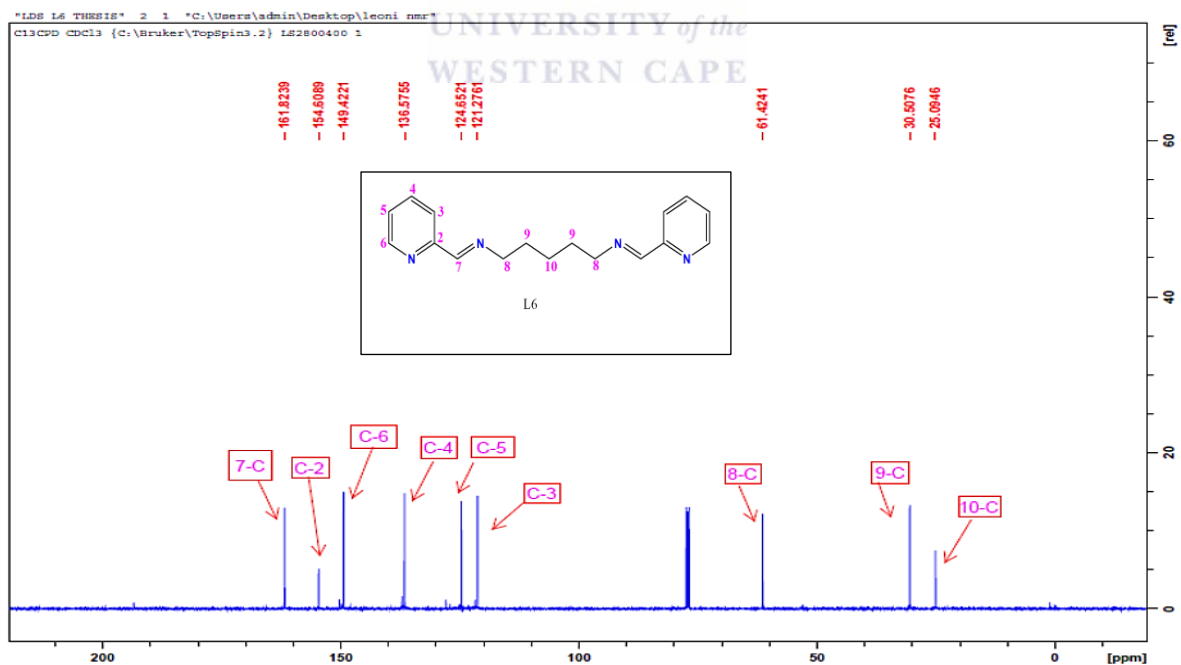
Appendix 7: ^1H NMR for N1,N5-bis((pyridin-2-yl)methylene)pentane-1,5-diamine,L6



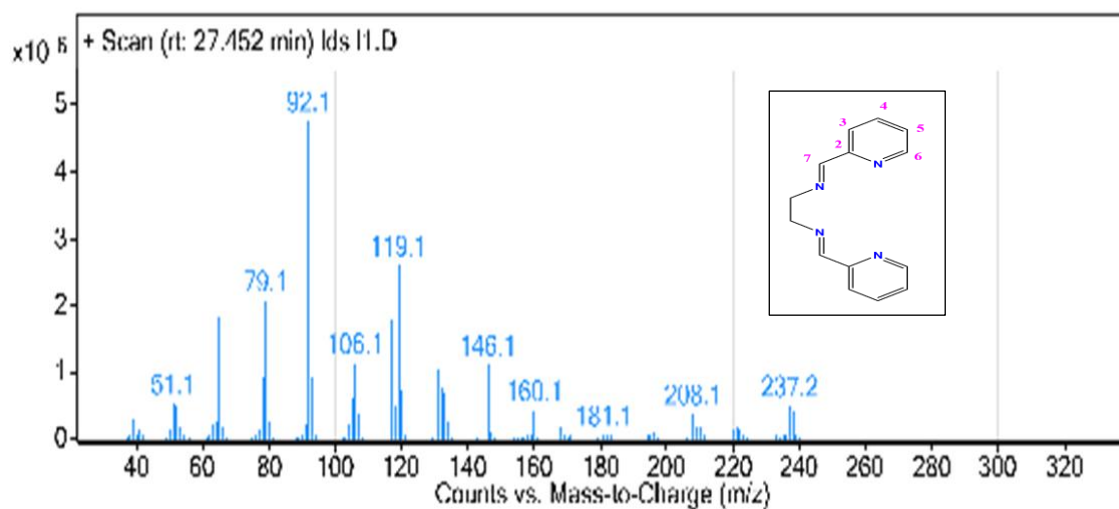
Appendix 8: ^{13}C NMR for N1,N2-bis((pyridin-2-yl)methylene)ethane-1,2-diamine,L1



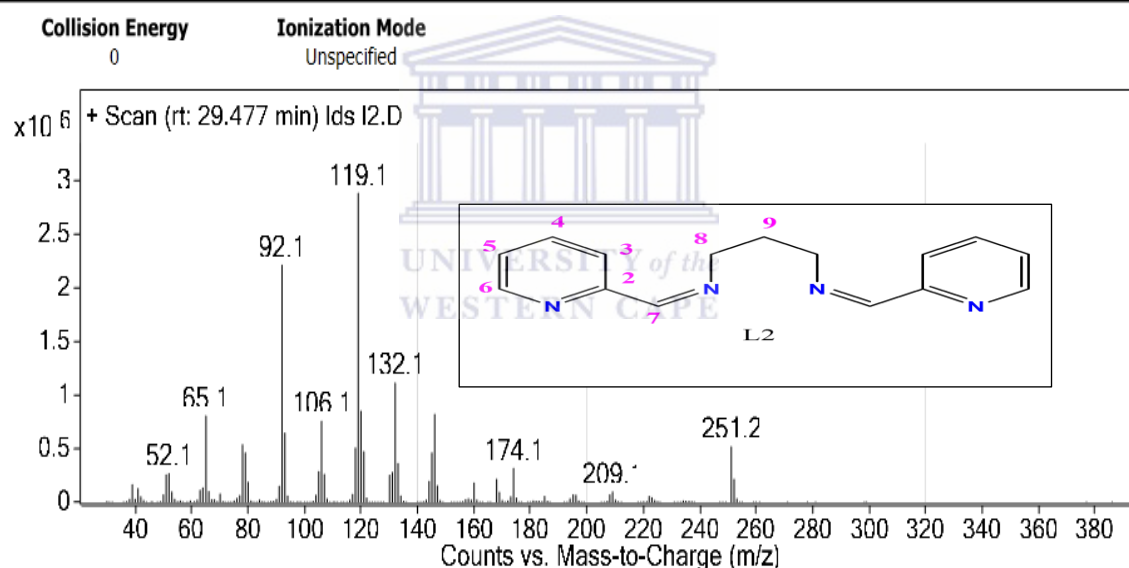
Appendix 9: ^{13}C NMR for N1,N3-bis(pyridin-2-ylmethylene)propane-1,3-diamine, L2



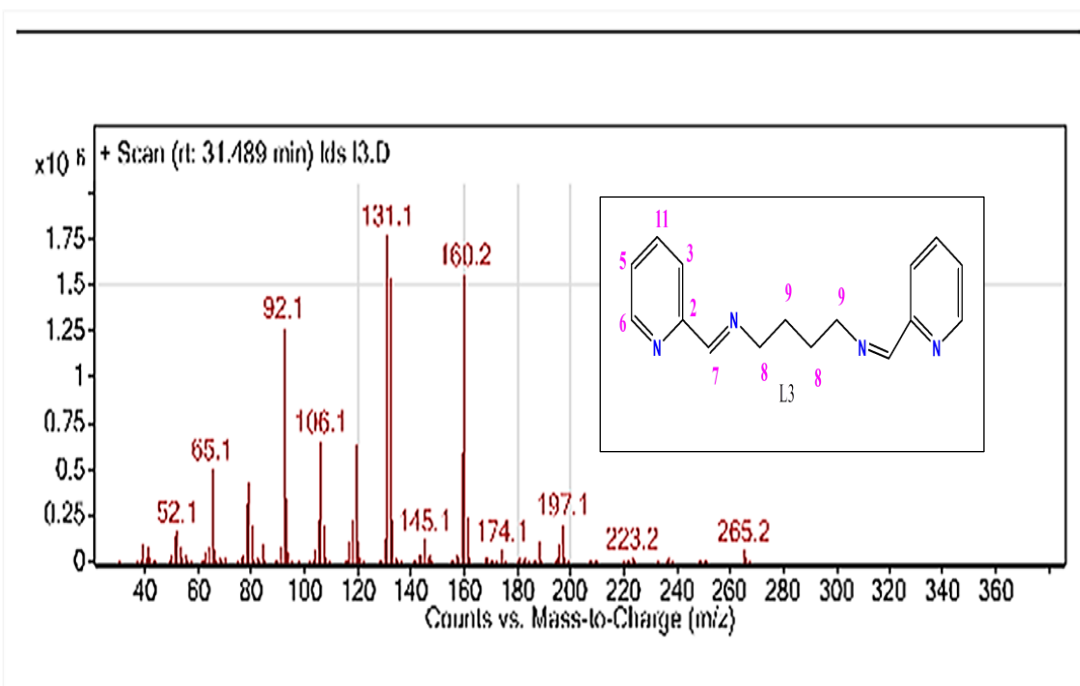
Appendix 10: ^{13}C NMR for N1,N5-bis(pyridin-2-ylmethylene)pentane-1,5-diamine, L6



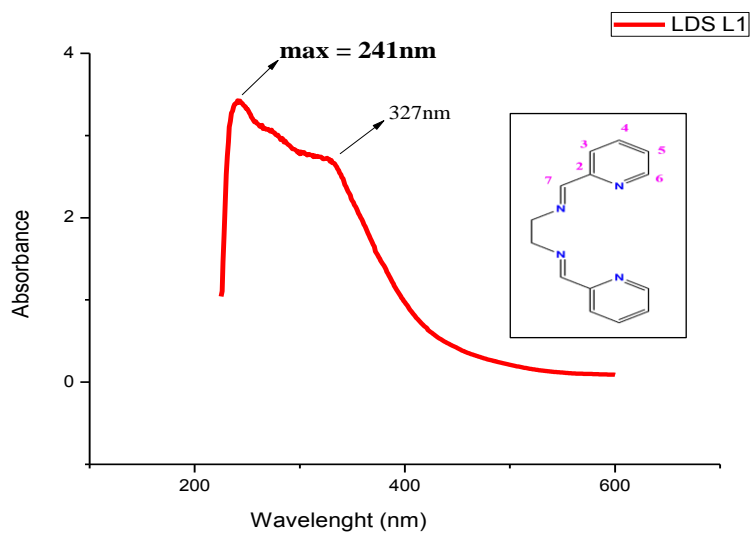
Appendix 11: Mass spectra for N1, N2-bis ((pyridin-2-yl) methylene) ethane-1, 2-diamine, L1



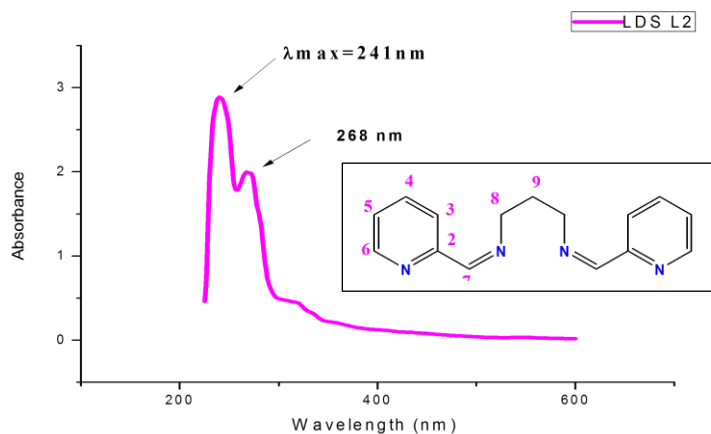
Appendix 12: Mass spectra for N1,N3-bis((pyridin-2-yl)methylene)propane-1,3-diamine, L2



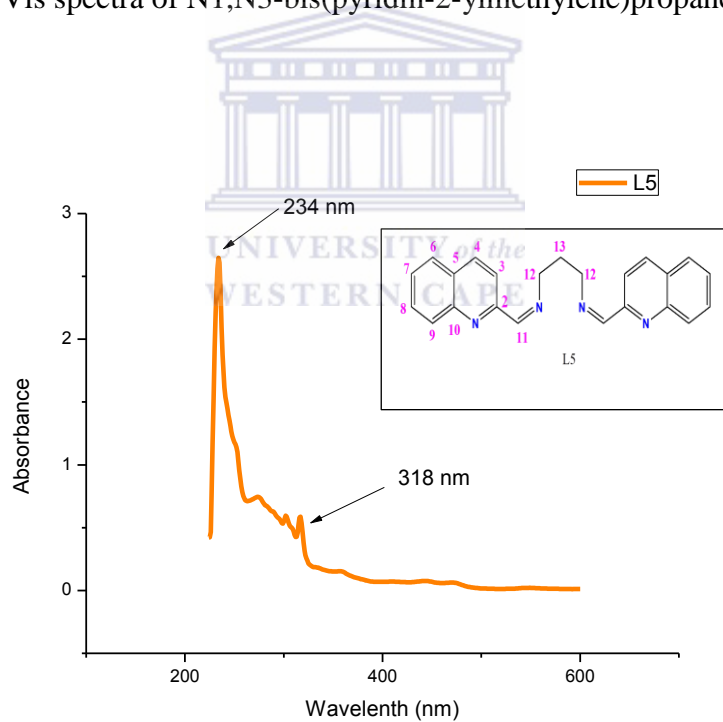
Appendix 13: Mass spectra of N1,N4-bis(pyridin-2-ylmethylene)butane-1,4-diamine, L3



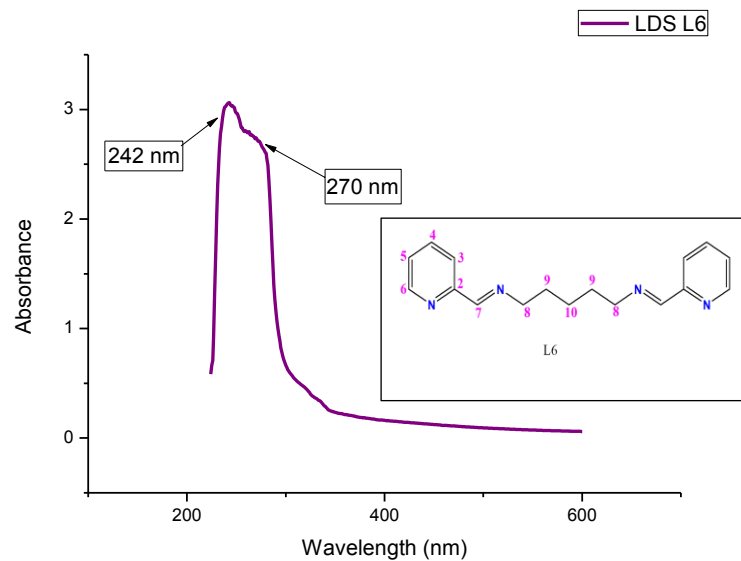
Appendix 14: UV/Vis spectra of N1,N2-bis((pyridin-2-yl)methylene)ethane-1,2-diamine, L1



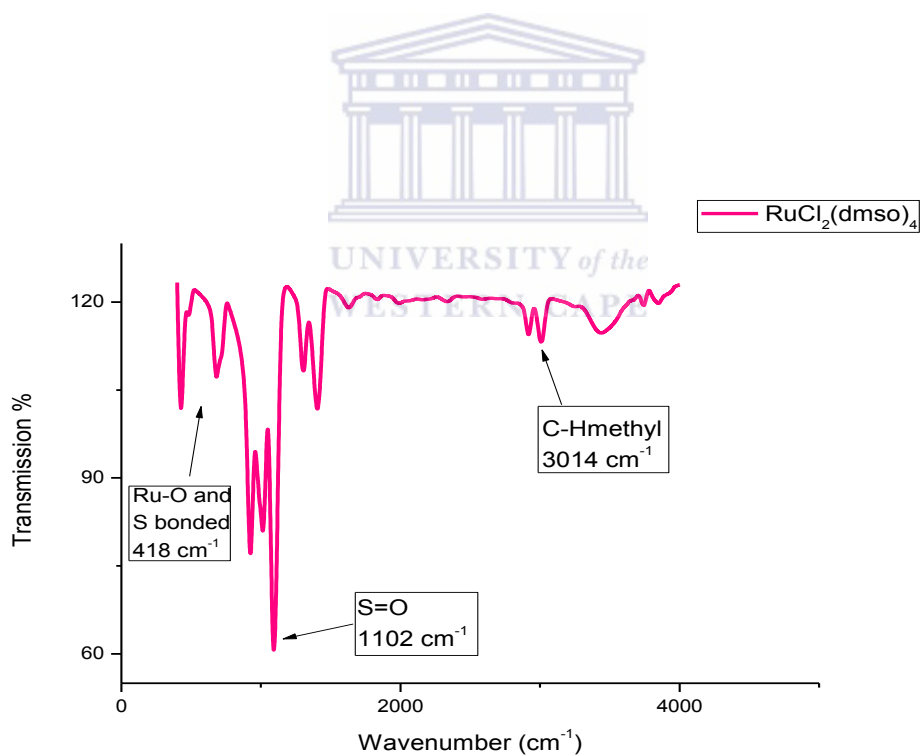
Appendix 15: UV/Vis spectra of N1,N3-bis(pyridin-2-ylmethylene)propane-1,3-diamine, L2



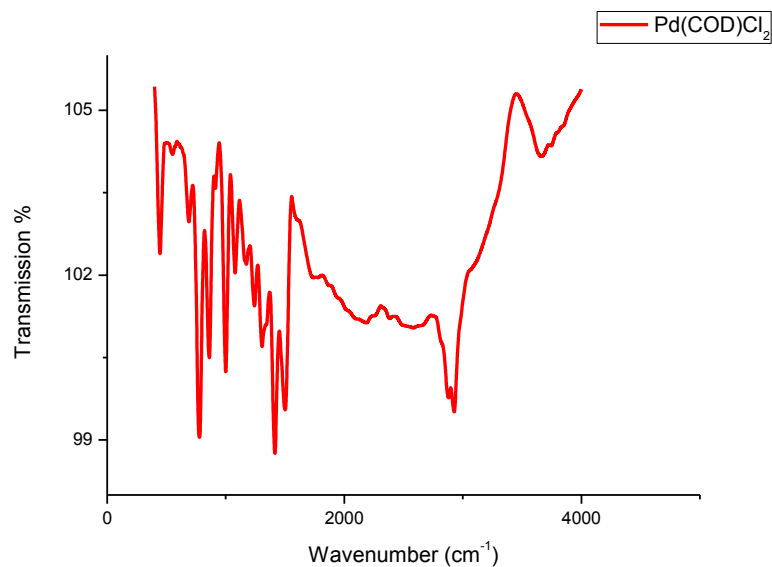
Appendix 16: UV/Vis spectra of N1,N3-bis(quinolin-2-ylmethylene)propane-1,3-diamine, L5



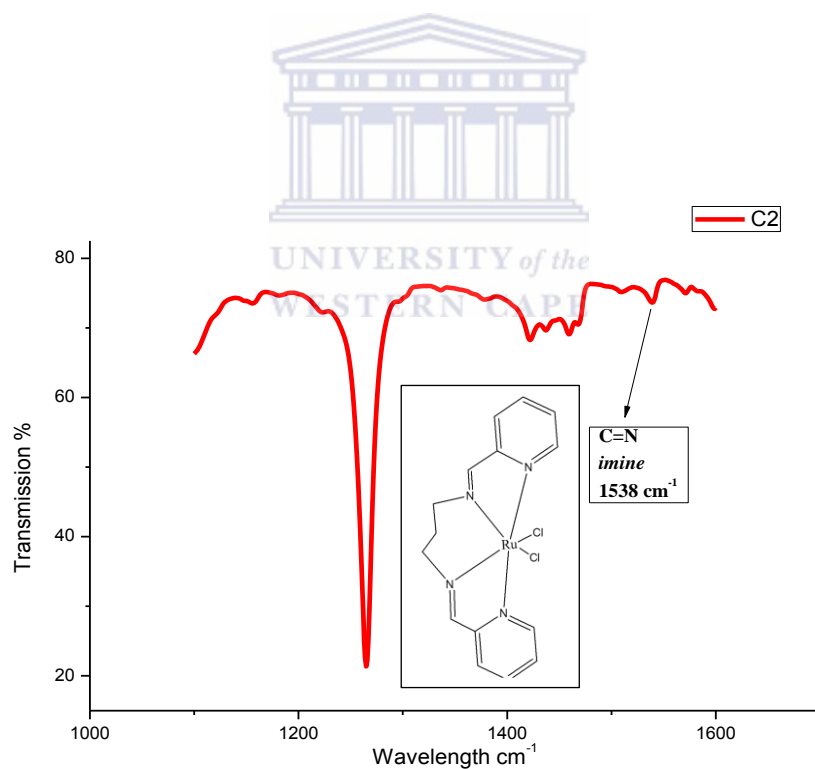
Appendix 17: UV/Vis for N1,N5-bis(pyridin-2-ylmethylene)pentane-1,5-diamine, L6



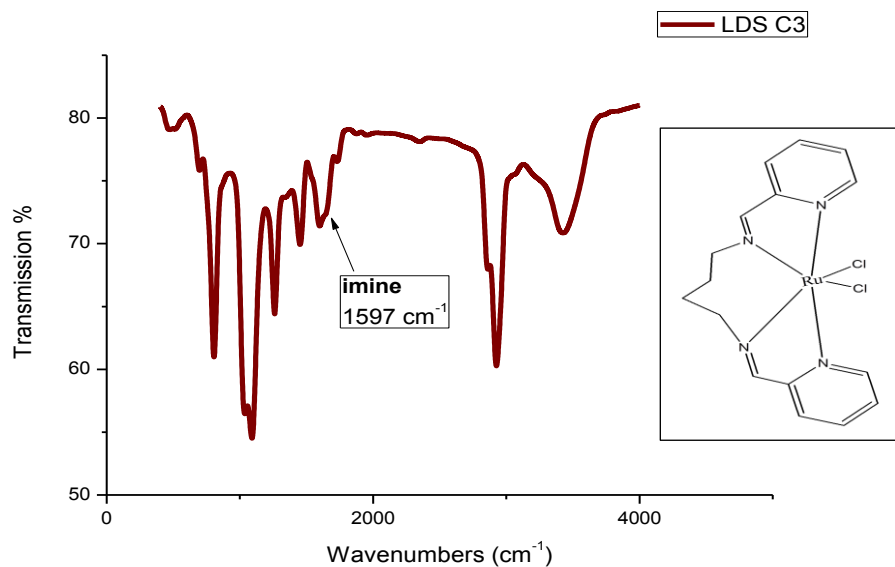
Appendix 18: FT-IR spectra of precursor, RuCl₂(dmsO₄)



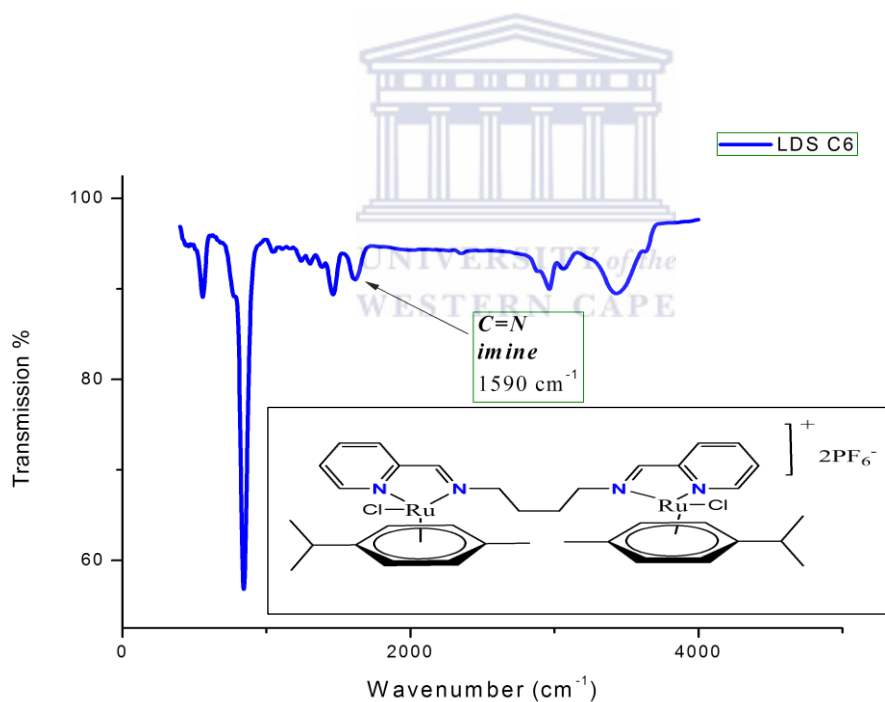
Appendix 19: FT-IR spectra of precursor, Pd(COD)Cl₂



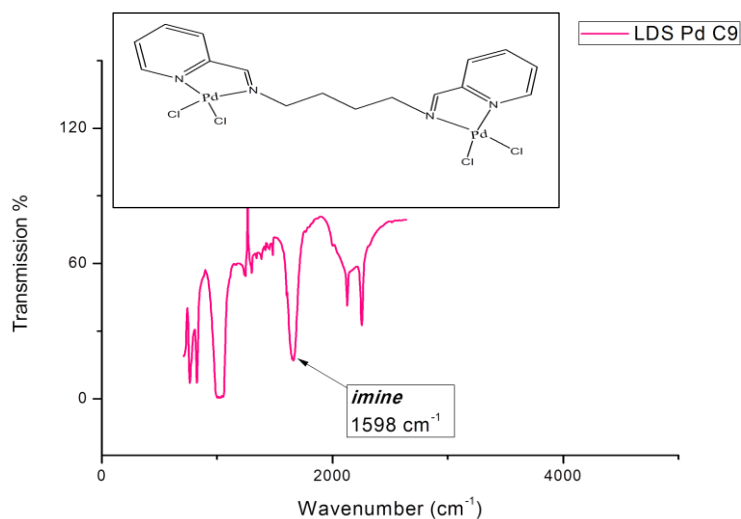
Appendix 20: FT-IR spectra for N1,N3-bis(pyridin-2-ylmethylene)propane-1,3-diamine)Cl₂], C2



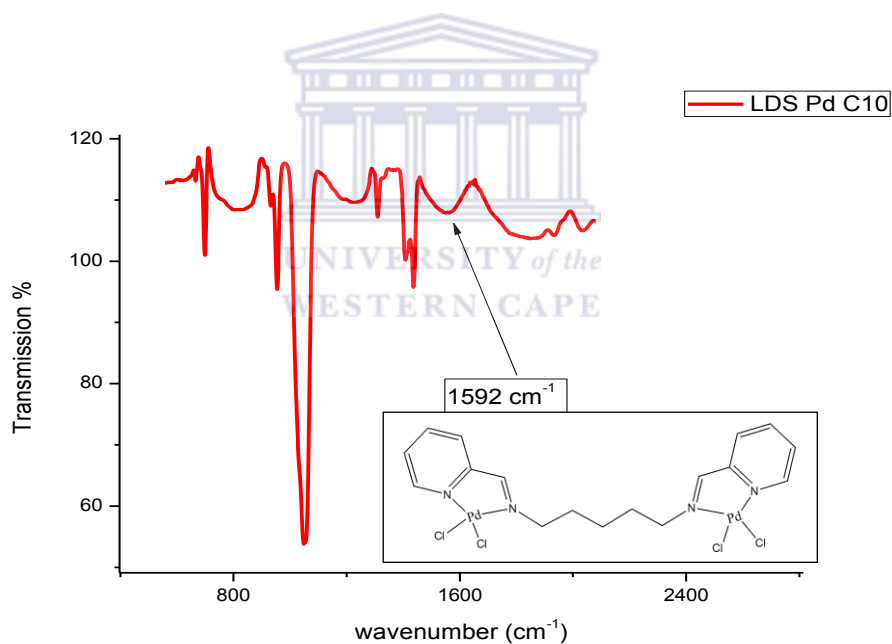
Appendix 21: FT-IR spectra for dichloro-N1,N4-bis(pyridin-2-ylmethylene)butane-1,4-diamine-ruthenium (II),C3



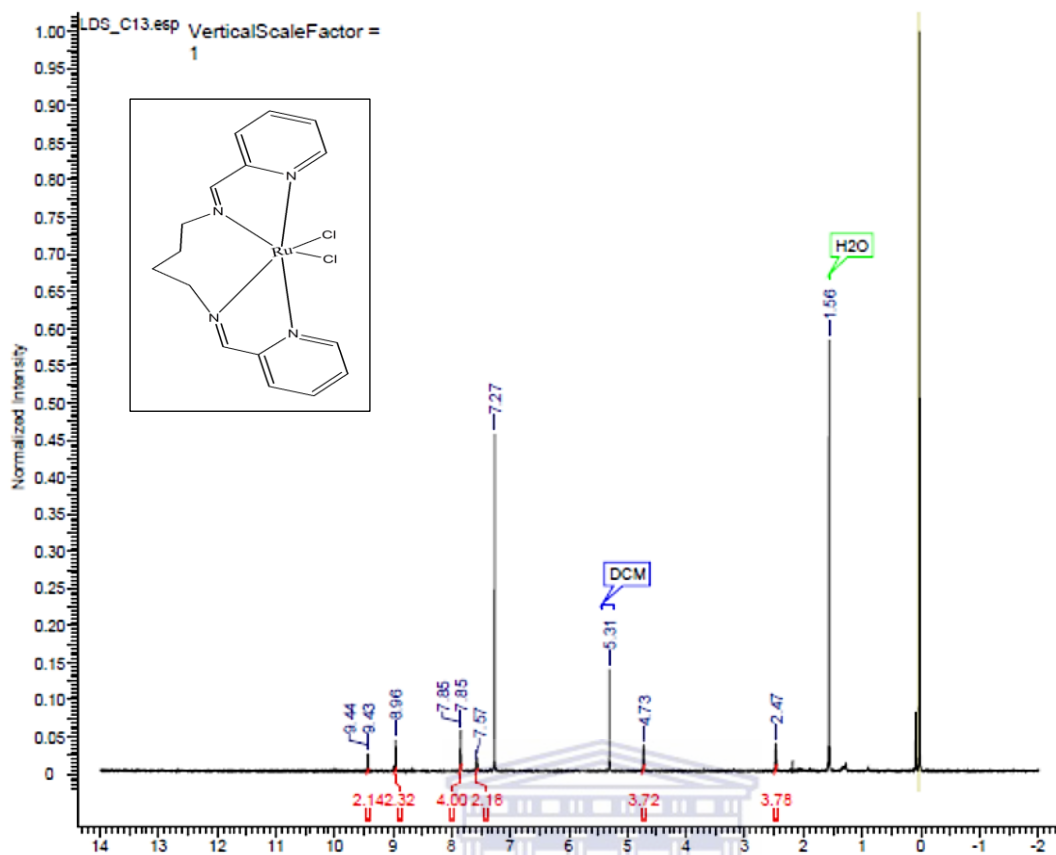
Appendix 22: FT-IR for cationic homobimetallic ruthenium(II) complex ,C6



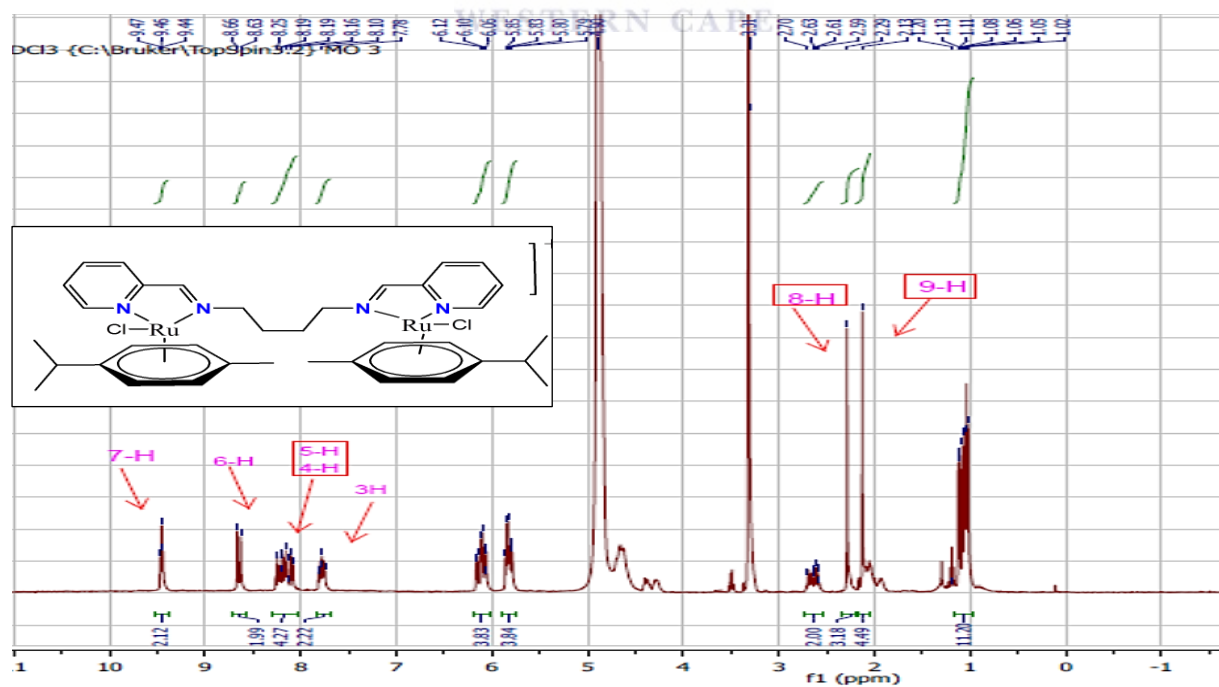
Appendix 23: dichloro-N1,N4-bis(pyridin-2-ylmethylene)butane-1,4-diamine palladium(II), C9



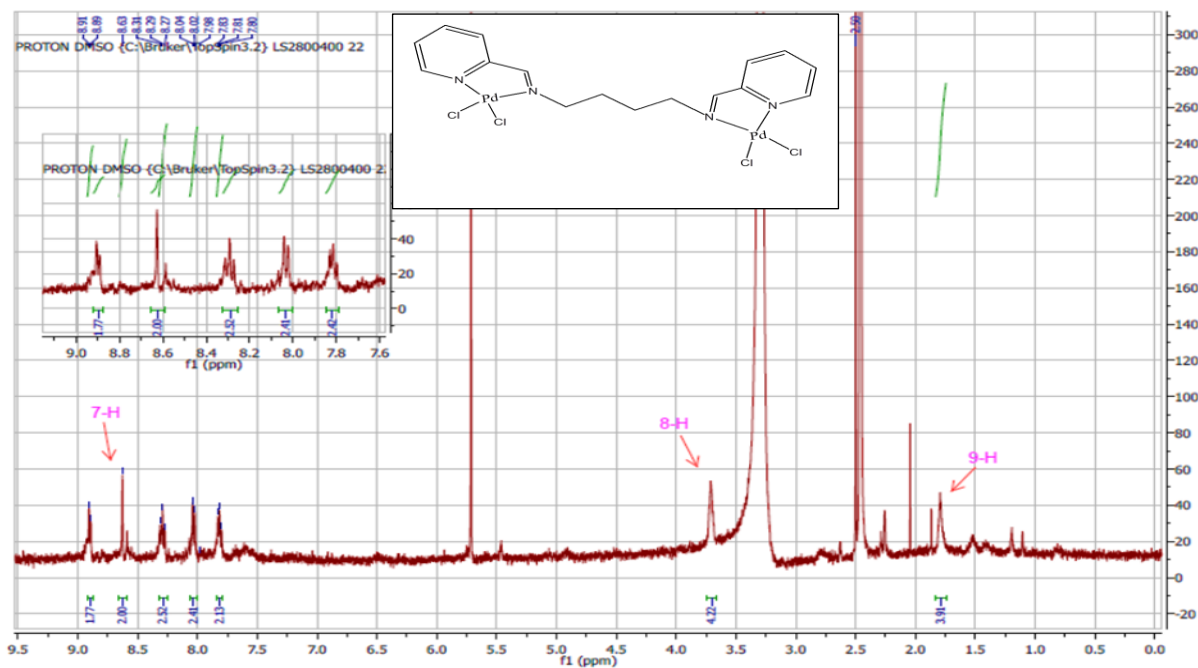
Appendix 24: dichloro-N1,N5-bis(pyridin-2-ylmethylene)pentane-1,5-diamine palladium(II), C10



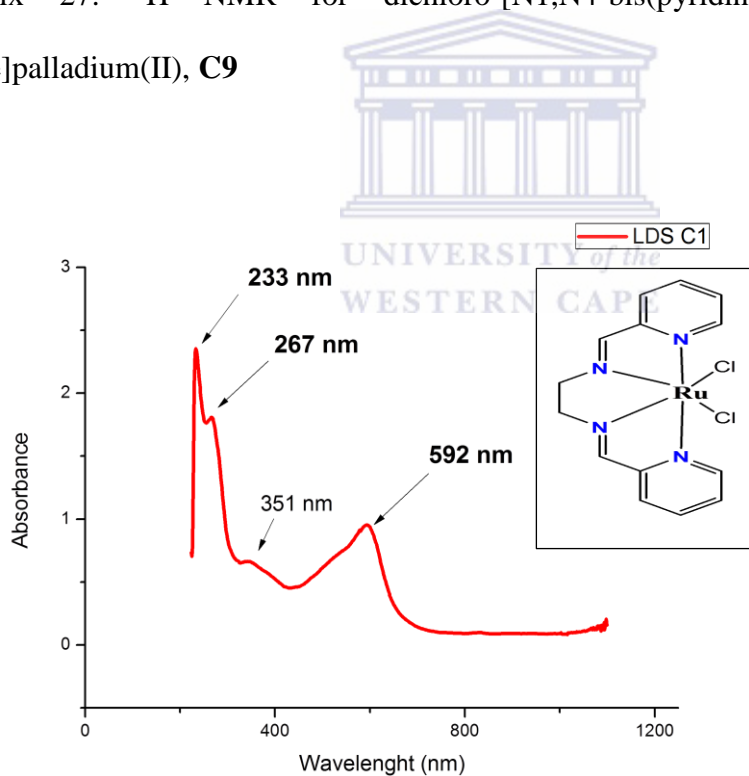
Appendix 25: ^1H NMR for dichloro-N1,N4-bis(pyridin-2-ylmethylene)butane-1,4-diamine-ruthenium(II), C3



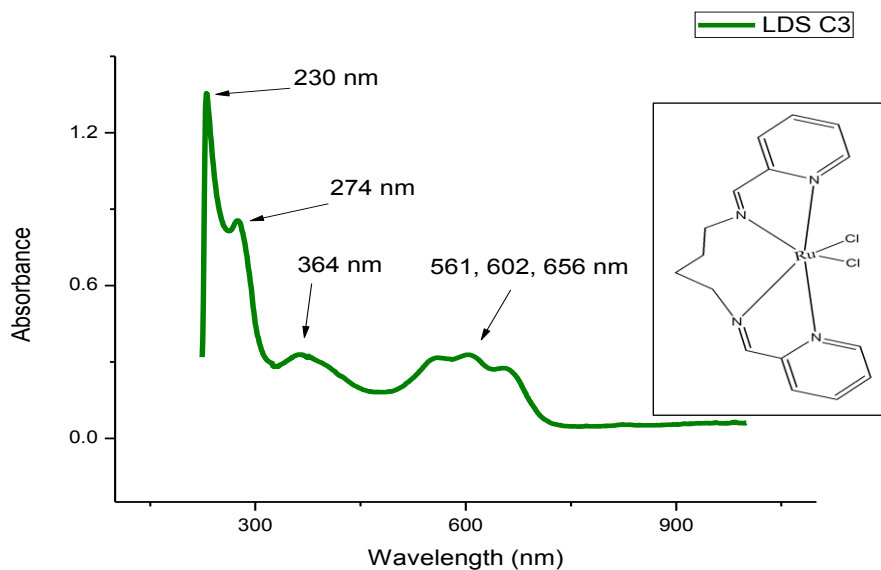
Appendix 26: ^1H NMR for homobimetallic ruthenium(II) complex, C6



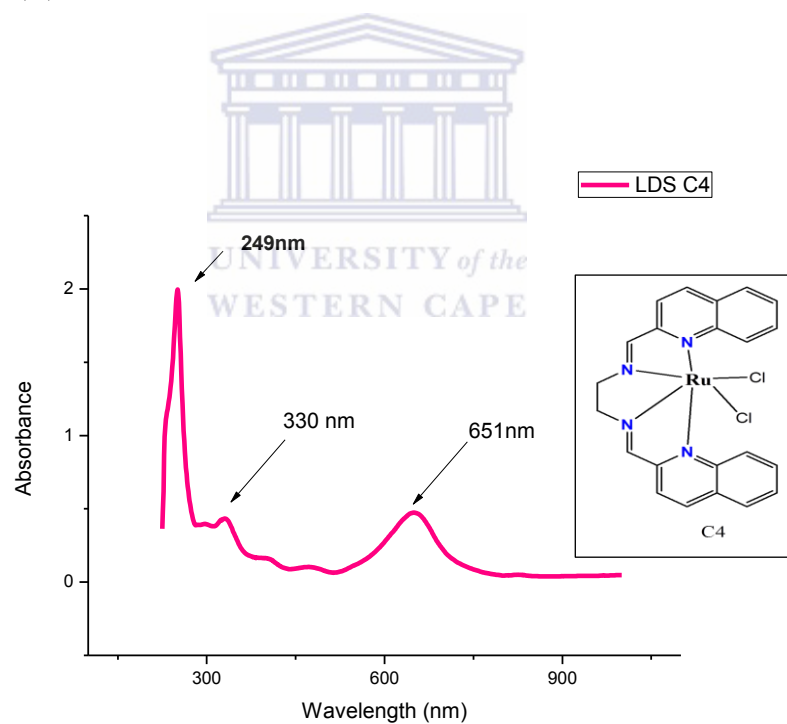
Appendix 27: ^1H NMR for dichloro-[N1,N4-bis(pyridin-2-ylmethylene)butane-1,4-diamine]palladium(II), C9



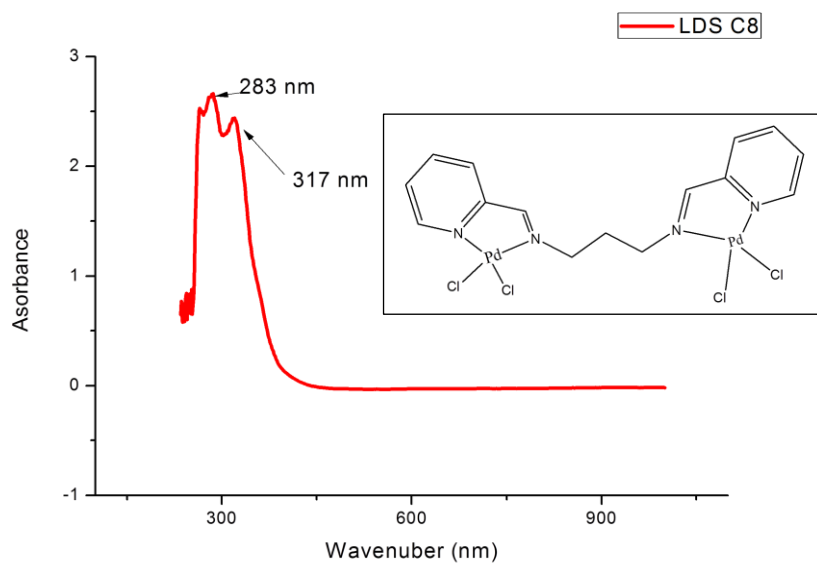
Appendix 28: UV/Vis spectra of Dichloro-N1,N2-bis((pyridin-2-yl)methylene)ethane-1,2-diamine ruthenium(II), C1



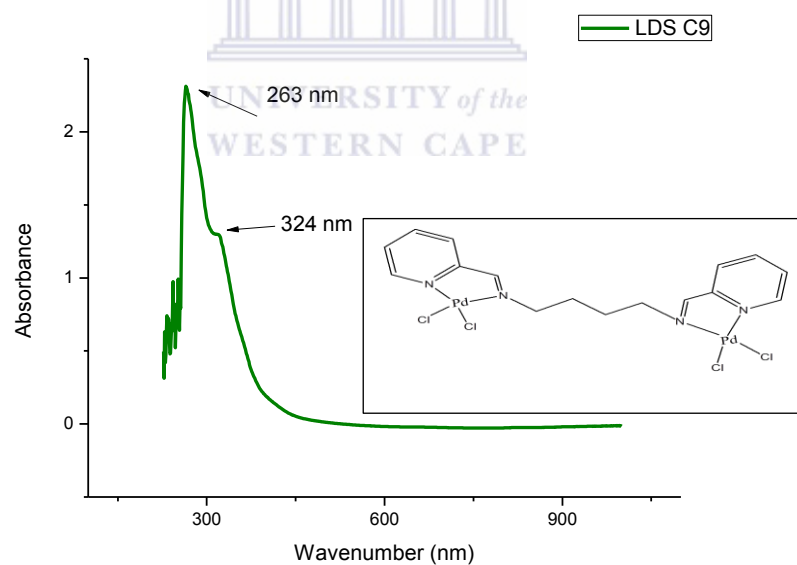
Appendix 29: UV/Vis spectra of Dichloro-N1,N4-bis(pyridin-2-ylmethylene)butane-1,4-diamine ruthenium (II),C3



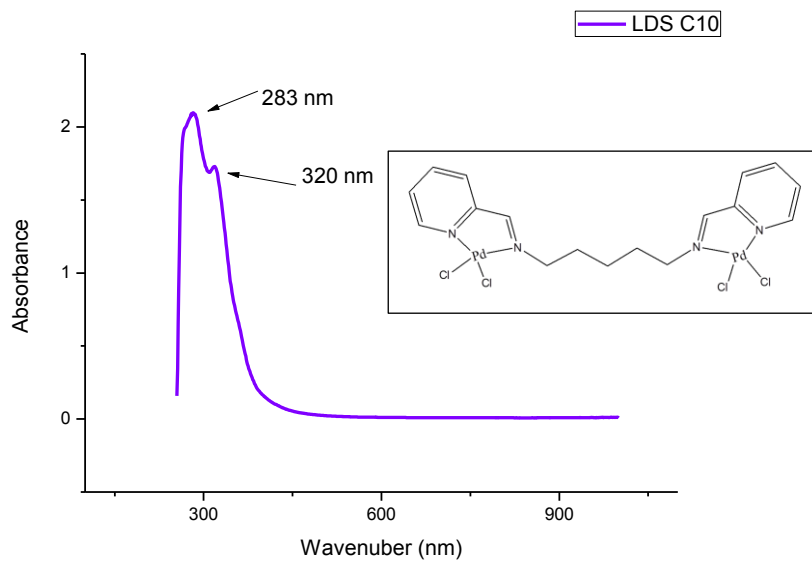
Appendix 30: UV/Vis spectra of Dichloro-N1,N2-bis((quinolin-2-yl)methylene)ethane-1,3-diamine ruthenium(II), C4



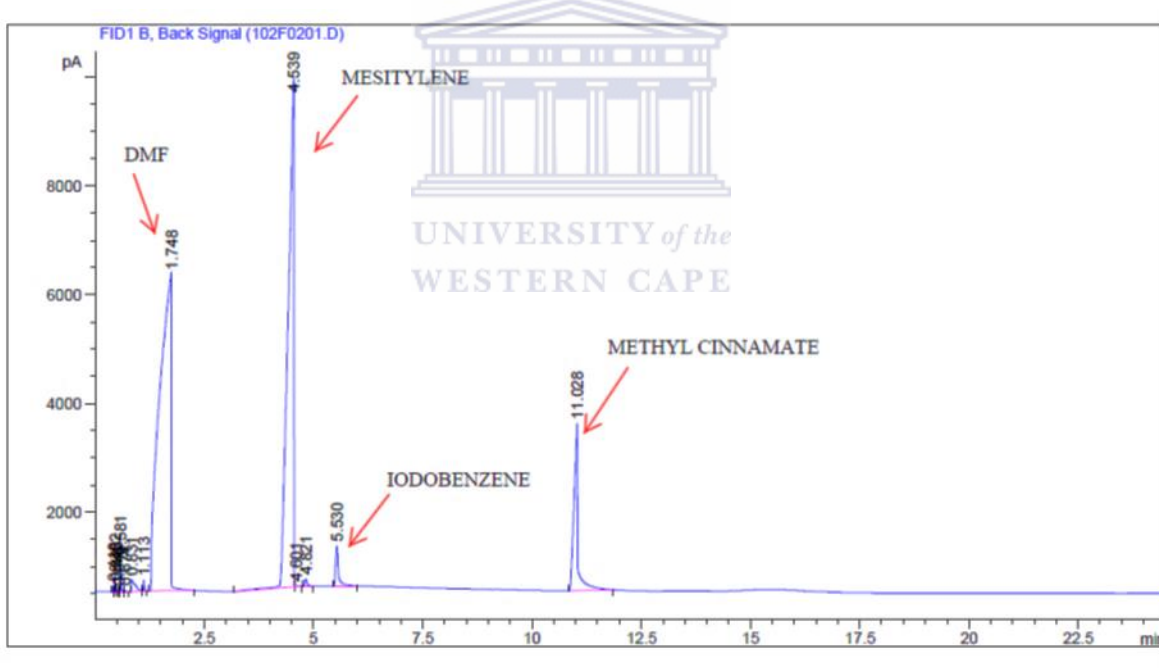
Appendix 31: dichloro-[N1,N3-bis(pyridin-2-ylmethylene)propane-1,3-diamine]palladium(II), C8



Appendix 31: UV/Vis for dichloro-[N1,N4-bis(pyridin-2-ylmethylene)butane-1,4-diamine]palladium(II), C9



Appendix 32: UV/Vis for dichloro-[N1,N5-bis(pyridin-2-ylmethylene)pentane-1,5-diamine]palladium(II), **C10**



Appendix 33: GC-chromatogram of arylation of iodobenzene, catalysed by complex **C8**.